

Natural balancing of the neutral-point-clamped converter

By

ISAAC MAHIJOKO SALAGAE



Thesis presented in partial fulfilment of the requirements for the
degree of Master of Science (Engineering Science) at the
University of Stellenbosch

Supervisor: Prof H Du T Mouton

December, 2003

Declaration

I, the undersigned, hereby declare that the work contained in this thesis is my own original work, unless otherwise stated, and has not previously, in its entirety or in part, been admitted at any university for a degree.

Isaac Mahijoko Salagae

1 October 2003

Summary

The three-level neutral-point-clamped(NPC) converter, being a widely used multilevel inverter, received a lot of attention recently due to problems associated with dc-link capacitor voltage balancing. There are mainly two problems associated with the neutral-point voltage of the NPC inverter:

1. At high modulation indices a low frequency ripple occurs on the neutral-point voltage.
2. Steady-state unbalance in the neutral-point voltage may arise due to a variety of factors including component imperfections, transients and other non-idealities and imbalances.

In this thesis we study the balancing problem with focus on the steady-state imbalance. This is achieved by a systematic and mathematically rigorous study of the natural balancing mechanisms of the three-level three-phase NPC inverter. Orthogonality of two sets of switching spectra in the frequency domain would imply that the DC-bus voltages balance in the steady state. This is done through mathematical analysis using Carrara's PWM strategy of alternative phase opposition disposition(APOD), phase opposition disposition(POD) and phase disposition(PD); and Bennet's geometric model for double Fourier series adapted for use with power converter systems by Bowes. The theory is verified through simulation.

Opsomming

Aangesien die drie-vlak, geklemde, neutrale-punt omsetter(NPC) 'n algemene omsetter konfigurasie is, is daar onlangs baie aandag gegee aan die probleme wat geassosieer word met die balansering van die omsetter se gelykstroombuskapasitorspanning. Die twee hoof probleme wat gepaart gaan met die neutraalpunktspanning van die NPC omsetter is:

1. Met 'n ho modulasie-indeks ontstaan daar 'n lae frekwensie rippel op die neutrale-puntspanning.
2. 'n Bestendige toestand wanbalans van die neutrale-puntspanning kan ontstaan as gevolg van 'n verskeidenheid faktore, onder andere komponent nie-idealiteit, oorgangs- en ander wanbalanse.

In hierdie tesis word op die bestendige-toestandwanbalans gefokus. Dit word gedoen deur middel van die neutraalbalanseeringsmeganisme van die drie-vlak, drie-fase NPC omsetter, sistematies en gedetaileerd wiskundig te bestudeer. In die bestendige toestand sal orgonaliteit van twee stelle skakel spektras in die frekwensie gebied, GS-bus spanning balans impliseer. Dit word wiskundig geanalyseer deur gebruik te maak van Carrara se alternatiewe fase opposisie disposisie (APOS), fase oposisie disposisie (POD) en fase disposisie(PD), puls-wydte modulasie strategie, asook Bennet se geometriese modelle vir die dubbel Fourier reeks wat aangepas is vir drywingsomsetters deur Bowes. Ten slotte is die teorie geverifieer deur simulasies.

Acknowledgements

I would like to thank God almighty, *Great is Thine faithfulness Lord unto me.*
Lamentations 3:22,23.

I would also like to thank the following people and institutions:

Prof. H. du T. Mouton for his extraordinary patience in guiding and supporting me; and for giving me the opportunity to do this project.

Batsadi ba me Sikhi le Gaetshelwe Salagae, ka bopelotelele, lorato le thotloetso e ba nneileng yone mo dithutong tsa me.

My relatives and friends for their support during difficult times.

The members of the Power Electronics Research Group of the University of Stellenbosch for their support. In particular I would like to thank Richardt Wilkinson, Aniel le Roux and Daleen Kleyn.

NRF and University of Stellenbosch's Electrical and Electronic Engineering department for their financial support.

Contents

1	Introduction	1
1.1	Historical Overview	1
1.2	Advantages and Applications of the NPC Inverter	4
1.3	Disadvantages of NPC Inverter	4
1.4	Research Objective	6
2	Background	8
2.1	PWM Modulation	8
2.1.1	Natural Sampling	9
2.1.2	Regular Sampling	11
2.1.3	Method of Analysis	12
2.1.4	PWM Technique	13
2.2	Vector Modulation	15
2.2.1	Generation of space vector modulation	16
2.2.2	Method of analysis	20
2.3	Strategies used by some authors	26
2.3.1	Avoid the narrow pulse problem	26
2.3.2	Model in DQ coordinate frame utilising current switching functions	27
2.3.3	Neutral-point voltage balancing circuit for DC-DC technology	28
2.3.4	Other strategies	29
2.4	Conclusion	29
3	Balancing Theory	30
3.1	$\alpha\beta$ transformation of the switching states	30
3.2	Load Transformation	35
3.3	Transformation to $\alpha\beta$ Parameters	37
3.4	Operation of a two-port switching circuit	41
3.5	Steady-State Balancing of the Capacitor Voltages	42
3.6	Time Constant	43

3.7	Filter Design	45
3.8	Balancing Circuit	48
3.9	Conclusion	52
4	Spectra of the switching functions	54
4.1	Theoretical Analysis using APOD/POD	
	PWM technique	54
4.1.1	Spectral Analysis for Harmonics	57
4.1.2	Steady-State Balancing using $F_1(\omega)$ and $F_2(\omega)$	64
4.2	Theoretical Analysis using PD PWM	
	technique	68
4.2.1	Spectral Analysis for Harmonics	70
4.2.2	Steady-State Balancing for $F_1(\omega)$ and $F_2(\omega)$	74
4.3	Conclusion	78
5	Simulations	81
5.1	Output voltage waveform	81
5.2	Natural balancing under APOD/POD	
	modulation	85
5.3	Natural balancing under PD modulation	89
5.4	Conclusion	93
6	Simulations of NPC Inverter under Vector Control	94
6.1	Switching Vectors	94
6.2	Duty Cycles	97
6.3	Simulation results	103
6.4	Conclusion	109
7	Conclusion	110
7.1	Summary	110
7.2	Thesis Contribution	111
7.3	Future Work	111
A	Harmonics using APOD/POD PWM technique	117
A.1	Coefficients of $(s_\alpha \times \frac{V_t}{2})$ and $(s_\beta \times \frac{V_t}{2})$	
	under APOD/POD PWM.	117
A.2	Derivation of s_α under APOD/POD PWM	119
A.3	Derivation of s_β under APOD/POD PWM.	123
A.4	Harmonics for S_α and S_β using theory and	
	MATLAB package under APOD/POD	127

A.5 Coefficients of $(s'_\alpha \times \frac{V_t}{2})$ and $(s'_\beta \times \frac{V_t}{2})$ under APOD/POD PWM	129
A.6 Harmonics for S'_α and S'_β under APOD/POD PWM using theory and MAPLE package	131
A.7 Harmonics for $ F_1 $ under APOD/POD PWM	134
A.8 Harmonics for $ F_2 $ under APOD/POD	138
B Harmonics using PD PWM technique	142
B.1 Coefficients of $(s_\alpha \times \frac{V_t}{2})$ and $(s_\beta \times \frac{V_t}{2})$ under PD PWM	142
B.2 Coefficients of $(s'_\alpha \times \frac{V_t}{2})$ and $(s'_\beta \times \frac{V_t}{2})$ under PD PWM	145
B.3 Maple program for S_α and S_β under PD PWM	148
B.4 Maple program for S'_α and S'_β under PD PWM	152
B.5 Maple program for $ F_1 $ under PD PWM	158
B.6 Maple program for $ F_2 $ under PD PWM	164
C Exponential decay	172
C.1 Exponential decay of v_δ under APOD/POD PWM	172
C.2 Exponential decay of v_δ under PD PWM	173
D FFT analysis and simulation setup	175
D.1 FFT for switching functions	175
D.2 Simulation setup using APOD/POD and PD.	176
D.3 Simulation setup using vector control	177

List of Figures

1.1	Three-level neutral-point-clamped inverter	2
1.2	Phase output voltage waveform	3
1.3	Line output voltage waveform	3
1.4	Single phase five-level diode-clamped inveter	5
2.1	Pulse-width modulation	9
2.2	Single-phase modulation	10
2.3	Three-phase modulation	10
2.4	Natural-sampled PWM	10
2.5	a) Regular sampling b) Symmetrical c) Asymmetrical	11
2.6	Model for double Fourier series	12
2.7	APOD system	14
2.8	POD system	14
2.9	PD system	15
2.10	Two-level three-phase inverter	16
2.11	Voltage space vector	16
2.12	Asymmetrical space vector pulse pattern	18
2.13	Phase A switching functions obtained from space vector waveform	20
2.14	a) Fundamental sinusoid, b) Space vector phase voltage ($b = a + c$) and c) Third harmonic triangle wave distortion	21
2.15	Zero crossings of three-phase sinusoids	21
2.16	Wall model for space vector modulation	22
2.17	14 regions for the minimum on/off time and the dc-link voltage balancing .	26
2.18	First sector for the switching state vectors of the three-level NPC inverter .	27
2.19	Neutral-point voltage balancing circuit	28
3.1	NPC inverter	31
3.2	Phase A of NPC inverter	32
3.3	Circuit A connected to the NPC inverter	35
3.4	Circuit B connected to the NPC inverter	35
3.5	Load 1	35

3.6	Load 2	36
3.7	Load 3	36
3.8	Load 4	36
3.9	Load 5	37
3.10	Load 6	37
3.11	Load 7	37
3.12	Load 8	39
3.13	Equivalent circuit of the three level NPC inverter	40
3.14	Two-port switching circuit	41
3.15	NPC equivalent circuit after shortcircuiting the voltage source $\frac{V_t}{2}$	44
3.16	Single-phase converter	46
3.17	Ripple current of the inductor	47
3.18	APOD/POD/PD PWM switching	47
3.19	Balancing filter	49
3.20	NPC inverter with a balancing circuit connected.	49
3.21	The frequency response plot for the RLC balance booster circuit	50
3.22	Effect of the quality factor	52
4.1	Carrier and reference waveform using APOD/POD strategy	55
4.2	Building of mathematical model by stretching triangular carriers	56
4.3	APOD/POD mathematical model for three-level NPC inverter	56
4.4	Harmonics	58
4.5	Harmonics of S_α and S_β derived from theory	61
4.6	APOD/POD mathematical model for three-level NPC inverter	62
4.7	Harmonics of S'_α and S'_β derived from theory	64
4.8	Absolute value of switching function F_1	68
4.9	Absolute value of switching function F_2	68
4.10	Carrier and reference waveform for three-level NPC inverter using PD strategy	69
4.11	Building of mathematical model by stretching triangular carriers	69
4.12	PD mathematical model for three-level NPC inverter	70
4.13	Harmonics of S_α and S_β derived from theory	72
4.14	PD mathematical model for three-level NPC inverter	73
4.15	Harmonics of S'_α and S'_β derived from theory	74
4.16	Absolute value of switching function F_1	78
4.17	Absolute value of switching function F_2	78
5.1	Output voltage for phase A	82
5.2	Output voltage for phase B	82

LIST OF FIGURES

5.3	Output voltage for phase C	82
5.4	Output voltage waveform NPC inverter	82
5.5	Output voltage for phases A, B and C.	84
5.6	Line output voltage waveform	84
5.7	Harmonics for S_α and S_β derived from simulation of practical converter . .	85
5.8	Harmonics for S_α and S_β derived from theory	86
5.9	Harmonics for S'_α and S'_β derived from simulation of practical converter . .	86
5.10	Harmonics for S'_α and S'_β derived from theory	86
5.11	Natural balancing of v_δ using theory	87
5.12	Natural balancing of capacitor voltage difference v_δ using simulation of practical converter	87
5.13	Natural balancing v_δ using simulation of practical converter with a balancing booster	89
5.14	Harmonics for S_α and S_β derived from simulation of practical converter . .	90
5.15	Harmonics of S_α and S_β derived from theory	90
5.16	Harmonics for S'_α and S'_β derived from simulation of practical converter . .	90
5.17	Harmonics of S'_α and S'_β derived from theory	91
5.18	Natural balancing of v_δ using theory	91
5.19	Natural balancing v_δ using simulation of practical converter with a balancing booster	92
5.20	Natural balancing using simulation of practical converter with a balancing booster	93
6.1	Switching vectors of a three-level NPC inverter	95
6.2	Regions of vector modulation of the NPC inverter in the first sector.	97
6.3	Sector I with coordinates for each region	101
6.4	Unfiltered line-to-line output voltage waveform	104
6.5	Unfiltered phase voltage waveform	104
6.6	Switching function of s_α in time domain	104
6.7	Switching function of s_β in time domain	105
6.8	Switching function of s'_α in time domain	105
6.9	Switching function of s'_β in time domain	105
6.10	Switching function of s_α in frequency domain	106
6.11	Switching function of s_β in frequency domain	106
6.12	Switching function of s'_α in frequency domain	106
6.13	Switching function of s'_β in frequency domain	107
6.14	Natural balancing of capacitor voltages of NPC inverter	107
6.15	Natural balancing with balancing booster	107
6.16	Load replaced by sinusoidal current source	108

6.17 Load replaced by sinusoidal current source with balancing circuit connected	109
D.1 Simulation setup for NPC inverter using APOD/POD and PD PWM.	176
D.2 Simulation setup for NPC inverter using vector control.	177

List of Tables

2.1	Switching vectors for two-level inverter	17
4.1	Simulation parameters for S_α and S_β under APOD/POD	61
4.2	Simulation parameters of S'_α and S'_β under APOD/POD	64
4.3	Simulation parameters for F_1 and F_2 under APOD/POD	67
4.4	Simulation parameters for S_α and S_β under PD	71
4.5	Simulation parameters for S'_α and S'_β under PD	74
4.6	Simulation parameters for F_1 and F_2 under PD	77
5.1	Simulation parameters for calculating filter capacitance and inductance . .	81
5.2	Simulation parameters for calculating filter capacitance and inductance . .	83
5.3	Simulation parameters without using balancing circuit under APOD/POD .	85
5.4	Balancing circuit parameters under APOD/POD	88
5.5	Simulation parameters without using balancing circuit under PD	89
5.6	Balancing circuit parameters under PD	92
6.1	Zero switching vectors	96
6.2	Small switching vectors	96
6.3	Medium switching vectors	96
6.4	Large switching vectors	97
6.5	Simulation parameters	103
6.6	Simulation parameters	108

Glossary

Abbreviations

NPC	:	Neutral point clamped converter
APOD	:	Alternative phase opposition disposition
DC	:	Direct current
DSP	:	Digital signal processors
HVDC	:	High voltage direct current
NP	:	Neutral point
PD	:	Phase disposition
POD	:	Phase opposition disposition
PWM	:	Pulsewidth modulation
SVM	:	Space vector modulation

Symbols

A_c	: Current source amplitude
β	: Bandwidth
d	: Duty cycle (in vector control)
D_T	: Duty cycle (in APOD/POD PD PWM)
C	: Capacitance
C_1 and C_2	: DC-bus capacitors (in ABC plane)
C_d	: DC-bus capacitor (in $\alpha\beta$ plane)
D_{a1} and D_{a2}	: Diodes for phase A
D_{b1} and D_{b2}	: Diodes for phase B
D_{c1} and D_{c2}	: Diodes for phase C
E	: Weber function
f_1	: Fundamental frequency
f_c	: Current source frequency
f_s	: Switching frequency
G	: Eigenvalue
Γ	: Gamma function
H	: Transfer function
H_0	: Struve function
i_a , i_b and i_c	: Phase currents
i_α and i_β	: Currents in the $\alpha\beta$ -plane.
i_{NP}	: Neutral point current
J	: Bessel/Anger function
L	: Inductance
m	: Current modulation index
M	: Modulation depth
M_a , M_b , M_c , M_d and M_q	: Current switching functions for medium vectors.
m_a	: Modulation index
m_f	: Frequency modulation ratio
Q	: Quality factor
R	: Resistance
$S0_d$ and $S0_q$: Current switching functions for zero vectors.
$S0_d$ and $S0_q$: Current switching functions for small vectors.

s_a	: Switching function of phase A.
S_{a1}, S_{a2}, S_{a3} and S_{a4}	: Switches for phase A of NPC inverter.
S_{a5}, S_{a6}, S_{a7} and S_{a8}	: Switches for phase A of NPC inverter.
s_b	: Switching function of phase B.
S_{b1}, S_{b2}, S_{b3} and S_{b4}	: Switches for phase B of NPC inverter.
s_c	: Switching function of phase C.
S_{c1}, S_{c2}, S_{c3} and S_{c4}	: Switches for phase C of NPC inverter.
$s_\alpha, s'_\alpha, s_\beta$ and s'_β	: Switching functions in the time domain in the $\alpha\beta$ -plane.
$S_\alpha, S'_\alpha, S_\beta$ and S'_β	: Switching functions in the frequency domain in the $\alpha\beta$ -plane.
t	: Time
T_0, T_7, T'_0 and T'_7	: State times
T_c	: Carrier period
T_{sc}	: Subcycle period
T_x, T_y, T'_x and T'_y	: Active state times
$V_0, V_1, V_2, V_3, V_4, V_5, V_6$ and V_7	: Voltage space vectors
v_0	: Output voltage
v_1	: Capacitor voltage of top DC-bus capacitor C_1 .
v_2	: Capacitor voltage of bottom DC-bus capacitor C_2 .
v_{ab}, v_{bc} and v_{ac}	: Line voltages
v_{an}	: Phase voltage for phase A.
v_{bn}	: Phase voltage for phase B.
v_{cn}	: Phase voltage for phase C.
v_{ca}	: Voltage across the load capacitor for phase A
v_{cb}	: Voltage across the load capacitor for phase B
v_{cc}	: Voltage across the load capacitor for phase C
$v_{c\alpha}$ and $v_{c\beta}$: Voltages across the load capacitors in the $\alpha\beta$ -plane.
v_α and v_β	: Voltages in the $\alpha\beta$ -plane.
$v_{carrier}$: Carrier signal
$v_{control}$: Control signal
v_δ	: DC-bus capacitor voltage difference
v_L	: Voltage across the inductor

\hat{V}_{sin}	: Peak value of the sinusoidal signal
$v_{svm}(\omega t)$: Space vector phase voltage waveform
V_t	: DC-bus voltage
\hat{V}_{tri}	: Amplitude of the triangular signal
v_x and v_y	: Active voltage vectors
v_*	: Reference voltage vector
ω_1	: Fundamental angular frequency
ω_c	: Cutoff frequency
ω_m	: Fundamental angular frequency
ω_s	: Switching angular frequency
Z	: Impedance

Chapter 1

Introduction

This chapter introduces the reader to what motivated the research on the balancing of three-level neutral-point-clamped inverter. We will start with the historical background to multilevel inverters, with an emphasis on recent work done on them, their advantages and their shortcomings. We will then introduce the neutral-point-clamped inverter and its advantages, and focus on the neutral-point voltage balancing problem. We will also give a short description of each chapter of the thesis.

1.1 Historical Overview

When an inverter is applied to an ac motor-drive system, harmonics cause losses and pulsating torques in the motor. From the energy-saving viewpoint, it is necessary to develop a high-efficiency motor-drive system. The multilevel inverter structure was introduced as a means of eliminating the need for the step-up transformer in high-voltage drives and reducing the output waveform harmonic content.

The multilevel inverter topology attempts to address some of the limitations of the standard two level inverter. Motor damage and failure caused by adjustable-speed drives inverters' high-voltage change rates(dv/dt)[14] was overcome by multilevel inverters because their individual devices have a much lower (dv/dt) per switching and they operate at high efficiency because they can switch at a much lower frequency than PWM-controlled inverters.

Increasing the output voltage meant raising the DC-bus voltage which leads to significant problems with voltage sharing among switching devices connected in series during turn-on and turn-off[13],[15], thus limiting the number of devices to a maximum of five. This problem is avoided by employing multilevel inverters because as the DC-bus voltage is raised, the voltage stress on each switching device can be held constant by adding more levels to the inverter. This helps in reducing the harmonics, because the increase in voltage levels leads to improved harmonic performance without increased switching loss

and also reduces the filter size. Multilevel converters are used extensively in high-power applications with medium-voltage levels. Applications include laminators, mills, conveyors, pumps, fans, blowers and compressors[6]. The three most often used topologies for multilevel inverters are:

1. diode-clamped (neutral-point-clamped) initially proposed by Nabae *et al.*[1], which consists of $m-1$ capacitors on the DC-bus, $(m-1)(m-2)$ clamping diodes producing n levels of the phase voltage and one of its application being in distribution system static synchronous compensator[15];
2. capacitor-clamped (flying capacitor)[5],[2], which consists of independent capacitors clamping the device voltage to one capacitor voltage level and having application in high-voltage dc transmission;
3. cascaded multicell with separate DC source[14], which consists of half-bridge inverter units connected in series with application in hybrid electric vehicles.

Other types of multilevel inverters were further discussed by Meynard and Foch[5], who introduced the versatile multilevel commutation cell. This work concentrates on a type of multilevel inverter called the neutral-point-clamped inverter(NPC inverter). Figure 1.1 shows the topology of a three-level neutral-point-clamped inverter.

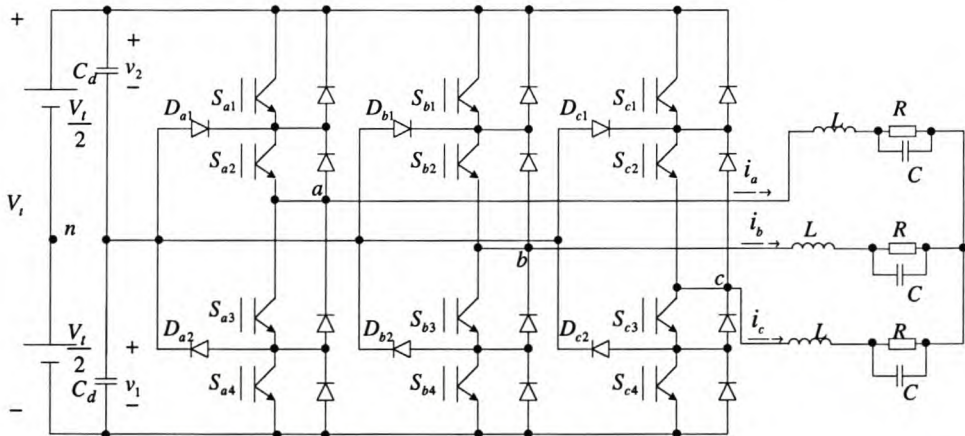


Figure 1.1: Three-level neutral-point-clamped inverter

This topology has appeared in several papers in recent years, including the study of vector control[7][8] and PWM strategies[20]. We have two capacitors that divide the DC-bus voltage in half. Each phase leg consists of a number of switches in series connected via diodes to the tap points, which are connected to the neutral point between the two DC-bus capacitors. The forward voltage across each switch is clamped by the connection

of diodes between the switch and tap points along the string of DC-bus capacitors. The tap points provide clamping voltage levels.

In the case of single-phase, output terminal potential varies between $+V_t/2$ and 0 or $-V_t/2$ and 0 as shown in Figure 1.2 below.

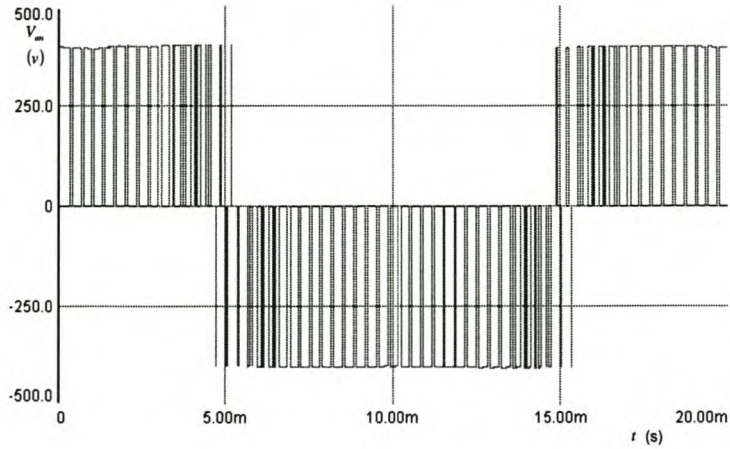


Figure 1.2: Phase output voltage waveform

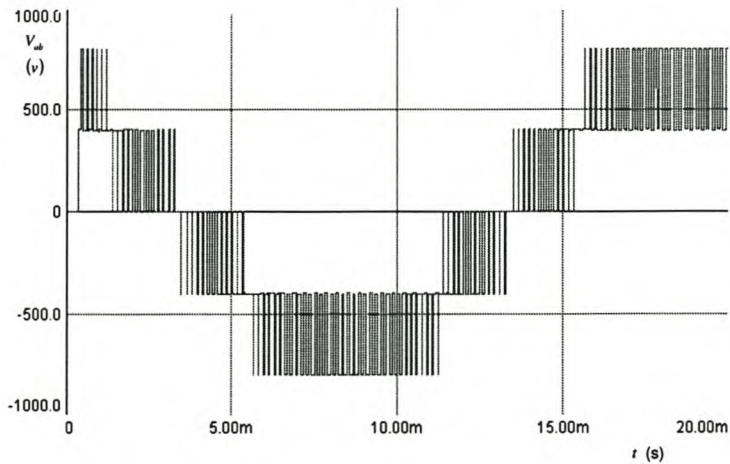


Figure 1.3: Line output voltage waveform

The two voltage sources $V_t/2$ are two capacitors charged at $V_t/2$ each. They are equivalent provided that the average current in each capacitor is zero. Using phase a, for the voltage level $V_t/2$ switches S_{a1} and S_{a2} are switched on; for the voltage level $-V_t/2$ switches S_{a3} and S_{a4} are switched on; and for the 0 level switches S_{a2} and S_{a3} are switched on. The two diodes D_{a1} and D_{a2} clamp the switch voltage to half the level of the DC-bus voltage. The point in the middle of two capacitors C_1 and C_2 is defined as the neutral point. The neutral point is the output phase voltage reference point. Figure 1.2 and

Figure 1.3 show the output voltage waveform of the three-level NPC inverter for single and three phase respectively. The phase voltage is a three-level waveform and the line voltage is a five-level waveform. For Figures 1.2 and 1.3 the DC-bus voltage is 800V.

1.2 Advantages and Applications of the NPC Inverter

The major advantages of the neutral-point-clamped inverter are: 1)improved quality of the output voltage waveform compared with conventional two-level inverters, and 2)higher DC-bus voltage because two switches are connected in series. Though initially intended for use in reduction of current harmonics caused by nonsinusoidal voltage feeding that caused power losses, electromagnetic interferences and pulsating torques in ac motor drives[19], this inverter's applications now include:

1. static var compensation system[15],[11]. This system is the most valuable tool to meet the requirements of VAR management and voltage control. It is used to regulate and stabilise transmission lines and to compensate industrial lagging loads;
2. high-voltage direct-current(HVDC) transmission system[16]. This system features easy powerflow control, stable cable transmission, and economical operation for long-distance transmission;
3. active filtering[16], which is useful for high-quality supply to critical loads in industrial distribution systems.

Other applications include power conditioning systems for superconductive magnetic energy storage[16].

1.3 Disadvantages of NPC Inverter

When the voltage levels increase, the number of diodes required will make the system impractical to implement[2]. Figure 1.4 shows a single-phase five-level diode-clamped inverter. For PWM modulation strategy, the diode reverse recovery of these clamping diodes becomes the major design challenge in high-voltage high-power applications[6]. This voltage source inverter requires a high number of devices compared to the conventional inverter. The complexity of the controller increases if large number of gating signals need to be generated. Imbalance of the capacitor voltages inherent in these inverters may result in over-voltage of one or more of the switches[3]. The balance of the neutral-point

has to be assured[9],[10],[3][16]. The problems associated with the neutral-point voltage of the three-level inverter are[3]:

1. at high modulation indices a low-frequency ripple(at three times the fundamental frequency) occurs on the neutral-point voltage. Although balancing techniques can be used to reduce this voltage, there are still limitations on the maximum amount of reduction;
2. steady-state imbalance in the neutral-point voltage may arise due to a variety of factors including component imperfections, transients and other non-idealities and imbalances.

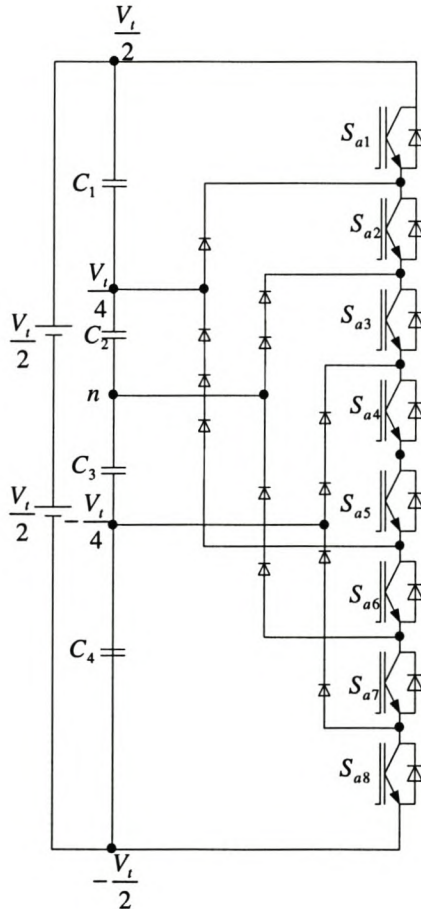


Figure 1.4: Single phase five-level diode-clamped inverter

1.4 Research Objective

The aim of this thesis is to study the neutral-point voltage problem of the three-level NPC inverter, with a focus on the steady-state imbalance. This will be achieved by a systematic and mathematically rigorous study of the natural balancing mechanism of the three-phase NPC converter. This will in turn be done through mathematical analysis and simulations of practical converters. The main conclusions will be based on the following equation[3]:

$$\begin{aligned} \frac{v_\delta}{V_t} &= \frac{\int_{-\infty}^{\infty} \left(\frac{S_\alpha(u)\bar{S}_\alpha(u)}{Z(u)} + \frac{S_\beta(u)\bar{S}_\beta(u)}{Z(u)} \right) du}{\int_{-\infty}^{\infty} \left(\frac{S'_\alpha(u)\bar{S}'_\alpha(u)}{Z(u)} + \frac{S'_\beta(u)\bar{S}'_\beta(u)}{Z(u)} \right) du} \\ &= \frac{\int_{-\infty}^{\infty} \frac{F_1(u)}{Z(u)} du}{\int_{-\infty}^{\infty} \frac{F_2(u)}{Z(u)} du} \end{aligned}$$

where

$$F_1(u) = S_\alpha(u)\bar{S}'_\alpha(u) + S_\beta(u)\bar{S}'_\beta(u)$$

$$F_2(u) = |S'_\alpha(u)|^2 + |S'_\beta(u)|^2$$

(NB: \bar{z} denotes the complex conjugate of z .)

V_t is the DC supply voltage and v_δ is the voltage difference $v_1 - v_2$ of the two capacitors C_1 and C_2 . $F_1(u)$ and $F_2(u)$ depend on the harmonic spectra of the switching functions as well as the load impedance. The exact meaning of these quantities will become clear later in the thesis.

To achieve this objective, the thesis includes the following chapters:

1. Introduction, which introduces the reader to what motivated the research on the balancing of the DC-bus capacitor voltages of the three-level neutral-point-clamped inverter;
2. Background, which reviews the literature that is necessary for understanding methods and strategies used in this thesis;
3. Balancing theory, which develops further the theory that studies the balancing problem of the DC-bus capacitor voltages of the NPC inverter;
4. Spectra of the switching functions, which analyses the switching functions of the NPC inverter under alternative phase opposition disposition(APOD), phase opposition disposition(POD) and phase disposition(PD) PWM strategies in order to prove the natural balancing of DC-bus capacitor voltages;

5. Simulations, which gives the simulation results derived from both the theoretical results and from the practical converter and verify the theoretical results obtained;
6. Simulations of NPC inverter under vector control, which discusses simulations for natural balancing of the three-level NPC PWM inverter under vector control;
7. Conclusion, which summarises the work done in this thesis and indicates further research opportunities in natural balancing.

Chapter 2

Background

In this chapter we review the literature that is necessary for understanding the methods and strategies used in this thesis. Two modulation strategies, PWM and vector modulation, are discussed since, given time, both of them can be used for harmonic analysis. We also briefly discuss some of the strategies used by other authors to give the reader an insight into what has been done.

2.1 PWM Modulation

A pulse-width-modulated(PWM) switching scheme in inverter circuits requires the output to be sinusoidal with controllable magnitude and frequency[4]. For this to be achieved a sinusoidal control signal at the desired frequency is compared with the triangular carrier waveform to determine how each phase leg should switch. In most PWM strategies a sinusoidal low-frequency fundamental reference waveform is compared to a high-frequency carrier waveform, where the carrier waveform is either triangular, sawtooth or trapezoidal. The PWM switching scheme can be obtained by either using natural sampling or regular sampling. The two sampling methods are discussed in the subsections 2.1.1 and 2.1.2. The inverter switching frequency is established by the frequency of the triangular waveform and kept constant at $\pm 5\text{kHz}$. The control/modulating signal is used to modulate the switch duty ratio and has the fundamental/modulation frequency($\pm 50\text{Hz}$) of the inverter output voltage. In the case of a half-bridge inverter, the output voltage(v_{A0}) fluctuates between $\frac{V_t}{2}$ and $-\frac{V_t}{2}$. When $v_{control} > v_{carrier}$ we have $v_{A0} = \frac{V_t}{2}$ and when $v_{control} < v_{carrier}$ we have $v_{A0} = -\frac{V_t}{2}$. Figure 2.1(a) shows the carrier waveform and the control/modulating waveform, whilst Figure 2.1(b) shows the output voltage waveform with the control/modulating waveform using natural sampling.

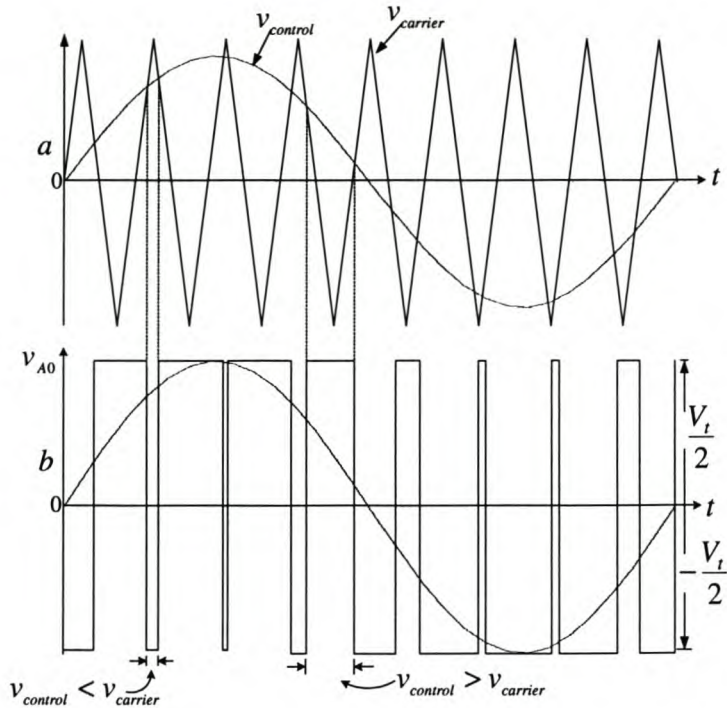


Figure 2.1: Pulse-width modulation

2.1.1 Natural Sampling

In natural sampling a triangular carrier, or sweep wave, is compared directly to a sinusoidal modulating wave[21][23] to determine the switching instants and therefore the resultant pulse widths. This is done by ascertaining the value of the sample during the intervals between those in time at which the two signals are equal in value. Therefore natural sampling can be defined as a process of intrinsic natural selection of the sampling points, when the time of sampling coincides with the time of appearance of the width-modulated pulse.

The modulating wave thus varies while the sampling process is taking place, resulting in the width of the pulse being proportional to the amplitude of the modulating wave at the instant that switching occurs. The edges of the pulses are generated by the crossing points of these two signals and the width of the pulse is proportional to the area under the sine wave, and approximately proportional to the average amplitude of the sine wave between the crossing points.

In the case of a three-phase system[22] there are two ways in which this natural sampling can be carried out. Both methods need three 120° phase-shifted reference sinusoids. In the first method a single carrier signal can be used to compare with the three different reference sinusoids(single-phase modulation) as shown in Figure 2.2. In the second method three different carrier signals with 120° phase displacements among themselves may be

used, one for each reference sinusoid (three-phase modulation) as shown in Figure 2.3. A natural-sampled PWM is shown in Figure 2.4.

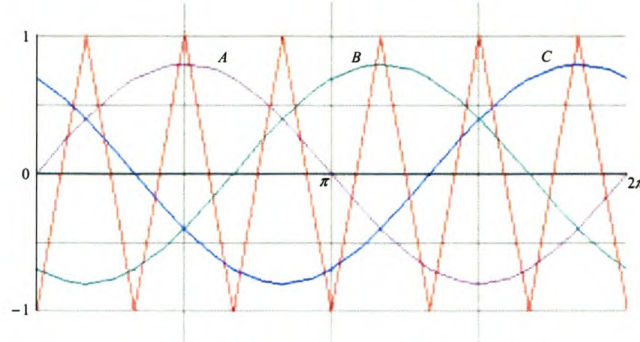


Figure 2.2: Single-phase modulation

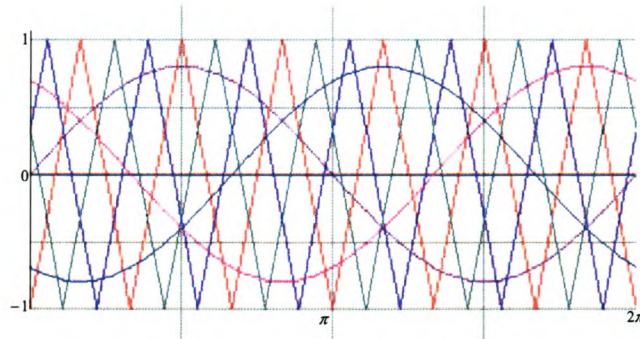


Figure 2.3: Three-phase modulation

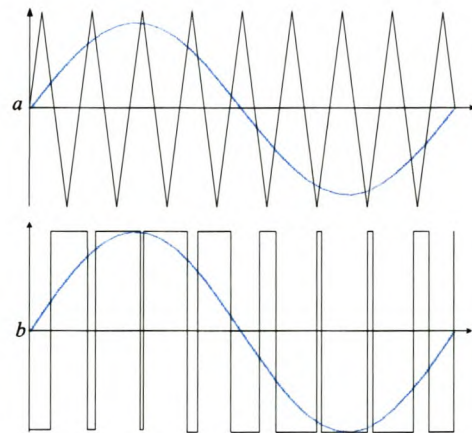


Figure 2.4: Natural-sampled PWM

2.1.2 Regular Sampling

Regular sampled PWM can be either symmetrical, where the reference sinusoidal waveform is kept constant for the entire carrier interval, or assymmetrical, where the reference sinusoidal waveform is resampled midway through the carrier interval. Figure 2.5 shows the switching functions of the regular sampled waveform using two regular sampling methods.

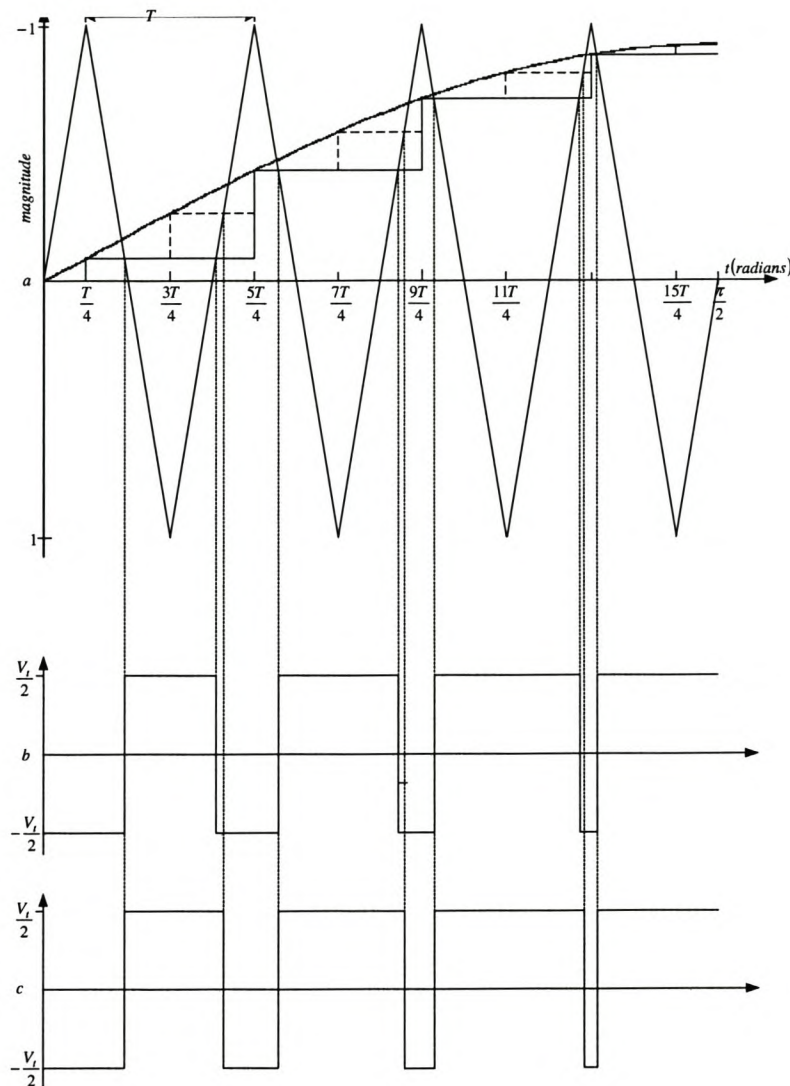


Figure 2.5: a) Regular sampling b) Symmetrical c) Assymetrical

2.1.3 Method of Analysis

In general no rational relationship exists between the modulating frequency and the carrier frequency and hence a single Fourier series approach is evidently inapplicable, since the PWM waveform will not be periodic. Bennet represented the duration-modulated pulses by the three-dimensional geometrical configuration [17], which was later modified by Bowes [18]. Natural sampling is assumed and the modulating wave is a single sinusoid represented by $A_m \cos \omega_m t$. The walls, which are parallel with and identical to each other, rest upon a flat surface referred to as the XOY plane and the positions they occupied are indicated by the shaded areas. The walls are of the same height, their tops are flat and their sides are perpendicular to the XOY plane.

There is one wall for every 2π units of length along the x-axis and one complete cycle of $Q \cos y$ for every 2π units of length in the y-direction. Now suppose the plane

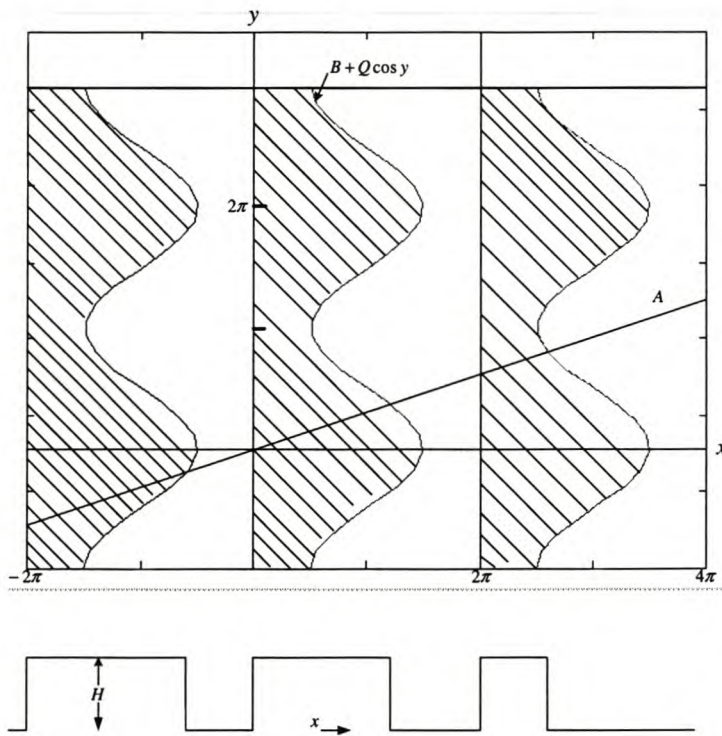


Figure 2.6: Model for double Fourier series

perpendicular to the XOY surface including the origin is passed through the walls along the line OA in the figure. Then the intersection of this plane with the walls is projected upon a second plane perpendicular to the XOY surface including the x-axis; the resulting curve will have the shape shown at the bottom of the figure, where H represents the height of the walls. Representing a given train of duration-modulated pulses by the configuration of Figure 2.6, x and y must be related to time as follows:

$$x = \omega_c t$$

and

$$y = \omega_m t$$

where ω_c is the carrier frequency(frequency of the triangular waveform/switching frequency) and ω_m is the modulating frequency/fundamental frequency. These relationships have the significance that for each value of time a point is specified in the XOY plane. The locus of all such points represents a straight line passing through the origin of slope ω_m/ω_c corresponding to line OA in Figure 2.6. If the plane in the configuration of Figure 2.6 is sectioned into elementary squares with edges 2π units long, then the portions of the walls within the different squares are identical, and thus the wall configuration is periodic in both the x and y axes. Hence this suggests that the height of the configuration can be expressed as a function of x and y by means of a double Fourier series designated by $F(x, y)$ [17]. One Fourier series represents the configuration of the model in the x direction and a second Fourier series represents the model configuration in the y direction. Combining these two Fourier series provides a double Fourier series which can be represented as follows:

$$\begin{aligned} F(x, y) = & \frac{1}{2}A_{00} + \sum_{n=1}^{\infty} (A_{0n}\cos ny + B_{0n}\sin ny) + \sum_{m=1}^{\infty} (A_{m0}\cos mx + B_{m0}\sin mx) \\ & + \sum_{m=1}^{\infty} \sum_{n=\pm 1}^{\pm \infty} (A_{mn}\cos(mx + ny) + B_{mn}\sin(mx + ny)) \end{aligned}$$

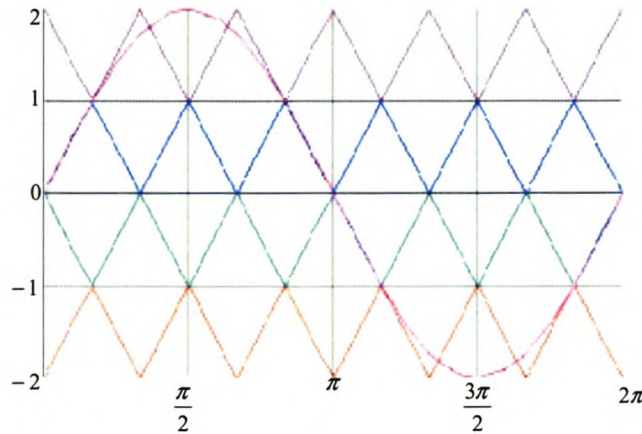
The Fourier coefficients are represented by

$$A_{mn} + jB_{mn} = \frac{1}{2\pi^2} \int_0^{2\pi} \int_0^{2\pi} F(x, y) e^{j(mx+ny)} dx dy$$

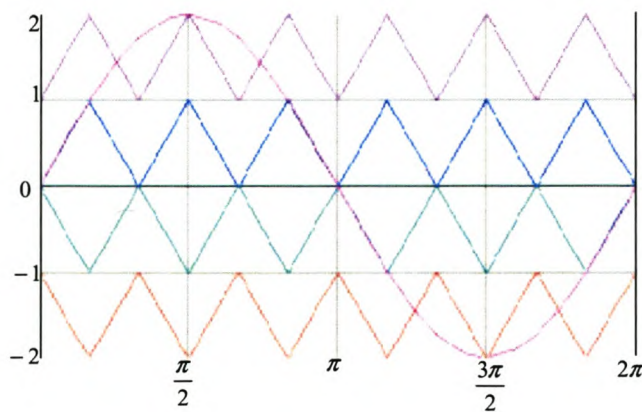
2.1.4 PWM Technique

The technique we discuss in this subsection was first developed by Carrara *et al*[19] and later modified by McGrath and Holmes[20]. In the case of an NPC inverter with N levels (where N is odd and more than 2), N-1 triangular carriers with the same frequency and amplitude are arranged so that they fully occupy contiguous bands in the range of $+V_t$ and $-V_t$. Then a sinusoidal reference centred in the middle of the carrier set is compared with each carrier to determine the voltage level that the converter should switch to. For a three-phase system, we need three 120° phase-shifted modulating sinusoids. Three alternative PWM strategies with differing phase relationships between the carriers are considered:

1. Alternative phase opposition disposition(APOD), where each carrier is phase shifted by 180° from its adjacent carriers as shown in Figure 2.7;

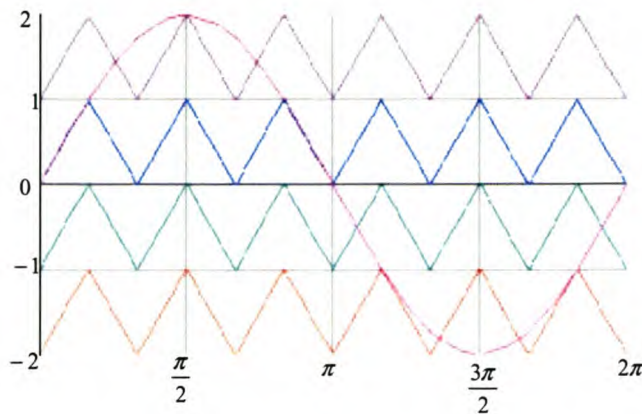
**Figure 2.7:** APOD system

2. Phase opposition disposition(POD), where the carriers above the reference zero point are out of phase with those below the zero point by 180° as shown in Figure 2.8;

**Figure 2.8:** POD system

3. Phase disposition(PD) where all carriers are in phase as shown in Figure 2.9.

In the case of three-level converters the APOD and POD strategies are equivalent. To build a mathematical model of the modulation process, we stretch the carrier turning it over at each corner, obtaining a ramp. Then the modulating signal is turned over together with the carrier.

**Figure 2.9:** *PD system*

2.2 Vector Modulation

Pulsewidth modulation is one of the cornerstones of power electronics and much work has investigated the harmonics that are inevitably produced as part of the modulation process, with a view of minimising the low order harmonics to reduce their impact on the converter load since higher frequency harmonics are more easily filtered [23]. Three-phase sinusoidal pulsewidth modulation and space vector pulsewidth modulation are mostly used techniques for pulsewidth modulation of three-phase converters. Space vector pulsewidth modulation has the advantage of lower inverter output voltage and current harmonics and a possible higher modulation index compared with the sinusoidal pulsewidth modulation [26]. Vector control techniques have made possible the application of induction motors for high performance applications where traditionally only dc drives were applied. The disadvantages of the space vector pulsewidth modulation include the difficulty of calculating the harmonic spectra [24].

In this section we study space vector modulation of a two-level three-phase inverter. We start by derivation of voltage vectors from switching states. We then derive and plot the space vector phase voltage waveform equation. From the space vector waveform we obtain the switching functions using asymmetric regular sampling. We then use the construction of three-dimensional geometrical models discovered by Bennett to construct a wall model for space vector modulation. This model is then used to express the harmonic spectrum of the general space vector modulation signal as a double Fourier series. This section serve as a basis for the work that can be done for the analysis of the switching spectra for a three-level three-phase NPC inverter under vector control as an alternative to the theory developed in Chapter 4.

2.2.1 Generation of space vector modulation

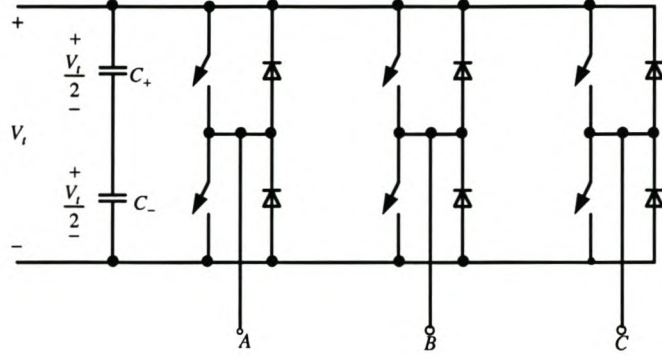


Figure 2.10: Two-level three-phase inverter

Space vector modulation has notable features such as easy digital implementation and a wide linear modulation range for output line-to-line voltages[31]. Figure 2.10 shows a two-level three-phase inverter. For a two-level three-phase inverter there are eight switching states which compose the output voltage. Figure 2.11 shows voltage space

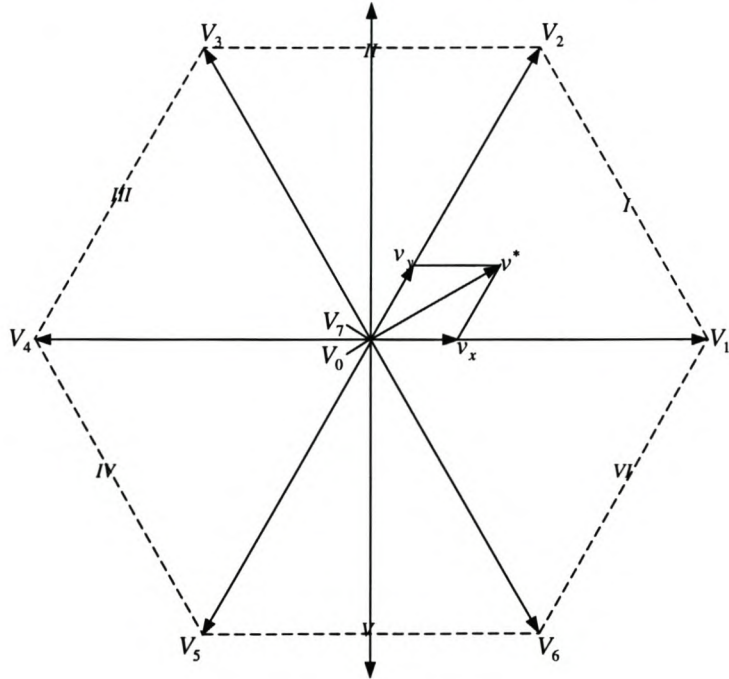


Figure 2.11: Voltage space vector

vectors of a two-level three-phase voltage source inverter which is divided into six sectors. The active vectors $V_1 - V_6$ are equal in magnitude and are mutually phase displaced by

$\pi/3$ such that[24]:

$$V_k = \frac{2}{3} V_t \exp\left(j \frac{k-1}{3}\pi\right)$$

$$k = 1, \dots, 6$$

where V_t is the DC-bus voltage.

Vectors	Switching states
V_0	111
V_7	-1-1-1
V_1	1-1-1
V_2	11-1
V_3	-11-1
V_4	-111
V_5	-1-11
V_6	1-11

Table 2.1: Switching vectors for two-level inverter

Table 2.1 shows the vectors and the switching states for two-level inverters. Any desired voltage vector v^* within the hexagonal limit of Figure 2.11 may be synthesised by decomposing it into components which lie along the active voltage vectors as follows for sector I:

$$v^* = v_x + v_y = \frac{T_x}{T_{sc}} V_1 + \frac{T_y}{T_{sc}} V_2$$

where T_{sc} is the subcycle period and T_x and T_y are the active state times. The reference voltage vector is given by

$$v^* = M \frac{V_t}{2} \exp(j\omega_m t)$$

where M is the modulation depth with a maximum value of 1.15 and ω_m is the desired fundamental angular frequency. Solving this equation we obtain the following:

$$\frac{3}{2} \frac{T_{sc}M}{2} \exp(j\omega_m t) = T_x \exp(0) + T_y \exp(j\frac{\pi}{3})$$

$$\frac{3}{4} T_{sc}M (\cos\omega_m t + j\sin\omega_m t) = T_x + T_y \left(\frac{1}{2} + j\frac{\sqrt{3}}{2}\right)$$

$$\frac{\frac{3}{4}T_{sc}M \left(\cos(\omega_m t + \frac{\pi}{6}) + \sin \omega_m t \sin \frac{\pi}{6} \right)}{\frac{\sqrt{3}}{2}} + \frac{3}{4}T_{sc}M j \sin \omega_m t = T_x + T_y \left(\frac{1}{2} + j \frac{\sqrt{3}}{2} \right)$$

$$\frac{1}{2}T_y + T_x = \frac{\sqrt{3}}{2}T_{sc}M \cos(\omega_m t + \frac{\pi}{6}) + \frac{\sqrt{3}}{2}T_{sc}M \sin \omega_m t \sin \frac{\pi}{6}$$

$$T_x = \frac{\sqrt{3}T_{sc}M}{2} \cos(\omega_m t + \frac{\pi}{6})$$

$$T_y = \frac{\sqrt{3}T_{sc}M}{2} \sin(\omega_m t)$$

The same procedure is followed to derive the state times for operation in each of the other five sectors. The remainder of the subcycle period is divided equally between the zero vectors such that:

$$T_0 = T_7 = \frac{1}{2} (T_{sc} - T_x - T_y)$$

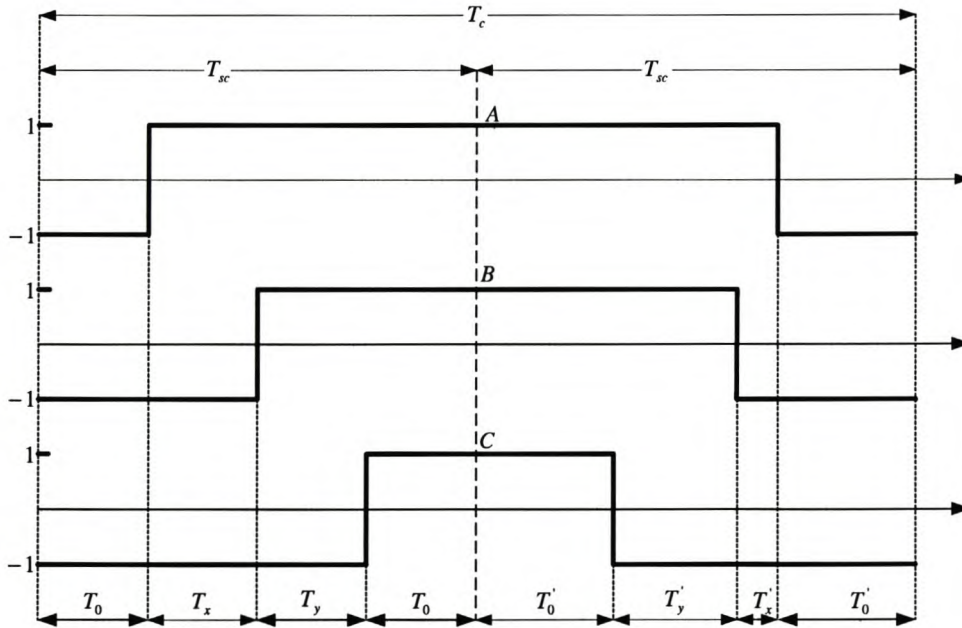


Figure 2.12: Asymmetrical space vector pulse pattern

The generation of the inverter-switching signals over two subcycle periods is depicted in Figure 2.12 . These are the switching functions for phases A, B and C. The voltage vector sequence is reversed in alternate subcycles and this modulation scheme is termed asymmetrical regularly sampled space vector modulation(SVM). For phase A we have:

For $0 \leq \omega_m t \leq \frac{\pi}{3}$

$$T_x = \frac{\sqrt{3}T_{sc}M}{2} \cos(\omega_m t + \frac{\pi}{6})$$

$$T_y = \frac{\sqrt{3}T_{sc}M}{2} \sin(\omega_m t)$$

Now we introduce a new variable $v_{svm}(\omega_m t)$, which is the space vector phase voltage waveform for phase A.

$$\begin{aligned} v_{svm}(\omega_m t) &= \frac{1}{T_{sc}} ((-T_0) + T_x + T_y + (+T_0)) \\ &= \frac{T_x}{T_{sc}} + \frac{T_y}{T_{sc}} \\ &= \frac{\sqrt{3}}{2} M \left(\cos\left(\omega_m t + \frac{\pi}{6}\right) + \cos\left(\omega_m t - \frac{\pi}{2}\right) \right) \\ &= \cos(\omega_m t) \cos \frac{\pi}{6} - \sin(\omega_m t) \sin \frac{\pi}{6} + \cos(\omega_m t) \cos \frac{\pi}{2} + \sin(\omega_m t) \sin \frac{\pi}{2} \\ &\quad + \left[\sin \omega_m t \sin \frac{\pi}{6} - \sin \omega_m t \sin \frac{\pi}{6} \right] \\ &= \cos\left(\omega_m t - \frac{\pi}{6}\right) \end{aligned}$$

For $\frac{\pi}{3} \leq \omega_m t \leq \frac{\pi}{2}$

$$\frac{3}{4}T_{sc}M \exp(j\omega_m t) = T_y \exp(j\frac{\pi}{3}) + T_x \exp(j\frac{\pi}{2})$$

$$T_y = \frac{3}{2}T_{sc}M \cos \omega_m t$$

$$T_x = \frac{3}{2}T_{sc}M \left(\sin\left(\omega_m t - \frac{\pi}{3}\right) \right)$$

Figure 2.13 shows the phase-A switching function obtained by comparing v_{svm} with a triangular carrier of amplitude 1 and frequency 300 Hz.

$$\begin{aligned} v_{svm}(\omega_m t) &= \frac{1}{T_{sc}} ((-T_0) + T_y + ((0)T_x) + (+T_0)) \\ &= \frac{1}{T_{sc}} \frac{3}{2}T_{sc}M \cos(\omega_m t) \\ &= \frac{3}{2}M \cos(\omega_m t) \\ &= \frac{\sqrt{3}}{2}M \left(\sqrt{3} \cos(\omega_m t) \right) \end{aligned}$$

Hence

$$v_{svm}(\omega_m t) = \frac{\sqrt{3}M}{2} \begin{cases} \cos\left(\omega_m t - \frac{\pi}{6}\right) & 0 \leq \omega_m t \leq \frac{\pi}{3} \\ \sqrt{3} \cos(\omega_m t) & \frac{\pi}{3} \leq \omega_m t \leq \frac{\pi}{2} \end{cases} \quad (2.1)$$

To define the remainder of the waveform half- and quarter-wave symmetry are used. The process described above requires for each subcycle the computation of new state times.

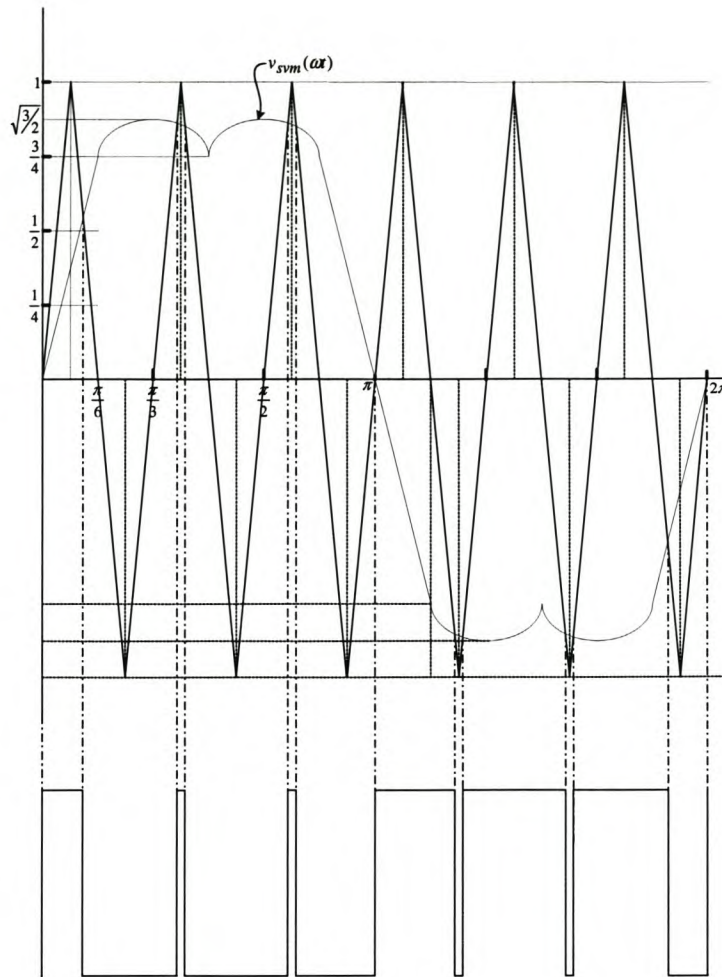


Figure 2.13: Phase A switching functions obtained from space vector waveform

For the symmetrical regular sampled modulation technique, the state sequence of the first subcycle is simply reversed with the same state times so that $T'_x = T_x$, $T'_y = T_y$ and $T'_0 = T_0$. This technique results in inverter-switching signals which exhibit symmetry about the midpoint of the carrier period T_c .

2.2.2 Method of analysis

Space vector modulation waveforms can be regarded as the sum of a desired fundamental sinewave component and an essentially triangular third harmonic waveform shown in Figure 2.14, which is half the magnitude of the triangle waveform formed by the zero-crossing segments of the three phase sinewaves[25] shown in Figure 2.15.

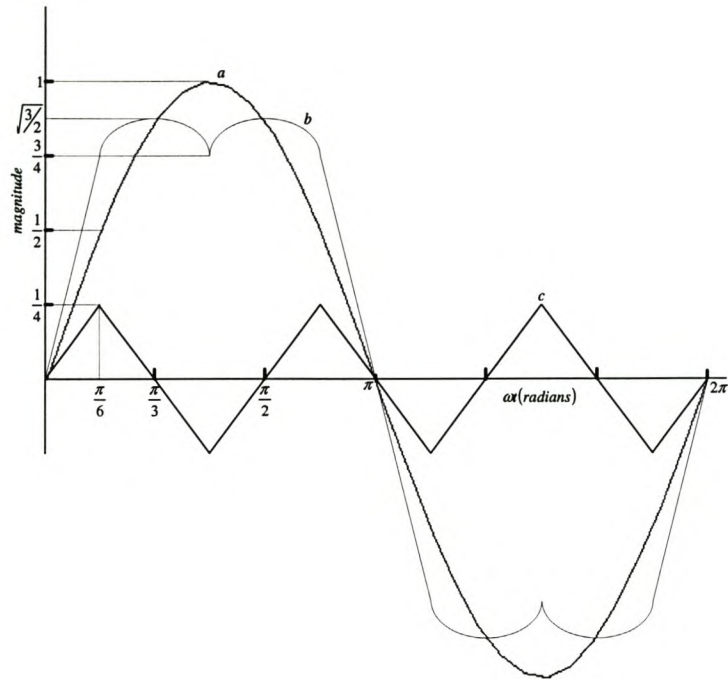


Figure 2.14: a) Fundamental sinusoid, b) Space vector phase voltage ($b = a + c$) and c) Third harmonic triangle wave distortion

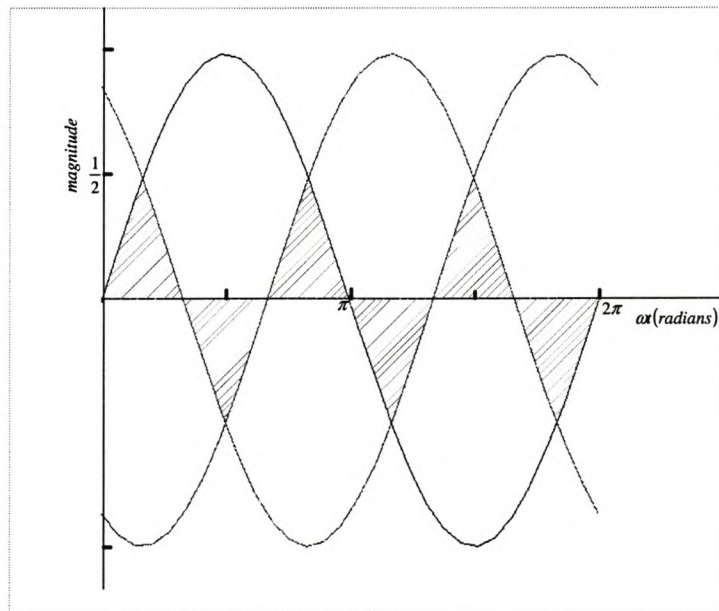


Figure 2.15: Zero crossings of three-phase sinusoids

Using the construction of three-dimensional geometrical models discovered by Bennett[27] and further expanded by Black[17] and Bowes[18][21] for analysis of asynchronous sinusoidal modulation schemes, Figure 2.16 below is constructed.

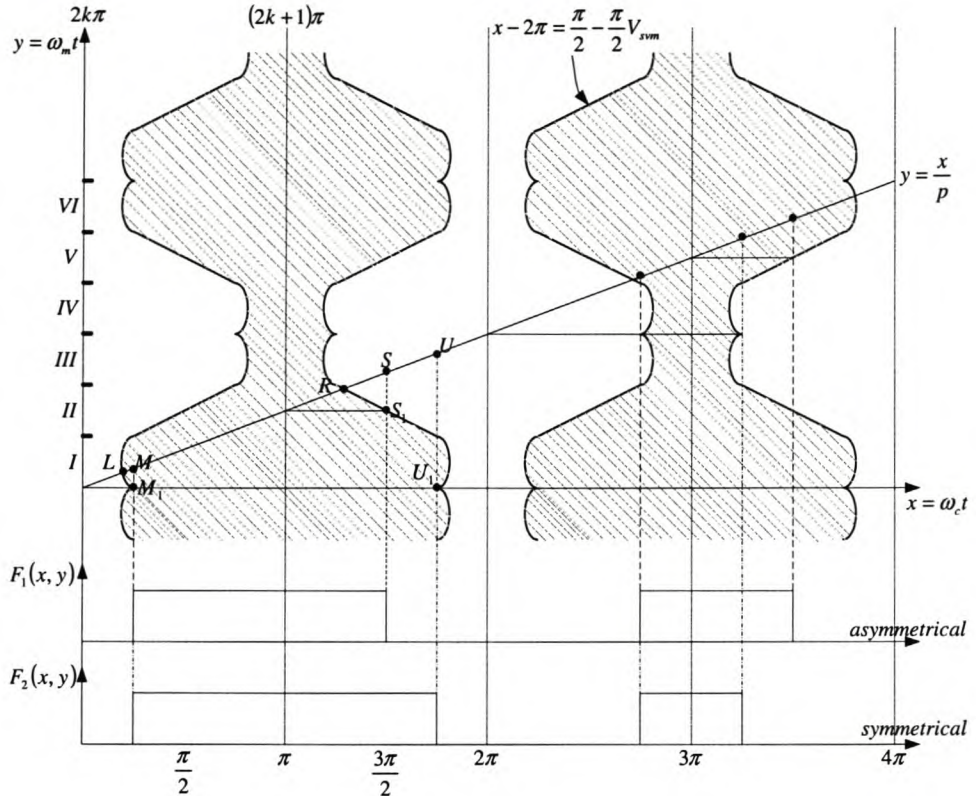


Figure 2.16: Wall model for space vector modulation

The figure shows regions I to VI along the y-axis corresponding to the six setors of operation shown in Figure 2.16, and the walls in the figure follow the characteristic SVM modulating function of equation 2.1. Using natural sampling the walls may be described by

$$x - 2k\pi = \frac{\pi}{2} - \frac{\pi}{2}v_{svm}(y)$$

for the wall between $2k\pi$ and $2k\pi + 1$, and

$$x - 2k\pi = \frac{3\pi}{2} + \frac{\pi}{2}v_{svm}(y) \quad (2.2)$$

for the wall between $2k\pi + 1$ and $2k\pi$, for all integer $k \in [-\infty, +\infty]$ so that the wall model is valid only for continuous modulation. The points of intersection for this natural sampling process are L and R. For asymetrical regular sampling, the points of intersection are M and S and the resulting pulsewidth-modulation signal is $F_2(x, y)$. The intersections for symmetrical regular sampling are M and U and the PWM signal is $F_2(x, y)$ which exhibits the expected symmetry about the midpoint of the carrier period. For symmetrical regular sampling the walls may be described by

$$x_M = x_{M_1} = 2k\pi + \frac{\pi}{2} - \frac{\pi}{2}v_{svm}(y_{M_1})$$

$$x_U = x_{U_1} = 2k\pi + \frac{3\pi}{2} + \frac{\pi}{2}v_{svm}(y_{U_1})$$

$$y_{M_1} = y_M - [x_{M_1} - 2k\pi] \frac{\omega_m}{\omega_c}$$

$$y_{U_1} = y_U - [x_{U_1} - 2k\pi] \frac{\omega_m}{\omega_c}$$

$$x_M = 2k\pi + \frac{\pi}{2} - \frac{\pi}{2}v_{svm}\left(y_M - [x_M - 2k\pi] \frac{1}{p}\right)$$

$$x_U = 2k\pi + \frac{3\pi}{2} + \frac{\pi}{2}v_{svm}\left(y_U - [x_U - 2k\pi] \frac{1}{p}\right)$$

$$x = \frac{\pi}{2} - \frac{\pi}{2}v_{svm}\left(y - \frac{x}{p}\right)$$

$$x = \frac{3\pi}{2} + \frac{\pi}{2}v_{svm}\left(y - \frac{x}{p}\right)$$

and for asymmetrical regular sampling by

$$x_M = 2k\pi + \frac{\pi}{2} - \frac{\pi}{2}v_{svm}(y_{M_1})$$

$$x_S = 2k\pi + \frac{3\pi}{2} + \frac{\pi}{2}v_{svm}(y_{S_1})$$

$$y_{M_1} = y_M - [x_{M_1} - 2k\pi] \frac{\omega_m}{\omega_c}$$

$$y_{S_1} = y_U - [x_{U_1} - (2k+1)\pi] \frac{\omega_m}{\omega_c}$$

$$x_M = 2k\pi + \frac{\pi}{2} - \frac{\pi}{2}v_{svm}\left(y_M - [x_{M_1} - 2k\pi] \frac{1}{p}\right)$$

$$x_S = 2k\pi + \frac{3\pi}{2} + \frac{\pi}{2}v_{svm}\left(y_S - [x_S - 2k\pi] \frac{1}{p}\right) + \frac{\pi}{2}$$

$$x = \frac{\pi}{2} - \frac{\pi}{2}v_{svm}\left(y - \frac{x}{p}\right)$$

$$x = \frac{3\pi}{2} + \frac{\pi}{2}v_{svm}\left(y - \frac{x}{p} + \frac{\pi}{p}\right)$$

That is

$$x - 2k\pi = \frac{\pi}{2} - \frac{\pi}{2}v_{svm}\left(y - \frac{x}{p}\right)$$

$$x - 2k\pi = \frac{3\pi}{2} + \frac{\pi}{2}v_{svm} \left(y - \frac{x}{p} + \frac{\pi}{p} \right) \quad (2.3)$$

where $p = \frac{\omega_c}{\omega_m}$, $\delta = 0$ for symmetrical regular sampling and $\delta = 1$ for asymmetrical regular sampling.

The harmonic spectrum of the general SVM signal $F(x, y)$ may be expressed as a double Fourier series:

$$\begin{aligned} F(x, y) = & \frac{1}{2}A_{00} + \sum_{n=1}^{\infty} (A_{0n} \cos ny + B_{0n} \sin ny) + \sum_{m=1}^{\infty} (A_{m0} \cos mx + B_{m0} \sin mx) \\ & + \sum_{m=1}^{\infty} \sum_{n=\pm 1}^{\pm \infty} (A_{mn} \cos(mx + ny) + B_{mn} \sin(mx + ny)) \end{aligned} \quad (2.4)$$

The Fourier coefficients are represented by

$$A_{mn} + jB_{mn} = \frac{1}{2\pi^2} \int_0^{2\pi} \int_0^{2\pi} F(x, y) e^{j(mx+ny)} dx dy$$

where m and n are indices on the carrier and modulating frequencies respectively.

$F(x, y)$ assumes a value $2E$ inside the walls defined by equation 2.3 and a zero outside this region.

We now apply the variable transformation $(x, y) \rightarrow (x, y - \frac{x}{p})$. Let:

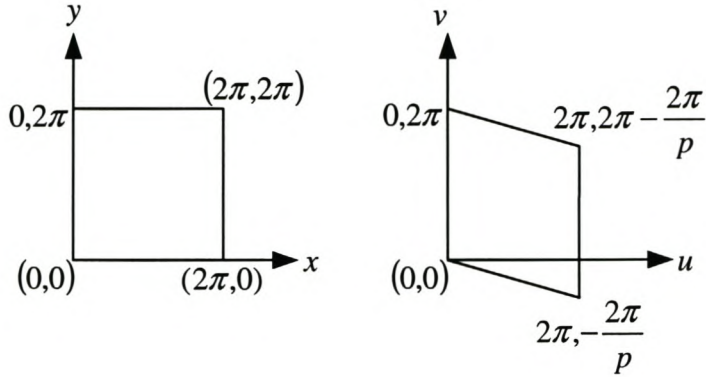
$$u = x$$

$$v = y - \frac{x}{p}$$

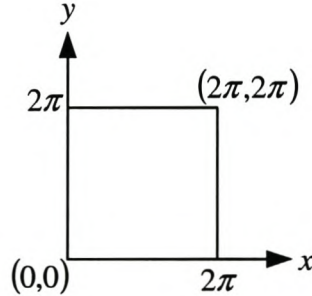
Then the Jacobian transformation J is given by

$$\begin{aligned} J(u, v) &= \begin{vmatrix} \frac{\delta x}{\delta u} & \frac{\delta x}{\delta v} \\ \frac{\delta y}{\delta u} & \frac{\delta y}{\delta v} \end{vmatrix} \\ &= \begin{vmatrix} 1 & 0 \\ -\frac{1}{p} & 1 \end{vmatrix} \\ &= 1 \end{aligned}$$

Region of integration is transformed in the following way:



Because $F(u,v)$ is periodic in u and v , the second region can be replaced by the following square:



Furthermore:

$$\begin{aligned} \frac{\pi}{2} - \frac{\pi}{2}v_{svm}(y - \frac{x}{p}) &= \frac{\pi}{2} - \frac{\pi}{2}v_{svm}(v) \\ \frac{3\pi}{2} + \frac{\pi}{2}v_{svm}(y - \frac{x}{p} + \frac{\delta\pi}{p}) &= \frac{3\pi}{2} + \frac{\pi}{2}v_{svm}(v + \frac{\delta\pi}{p}) \end{aligned}$$

Hence

$$K_{mn} = \frac{2E}{2\pi^2} \int_0^{2\pi} \int_{\frac{\pi}{2} - \frac{\pi}{2}v_{svm}(v)}^{\frac{3\pi}{2} + \frac{\pi}{2}v_{svm}(v + \frac{\delta\pi}{p})} e^{j(mu + n(v + \frac{u}{p}))} du dv$$

But

$$e^{j(mu + nv + n\frac{u}{p})} = e^{jnv} e^{jqu}$$

where $q = mp + n$.

Thus the general harmonic amplitude for both symmetrical and asymmetrical sampling becomes

$$K_{mn} = \frac{E}{\pi^2} \int_0^{2\pi} e^{jny} \int_{\frac{\pi}{2} - \frac{\pi}{2}v_{svm}(y)}^{\frac{3\pi}{2} + \frac{\pi}{2}v_{svm}(y + \frac{\delta\pi}{p})} \exp\left\{j\frac{q}{p}x\right\} dx dy$$

where $q = mp + n$ is the harmonic order.

2.3 Strategies used by some authors

In this section we give a short overview of the strategies used by some authors for solving the voltage balancing problem associated with the neutral point of the three-level three-phase NPC inverter.

2.3.1 Avoid the narrow pulse problem

This strategy was proposed by Lee *et al*[10]. They present a PWM method based on the space voltage vectors. They claim that this method solves the voltage imbalance problem and avoids the narrow pulse which is shorter than the minimum on/off time of the gate turn-off thyristors.

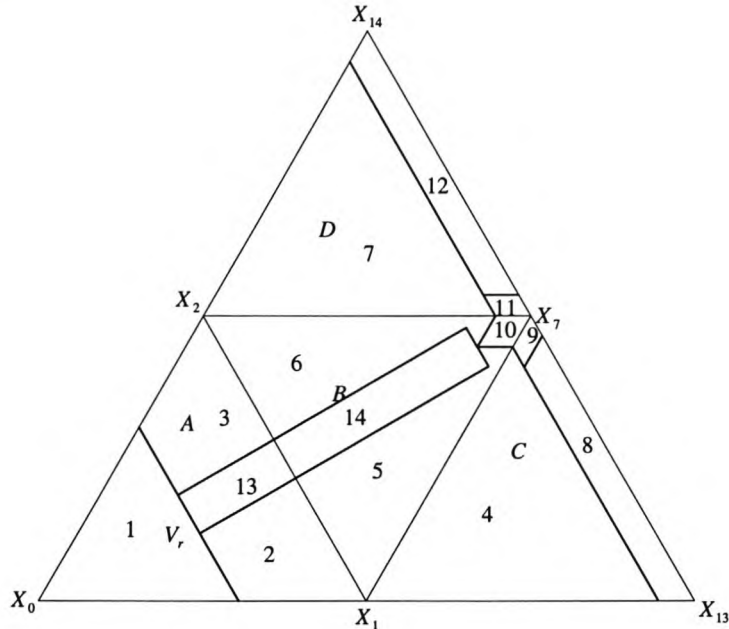


Figure 2.17: 14 regions for the minimum on/off time and the dc-link voltage balancing.

The causes of the narrow pulses are the duration of the voltage vector and the output sequence of the voltage vectors. To solve this problem they utilised the fact that the zero voltage vector has three switching states and the small voltage vector has two switching states. Alternatively they used the dominant voltage vector in each region and divided the dominant vector that is longer than the minimum on/off time into parts equal to the minimum on/off time. Figure 2.17 shows the 14 regions formed from the four regions of the first sector of the switching states. The voltage imbalance in regions 1, 4, 7, 8, 9, 10, 11 and 12 can be solved since the difference between the duration of the upper small voltage vectors and the lower small voltage vectors can be naturally compensated.

For regions 2, 3, 5, 6, 13 and 14 time compensation method is used to solve the voltage balancing problem.

2.3.2 Model in DQ coordinate frame utilising current switching functions

In this method the authors[16] discuss the neutral-point control using vector modulation. They utilise four regions A, B, C and D as shown in Figure 2.18 to develop the mathematical formulation of the NP balancing problem. The regions that are advantageous for

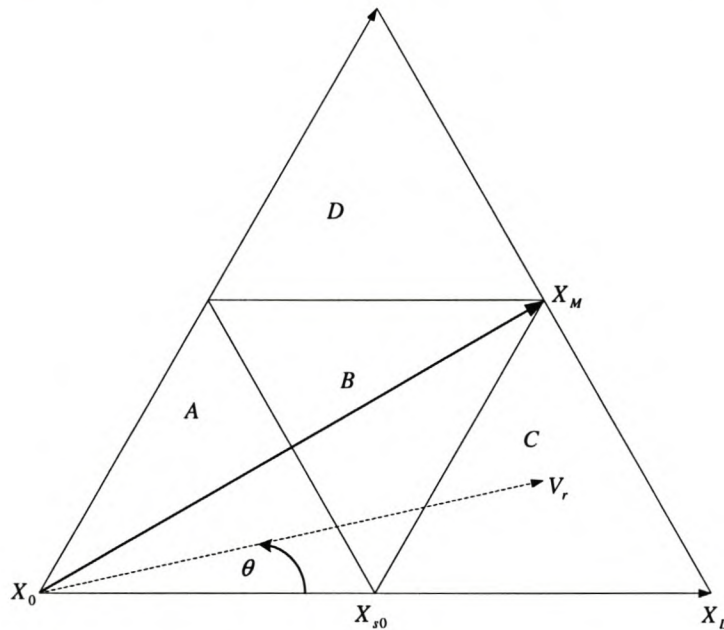


Figure 2.18: First sector for the switching state vectors of the three-level NPC inverter

the neutral-point balancing problem are A, B and C. The neutral point currents for these regions are:

Region A

$$i_{NP} = m_{s0} \cdot d_{s0} \cdot i_a + m_{s1} \cdot d_{s1} \cdot i_c \quad (2.5)$$

Region B

$$i_{NP} = d_M \cdot i_b + (m_{s0} \cdot d_{s0} \cdot i_a + m_{s1} \cdot d_{s1} \cdot i_c) \quad (2.6)$$

Region C

$$i_{NP} = d_M \cdot i_b + m_{s0} \cdot d_{s0} \cdot i_a \quad (2.7)$$

where m is the current modulation index,
 d is the duty cycle,

subscripts s_0 , s_1 and M are zero, small and middle vector respectively, i_a , i_b and i_c are phase currents.

Periodic variation in the components of equations 2.5, 2.6 and 2.7 cause steady-state low-frequency ripple in the neutral-point current over the output voltage line cycle. The composite expression combining equations 2.5, 2.6 and 2.7 into one matrix equation valid over the full line cycle of the output voltage transformed to $d - q$ parameters is

$$i_{NP} = \begin{bmatrix} d_M \cdot M_d & d_M \cdot M_q \end{bmatrix} \cdot \begin{bmatrix} i_d \\ i_q \end{bmatrix} + \begin{bmatrix} m_{s0} \cdot d_{s0} \cdot SO_d & m_{s0} \cdot d_{s0} \cdot SO_q \\ m_{s1} \cdot d_{s1} \cdot S1_d & m_{s1} \cdot d_{s1} \cdot S1_q \end{bmatrix} \quad (2.8)$$

where

$$M_d = M_a \cdot \cos(\theta) + M_b \cdot \cos(\theta - 2\pi/3) + M_c \cdot \cos(\theta + 2\pi/3)$$

and M , $S1$ and $S0$ are current switching functions for medium, small and zero vectors respectively.

Equation 2.8 is the fundamental equation used in the balancing of the DC-link capacitors.

2.3.3 Neutral-point voltage balancing circuit for DC-DC technology

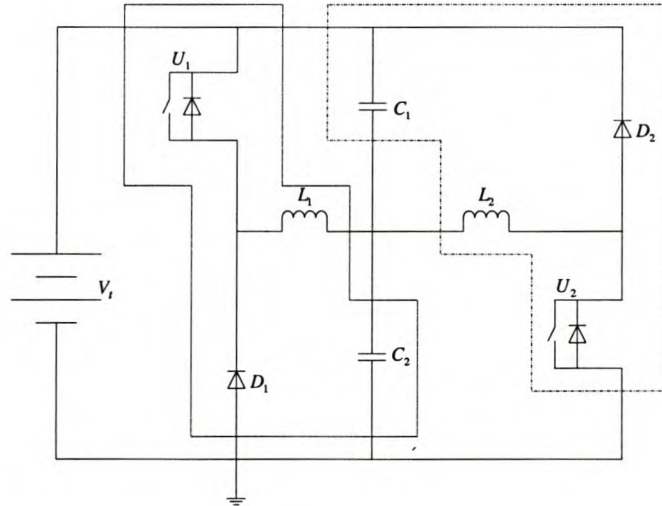


Figure 2.19: Neutral-point voltage balancing circuit

This strategy was proposed by Jouanne *et al.*[28]. The circuit shown in Figure 2.19 consists of boost and buck converters which work in complementary periods. C_1 and C_2 are the DC-link capacitors; U_1 , D_1 , L_1 and C_1 work in buck DC-DC converter mode; U_2 , D_2 , L_2 and C_2 work in boost DC-DC converter mode. For

$V_{C1} > V_{C2}$ the buck converter operates and the boost operator does not operate. Within this period V_{C2} increases and V_{C1} decreases, while V_t is kept constant. When U_1 is switched on, the current flows from U_1 to L_1 to charge C_2 . When U_1 is switched off, the energy stored in L_1 is transmitted to C_2 through the loop D_1 , L_1 and C_2 .

For boost DC-DC mode where $V_{C2} > V_{C1}$, the buck converter does not operate and the energy in C_2 is indirectly transferred to capacitor C_1 . When U_2 is on, the current flows from C_2 to L_2 to U_2 to the ground. When U_2 is switched off, the energy stored in L_2 is transmitted to C_1 through the loop D_2 , L_2 and C_1 . Within this period V_{C1} increases and V_{C2} decreases, while V_t is kept constant.

2.3.4 Other strategies

Other strategies include:

1. Minimise losses by not switching the highest current[16];
2. Closed-loop system of the line-to-line voltage vectors[8],[7];
3. Self-balancing space vector modulator[29];
4. Control method based for NPC converter based on a state-space model[30];
5. Share the balancing task with front-end converter[16];
6. Switching frequency optimal-PWM method[12].

2.4 Conclusion

This chapter provides an insight into the background information needed in order to better understand what is entailed in this thesis. We started by discussing the PWM switching scheme in inverter circuits and the natural and regular sampling associated with this scheme. We then discussed the method of analysis for the PWM switching scheme using Bennet's geometric model method. Three alternative PWM strategies with differing phase relationships between the carriers introduced by Carrara *et al* known as alternative phase opposition disposition(APOD), phase opposition disposition(POD) and phase disposition(PD) were discussed. We use these PWM modulation strategies in our analysis of switching functions in Chapter 4.

This chapter further provided vector modulation for two-level three-phase inverters. Under this section on vector modulation we demonstrated the generation of space vector modulation and the method used for the analysis of two-level three-phase inverters. We then gave an overview of strategies used by other authors for solving the balancing problem of the neutral point of the NPC inverter

Chapter 3

Balancing Theory

This chapter develops further the balancing theory first introduced in [3]. In [3] natural balancing under vector control was studied; the simulation results are shown in section 6.3. In this thesis we study natural balancing under phase opposition disposition pulse-width modulation using the theory and simulation of practical converters as shown in Chapters 4 and 5. The transformation of the three-level NPC circuit into a two-port circuit is discussed. We then give the fundamental equation that describes the factors influencing the steady-state balancing of the capacitor voltages. The two factors are the impedance of the output filter and load and the overlap of the Fourier transforms of the switching functions. This thesis is based on the study of these factors. We further develop the theory for the rebalancing time constant that will be used to compare the exponential decay of capacitor voltage difference using a practical converter and the theory developed in Chapter 4. We end the chapter by formulating equations used for designing the filter and the balance booster.

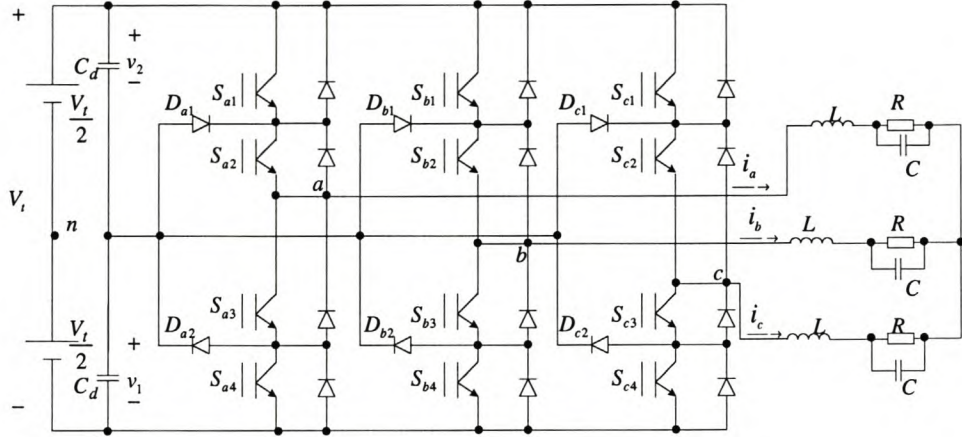
3.1 $\alpha\beta$ transformation of the switching states

In this section we transform the switching states from ABC parameters to $\alpha\beta$ parameters. We first develop the theory that is necessary for the transformation of the three-level neutral-point-clamped (NPC) inverter to its equivalent two-port circuit. Figure 3.1 shows the three-level neutral-point-clamped (NPC) inverter. The load consists of a low-pass LC filter and a load resistor. The DC supply voltage is denoted by V_t and the imbalance in the DC-bus capacitor voltages by v_δ . The equations used to denote V_t and v_δ are

$$V_t = v_1 + v_2$$

and

$$v_\delta = v_1 - v_2$$

**Figure 3.1:** NPC inverter

where v_δ denotes the imbalance in the DC capacitor voltages.

Let s_a , s_b and s_c represent the switching states of phases A, B and C respectively. We define them as follows

$$s_a = \begin{cases} 1 & \text{if } S_{a1} \text{ and } S_{a2} \text{ are closed} \\ 0 & \text{if } S_{a2} \text{ and } S_{a3} \text{ are closed} \\ -1 & \text{if } S_{a3} \text{ and } S_{a4} \text{ are closed} \end{cases} \quad (3.1)$$

$$s_b = \begin{cases} 1 & \text{if } S_{b1} \text{ and } S_{b2} \text{ are closed} \\ 0 & \text{if } S_{b2} \text{ and } S_{b3} \text{ are closed} \\ -1 & \text{if } S_{b3} \text{ and } S_{b4} \text{ are closed} \end{cases} \quad (3.2)$$

and

$$s_c = \begin{cases} 1 & \text{if } S_{c1} \text{ and } S_{c2} \text{ are closed} \\ 0 & \text{if } S_{c2} \text{ and } S_{c3} \text{ are closed} \\ -1 & \text{if } S_{c3} \text{ and } S_{c4} \text{ are closed} \end{cases} \quad (3.3)$$

Expressing v_{an} , v_{bn} and v_{cn} in terms of the a, b and c switching states results in

$$\begin{bmatrix} v_{an} \\ v_{bn} \\ v_{cn} \end{bmatrix} = \begin{bmatrix} s_a \\ s_b \\ s_c \end{bmatrix} \frac{V_t}{2} + \begin{bmatrix} (1 - |s_a|) \\ (1 - |s_b|) \\ (1 - |s_c|) \end{bmatrix} \frac{v_\delta}{2} \quad (3.4)$$

We now show that equation 3.4 holds. We use phase A of Figure 3.1 to prove validity of v_{an} in equation 3.4. The same method is used to prove the validity of v_{bn} and v_{cn} in equation 3.4.

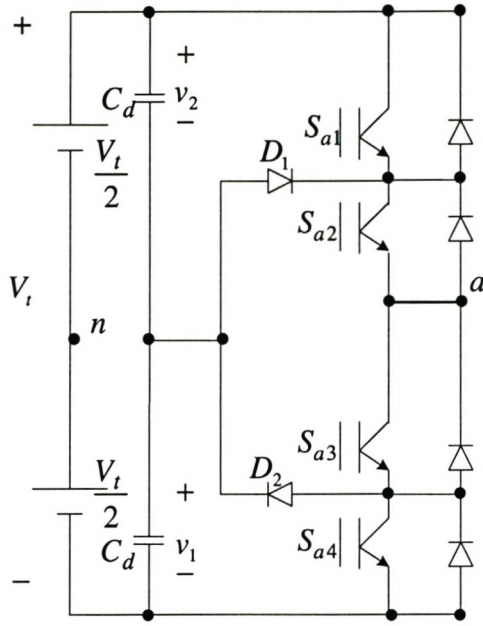


Figure 3.2: Phase A of NPC inverter

For $s_a = 1$

Substituting $s_a = 1$ in equation 3.4 results in

$$v_{an} = V_t/2$$

and with S_{a1} and S_{a2} closed in Figure 3.2 we have

$$v_{an} = V_t/2$$

For $s_a = 0$

Substituting $s_a = 0$ in equation 3.4 results in

$$\begin{aligned} v_{an} &= \frac{V_t}{2} - v_2 \\ &= \frac{1}{2}(v_1 + v_2) - v_2 \\ &= \frac{1}{2}v_1 - \frac{1}{2}v_2 \\ &= \frac{1}{2}v_\delta \end{aligned}$$

and with S_{a2} and S_{a3} closed in Figure 3.2 we have

$$v_{an} = v_\delta/2$$

For $s_a = -1$

Substituting $s_a = -1$ in equation 3.4 results in

$$v_{an} = -V_t/2$$

and with S_{a3} and S_{a4} closed in Figure 3.2 we have

$$v_{an} = -V_t/2$$

Since $v_1 + v_2 = V_t$, which is constant, it follows that

$$\begin{aligned} \frac{dv_\delta}{dt} &= \frac{dv_1}{dt} - \frac{dv_2}{dt} = \frac{dv_1}{dt} - \frac{dV_t}{dt} + \frac{dv_1}{dt} \\ &= 2\frac{dv_1}{dt} - \frac{dV_t}{dt} \\ &= 2\frac{dv_1}{dt} - 0 \quad V_t \text{ is a constant} \\ &= 2\frac{dv_1}{dt} \end{aligned}$$

By considering the current flowing into the centre point of the DC-bus capacitor bank, it is easy to see that

$$\begin{aligned} \frac{dv_\delta}{dt} &= -\frac{1}{C_d}(i_a(1 - |s_a|) + i_b(1 - |s_b|) + i_c(1 - |s_c|)) \\ &= \frac{1}{C_d}(i_a|s_a| + i_b|s_b| + i_c|s_c|) \end{aligned}$$

The next step in the analysis is to transform the three-phase quantities to the $\alpha\beta$ -plane. In 1983 Akagi *et al.*[34], [35] proposed the instantaneous power theory or p-q theory. It is based on instantaneous values in three-phase power systems with or without neutral wire, and is valid for steady-state or transitory operations, as well as for generic voltage and current waveforms. This theory consists of an algebraic transformation (Clarke transformation) of the three-phase voltages and currents in the a-b-c coordinates into the $\alpha - \beta - 0$ coordinates, followed by the calculation of the p-q theory instantaneous power components.

We use this theory to obtain the following transformations

$$\begin{bmatrix} v_\alpha \\ v_\beta \end{bmatrix} = A \begin{bmatrix} v_{an} \\ v_{bn} \\ v_{cn} \end{bmatrix}, \begin{bmatrix} i_\alpha \\ i_\beta \end{bmatrix} = A \begin{bmatrix} i_a \\ i_b \\ i_c \end{bmatrix}, \begin{bmatrix} s_\alpha \\ s_\beta \end{bmatrix} = A \begin{bmatrix} s_a \\ s_b \\ s_c \end{bmatrix} \text{ and } \begin{bmatrix} s'_\alpha \\ s'_\beta \end{bmatrix} = A \begin{bmatrix} |s_a| \\ |s_b| \\ |s_c| \end{bmatrix}$$

where

$$A = \sqrt{\frac{2}{3}} \begin{bmatrix} 1 & -1/2 & -1/2 \\ 0 & \sqrt{3}/2 & -\sqrt{3}/2 \end{bmatrix}$$

is the Clarke transformation.

By making use of the above definitions, it can be shown that

$$\frac{dv_\delta}{dt} = \frac{1}{C_d}(i_\alpha s'_\alpha + i_\beta s'_\beta)$$

since

$$\begin{aligned} i_\alpha s'_\alpha + i_\beta s'_\beta &= \begin{bmatrix} i_\alpha \\ i_\beta \end{bmatrix}^T \begin{bmatrix} s'_\alpha \\ s'_\beta \end{bmatrix} \\ &= \frac{2}{3}[i_a \ i_b \ i_c] \begin{bmatrix} 1 & 0 \\ -1/2 & \sqrt{3}/2 \\ -1/2 & -\sqrt{3}/2 \end{bmatrix} \begin{bmatrix} 1 & -1/2 & -1/2 \\ 0 & \sqrt{3}/2 & -\sqrt{3}/2 \end{bmatrix} \begin{bmatrix} |s_a| \\ |s_b| \\ |s_c| \end{bmatrix} \\ &= \frac{2}{3}[i_a \ i_b \ i_c] \begin{bmatrix} 1 & -1/2 & -1/2 \\ -1/2 & 1 & -1/2 \\ -1/2 & -1/2 & 1 \end{bmatrix} \begin{bmatrix} |s_a| \\ |s_b| \\ |s_c| \end{bmatrix} \\ &= \frac{2}{3}[i_a(|s_a| - \frac{1}{2}|s_b| - \frac{1}{2}|s_c|) + i_b(-\frac{1}{2}|s_a| + |s_b| - \frac{1}{2}|s_c|) \\ &\quad + i_c(-\frac{1}{2}|s_a| - \frac{1}{2}|s_b| + |s_c|)] \\ &= \frac{2}{3}[|s_a|(i_a - \frac{1}{2}i_b - \frac{1}{2}i_c) + |s_b|(-\frac{1}{2}i_a + i_b - \frac{1}{2}i_c) + |s_c|(-\frac{1}{2}i_a + \frac{1}{2}i_b + i_c)] \end{aligned}$$

But

$$i_a + i_b + i_c = 0$$

That is

$$i_\alpha s'_\alpha + i_\beta s'_\beta = |s_a|i_a + |s_b|i_b + |s_c|i_c$$

and

$$\frac{dv_\delta}{dt} = \frac{1}{C_d}(i_\alpha s'_\alpha + i_\beta s'_\beta) \tag{3.5}$$

Applying $\alpha\beta$ transformation to equation 3.4 results in

$$\begin{bmatrix} v_\alpha \\ v_\beta \end{bmatrix} = \begin{bmatrix} s_\alpha \\ s_\beta \end{bmatrix} \frac{V_t}{2} - \begin{bmatrix} s'_\alpha \\ s'_\beta \end{bmatrix} \frac{v_\delta}{2} \tag{3.6}$$

3.2 Load Transformation

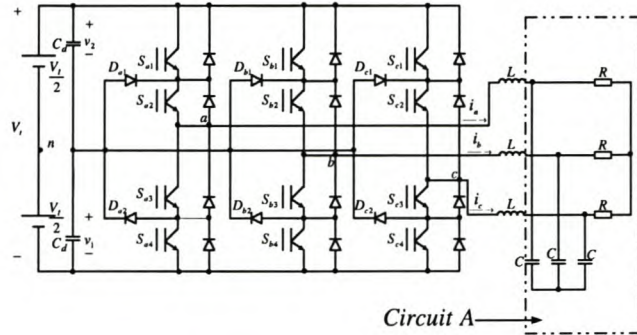


Figure 3.3: Circuit A connected to the NPC inverter

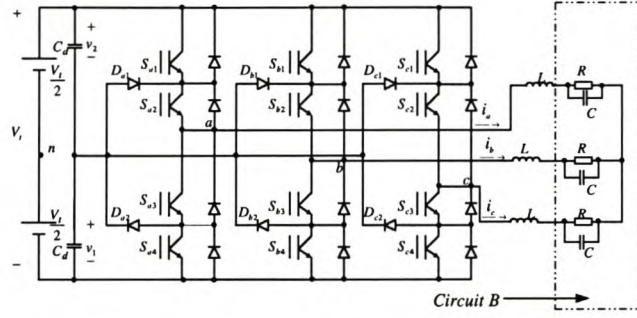


Figure 3.4: Circuit B connected to the NPC inverter

There are two ways in which the filter capacitors can be connected in a practical converter. Circuit A of Figure 3.3 and circuit B of Figure 3.4 show these two ways. The aim of this section is to show that the two circuits are essentially the same and can be treated by the same techniques. This is necessary since it is easy to use Figure 3.4 for the $\alpha\beta$ transformation of NPC inverter into its equivalent two-port circuit. We use $Y - \Delta$ and $\Delta - Y$ transforms [33] to simplify circuit A given in Figure 3.3 in order for it to be further transformed into $\alpha\beta$ parameters. Now we consider load transformation.

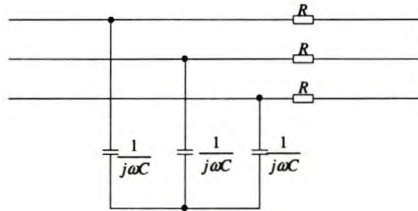
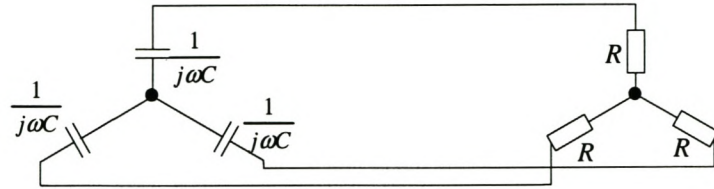
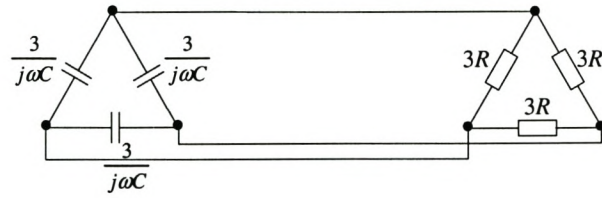


Figure 3.5: Load 1

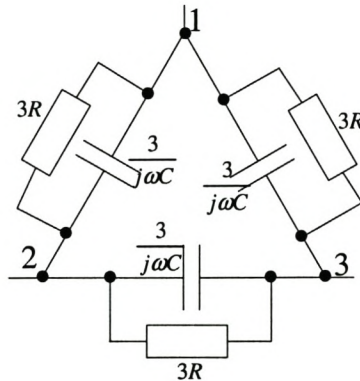
The equivalent circuit of Figure 3.5 is given by Figure 3.6

**Figure 3.6: Load 2**

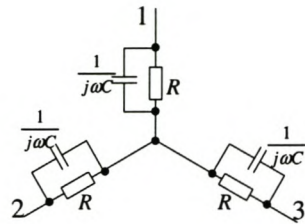
Applying $Y - \Delta$ transform [33] to Figure 3.6, we obtain Figure 3.7

**Figure 3.7: Load 3**

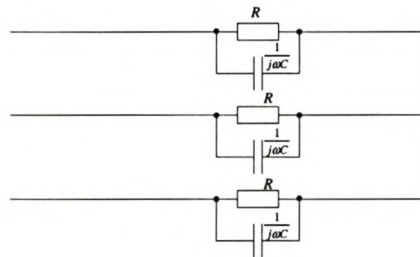
The equivalent circuit is given by Figure 3.8

**Figure 3.8: Load 4**

Applying the $\Delta - Y$ transform to Figure 3.8, we obtain Figure 3.9

**Figure 3.9: Load 5**

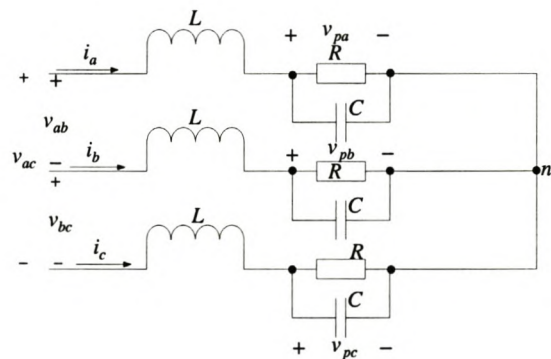
The equivalent circuit of Figure 3.9 is given by Figure 3.10

**Figure 3.10: Load 6**

3.3 Transformation to $\alpha\beta$ Parameters

In this section we derive an equivalent circuit in terms of α and β parameters that makes it easy to understand the balancing mechanisms.

We start by transforming the load to $\alpha\beta$ parameters. Using Figure 3.10 we can now represent the load of Figure 3.1 by Figure 3.11.

**Figure 3.11: Load 7**

From Figure 3.11 we derive the following equations that lead to the transformation of Figure 3.11 into $\alpha\beta$ parameters as shown in Figure 3.12.

Considering the v_{ab} loop, we have the following

$$v_{ab} = v_{an} - v_{bn} = L \frac{di_a}{dt} + v_{pa} - v_{pb} - L \frac{di_b}{dt}$$

which can be written as

$$\frac{di_a}{dt} - \frac{di_b}{dt} = \frac{1}{L}(v_{an} - v_{bn} - v_{pa} + v_{pb}) \quad (3.7)$$

Considering the v_{bc} loop, we have the following

$$v_{bc} = v_{bn} - v_{cn} = L \frac{di_b}{dt} + v_{pb} - v_{pc} - L \frac{di_c}{dt}$$

which can be written as

$$\frac{di_b}{dt} - \frac{di_c}{dt} = \frac{1}{L}(v_{bn} - v_{cn} - v_{pb} + v_{pc}) \quad (3.8)$$

Considering the v_{ac} loop, we have the following

$$v_{ac} = v_{cn} - v_{an} = L \frac{di_a}{dt} + v_{pa} - v_{pc} - L \frac{di_c}{dt}$$

which can be written as

$$\frac{di_c}{dt} - \frac{di_a}{dt} = \frac{1}{L}(v_{cn} - v_{an} - v_{pc} + v_{pa}) \quad (3.9)$$

We also note that

$$i_a + i_b + i_c = 0$$

Subtracting equation 3.9 from equation 3.7 results in

$$2 \frac{di_a}{dt} - \frac{di_b}{dt} - \frac{di_c}{dt} = \frac{1}{L}(2v_{an} - v_{bn} - v_{cn} - 2v_{pa} + v_{pb} + v_{pc})$$

which simplifies to

$$\frac{di_a}{dt} = \frac{1}{3L}(2v_{an} - v_{bn} - v_{cn} - 2v_{pa} + v_{pb} + v_{pc})$$

Subtracting equation 3.7 from equation 3.8 results in

$$2 \frac{di_b}{dt} - \frac{di_c}{dt} - \frac{di_a}{dt} = \frac{1}{L}(2v_{bn} - v_{cn} - v_{an} - 2v_{pb} + v_{pc} + v_{pa})$$

which simplifies to

$$\frac{di_b}{dt} = \frac{1}{3L}(2v_{bn} - v_{cn} - v_{an} - 2v_{pb} + v_{pc} + v_{pa})$$

Subtracting equation 3.8 from equation 3.9 results in

$$2\frac{di_c}{dt} - \frac{di_a}{dt} - \frac{di_b}{dt} = \frac{1}{L}(2v_{cn} - v_{an} - v_{bn} - 2v_{pc} + v_{pa} + v_{pb})$$

which simplifies to

$$\frac{di_c}{dt} = \frac{1}{3L}(2v_{cn} - v_{an} - v_{bn} - 2v_{pc} + v_{pa} + v_{pb})$$

Writing these equations in matrix form results in:

$$\begin{bmatrix} \frac{di_a}{dt} \\ \frac{di_b}{dt} \\ \frac{di_c}{dt} \end{bmatrix} = \frac{1}{3L} \begin{bmatrix} 2 & -1 & -1 \\ -1 & 2 & -1 \\ -1 & -1 & 2 \end{bmatrix} \begin{bmatrix} v_{an} \\ v_{bn} \\ v_{cn} \end{bmatrix} - \frac{1}{3L} \begin{bmatrix} 2 & -1 & -1 \\ -1 & 2 & -1 \\ -1 & -1 & 2 \end{bmatrix} \begin{bmatrix} v_{pa} \\ v_{pb} \\ v_{pc} \end{bmatrix} \quad (3.10)$$

Now applying $\alpha\beta$ transformation results in

$$\sqrt{\frac{2}{3}} \begin{bmatrix} 1 & -1/2 & -1/2 \\ -1 & \sqrt{3}/2 & -\sqrt{3}/2 \end{bmatrix} \frac{1}{3} \begin{bmatrix} 2 & -1 & -1 \\ -1 & 2 & -1 \\ -1 & -1 & 2 \end{bmatrix} = \sqrt{\frac{2}{3}} \begin{bmatrix} 1 & -1/2 & -1/2 \\ 0 & \sqrt{3}/2 & -\sqrt{3}/2 \end{bmatrix} \quad (3.11)$$

That is

$$\begin{bmatrix} \frac{di_\alpha}{dt} \\ \frac{di_\beta}{dt} \end{bmatrix} = \frac{1}{L} \begin{bmatrix} v_\alpha \\ v_\beta \end{bmatrix} - \frac{1}{L} \begin{bmatrix} v_{c\alpha} \\ v_{c\beta} \end{bmatrix}$$

which is represented by Figure 3.12

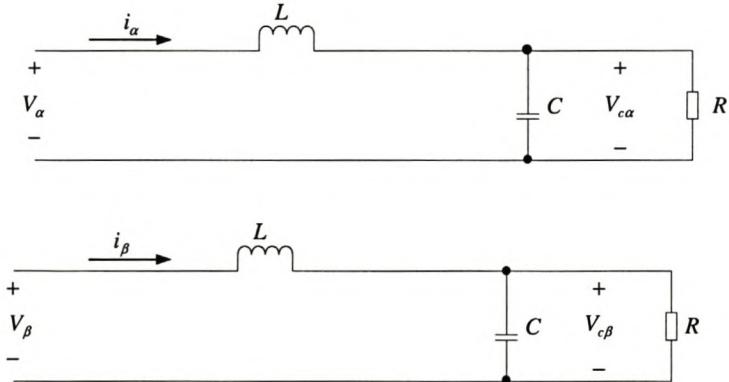


Figure 3.12: Load 8

Figure 3.12 represent the $\alpha\beta$ transformation of the load of Figure 3.1.

We rewrite equation 3.5 from section 3.1 as follows:

$$\frac{d\frac{v_\delta}{2}}{dt} = \frac{1}{2C_d}(i_\alpha s'_\alpha + i_\beta s'_\beta) \quad (3.12)$$

where the capacitor current i_d is given by

$$i_d = i_\alpha s'_\alpha + i_\beta s'_\beta$$

We also rewrite equation 3.6 from section 3.1 as follows:

$$v_\alpha = \frac{V_t}{2}s_\alpha - \frac{v_\delta}{2}s'_\alpha \quad (3.13)$$

$$v_\beta = \frac{V_t}{2}s_\beta - \frac{v_\delta}{2}s'_\beta \quad (3.14)$$

Using equations 3.12, 3.13 and 3.14 and Figure 3.12 we obtain the equivalent circuit of the three-level NPC inverter given in section 3.1 by Figure 3.1. The equivalent two-port circuit is given by Figure 3.13.

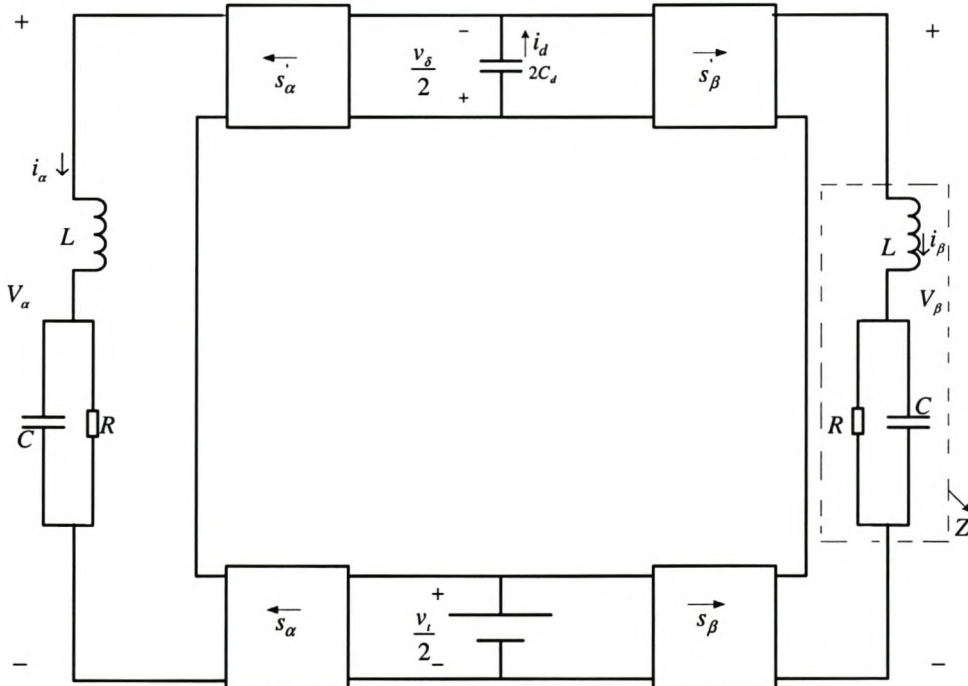


Figure 3.13: Equivalent circuit of the three level NPC inverter

Furthermore from Figure 3.11

$$i_a = C \frac{dv_{pa}}{dt} + \frac{v_{pa}}{R} \Rightarrow \frac{dv_{pa}}{dt} = \frac{1}{C} (i_a - \frac{v_{pa}}{R})$$

$$i_b = C \frac{dv_{pb}}{dt} + \frac{v_{pb}}{R} \Rightarrow \frac{dv_{pb}}{dt} = \frac{1}{C} (i_b - \frac{v_{pb}}{R})$$

$$i_c = C \frac{dv_{pc}}{dt} + \frac{v_{pc}}{R} \Rightarrow \frac{dv_{pc}}{dt} = \frac{1}{C} (i_c - \frac{v_{pc}}{R})$$

That is

$$\begin{bmatrix} \dot{v}_{c\alpha} \\ \dot{v}_{c\beta} \end{bmatrix} = \frac{1}{C} \begin{bmatrix} i_\alpha \\ i_\beta \end{bmatrix} - \frac{1}{RC} \begin{bmatrix} v_{c\alpha} \\ v_{c\beta} \end{bmatrix}$$

3.4 Operation of a two-port switching circuit

Figure 3.13 shows an equivalent circuit based on equations 3.12, 3.13 and 3.14. This equivalent circuit provides an intuitive way of understanding the balancing mechanisms of the three-level NPC inverter. Each of the switching blocks of Figure 3.13 can be thought of as a two-port switching circuit. Figure 3.14 gives an explanation of how the blocks of

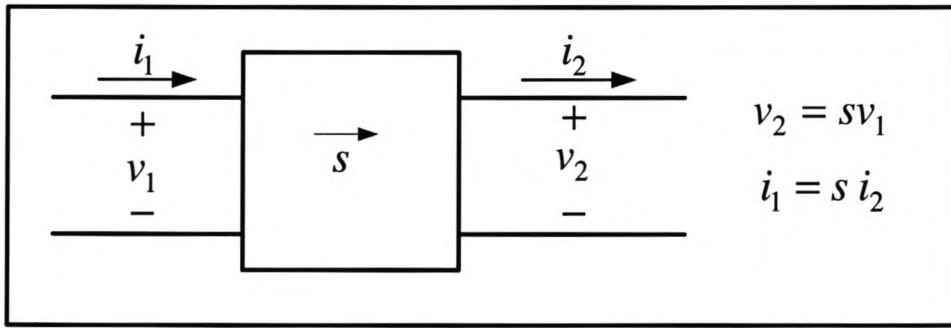


Figure 3.14: Two-port switching circuit

Figure 3.13 are defined. Figure 3.14 shows the basic two-port switching function s . The arrow points from port 1 to port 2. The relations between voltages v_1 and v_2 and currents i_1 and i_2 are given by

$$v_2 = sv_1$$

and

$$i_1 = si_2$$

In general this circuit can only be analysed through simulation.

3.5 Steady-State Balancing of the Capacitor Voltages

In this section we derive the fundamental equation that shows the factors that influence the steady-state balancing of the capacitor voltages. In order to achieve this, we make use of Figure 3.13.

Since we study the case where the bus capacitance C_d is large in the sense that the voltage across v_δ varies slowly compared to the dynamics of the rest of the system and contains relatively small voltage ripple, we assume that the system is in the steady state. Let Z denote the impedance of the filter inductor. Then the following equations hold in the frequency domain: V_δ is a DC voltage

$$I_\alpha(\omega) = \frac{\frac{V_t}{2}S_\alpha(\omega) - \frac{V_\delta}{2}S'_\alpha(\omega)}{Z(\omega)}$$

and

$$I_\beta(\omega) = \frac{\frac{V_t}{2}S_\beta(\omega) - \frac{V_\delta}{2}S'_\beta(\omega)}{Z(\omega)}$$

where

$$\frac{V_t}{2}S_\alpha(\omega) - \frac{V_\delta}{2}S'_\alpha(\omega)$$

and

$$\frac{V_t}{2}S_\beta(\omega) - \frac{V_\delta}{2}S'_\beta(\omega)$$

are the voltages across the load.

Since capacitor current i_d is given by

$$i_d = i_\alpha s'_\alpha + i_\beta s'_\beta$$

in the time domain, it follows that

$$I_d(\omega) = I_\alpha(\omega) * S'_\alpha(\omega) + I_\beta(\omega) * S'_\beta(\omega)$$

in the frequency domain.

Hence

$$\begin{aligned} I_d(\omega) &= \frac{V_t}{2} \left\{ \left(\frac{S_\alpha(\omega)}{Z(\omega)} \right) * S'_\alpha + \left(\frac{S_\beta(\omega)}{Z(\omega)} \right) * S'_\beta(\omega) \right\} - \frac{V_\delta}{2} \left\{ \left(\frac{S'_\alpha(\omega)}{Z(\omega)} \right) * S'_\alpha(\omega) \right. \\ &\quad \left. + \left(\frac{S'_\beta(\omega)}{Z(\omega)} \right) * S'_\beta(\omega) \right\} \end{aligned}$$

Since the average value of i_d is equal to zero Amperes at steady state, we have

$$I_d(\omega)_{/\omega=0} = 0$$

Thus applying the definition of the convolution integral; we have

$$\begin{aligned} \left(\frac{V_t}{2} \cdot \frac{S_\alpha(\omega)}{Z(\omega)} \right) * S'_\alpha(\omega) &= \frac{1}{2\pi} \int_{-\infty}^{\infty} \left(\frac{v_t}{2} \cdot \frac{S_\alpha(u)}{Z(u)} \right) S'_\alpha(0-u) du \\ &= \frac{1}{2\pi} \cdot \frac{V_t}{2} \int_{-\infty}^{\infty} \frac{S_\alpha(u) \bar{S}'_\alpha(u)}{Z(u)} du \quad S'_\alpha(-u) = \bar{S}'_\alpha(u) \end{aligned}$$

Now we obtain the key equation that will be used in the study of the natural balancing of the capacitor voltages of the NPC inverter given by:

$$\begin{aligned} \frac{V_\delta}{V_t} &= \frac{\int_{-\infty}^{\infty} \left(\frac{S_\alpha(u) \bar{S}'_\alpha(u)}{Z(u)} + \frac{S_\beta(u) \bar{S}'_\beta(u)}{Z(u)} \right) du}{\int_{-\infty}^{\infty} \left(\frac{S'_\alpha(u) \bar{S}'_\alpha(u)}{Z(u)} + \frac{S'_\beta(u) \bar{S}'_\beta(u)}{Z(u)} \right) du} \quad (3.15) \\ &= \frac{\int_{-\infty}^{\infty} \frac{F_1(u)}{Z(u)} du}{\int_{-\infty}^{\infty} \frac{F_2(u)}{Z(u)} du} \end{aligned}$$

where

$$F_1(u) = S_\alpha(u) \bar{S}'_\alpha(u) + S_\beta(u) \bar{S}'_\beta(u)$$

$$F_2(u) = |S'_\alpha(u)|^2 + |S'_\beta(u)|^2$$

(NB: \bar{z} denotes the complex conjugate of z .)

This fundamental equation shows that the steady-state balancing of the capacitor voltages is influenced by the following two factors:

1. The impedance of the output filter and load;
2. The values of $F_1(\omega)$ and $F_2(\omega)$.

3.6 Time Constant

Time constant is the interval required for a circuit to change a specified fraction from one state or condition to another. The time constant is used in the expression

$$G(t) = G(0)e^{-\frac{t}{\tau}}$$

where $G(t)$ is the value of the state at time t , $G(0)$ is the value of the state at time $t = 0$, τ is the time constant, and t is the time that has elapsed from the start of the exponential decay.

In this section we calculate the time constant associated with the rebalancing of the DC-bus voltages following a perturbation. This time constant can be seen as a measure of the strength of the balancing mechanisms.

The exponential decay is associated with the DC current I_d . Referring to the equivalent circuit of the NPC inverter given in Figure 3.13, the change in the capacitor voltage of $2C_d$ is slow; hence the state of the circuit can be taken as steady state. For calculating time constant we use the first order differential equation given by

$$\dot{x} = Gx + B$$

where G is the eigenvalue and $B = 0$ since we are only interested in the homogeneous solution. This implies that $V_t = 0$, that is we short-circuit voltage source $\frac{V_t}{2}$ in the equivalent circuit to obtain $V_t = 0$. The resulting circuit is shown in Figure 3.15.

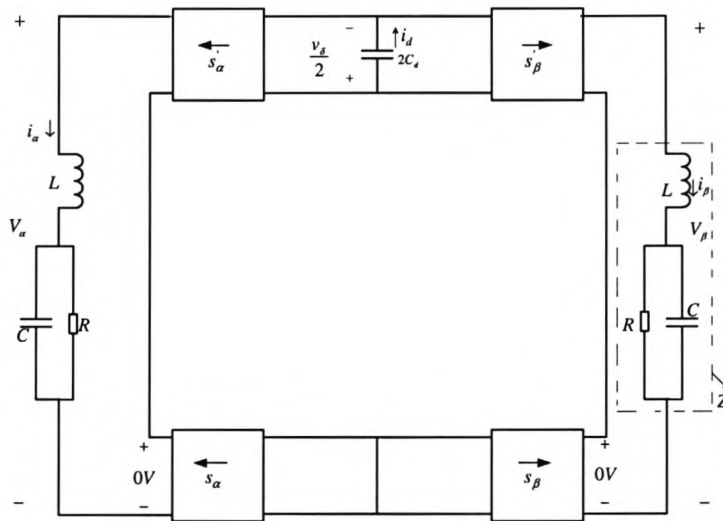


Figure 3.15: NPC equivalent circuit after shortcircuiting the voltage source $\frac{V_t}{2}$

$$I_d(0) = C_d \frac{dv_\delta}{dt}$$

$$I_d(\omega) = I_\alpha(\omega) * S'_\alpha(\omega) + I_\beta(\omega) * S'_\beta(\omega)$$

$$I_\alpha(\omega) = \frac{-\frac{v_\delta}{2} S'_\alpha(\omega)}{Z(\omega)}$$

$$I_\beta(\omega) = \frac{-\frac{v_\delta}{2} S'_\beta(\omega)}{Z(\omega)}$$

$$\begin{aligned} \frac{dv_\delta}{dt} &= \frac{1}{C_d} (I_\alpha(\omega) * S'_\alpha(\omega) + I_\beta(\omega) * S'_\beta(\omega))|_{\omega=0} \\ &= \frac{1}{C_d} \left[\left(\frac{-\frac{v_\delta}{2} S'_\alpha(\omega)}{Z(\omega)} \right) * S'_\alpha(\omega) - \left(\frac{\frac{v_\delta}{2} S'_\beta(\omega)}{Z(\omega)} \right) * S'_\beta \right] |_{\omega=0} \end{aligned}$$

Using the definition of the convolution integral we have

$$\begin{aligned}\frac{dv_\delta}{dt} &= \frac{1}{C_d} \left\{ - \int_{-\infty}^{\infty} \left(\frac{\frac{v_\delta}{2} S'_\alpha(u)}{Z(u)} \right) S'_\alpha(0-u) du - \int_{-\infty}^{\infty} \left(\frac{\frac{v_\delta}{2} S'_\beta(u)}{Z(u)} \right) S'_\beta(0-u) du \right\} \\ &= -\frac{1}{C_d} \left\{ \frac{v_\delta}{2} \int_{-\infty}^{\infty} \left(\frac{S'_\alpha(u)}{Z(u)} \right) \overline{S'_\alpha}(u) du + \frac{v_\delta}{2} \int_{-\infty}^{\infty} \left(\frac{S'_\beta(u)}{Z(u)} \right) \overline{S'_\beta}(u) du \right\} \\ &= -\frac{v_\delta}{2C_d} \left\{ \int_{-\infty}^{\infty} \left(\frac{S'_\alpha(u) \overline{S'_\alpha}(u)}{Z(u)} + \frac{S'_\beta(u) \overline{S'_\beta}(u)}{Z(u)} \right) du \right\} \\ \frac{dv_\delta}{v_\delta} &= -\frac{1}{2C_d} \left\{ \int_{-\infty}^{\infty} \left(\frac{S'_\alpha(u) \overline{S'_\alpha}(u)}{Z(u)} + \frac{S'_\beta(u) \overline{S'_\beta}(u)}{Z(u)} \right) du \right\} dt\end{aligned}$$

Time constant(τ) is given by

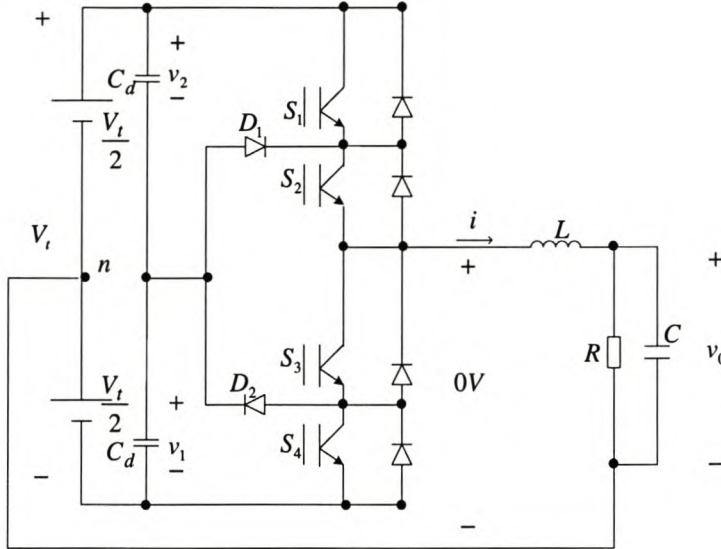
$$\begin{aligned}\tau &= \frac{1}{\frac{1}{2C_d} \left\{ \int_{-\infty}^{\infty} \left(\frac{S'_\alpha(u)}{Z(u)} \right) \overline{S'_\alpha}(u) du + \int_{-\infty}^{\infty} \left(\frac{S'_\beta(u)}{Z(u)} \right) \overline{S'_\beta}(u) du \right\}} \\ &= \frac{2C_d}{\left\{ \int_{-\infty}^{\infty} \left(\frac{S'_\alpha(u)}{Z(u)} \right) \overline{S'_\alpha}(u) du + \int_{-\infty}^{\infty} \left(\frac{S'_\beta(u)}{Z(u)} \right) \overline{S'_\beta}(u) du \right\}} \\ &= \frac{2C_d}{\int_{-\infty}^{\infty} \frac{F_2(u)}{Z(u)} du} \\ &= \frac{2C_d}{2\Re e \int_0^{\infty} \frac{F_2(u)}{Z(u)} du} \\ &= \frac{C_d}{\Re e \int_0^{\infty} \frac{F_2(u)}{Z(u)} du}\end{aligned}\tag{3.16}$$

From equation 3.16 we observe that factors influencing the value of the time constant associated with the rebalancing of the DC-bus voltage are:

1. The impedance of the output filter and load;
2. The value of $F_2(u)$, that is, the overlap of the spectra of $S'_\alpha(u)$ and $\overline{S'_\alpha}(u)$ as well as $S'_\beta(u)$ and $\overline{S'_\beta}(u)$ in the frequency domain.

3.7 Filter Design

This section is aimed at deriving the equations for the filter inductor and filter capacitor. We consider a single-phase converter shown in Figure 3.16 in order to derive the equations of the filter inductor and filter capacitor. The procedure we derive here is only an approximate design of the filter design for a three-phase converter.

**Figure 3.16:** Single-phase converter

Voltage across the inductor of the filter(v_L) is given by

$$v_L = L \frac{di}{dt}$$

When the two middle switches S_2 and S_3 are closed, then the voltage across the inductor is given by

$$v_L = -v_0 \quad (3.17)$$

In inverter circuits the aim of the PWM switching scheme is to produce an inverter output that is sinusoidal with magnitude and frequency controllable. This is done by comparing the sinusoidal control signal at the desired frequency with a triangular waveform. In this section we use the APOD/POD/PD PWM switching scheme.

The output voltage v_0 is given by

$$v_0 = m_a \frac{V_t}{2} \sin \omega_1 t$$

where $\sin \omega_1 t$ is the control signal with peak amplitude $\hat{V}_{control}$ and m_a is the amplitude modulation ratio given by

$$m_a = \frac{\hat{V}_{control}}{\hat{V}_{tri}}$$

where \hat{V}_{tri} is the peak value of the triangular signal.

Then

$$di = \frac{-m_a \frac{V_t}{2} \sin \omega_1 t}{L} dt \quad (3.18)$$

Equation 3.18 is only true during the period when the two middle switches are on.

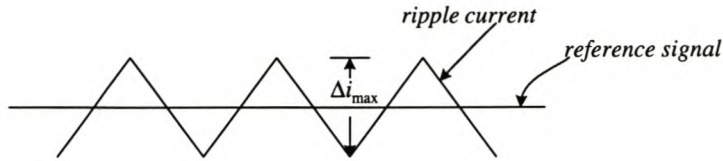


Figure 3.17: Ripple current of the inductor

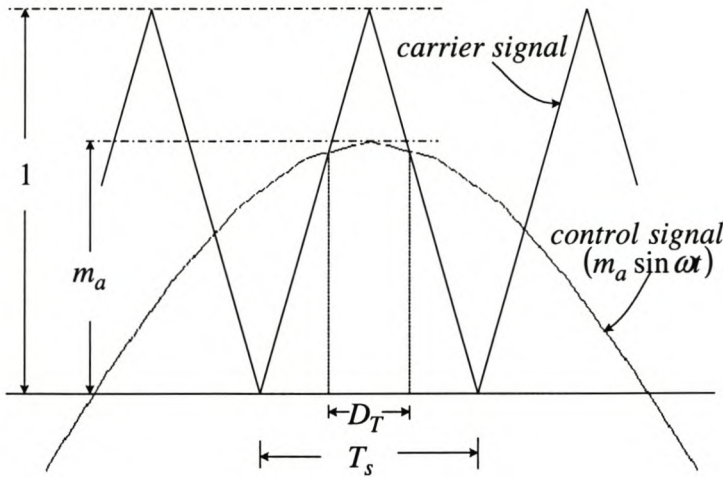


Figure 3.18: APOD/POD/PD PWM switching

Figures 3.17 and 3.18 show the ripple current in the filter inductor and the duty cycle for APOD/POD/PD PWM switching respectively. Assuming constant duty cycle for approximating v_0 we then obtain the following expression for the ripple current

$$\Delta i = \frac{-m_a \frac{V_t}{2} \sin \omega_1 t}{L} \Delta t$$

where

$$\frac{-m_a \frac{V_t}{2} \sin \omega_1 t}{L}$$

is the gradient of the ripple current and Δt is the time that both S_2 and S_3 are on.

Thus for the period when S_2 and S_3 are switched on we have

$$D_T = T_s (1 - m_a \sin \omega_1 t) \quad (3.19)$$

where D_T is the duty cycle of S_2 and S_3 , T_s is the switching period and $m_a \sin \omega_1 t$ is the reference signal applied to the pulse-width modulator.

Equation 3.19 holds since the duty cycle is not constant. Therefore the peak-to-peak ripple current in the inductor is given by

$$\begin{aligned}\Delta i &= \frac{V_t T_s}{2L} (-m_a \sin \omega_1 t) (1 - m_a \sin \omega_1 t) \\ &= \frac{V_t T_s}{2L} (-m_a \sin \omega_1 t + m_a^2 \sin^2 \omega_1 t)\end{aligned}$$

For maximum ripple current

$$\frac{d\Delta i}{dt} = -\frac{V_t T_s}{2L} m_a \omega_1 \cos \omega_1 t = 0$$

Using the second derivative we observe that the ripple current(Δi) is maximum when $\omega_1 t = \frac{\pi}{2}(4n - 1)$ where n is a positive integer.

The maximum ripple current is then given by

$$\Delta i_{max} = \frac{V_t T_s}{2L} (m_a + m_a^2)$$

Therefore

$$L = \frac{V_t m_a}{2 f_s \Delta i_{max}} (1 + m_a) \quad (3.20)$$

The cut-off frequency(ω_c) is given by

$$\omega_c = \frac{1}{\sqrt{LC}}$$

The cut-off frequency occurs at 10 percent of the magnitude where the largest harmonics occur, that is, if the largest frequency occurs at 12kHz, then the cut-off frequency occurs at 1200Hz and is given by

$$\omega_c = \frac{1}{\sqrt{LC}} = 1200 \times 2\pi$$

Hence the equation for the filter capacitor is given by

$$C = \frac{1}{L \omega_c^2} \quad (3.21)$$

3.8 Balancing Circuit

From equation 3.15 one of the factors affecting the balancing of the capacitor voltages is the impedance of the output filter and load. Decreasing the load impedance is done by connecting the balancing circuit at the frequency where the largest component of harmonics of F_2 occurs. In this section we derive the equations that are used in the design of the balancing booster [32]. Figure 3.19 shows the balancing circuit that acts as a band-pass filter providing a low impedance at twice the switching frequency.

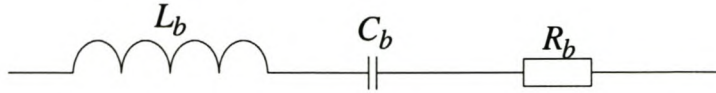
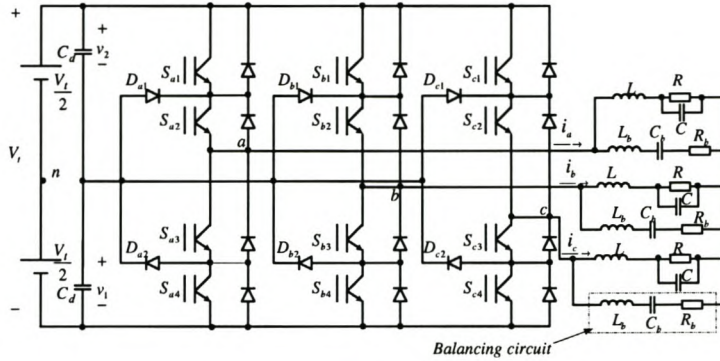
**Figure 3.19:** Balancing filter**Figure 3.20:** NPC inverter with a balancing circuit connected.

Figure 3.20 shows the NPC inverter with the balancing circuit connected.

The impedance $Z(s)$ is given by

$$Z(s) = Ls + \frac{1}{sC} + R$$

and

$$\begin{aligned} Z(j\omega) &= j\omega L + \frac{1}{j\omega C} + R \\ &= j\omega L - \frac{j}{\omega C} + R \end{aligned}$$

Hence

$$|Z(j\omega)| = \sqrt{\left(L\omega - \frac{1}{\omega C}\right)^2 + R^2}$$

The minimum magnitude of $|Z(j\omega)|$ is given by

$$\begin{aligned} Z_{min} &= |Z(j\omega_0)| \\ &= \sqrt{\left(L\omega_0 - \frac{1}{\omega_0 C}\right)^2 + R^2} \end{aligned}$$

Since $\omega_0 = \frac{1}{\sqrt{LC}}$

$$\begin{aligned} Z_{min} &= \sqrt{R^2} \\ &= R \end{aligned}$$

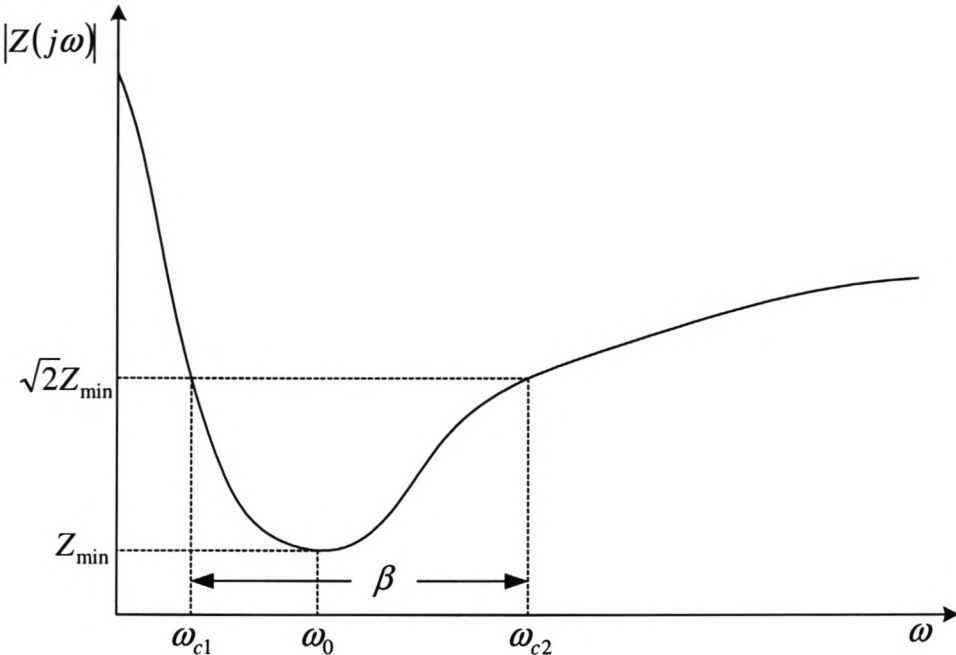


Figure 3.21: The frequency response plot for the RLC balance booster circuit

Figure 3.21 shows the frequency response plot for the RLC balance booster circuit. At the cut-off frequencies, the magnitude of the transfer function is $\sqrt{2}H_{min} = \sqrt{2}R$.

Solving for ω_c yields

$$\sqrt{2}R = \sqrt{(L\omega_c - \frac{1}{\omega_c C})^2 + R^2}$$

$$2R^2 = (L\omega_c - \frac{1}{\omega_c C})^2 + R^2$$

$$R^2 = (L\omega_c - \frac{1}{\omega_c C})^2$$

$$\pm R = L\omega_c - \frac{1}{\omega_c C}$$

$$\omega_c^2 L \pm \omega_c R - \frac{1}{C}$$

$$\omega_c^2 \pm \frac{\omega_c R}{L} - \frac{1}{LC} = 0$$

$$\omega_c = -\frac{R}{2L} \pm \sqrt{\left(\frac{R}{2L}\right)^2 + \frac{1}{LC}}$$

or

$$\omega_c = \frac{R}{2L} \pm \sqrt{\left(\frac{R}{2L}\right)^2 + \frac{1}{LC}}$$

Taking only the positive values we have

$$\omega_{c1} = -\frac{R}{2L} + \sqrt{\left(\frac{R}{2L}\right)^2 + \frac{1}{LC}}$$

$$\omega_{c2} = \frac{R}{2L} + \sqrt{\left(\frac{R}{2L}\right)^2 + \frac{1}{LC}}$$

Bandwidth(β), which is the width of the passband, is given by

$$\begin{aligned}\beta &= \omega_{c1} - \omega_{c2} \\ &= \left(\frac{R}{2L} + \sqrt{\left(\frac{R}{2L}\right)^2 + \frac{1}{LC}} \right) - \left(-\frac{R}{2L} + \sqrt{\left(\frac{R}{2L}\right)^2 + \frac{1}{LC}} \right) \\ &= \frac{R}{L}\end{aligned}$$

Quality factor(Q), which is the ratio of the centre frequency to the bandwidth, is given by

$$\begin{aligned}Q &= \frac{\omega_0}{\beta} \\ &= \frac{\frac{1}{\sqrt{LC}}}{\frac{R}{L}} \\ &= \sqrt{\frac{L}{R^2C}}\end{aligned}$$

Let Q_1, Q_2, Q_3, Q_4 and Q_5 be quality factors such that

$$Q_1 > Q_2 > Q_3 > Q_4 > Q_5$$

Then Figure 3.22 shows the effect of the quality factor. This shows that the smaller quality factor corresponds to the larger bandwidth and conversely.

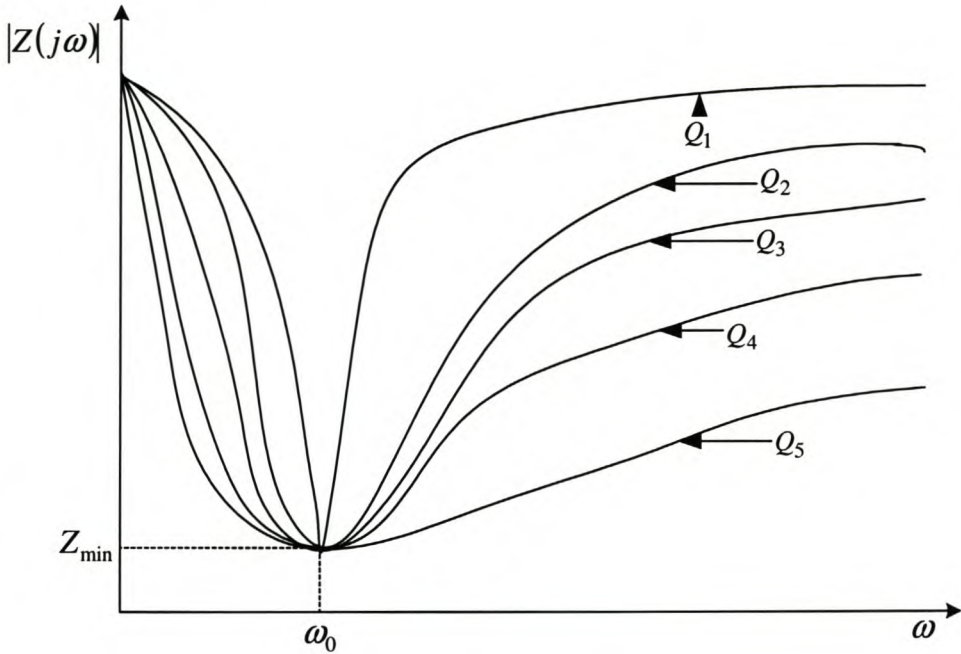


Figure 3.22: Effect of the quality factor

3.9 Conclusion

This chapter presented the theory that is used in the analysis of capacitor voltage balancing of the NPC inverter. The theory presented in the paper by [3] was elaborated and the key equation that is used in the analysis of capacitor voltage balancing was presented. The key equation is given by

$$\frac{V_\delta}{V_t} = \frac{\int_{-\infty}^{\infty} \left(\frac{S_\alpha(u) \overline{S'_\alpha}(u)}{Z(u)} + \frac{S_\beta(u) \overline{S'_\beta}(u)}{Z(u)} \right) du}{\int_{-\infty}^{\infty} \left(\frac{S'_\alpha(u) \overline{S'_\alpha}(u)}{Z(u)} + \frac{S'_\beta(u) \overline{S'_\beta}(u)}{Z(u)} \right) du}$$

Factors influencing the balancing of the capacitor voltages of the NPC inverter are

- the impedance of the output filter and load;
- the overlap of the spectra of the switching function.

We further derived the equation for the time constant given by

$$\text{Time Constant} = \frac{2C_d}{\left\{ \int_{-\infty}^{\infty} \left(\frac{S'_\alpha(u)}{Z(u)} \right) \overline{S'_\alpha}(u) du + \int_{-\infty}^{\infty} \left(\frac{S'_\beta(u)}{Z(u)} \right) \overline{S'_\beta}(u) du \right\}}$$

The time constant will be used to calculate and plot the exponential decay of capacitor voltage difference v_δ using the theory developed in Chapter 4.

The design of the output filter was discussed and the equation for the inductance of the filter inductor is given by

$$L = \frac{m_a v_t}{2f_s \Delta i_{max}} (1 - m_a)$$

This equation is used to determine the parameters of the filter inductor and filter capacitor for the simulation of the practical converter discussed in Chapter 5.

Finally we gave the equations that will be used in determining the parameters of the balancing circuit.

Chapter 4

Spectra of the switching functions

In this chapter we analyse the switching functions of the NPC converter under the APOD, POD and PD PWM strategies in order to prove the natural balancing of DC-capacitor voltages. We develop a mathematical model using Carrara's PWM technique and Bennet's geometric technique. We then use Bowe's double Fourier series method to calculate the coefficients of the switching functions. We further derive Fourier series expansions of the switching functions. These results are then used to plot the harmonics of the switching functions using the Matlab and Maple packages. Using the theory developed we then prove that the difference in DC-capacitor voltage v_δ decays to zero under steady-state conditions. Throughout our analysis we assume that the frequency modulation ratio(m_f) is given by

$$m_f = \frac{f_s}{f_1} = 3k$$

where

f_s is the switching frequency

f_1 is the fundamental frequency and

k is an integer.

4.1 Theoretical Analysis using APOD/POD PWM technique

For the three-level three-phase NPC inverter, alternative phase opposition disposition (APOD) and phase opposition disposition(POD) are equivalent. In this section we study the switching functions of the three-level three-phase NPC inverter using APOD/POD PWM strategy. For an NPC inverter with 3 levels, 3-1 triangular carriers with the same frequency and amplitude are arranged so that they fully occupy contiguous bands in the range of $+\pi$ and $-\pi$. A sinusoidal reference centred in the middle of the carrier set is then compared with each carrier to determine the voltage level that the converter should

switch to.

In the APOD/POD PWM strategy the carriers above the reference zero point are out of phase with those below the zero point by 180° . To comply with the requirements for the three-phase system, we use three 120° phase-shifted modulating sinusoids.

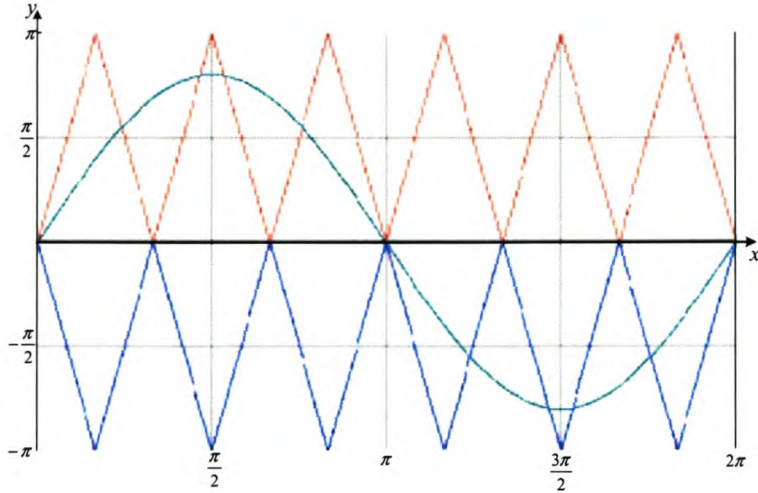


Figure 4.1: Carrier and reference waveform using APOD/POD strategy

The surface of Figure 4.1 is defined by a two-variable function $F(x, y)$ where $x = \omega_s t$ and $y = \omega_1 t$. The surface defined by $F(x, y)$ is composed of an infinite number of parallel walls with heights ranging from $+V_t/2$, 0 to $-V_t/2$. $F(x, y)$ assumes $+V_t/2$ and 0 for values above the zero reference and $-V_t/2$ and 0 for values below the zero reference. That is:

$$F(x, y) = \begin{cases} +\frac{V_t}{2} & if \quad 0 \leq y \leq \text{sinusoidal reference} \\ -\frac{V_t}{2} & if \quad \text{sinusoidal reference} \leq y \leq 0 \\ 0 & if \quad 0 \leq \text{sinusoidal reference} \leq y \leq \pi \\ 0 & if \quad -\pi \leq y \leq \text{sinusoidal reference} \leq 0 \end{cases} \quad (4.1)$$

Figure 4.2 shows the building of the mathematical model. This is done by stretching the triangular carrier by turning it at the first corner from the origin. The resulting triangular carriers will occupy regions between π and 2π for the carrier above the zero reference and $-\pi$ and -2π for the carrier below the zero reference.

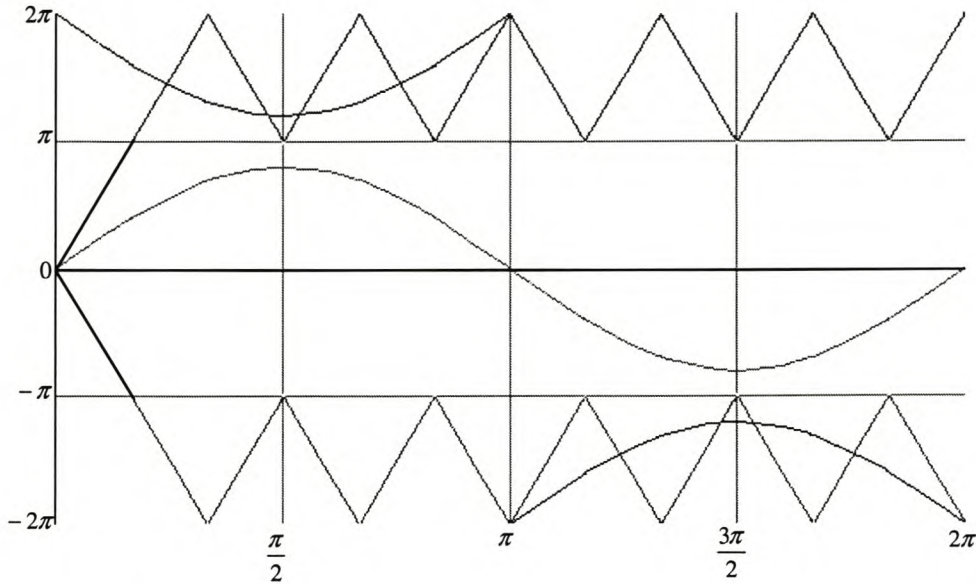


Figure 4.2: Building of mathematical model by stretching triangular carriers

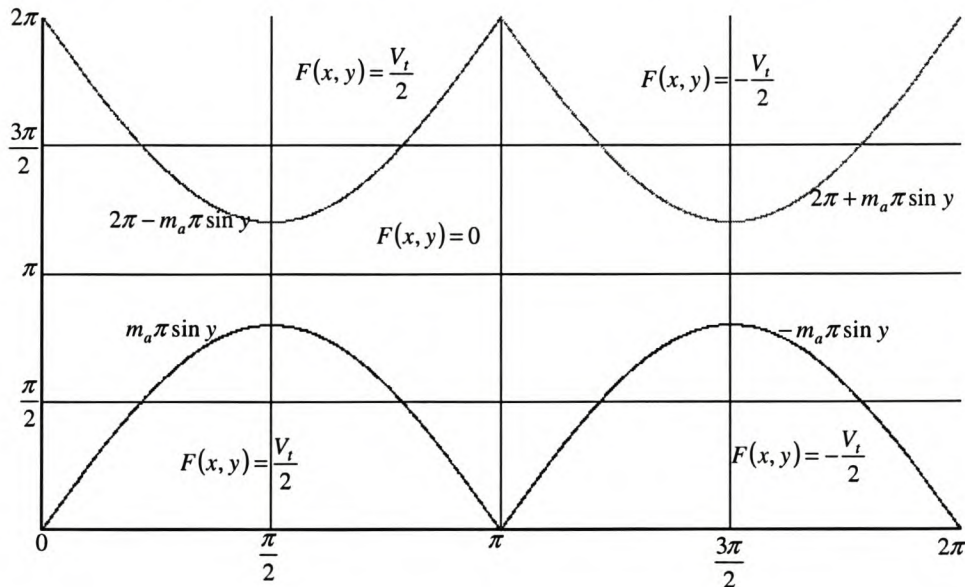


Figure 4.3: APOD/POD mathematical model for three-level NPC inverter

Now we superimpose the walls in Figure 4.2 to obtain final results of added functions $F(x, y)$ and equations for the resulting walls shown in Figure 4.3; m_a is the modulating index given by

$$m_a = \frac{\hat{V}_{sin}}{\hat{V}_{tri}}$$

where \hat{V}_{sin} is the peak value of the sinusoidal signal and \hat{V}_{tri} is the amplitude of the triangular signal.

4.1.1 Spectral Analysis for Harmonics

Time-varying waveforms can be described by an infinite series of harmonic components, but the non-periodic nature of PWM switched waveform makes the determination of these components difficult. This problem was first solved for communication theory by Bennet [17] and then adapted for use with power converter systems by Bowes [18] by representing the switched waveform as a two-dimensional function of the carrier and reference waveforms. The function is periodic in both dimensions even if the switched waveform is not periodic, and hence can be expressed in general harmonic form as a double Fourier series [17] given by equation 4.2

$$\begin{aligned} F(x, y) = & \frac{1}{2}A_{00} + \sum_{n=1}^{\infty} \{A_{0n}\cos(ny) + B_{0n}\sin(ny)\} + \sum_{m=1}^{\infty} \{A_{m0}\cos(mx) + B_{m0}\sin(mx)\} \\ & + \sum_{m=1}^{\infty} \sum_{\substack{n=-\infty \\ n \neq 0}}^{\infty} \{A_{mn}\cos(mx + ny) + B_{mn}\sin(mx + ny)\} \end{aligned} \quad (4.2)$$

In this section the double Fourier series technique is used to evaluate the harmonics of the switching functions obtained with the APOD/POD PWM strategy. This involves the calculation of the complex Fourier coefficients of the double Fourier series expansions of these functions based on the regions of Figure 4.3 for the analysis of S_{α} and S_{β} , and Figure 4.6 for the analysis of S'_{α} and S'_{β} . The harmonic coefficients of this series are obtained by evaluating the double integration for APOD/POD PWM strategy. This section is divided into two subsections to cover these two cases.

Case of s_{α} and s_{β}

For the analysis of switching functions s_{α} and s_{β} we make use of Figure 4.3 and the coefficient [17] is given by

$$C_{mn} = A_{mn} + jB_{mn} = \frac{1}{2\pi^2} \int_{-\pi}^{\pi} \int_{-\pi}^{\pi} F(x, y) e^{j(mx+ny)} dx dy$$

where $x = \omega_s t$, $y = \omega_1 t$.

The coefficients are given by equations 4.3, 4.4 and 4.5. Detailed calculations of the coefficients are shown in Appendix A.1.

For $m = 0$

$$A_{0n} + jB_{0n} = \frac{V_t m_a}{2\pi} \frac{(e^{2j\pi n} - 1)}{(n^2 - 1)} \quad (4.3)$$

For $m = 0$ and $n = 1$

$$A_{01} + jB_{01} = \frac{jV_t m_a}{2} \quad (4.4)$$

For $m \neq 0$

$$A_{mn} + jB_{mn} = \frac{-jV_t}{2m\pi} e^{jn\pi} \{ J_n(m\pi m_a) - (-1)^n J_n(m\pi m_a) \} \quad (4.5)$$

where J is a Bessel function given by

$$J_n(m\pi m_a) = \frac{1}{2\pi} \int_{-\pi}^{\pi} e^{-i(m\pi m_a)} e^{in\theta} d\theta$$

with $J_{-n}(-m\pi m_a) = J_n(m\pi m_a)$ and $J_{-n}(m\pi m_a) = (-1)^n J_n(m\pi m_a)$

The results can be interpreted as harmonics occurring as sidebands around integer multiples of the switching frequency. The results also contain a fundamental component. From Figure 4.4 f_s , $2f_s$ and $3f_s$ are integer multiples of switching frequency (f_s) where the coefficients of f_s represent the values of m in equation 4.5 and $f_s + 1$, $2f_s + 3$ and $3f_s - 2$ are the sideband values where 1, 3 and -3 respectively represent the values of n in equation 4.5. Fundamental frequency is given by f_1 .

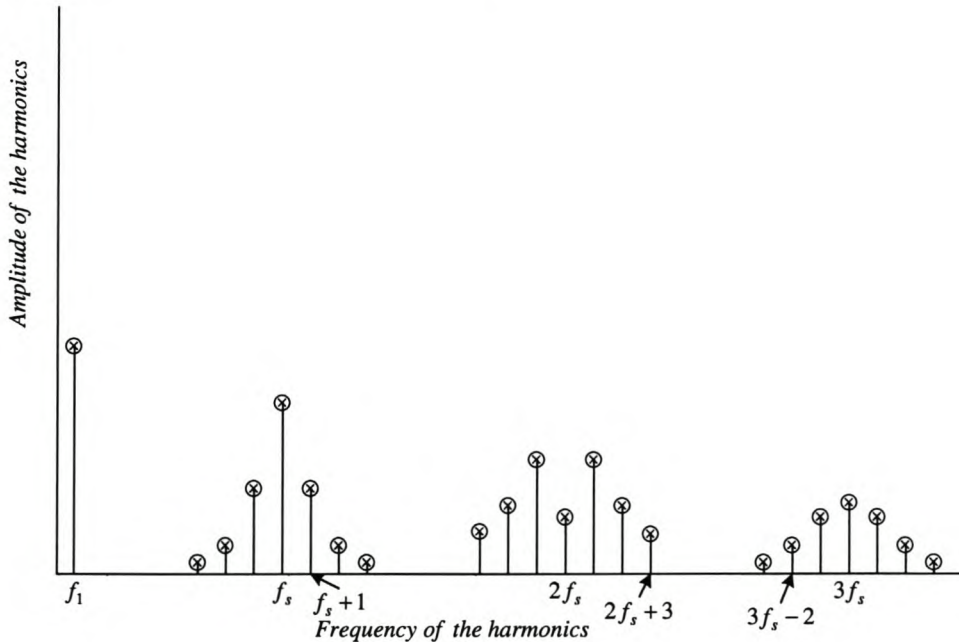


Figure 4.4: Harmonics

The Fourier series of the line-to-centre-point output voltages for phases A, B and C of the NPC converter are given by equations 4.6, 4.7 and 4.8. This we obtain by making use of the fact that the three output voltages are identical copies of each other shifted by 120 degrees in phase.

$$\begin{aligned}
s_a(t) &= \frac{1}{2}A_{00} + \sum_{n=1}^{\infty} (A_{0n} \cos n\omega_1 t + B_{0n} \sin n\omega_1 t) \\
&\quad + \sum_{m=1}^{\infty} (A_{m0} \cos m\omega_s t + B_{m0} \sin m\omega_s t) \\
&\quad + \sum_{m=1}^{\infty} \sum_{n=\pm 1}^{\pm \infty} (A_{mn} \cos ((m\omega_s + n\omega_1) t) + B_{mn} \sin ((m\omega_s + n\omega_1) t)) \tag{4.6}
\end{aligned}$$

$$\begin{aligned}
s_b(t) &= \frac{1}{2}A_{00} + \sum_{n=1}^{\infty} \left(A_{0n} \cos n\omega_1 \left(t - \frac{2\pi}{3\omega_1} \right) + B_{0n} \sin n\omega_1 \left(t - \frac{2\pi}{3\omega_1} \right) \right) \\
&\quad + \sum_{m=1}^{\infty} \left(A_{m0} \cos m\omega_s \left(t - \frac{2\pi}{3\omega_s} \right) + B_{m0} \sin m\omega_s \left(t - \frac{2\pi}{3\omega_1} \right) \right) \\
&\quad + \sum_{m=1}^{\infty} \sum_{n=\pm 1}^{\pm \infty} \left\{ A_{mn} \cos \left((m\omega_s + n\omega_1) \left(t - \frac{2\pi}{3\omega_1} \right) \right) \right. \\
&\quad \left. + B_{mn} \sin \left((m\omega_s + n\omega_1) \left(t - \frac{2\pi}{3\omega_1} \right) \right) \right\} \tag{4.7}
\end{aligned}$$

$$\begin{aligned}
s_c(t) &= \frac{1}{2}A_{00} + \sum_{n=1}^{\infty} \left(A_{0n} \cos n\omega_1 \left(t + \frac{2\pi}{3\omega_1} \right) + B_{0n} \sin n\omega_1 \left(t + \frac{2\pi}{3\omega_1} \right) \right) \\
&\quad + \sum_{m=1}^{\infty} \left(A_{m0} \cos m\omega_s \left(t + \frac{2\pi}{3\omega_s} \right) + B_{m0} \sin m\omega_s \left(t + \frac{2\pi}{3\omega_1} \right) \right) \\
&\quad + \sum_{m=1}^{\infty} \sum_{n=\pm 1}^{\pm \infty} \left\{ A_{mn} \cos \left((m\omega_s + n\omega_1) \left(t + \frac{2\pi}{3\omega_1} \right) \right) \right. \\
&\quad \left. + B_{mn} \sin \left((m\omega_s + n\omega_1) \left(t + \frac{2\pi}{3\omega_1} \right) \right) \right\} \tag{4.8}
\end{aligned}$$

From section 3.1 of Chapter 3 we know that

$$\begin{aligned}
\begin{bmatrix} s_\alpha \\ s_\beta \end{bmatrix} &= A \begin{bmatrix} s_a \\ s_b \\ s_c \end{bmatrix} = \sqrt{\frac{2}{3}} \begin{bmatrix} 1 & -1/2 & -1/2 \\ 0 & \sqrt{3}/2 & -\sqrt{3}/2 \end{bmatrix} \begin{bmatrix} s_a \\ s_b \\ s_c \end{bmatrix} \\
&= \sqrt{\frac{2}{3}} \begin{bmatrix} s_a - s_b/2 - s_c/2 \\ \frac{\sqrt{3}}{2}s_b - \frac{\sqrt{3}}{2}s_c \end{bmatrix}
\end{aligned}$$

which can be written as

$$s_\alpha = \sqrt{\frac{2}{3}} (s_a - s_b/2 - s_c/2)$$

and

$$\begin{aligned}
s_\beta &= \sqrt{\frac{2}{3}} \frac{\sqrt{3}}{2} (s_b - s_c) \\
&= \frac{1}{\sqrt{2}} (s_b - s_c)
\end{aligned}$$

Similarly since

$$\begin{bmatrix} s'_\alpha \\ s'_\beta \end{bmatrix} = A \begin{bmatrix} |s_a| \\ |s_b| \\ |s_c| \end{bmatrix} = \sqrt{\frac{2}{3}} \begin{bmatrix} 1 & -1/2 & -1/2 \\ 0 & \sqrt{3}/2 & -\sqrt{3}/2 \end{bmatrix} \begin{bmatrix} |s_a| \\ |s_b| \\ |s_c| \end{bmatrix}$$

$$= \sqrt{\frac{2}{3}} \begin{bmatrix} |s_a| - |s_b|/2 - |s_c|/2 \\ \frac{\sqrt{3}}{2}|s_b| - \frac{\sqrt{3}}{2}|s_c| \end{bmatrix}$$

which can be written as

$$s'_\alpha = \sqrt{\frac{2}{3}} (|s_a| - |s_b|/2 - |s_c|/2)$$

and

$$\begin{aligned} s'_\beta &= \sqrt{\frac{2}{3}} \frac{\sqrt{3}}{2} (|s_b| - |s_c|) \\ &= \frac{1}{\sqrt{2}} (|s_b| - |s_c|) \end{aligned}$$

Using derivations discussed in Appendix A.2 we obtain Fourier series equation for s_α given by

$$s_\alpha = \sqrt{\frac{3}{2}} \left[\sum_{\substack{n=1 \\ n \neq 3k}}^{\infty} \{A_{0n} \cos n\omega_1 t + B_{0n} \sin n\omega_1 t\} \right. \\ \left. + \sum_{m=1}^{\infty} \sum_{\substack{n=\pm 1 \\ n \neq 3k}}^{\pm \infty} \{A_{mn} \cos ((m\omega_s + n\omega_1) t) + B_{mn} \sin ((m\omega_s + n\omega_1) t)\} \right] \quad (4.9)$$

Similarly using derivations discussed in Appendix A.3 we obtain Fourier series equation for s_β given by

$$s_\beta = \sqrt{\frac{3}{2}} \left[\sum_{\substack{n=1 \\ n=3k+1}}^{\infty} \left\{ A_{0n} \cos \left(n\omega_1 t - \frac{\pi}{2} \right) + B_{0n} \sin \left(n\omega_1 t - \frac{\pi}{2} \right) \right\} \right. \\ - \sum_{\substack{n=1 \\ n=3k+2}}^{\infty} \left\{ A_{0n} \cos \left(n\omega_1 t - \frac{\pi}{2} \right) + B_{0n} \sin \left(n\omega_1 t - \frac{\pi}{2} \right) \right\} \\ + \sum_{m=1}^{\infty} \left[\sum_{\substack{n=\pm 1 \\ n=3k+1}}^{\pm \infty} \left\{ A_{mn} \cos \left((m\omega_s t + n\omega_1 t) - \frac{\pi}{2} \right) + B_{mn} \cos \left((m\omega_s t + n\omega_1 t) - \frac{\pi}{2} \right) \right\} \right. \\ \left. - \sum_{\substack{n=\pm 1 \\ n=3k+2}}^{\pm \infty} \left\{ A_{mn} \cos \left((m\omega_s t + n\omega_1 t) - \frac{\pi}{2} \right) + B_{mn} \cos \left((m\omega_s t + n\omega_1 t) - \frac{\pi}{2} \right) \right\} \right] \right] \quad (4.10)$$

for $m_f = \frac{\omega_s}{\omega_1} = 3k$ and $n \neq 3k$ where k is an integer.

Using equations 4.3, 4.4, 4.5 and 4.9 and the Matlab package we obtain the harmonics for S_α shown in Figure 4.5. Similarly using equations 4.3, 4.4, 4.5 and 4.10 and the Matlab package we obtain the harmonics for S_β shown in Figure 4.5. The Matlab program used to generate Figure 4.5 is shown in Appendix A.4. The simulation parameters are given by Table 4.1.

Table 4.1: *Simulation parameters for S_α and S_β under APOD/POD*

<i>DC – bus voltage</i>	V_t	800 V
<i>DC – bus capacitance</i>	C_d	2 500 μF
<i>Switching frequency</i>	f_s	6 kHz
<i>Modulation index</i>	m_a	0.8
<i>Filter inductance</i>	L	500 μH
<i>Filter capacitance</i>	C	100 μF
<i>Load resistance</i>	R	10 Ω

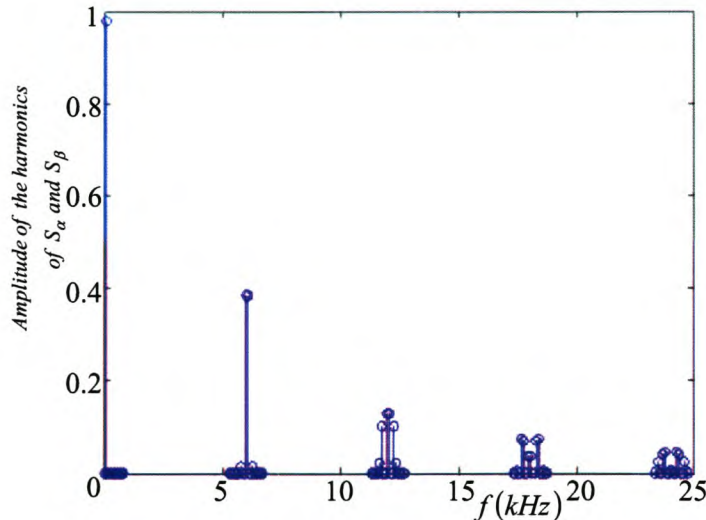


Figure 4.5: *Harmonics of S_α and S_β derived from theory*

The magnitudes of harmonics for S_β and S_α are the same, except that they are out of phase by $\pi/2$. Furthermore, the harmonics for both S_β and S_α do not contain third-order harmonics and are centred around the fundamental frequency and the integer multiples of the switching frequency.

Case of s'_α and s'_β

Since

$$\begin{bmatrix} s'_\alpha \\ s'_\beta \end{bmatrix} = \sqrt{\frac{2}{3}} \begin{bmatrix} |s_a| - |s_b|/2 - |s_c|/2 \\ \frac{\sqrt{3}}{2} |s_b| - \frac{\sqrt{3}}{2} |s_c| \end{bmatrix}$$

the wall of height $-V_t/2$ is replaced by one with height $V_t/2$ for the analysis of s'_α and s'_β . Thus for this case Figure 4.3 is modified to Figure 4.6. In this subsection we follow the same procedure used in the analysis for s_α and s_β .

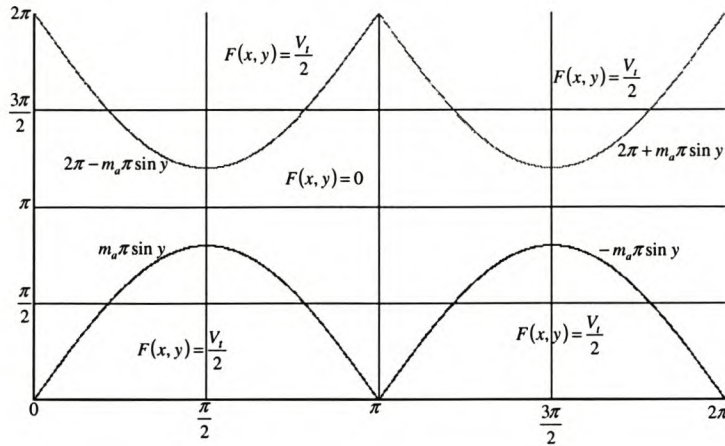


Figure 4.6: APOD/POD mathematical model for three-level NPC inverter

For the analysis of switching functions s'_α and s'_β we make use of Figure 4.6 and the coefficient [17] is given by

$$C_{mn} = A_{mn} + jB_{mn} = \frac{1}{2\pi^2} \int_{-\pi}^{\pi} \int_{-\pi}^{\pi} F(x, y) e^{j(mx+ny)} dx dy$$

where $x = \omega_s t$, $y = \omega_1 t$

The coefficients are given by equations 4.11, 4.12 and 4.13. Detailed calculations of the coefficients are shown in Appendix A.5.

For $m = 0$

$$A_{0n} + jB_{0n} = -\frac{1}{2} V_t m_a \left\{ \frac{2e^{jn\pi} + 1 + e^{2jn\pi}}{\pi(n^2 - 1)} \right\} \quad (4.11)$$

For $m = 0$ and $n = 1$

$$\begin{aligned} A_{01} + jB_{01} &= \frac{V_t}{4\pi^2} \left[\int_0^\pi e^{jy} (2m_a \pi \sin y) dy + \int_\pi^{2\pi} e^{jy} (-2m_a \pi \sin y) dy \right] \\ &= 0 \end{aligned} \quad (4.12)$$

For $m \neq 0$

$$A_{mn} + jB_{mn} = \frac{-jV_t}{4\pi m} [J_{-n}(m\pi m_a) - jE_{-n}(m\pi m_a) - J_{-n}(-m\pi m_a) + jE_{-n}(-m\pi m_a)] \{1 + (-1)^n\} \quad (4.13)$$

where J is an Anger function [36], [37] given by

$$J_n(m\pi m_a) = \frac{1}{\pi} \int_0^\pi \cos((m\pi m_a) \sin \theta - n\theta) d\theta$$

and E is a Weber function [36], [37] given by

$$E_n(m\pi m_a) = -\frac{1}{\pi} \int_0^\pi \sin((m\pi m_a) \sin \theta - n\theta) d\theta$$

Since double Fourier series for s'_α and s_α are the same except for the coefficients, we have

$$s'_\alpha = \sqrt{\frac{3}{2}} \left[\sum_{\substack{n=1 \\ n \neq 3k}}^{\infty} \{A_{0n} \cos n\omega_1 t + B_{0n} \sin n\omega_1 t\} + \sum_{m=1}^{\infty} \sum_{\substack{n=\pm 1 \\ n \neq 3k}}^{\pm \infty} \{A_{mn} \cos((m\omega_s + n\omega_1)t) + B_{mn} \sin((m\omega_s + n\omega_1)t)\} \right] \quad (4.14)$$

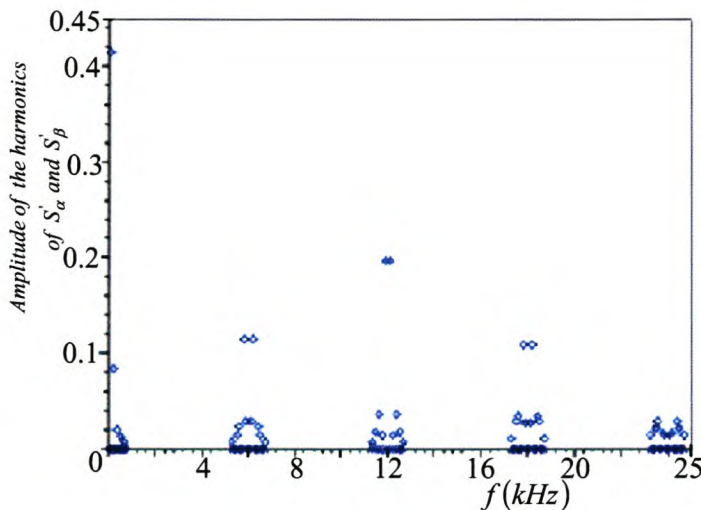
Similarly since double Fourier series for s'_β and s_β are the same except for the coefficients, we have

$$s'_\beta = \sqrt{\frac{3}{2}} \left[\sum_{\substack{n=1 \\ n=3k+1}}^{\infty} \left\{ A_{0n} \cos \left(n\omega_1 t - \frac{\pi}{2} \right) + B_{0n} \sin \left(n\omega_1 t - \frac{\pi}{2} \right) \right\} - \sum_{\substack{n=1 \\ n=3k+2}}^{\infty} \left\{ A_{0n} \cos \left(n\omega_1 t - \frac{\pi}{2} \right) + B_{0n} \sin \left(n\omega_1 t - \frac{\pi}{2} \right) \right\} + \sum_{m=1}^{\infty} \left[\sum_{\substack{n=\pm 1 \\ n=3k+1}}^{\pm \infty} \left\{ A_{mn} \cos \left((m\omega_s t + n\omega_1 t) - \frac{\pi}{2} \right) + B_{mn} \cos \left((m\omega_s t + n\omega_1 t) - \frac{\pi}{2} \right) \right\} - \sum_{\substack{n=\pm 1 \\ n=3k+2}}^{\pm \infty} \left\{ A_{mn} \cos \left((m\omega_s t + n\omega_1 t) - \frac{\pi}{2} \right) + B_{mn} \cos \left((m\omega_s t + n\omega_1 t) - \frac{\pi}{2} \right) \right\} \right] \right] \quad (4.15)$$

Using equations 4.11, 4.12, 4.13 and 4.14 and the Maple package we obtain the harmonics for S'_α shown in Figure 4.7. Similarly using equations 4.11, 4.12, 4.13 and 4.15 and the Maple package we obtain the harmonics for S'_β shown in Figure 4.7. The Maple program used to generate Figure 4.7 is shown in Appendix A.6. The simulation parameters are given by Table 4.2.

Table 4.2: Simulation parameters of S'_α and S'_β under APOD/POD

<i>DC – bus voltage</i>	V_t	800 V
<i>DC – bus capacitance</i>	C_d	2 500 μF
<i>Switching frequency</i>	f_s	6 kHz
<i>Modulation index</i>	m_a	0.8
<i>Filter inductance</i>	L	500 μH
<i>Filter capacitance</i>	C	100 μF
<i>Load resistance</i>	R	10 Ω

**Figure 4.7:** Harmonics of S'_α and S'_β derived from theory

The magnitudes of harmonics for S'_β and S'_α are the same, except that they are out of phase by $\pi/2$. Furthermore, the harmonics for both S'_β and S'_α do not contain third-order harmonics and are centred around the fundamental frequency and the integer multiples of the switching frequency. Except for the fundamental frequency the largest harmonic occurs at twice the switching frequency.

4.1.2 Steady-State Balancing using $F_1(\omega)$ and $F_2(\omega)$

In this section we use the theory developed in Chapter 3 and subsection 4.1.1 of this chapter to conclude that the DC-capacitor voltages of the NPC inverter balance naturally in the steady state.

From equation 3.15 given by

$$\frac{V_\delta}{V_t} = \frac{\int_{-\infty}^{\infty} \frac{F_1(\omega)}{Z(\omega)} d\omega}{\int_{-\infty}^{\infty} \frac{F_2(\omega)}{Z(\omega)} d\omega}, \quad (4.16)$$

where

$$F_1(\omega) = S_\alpha(\omega) \overline{S'_\alpha}(\omega) + S_\beta(\omega) \overline{S'_\beta}(\omega) \quad (4.17)$$

and

$$F_2(\omega) = S'_\alpha(\omega) \overline{S'_\alpha}(\omega) + S'_\beta(\omega) \overline{S'_\beta}(\omega) \quad (4.18)$$

we know that the values of $F_1(\omega)$ and $F_2(\omega)$ are dependent on the way the spectra of $S_\alpha(\omega)$ and $\overline{S'_\alpha}(\omega)$ as well as $S_\beta(\omega)$ and $\overline{S'_\beta}(\omega)$ overlap in the frequency domain. Orthogonality of these two sets of spectra would imply that the DC-bus voltages balance in the steady state.

From subsection 4.1.1 we arrive at the following results in the analysis of switching functions. The following holds for the results that follow:

H is a struve function [36], [37] given by

$$H_0(m\pi m_a) = \sum_{k=0}^{\infty} \frac{\frac{1}{2}(m\pi m_a)^{2k+1}}{\left(\Gamma(k + \frac{3}{2})\right)^2}$$

and Γ is a Gamma function [36], [37] given by

$$\Gamma\left(k + \frac{3}{2}\right) = \int_0^{\infty} e^{-\phi} \phi^{(k+\frac{3}{2})-1} d\phi$$

The results are as follows:

For $n = 0$

$$S_\alpha(\omega) = 0$$

$$\overline{S'_\alpha}(\omega) = \pm \frac{1}{2} \frac{j\sqrt{6}V_t H_0(m\pi m_a)}{m\pi}$$

$$S'_\alpha(\omega) = \pm \frac{1}{2} \frac{j\sqrt{6}V_t H_0(m\pi m_a)}{m\pi}$$

$$S_\beta(\omega) = 0$$

$$\overline{S'_\beta}(\omega) = \pm \frac{1}{2} \frac{j\sqrt{6}V_t H_0(m\pi m_a)}{m\pi}$$

$$S'_\beta(\omega) = \pm \frac{1}{2} \frac{j\sqrt{6}V_t H_0(m\pi m_a)}{m\pi}$$

For n even

$$S_\alpha(\omega) = 0$$

$$S'_\alpha(\omega) = \pm \frac{1}{4} \frac{\sqrt{6}V_t(-E_n(-m\pi m_a) + E_n(m\pi m_a))}{m\pi}$$

$$\overline{S'_\alpha}(\omega) = \pm \frac{1}{4} \frac{\sqrt{6}V_t(-E_n(-m\pi m_a) + E_n(m\pi m_a))}{m\pi}$$

$$S_\beta(\omega) = 0$$

$$S'_\beta(\omega) = \pm \frac{1}{4} \frac{\sqrt{6}V_t(-E_n(-m\pi m_a) + E_n(m\pi m_a))}{m\pi}$$

$$\overline{S'_\beta}(\omega) = \pm \frac{1}{4} \frac{\sqrt{6}V_t(-E_n(-m\pi m_a) + E_n(m\pi m_a))}{m\pi}$$

For n odd

$$S_\alpha(\omega) = \pm \frac{1}{2} \frac{j\sqrt{6}V_t J_n(m\pi m_a)}{m\pi}$$

$$S'_\alpha(\omega) = 0$$

$$\overline{S'_\alpha}(\omega) = 0$$

$$S_\beta(\omega) = \pm \frac{1}{2} \frac{j\sqrt{6}V_t J_n(m\pi m_a)}{m\pi}$$

$$S'_\beta(\omega) = 0$$

$$\overline{S'_\beta}(\omega) = 0$$

Substituting the above results into equation 4.17 and 4.18 we have the following

$$\begin{aligned} F_1(\omega) &= S_\alpha(\omega) \overline{S'_\alpha}(\omega) + S_\beta(\omega) \overline{S'_\beta}(\omega) \\ &= 0 \end{aligned} \tag{4.19}$$

$$\begin{aligned} F_2(\omega) &= |S'_\alpha(\omega)|^2 + |S'_\beta(\omega)|^2 \\ &= \left\{ \begin{array}{ll} 2 \left| \frac{1}{2} \frac{j\sqrt{6}V_t H_0(m\pi m_a)}{m\pi} \right|^2 & if \quad n = 0 \\ 2 \left| \frac{1}{2} \frac{j\sqrt{6}V_t J_n(m\pi m_a)}{m\pi} \right|^2 & if \quad n \text{ is even} \\ 0 & if \quad n \text{ is odd} \end{array} \right\} \\ &\neq 0 \end{aligned} \tag{4.20}$$

We now substitute equation 4.19 into equation 4.16 and obtain the following results

$$\begin{aligned}\frac{V_\delta}{V_t} &= \frac{\int_{-\infty}^{\infty} \frac{F_1(\omega)}{Z(\omega)} d\omega}{\int_{-\infty}^{\infty} \frac{F_2(\omega)}{Z(\omega)} d\omega} \\ &= \frac{\int_{-\infty}^{\infty} 0 d\omega}{\int_{-\infty}^{\infty} \frac{F_2(\omega)}{Z(\omega)} d\omega} \\ &= 0\end{aligned}$$

These results show that the difference in capacitor voltages v_δ decays to zero in the steady state.

Figures 4.8 and 4.9 show the harmonics for absolute values of $F_1(\omega)$ and $F_2(\omega)$ respectively derived from theory using the Maple package. The Maple programs used to obtain these figures are shown in Appendix A.7 and A.8 respectively. Table 4.3 show the parameters used to obtain these figures.

Table 4.3: *Simulation parameters for F_1 and F_2 under APOD/POD*

<i>DC – bus voltage</i>	V_t	800 V
<i>DC – bus capacitance</i>	C_d	2 500 μF
<i>Switching frequency</i>	f_s	6 kHz
<i>Modulation index</i>	m_a	0.8
<i>Filter inductance</i>	L	500 μH
<i>Filter capacitance</i>	C	100 μF
<i>Load resistance</i>	R	10 Ω

The harmonics of $|F_1|$ are zero as expected and the harmonics of $|F_2|$ have the largest value at twice the switching frequency.

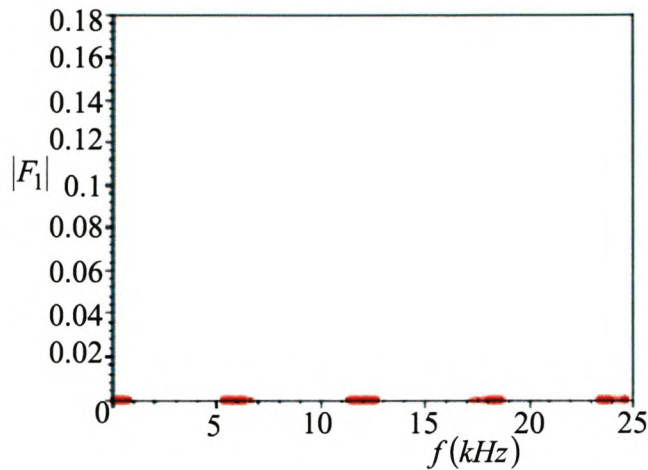


Figure 4.8: Absolute value of switching function F_1

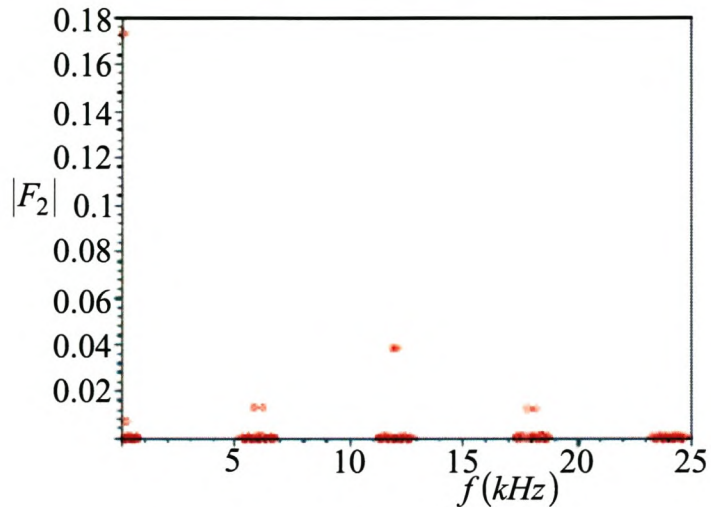


Figure 4.9: Absolute value of switching function F_2

4.2 Theoretical Analysis using PD PWM technique

In this section the PD strategy is considered. Figure 4.10 shows the carrier and reference waveform for a three-level NPC inverter using PD strategy.

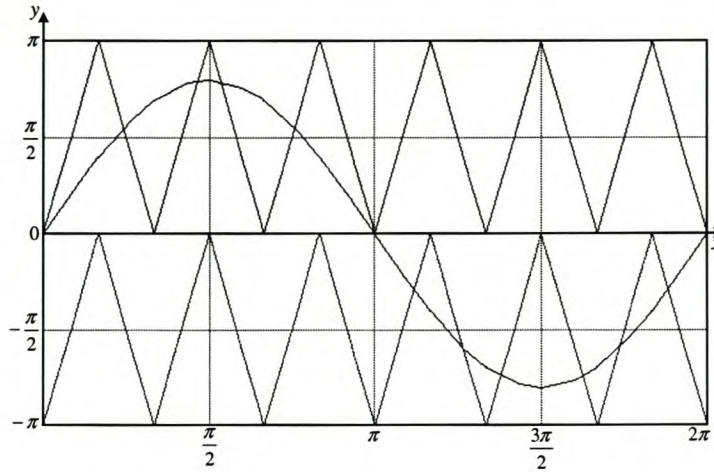


Figure 4.10: Carrier and reference waveform for three-level NPC inverter using PD strategy

The function $F(x, y)$ assumes $+V_t/2$ and 0 for values above the zero reference and $-V_t/2$ and 0 for values below the zero reference. That is:

$$F(x, y) = \begin{cases} +\frac{V_t}{2} & \text{if } 0 \leq y \leq \text{sinusoidal reference} \\ -\frac{V_t}{2} & \text{if } \text{sinusoidal reference} \leq y \leq 0 \\ 0 & \text{if } 0 \leq \text{sinusoidal reference} \leq y \leq \pi \\ 0 & \text{if } \pi \leq y \leq \text{sinusoidal reference} \leq 0 \end{cases} \quad (4.21)$$

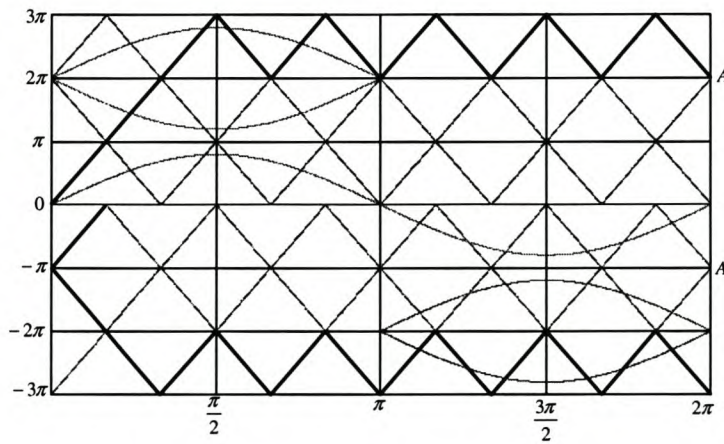


Figure 4.11: Building of mathematical model by stretching triangular carriers

Figure 4.11 shows the building of the mathematical model. This is done by stretching the triangular carrier by turning it twice at the first corner from the origin.

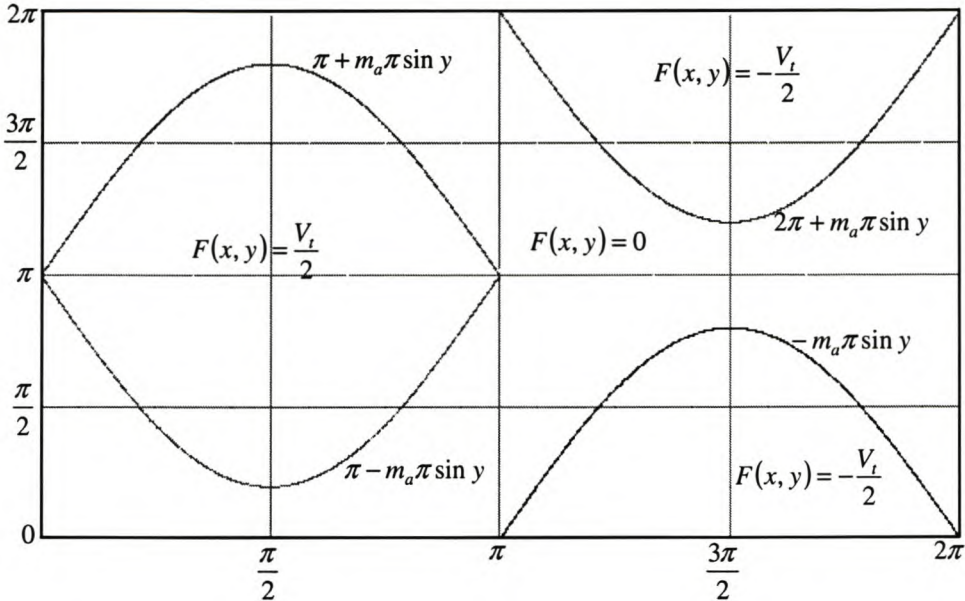


Figure 4.12: PD mathematical model for three-level NPC inverter

Now we superimpose the walls in Figure 4.11 in such a way to have coincidence of the points labeled A. We obtain final results of added functions $F(x, y)$ and equations for the resulting walls shown in Figure 4.12; m_a is the modulating index given by

$$m_a = \frac{\hat{V}_{sin}}{\hat{V}_{tri}}$$

where \hat{V}_{sin} is the peak value of the sinusoidal signal and \hat{V}_{tri} is the amplitude of the triangular signal.

4.2.1 Spectral Analysis for Harmonics

In this section the double Fourier series technique is used to evaluate the harmonics of the switching functions obtained with the PD PWM strategy. This involves the calculation of the complex Fourier coefficients of the double Fourier series expansions of these functions based on the regions of Figure 4.12 for the analysis of S_α and S_β , and for the analysis of S'_α and S'_β . The harmonic coefficients of this series are obtained by evaluating the double integration for PD PWM strategy. This section is divided into two subsections to cover these two cases.

Case of s_α and s_β

For the analysis of switching functions s_α and s_β we make use of Figure 4.12 and the coefficient [17] is given by

$$C_{mn} = A_{mn} + jB_{mn} = \frac{1}{2\pi^2} \int_{-\pi}^{\pi} \int_{-\pi}^{\pi} F(x, y) e^{j(mx+ny)} dx dy$$

The coefficients are given by equations 4.22, 4.23, 4.24 and 4.25. Detailed calculations of the coefficients are shown in Appendix A.9.

For $m = 0$

$$A_{0n} + jB_{0n} = \frac{V_t m_a}{2\pi} \frac{(e^{2j\pi n} - 1)}{(n^2 - 1)} \quad (4.22)$$

For $m = 0$ and $n = 1$

$$A_{01} + jB_{01} = \frac{jV_d m_a}{2} \quad (4.23)$$

For m even

$$A_{mn} + jB_{mn} = \frac{-jV_t}{2m\pi} e^{jn\pi} \{ J_n(m\pi m_a) - (-1)^n J_n(m\pi m_a) \} \quad (4.24)$$

For m odd

$$\begin{aligned} A_{mn} + jB_{mn} = & \frac{-jV_t}{4\pi m} [J_{-n}(-m\pi m_a) - jE_{-n}(-m\pi m_a) - J_{-n}(m\pi m_a) \\ & + jE_{-n}(m\pi m_a)] \{1 + (-1)^n\} \end{aligned} \quad (4.25)$$

Using equations 4.22, 4.23, 4.24, 4.25 and 4.9 and the Maple package we obtain the harmonics for S_α shown in Figure 4.13. Similarly using equations 4.22, 4.23, 4.24 and 4.10 and the Maple package we obtain the harmonics for S_β shown in Figure 4.13. The Maple program used to generate Figure 4.13 is shown in Appendix B.3. The simulation parameters are given by Table 4.4.

Table 4.4: Simulation parameters for S_α and S_β under PD

<i>DC – bus voltage</i>	V_t	800 V
<i>Fundamental frequency</i>	f_1	50 Hz
<i>Switching frequency</i>	f_s	6 kHz
<i>Modulation index</i>	m_a	0.8

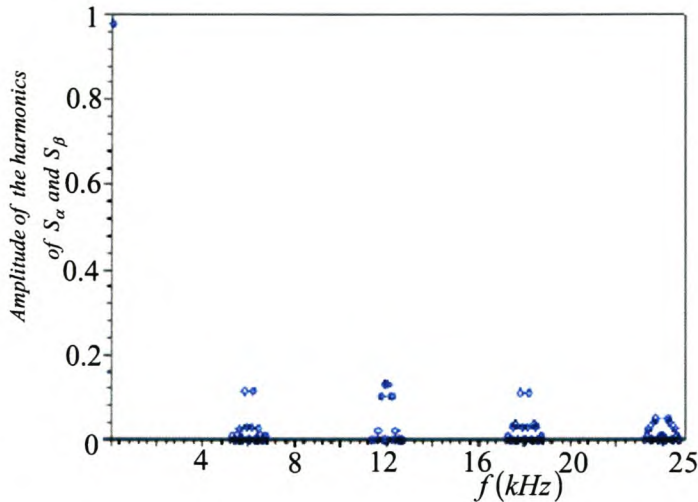


Figure 4.13: Harmonics of S_α and S_β derived from theory

The magnitudes of harmonics for S_β and S_α are the same; except that they are out of phase by $\pi/2$. Furthermore, the harmonics for both S_β and S_α do not contain third-order harmonics and are centred around the fundamental frequency and the integer multiples of the switching frequency.

Case of s'_α and s'_β

Since

$$\begin{bmatrix} s'_\alpha \\ s'_\beta \end{bmatrix} = \sqrt{\frac{2}{3}} \begin{bmatrix} |s_a| - |s_b|/2 - |s_c|/2 \\ \frac{\sqrt{3}}{2}|s_b| - \frac{\sqrt{3}}{2}|s_c| \end{bmatrix}$$

the wall of height $-V_t/2$ is replaced by one with height $V_t/2$. Thus for this case Figure 4.12 is modified to Figure 4.14. In this subsection we follow the same procedure used in the analysis for s_α and s_β .

For the analysis of switching functions s'_α and s'_β we make use of Figure 4.14 and the coefficient [17] is given by

$$C_{mn} = A_{mn} + jB_{mn} = \frac{1}{2\pi^2} \int_{-\pi}^{\pi} \int_{-\pi}^{\pi} F(x, y) e^{j(mx+ny)} dx dy$$

The coefficients are given by equations 4.26, 4.27, 4.28 and 4.29. Detailed calculations of the coefficients are shown in Appendix A.10.

For $m = 0$

$$A_{0n} + jB_{0n} = -\frac{1}{2} V_t m_a \left\{ \frac{2e^{jn\pi} + 1 + e^{2jn\pi}}{\pi(n^2 - 1)} \right\} \quad (4.26)$$

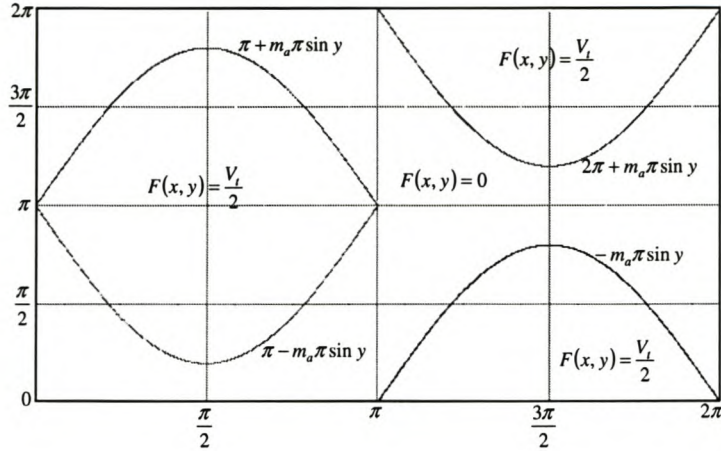


Figure 4.14: PD mathematical model for three-level NPC inverter

For $m = 0$ and $n = 1$

$$\begin{aligned}
 A_{01} + jB_{01} &= \frac{V_t}{4\pi^2} \left[\int_0^\pi e^{jy} (2m_a \pi \sin y) dy + \int_\pi^{2\pi} e^{jy} (-2m_a \pi \sin y) dy \right] \\
 &= 0
 \end{aligned} \tag{4.27}$$

For m even

$$\begin{aligned}
 A_{mn} + jB_{mn} &= \frac{-jV_t}{4\pi m} [J_{-n}(m\pi m_a) - jE_{-n}(m\pi m_a) - J_{-n}(-m\pi m_a) \\
 &\quad + jE_{-n}(-m\pi m_a)] \{1 + (-1)^n\}
 \end{aligned} \tag{4.28}$$

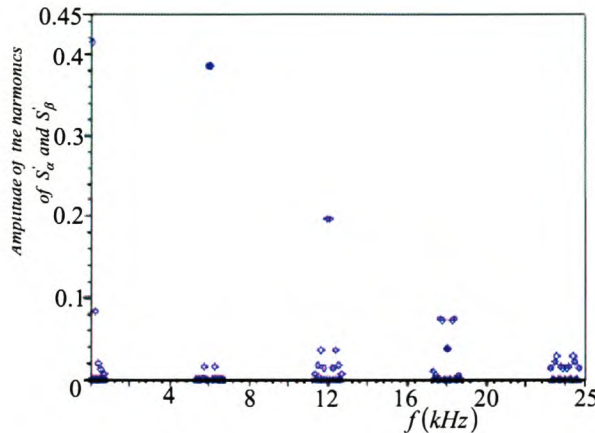
For m odd

$$A_{mn} + jB_{mn} = \frac{-jV_t}{2m\pi} e^{jn\pi} \{(-1)^n J_{-n}(m\pi m_a) - (-1)^n J_n(m\pi m_a)\} \tag{4.29}$$

Using equations 4.26, 4.27, 4.28, 4.29 and 4.14 and the Maple package we obtain the harmonics for S'_α shown in Figure 4.15. Similarly, using equations 4.26, 4.27, 4.28, 4.29 and 4.15 and the Maple package we obtain the harmonics for S'_β shown in Figure 4.15. The Maple program used to generate Figure 4.15 is shown in Appendix B.4. The simulation parameters are given by Table 4.5.

Table 4.5: Simulation parameters for S'_α and S'_β under PD

<i>DC – bus voltage</i>	V_t	800 V
<i>Fundamental frequency</i>	f_1	50 Hz
<i>Switching frequency</i>	f_s	6 kHz
<i>Modulation index</i>	m_a	0.8

**Figure 4.15:** Harmonics of S'_α and S'_β derived from theory

The magnitudes of harmonics for S'_β and S'_α are the same, except that they are out of phase by $\pi/2$. Furthermore, the harmonics for both S'_β and S'_α do not contain third-order harmonics and are centred around the fundamental frequency and the integer multiples of the switching frequency. Except for the fundamental frequency the largest harmonic occurs at twice the switching frequency.

4.2.2 Steady-State Balancing for $F_1(\omega)$ and $F_2(\omega)$

In this section we use the theory developed in Chapter 3 and subsection 4.2.1 of this chapter to conclude that the DC-capacitor voltages of the NPC inverter balance naturally in the steady state. From subsection 4.2.1 we arrive at the following results in the analysis of switching functions.

For m even

For $n = 0$

$$S_\alpha(\omega) = 0$$

$$\overline{S'_\alpha}(\omega) = \pm \frac{1}{2} \frac{j\sqrt{6}V_t H_0(m\pi m_a)}{m\pi}$$

$$S'_\alpha(\omega) = \pm \frac{1}{2} \frac{j\sqrt{6}V_t H_0(m\pi m_a)}{m\pi}$$

$$S_\beta(\omega) = 0$$

$$\overline{S'_\beta}(\omega) = \pm \overline{\frac{1}{2} \frac{j\sqrt{6}V_t H_0(m\pi m_a)}{m\pi}}$$

$$S'_\beta(\omega) = \pm \frac{1}{2} \frac{j\sqrt{6}V_t H_0(m\pi m_a)}{m\pi}$$

For n even

$$S_\alpha(\omega) = 0$$

$$S'_\alpha(\omega) = \pm \frac{1}{4} \frac{\sqrt{6}V_t (-E_{-n}(m\pi m_a) + E_{-n}(-m\pi m_a))}{m\pi}$$

$$\overline{S'_\alpha}(\omega) = \pm \overline{\frac{1}{4} \frac{\sqrt{6}V_t (-E_{-n}(m\pi m_a) + E_{-n}(-m\pi m_a))}{m\pi}}$$

$$S_\beta(\omega) = 0$$

$$S'_\beta(\omega) = \pm \frac{1}{4} \frac{\sqrt{6}V_t (-E_{-n}(m\pi m_a) + E_{-n}(-m\pi m_a))}{m\pi}$$

$$\overline{S'_\beta}(\omega) = \pm \overline{\frac{1}{4} \frac{\sqrt{6}V_t (-E_{-n}(m\pi m_a) + E_{-n}(-m\pi m_a))}{m\pi}}$$

For n odd

$$S_\alpha(\omega) = \pm \frac{1}{2} \frac{j\sqrt{6}V_t J_n(m\pi m_a)}{m\pi}$$

$$S'_\alpha(\omega) = 0$$

$$\overline{S'_\alpha}(\omega) = 0$$

$$S_\beta(\omega) = \pm \frac{1}{2} \frac{j\sqrt{6}V_t J_n(m\pi m_a)}{m\pi}$$

$$S'_\beta(\omega) = 0$$

$$\overline{S'_\beta}(\omega) = 0$$

For m odd

For $n = 0$

$$S_\alpha(\omega) = \pm \frac{1}{2} \frac{j\sqrt{6}V_t H_0(m\pi m_a)}{m\pi}$$

$$\overline{S'_\alpha}(\omega) = 0$$

$$S'_\alpha(\omega) = 0$$

$$S_\beta(\omega) = \pm \frac{1}{2} \frac{j\sqrt{6}V_t H_0(m\pi m_a)}{m\pi}$$

$$\overline{S'_\beta}(\omega) = 0$$

$$S'_\beta(\omega) = 0$$

For n even

$$S_\alpha(\omega) = \pm \frac{1}{4} \frac{\sqrt{6}V_t (-E_{-n}(m\pi m_a) + E_{-n}(-m\pi m_a))}{m\pi}$$

$$S'_\alpha(\omega) = 0$$

$$\overline{S'_\alpha}(\omega) = 0$$

$$S_\beta(\omega) = \pm \frac{1}{4} \frac{\sqrt{6}V_t (-E_{-n}(m\pi m_a) + E_{-n}(-m\pi m_a))}{m\pi}$$

$$S'_\beta(\omega) = 0$$

$$\overline{S'_\beta}(\omega) = 0$$

For n odd

$$S_\alpha(\omega) = 0$$

$$S'_\alpha(\omega) = \pm \frac{1}{2} \frac{j\sqrt{6}V_t J_n(m\pi m_a)}{m\pi}$$

$$\overline{S'_\alpha}(\omega) = \pm \frac{1}{2} \frac{j\sqrt{6}V_t J_n(m\pi m_a)}{m\pi}$$

$$S_\beta(\omega) = 0$$

$$S'_\beta(\omega) = \pm \frac{1}{2} \frac{j\sqrt{6}V_t J_n(m\pi m_a)}{m\pi}$$

$$\overline{S'_\beta}(\omega) = \pm \frac{1}{2} \frac{j\sqrt{6}V_t J_n(m\pi m_a)}{m\pi}$$

Substituting the above results into equation 4.17 and 4.18 we have the following

$$\begin{aligned} F_1(\omega) &= S_\alpha(\omega) \overline{S'_\alpha}(\omega) + S_\beta(\omega) \overline{S'_\beta}(\omega) \\ &= 0 \end{aligned} \tag{4.30}$$

For m even

$$\begin{aligned} F_2(\omega) &= |S'_\alpha(\omega)|^2 + |S'_\beta(\omega)|^2 \\ &= \left\{ \begin{array}{ll} 2 \left| \frac{1}{2} \frac{j\sqrt{6}V_t H_0(m\pi m_a)}{m\pi} \right|^2 & \text{if } n = 0 \\ 2 \left| \frac{1}{4} \frac{\sqrt{6}V_t(-E_{-n}(m\pi m_a) + E_{-n}(-m\pi m_a))}{m\pi} \right|^2 & \text{if } n \text{ is even} \\ 0 & \text{if } n \text{ is odd} \end{array} \right\} \\ &\neq 0 \end{aligned} \quad (4.31)$$

For m odd

$$\begin{aligned} F_2(\omega) &= |S'_\alpha(\omega)|^2 + |S'_\beta(\omega)|^2 \\ &= \left\{ \begin{array}{ll} 2 \left| \frac{1}{2} \frac{j\sqrt{6}V_t H_0(m\pi m_a)}{m\pi} \right|^2 & \text{if } n = 0 \\ 0 & \text{if } n \text{ is even} \\ 2 \left| \frac{1}{4} \frac{\sqrt{6}V_t(-E_{-n}(m\pi m_a) + E_{-n}(-m\pi m_a))}{m\pi} \right|^2 & \text{if } n \text{ is odd} \end{array} \right\} \\ &\neq 0 \end{aligned} \quad (4.32)$$

We now substitute equation 4.30 into equation 4.16 and obtain the following results

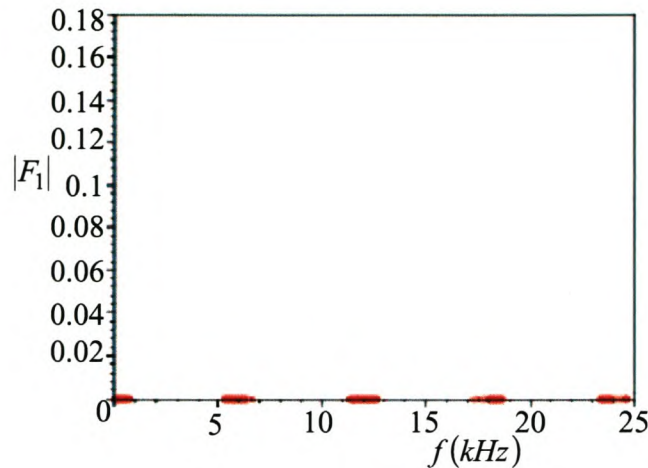
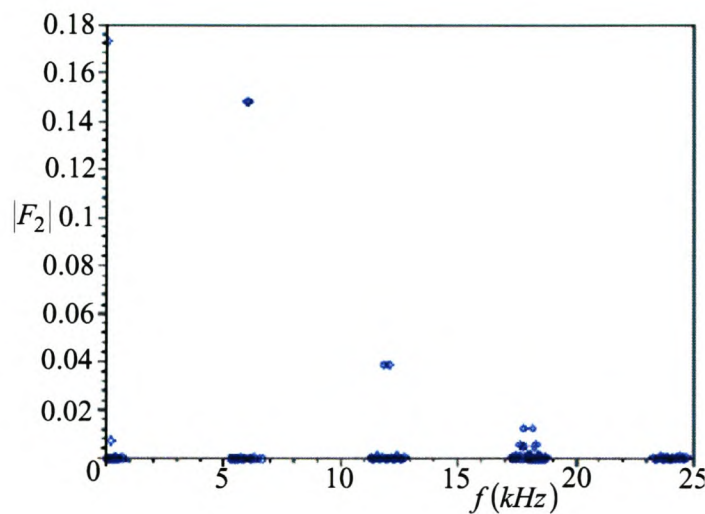
$$\begin{aligned} \frac{V_\delta}{V_t} &= \frac{\int_{-\infty}^{\infty} \frac{F_1(\omega)}{Z(\omega)} d\omega}{\int_{-\infty}^{\infty} \frac{F_2(\omega)}{Z(\omega)} d\omega} \\ &= \frac{\int_{-\infty}^{\infty} 0 d\omega}{\int_{-\infty}^{\infty} \frac{F_2(\omega)}{Z(\omega)} d\omega} \\ &= 0 \end{aligned}$$

These results show that the difference in capacitor voltages v_δ decays to zero in the steady state.

Figures 4.16 and 4.17 show the harmonics for absolute values of $F_1(\omega)$ and $F_2(\omega)$ respectively derived from theory using the Maple package. The Maple programs used to obtain these figures are shown in Appendix B.5 and B.6 respectively. Table 4.6 show the parameters used to obtain these figures.

Table 4.6: Simulation parameters for F_1 and F_2 under PD

<i>DC – bus voltage</i>	V_t	800 V
<i>Fundamental frequency</i>	f_1	50 Hz
<i>Switching frequency</i>	f_s	6 kHz
<i>Modulation index</i>	m_a	0.8

**Figure 4.16:** Absolute value of switching function F_1 **Figure 4.17:** Absolute value of switching function F_2

The harmonics of $|F_1|$ are zero as expected and the harmonics of $|F_2|$ have the largest value at the switching frequency.

4.3 Conclusion

This chapter studied the natural balancing of DC-bus capacitor voltages of the three-level NPC converter under APOD/POD and PD PWM modulation techniques. This was done by theoretically analysing the switching functions of the three-level NPC converter under APOD/POD and PD PWM modulation techniques. We derived equations for the

coefficients of the double Fourier series for the switching functions of the NPC inverter under APOD/POD and PD PWM modulation techniques.

For APOD/POD PWM modulation technique the coefficients for S_α and S_β are given by

$$A_{mn} + jB_{mn} = \frac{-jV_t}{2m\pi} e^{jn\pi} \{ J_n(m\pi m_a) - (-1)^n J_n(m\pi m_a) \} \quad (4.33)$$

where J is a Bessel function.

For S'_α and S'_β the coefficients are given by

$$\begin{aligned} A_{mn} + jB_{mn} = & \frac{-jV_t}{4\pi m} [J_{-n}(m\pi m_a) - jE_{-n}(m\pi m_a) - J_{-n}(-m\pi m_a) \\ & + jE_{-n}(-m\pi m_a)] \{1 + (-1)^n\} \end{aligned} \quad (4.34)$$

where J is an Anger function and E is a Weber function.

For PD PWM modulation technique the coefficients for S_α and S_β are given by

For m even

$$A_{mn} + jB_{mn} = \frac{-jV_t}{2m\pi} e^{jn\pi} \{ J_n(m\pi m_a) - (-1)^n J_n(m\pi m_a) \} \quad (4.35)$$

For m odd

$$\begin{aligned} A_{mn} + jB_{mn} = & \frac{-jV_t}{4\pi m} [J_{-n}(-m\pi m_a) - jE_{-n}(-m\pi m_a) - J_{-n}(m\pi m_a) \\ & + jE_{-n}(m\pi m_a)] \{1 + (-1)^n\} \end{aligned} \quad (4.36)$$

For S'_α and S'_β the coefficients are given by

For m even

$$\begin{aligned} A_{mn} + jB_{mn} = & \frac{-jV_t}{4\pi m} [J_{-n}(m\pi m_a) - jE_{-n}(m\pi m_a) - J_{-n}(-m\pi m_a) \\ & + jE_{-n}(-m\pi m_a)] \{1 + (-1)^n\} \end{aligned} \quad (4.37)$$

For m odd

$$A_{mn} + jB_{mn} = \frac{-jV_t}{2m\pi} e^{jn\pi} \{ (-1)^n J_{-n}(m\pi m_a) - (-1)^n J_n(m\pi m_a) \} \quad (4.38)$$

We further derived equations for S_α , S_β , S'_α and S'_β given by

$$\begin{aligned} S_\alpha &= S'_\alpha \\ &= \sqrt{\frac{3}{2}} \left[\sum_{\substack{n=1 \\ n \neq 3k}}^{\infty} \{ A_{0n} \cos n\omega_1 t + B_{0n} \sin n\omega_1 t \} \right. \\ &\quad \left. + \sum_{m=1}^{\infty} \sum_{\substack{n=\pm 1 \\ n \neq 3k}}^{\pm \infty} \{ A_{mn} \cos ((m\omega_s + n\omega_1) t) + B_{mn} \sin ((m\omega_s + n\omega_1) t) \} \right] \end{aligned} \quad (4.39)$$

$$\begin{aligned}
S_\beta &= S'_\beta \\
&= \sqrt{\frac{3}{2}} \left[\sum_{\substack{n=1 \\ n=3k+1}}^{\infty} \left\{ A_{0n} \cos \left(n\omega_1 t - \frac{\pi}{2} \right) + B_{0n} \sin \left(n\omega_1 t - \frac{\pi}{2} \right) \right\} \right. \\
&\quad - \sum_{\substack{n=1 \\ n=3k+2}}^{\infty} \left\{ A_{0n} \cos \left(n\omega_1 t - \frac{\pi}{2} \right) + B_{0n} \sin \left(n\omega_1 t - \frac{\pi}{2} \right) \right\} \\
&\quad + \sum_{m=1}^{\infty} \left[\sum_{\substack{n=\pm 1 \\ n=3k+1}}^{\pm\infty} \left\{ A_{mn} \cos \left((m\omega_s t + n\omega_1 t) - \frac{\pi}{2} \right) + B_{mn} \cos \left((m\omega_s t + n\omega_1 t) - \frac{\pi}{2} \right) \right\} \right. \\
&\quad \left. \left. - \sum_{\substack{n=\pm 1 \\ n=3k+2}}^{\pm\infty} \left\{ A_{mn} \cos \left((m\omega_s t + n\omega_1 t) - \frac{\pi}{2} \right) + B_{mn} \cos \left((m\omega_s t + n\omega_1 t) - \frac{\pi}{2} \right) \right\} \right] \right]
\end{aligned} \tag{4.40}$$

We proved that the overlap in the frequency domain of two sets of spectra given by $S_\alpha(\omega)$ and $\bar{S}'_\alpha(\omega)$ as well as $S_\beta(\omega)$ and $\bar{S}'_\beta(\omega)$ are orthogonal, which implies that the DC-bus voltages balance in the steady state.

This chapter provided a formal theoretical proof that APOD/POD and PD PWM modulation techniques satisfy the requirements for natural balancing.

Chapter 5

Simulations

To ensure the validity of the analytical solutions provided in Chapters 3 and 4, this chapter compares theoretical results obtained using Maple and Matlab packages with the simulated results of the practical converter using FFT analysis. We give the output voltage waveforms of the NPC inverter and then the harmonics for the switching functions s_α , s_β , s'_α and s'_β using both theory and FFT analysis. We finally show the exponential decay of the capacitor voltage difference v_δ without the balancing booster and with the balancing booster.

5.1 Output voltage waveform

In this section we show the output voltage waveform of NPC inverter under PWM modulation. The specifications of the converter are given by Table 5.1.

Table 5.1: *Simulation parameters for calculating filter capacitance and inductance*

<i>DC – bus voltage</i>	V_t	800 V
<i>DC – bus capacitance</i>	C_d	2 500 μF
<i>Switching frequency</i>	f_s	1.2 kHz
<i>Modulation index</i>	m_a	0.8
<i>Load resistance</i>	R	10 Ω

Figures 5.1, 5.2 and 5.3 show the unfiltered voltage waveform for phases A, B and C for the NPC inverter. The output voltage waveform varies between $(+V_t/2)$ and (0) or $(-V_t/2)$ and (0) .

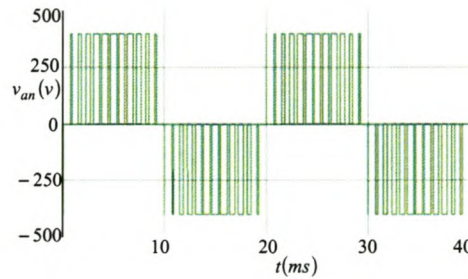
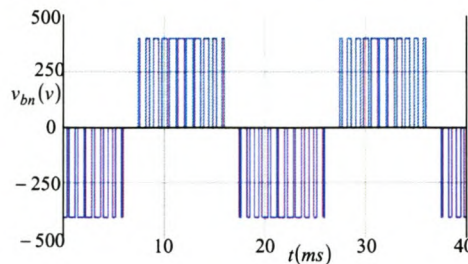
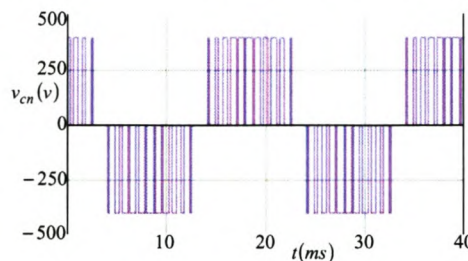
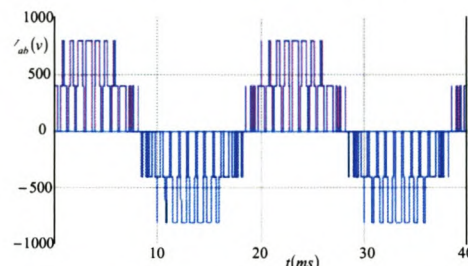
**Figure 5.1:** Output voltage for phase A**Figure 5.2:** Output voltage for phase B**Figure 5.3:** Output voltage for phase C**Figure 5.4:** Output voltage waveform NPC inverter

Figure 5.4 shows the five-level unfiltered output voltage waveform for the line voltage of NPC inverter.

We use equation 3.20 given by

$$L = \frac{m_a V_t}{2 f_s \Delta i_{max}} (1 + m_a)$$

to calculate the filter inductor.

For a system with the parameters given in Table 5.2,

Table 5.2: Simulation parameters for calculating filter capacitance and inductance

<i>DC – bus voltage</i>	V_t	800 V
<i>DC – bus capacitance</i>	C_d	2 500 μF
<i>Switching frequency</i>	f_s	6 kHz
<i>Modulation index</i>	m_a	0.8
<i>Load resistance</i>	R	10 Ω

the maximum output voltage is given by

$$\begin{aligned} v_{0(max)} &= \frac{V_t}{2} m_a \\ &= 320V \end{aligned}$$

$$\begin{aligned} I_{max} &= \frac{320V}{10\Omega} \\ &= 32A \end{aligned}$$

Now taking Δi_{max} to be 30 percent of I_{max} we have

$$\begin{aligned} \Delta i_{max} &= 0.3 \times I_{max} \\ &= 9.6A \end{aligned}$$

Hence the filter inductor is given by

$$L = 10mH$$

Now we calculate the filter capacitance.

For APOD/POD modulation we observe from Figure 4.9 that the largest component of harmonics occurs at twice the switching frequency, that is at 12kHz. The cut-off frequency f_c occurs at 10 percent of 12kHz, that is at 1.2kHz.

Hence

$$\omega_c = \frac{1}{\sqrt{LC}} = 1200 \times 2\pi$$

Thus the filter capacitor is given by

$$C = 1.759\mu F$$

For PD modulation we observe from Figure 4.17 that the largest component of harmonics occurs at the switching frequency, that is at $6kH z$. The cut-off frequency f_c occurs at 10 percent of $6kH z$, that is at $600H z$.

Hence

$$\omega_c = \frac{1}{\sqrt{LC}} = 600 \times 2\pi$$

Thus the filter capacitor is given by

$$C = 7.036\mu F$$

Figure 5.5 shows the filtered output voltages for phases A, B and C. Figure 5.6 shows the filtered line output voltage waveform.

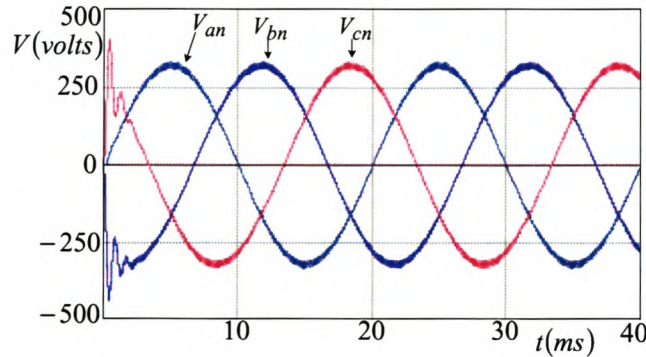


Figure 5.5: Output voltage for phases A, B and C.

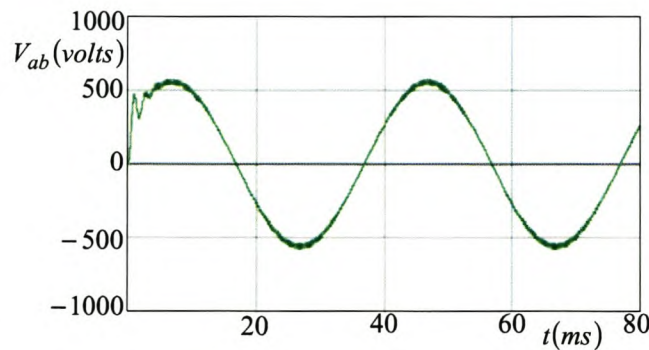


Figure 5.6: Line output voltage waveform

5.2 Natural balancing under APOD/POD modulation

In this section we give simulation results derived from both the theoretical results and from the simulated converter which proves the theoretical results obtained in Chapter 4 under APOD/POD modulation. Table 5.3 shows the parameters used to obtain the figures in this section. Appendix D.2 shows the Simplorer simulation setup used and Appendix D.1 shows the FFT program used.

Table 5.3: *Simulation parameters without using balancing circuit under APOD/POD*

<i>DC – bus voltage</i>	V_t	800 V
<i>DC – bus capacitance</i>	C_d	2 500 μF
<i>Switching frequency</i>	f_s	6 kHz
<i>Modulation index</i>	m_a	0.8
<i>Filter inductance</i>	L	10 mH
<i>Filter capacitance</i>	C	1.759 μF
<i>Load resistance</i>	R	10 Ω

Figures 5.7 and 5.8 show the simulated and theoretical values of the harmonics of S_α and S_β , while Figures 5.9 and 5.10 show the simulated and theoretical values of the harmonics of S'_α and S'_β . Close investigation of these figures shows that magnitudes of the harmonics of S_α and S_β ; and S'_α and S'_β are the same. The spectra shown in Figures 5.7 and 5.9(or 5.8 and 5.10) do not overlap. This ensures balancing in the steady state.

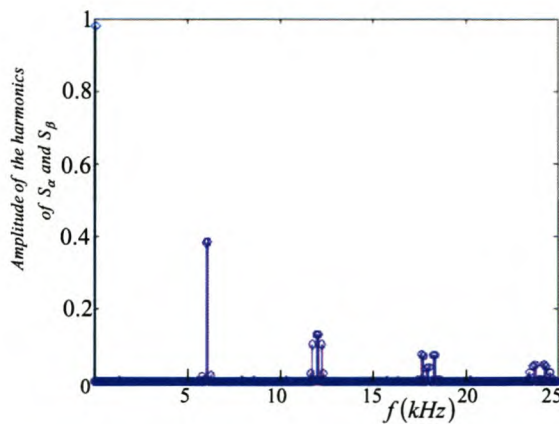


Figure 5.7: *Harmonics for S_α and S_β derived from simulation of practical converter*

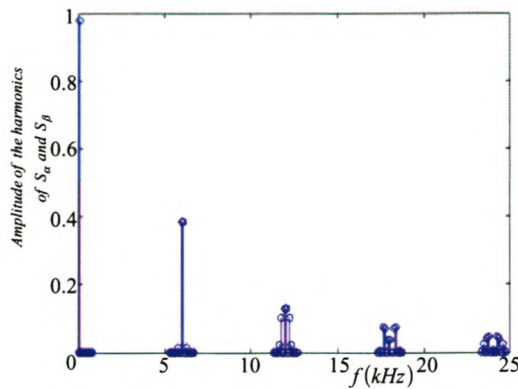


Figure 5.8: Harmonics for S_α and S_β derived from theory

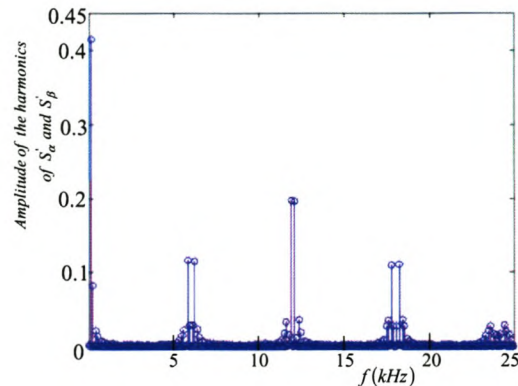


Figure 5.9: Harmonics for S'_α and S'_β derived from simulation of practical converter

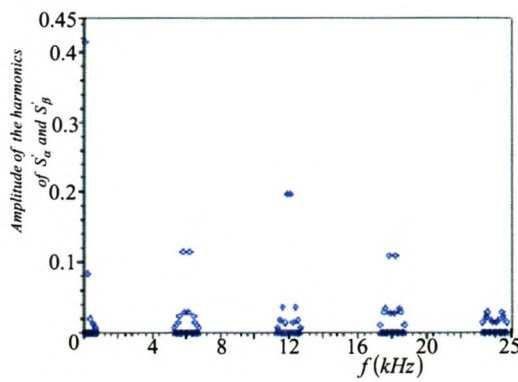


Figure 5.10: Harmonics for S'_α and S'_β derived from theory

We now plot the exponential decay of DC-capacitor voltage difference of the NPC inverter using the time constant equation derived in section 3.6, filter design equations derived in section 3.7 and the Maple package.

From equation 3.16 given by

$$\text{Time Constant} = \tau = \frac{C_d}{\Re e \int_0^\infty \frac{F_2(u)}{Z(u)} du} \quad (5.1)$$

where F_2 is given by equation 4.18; we give the equation that represents the exponential decay of capacitor voltage difference v_δ . Taking initial values v_1 and v_2 to be 500V and 300V respectively we have

$$\begin{aligned} v_\delta(t) &= v_\delta(0)e^{-\frac{t}{\tau}} \\ &= 200V e^{-t(\frac{\Re e \int_0^\infty \frac{F_2(u)}{Z(u)} du}{C_d})} \end{aligned} \quad (5.2)$$

Using equation 5.2 and Appendix C.1, the plot of v_δ versus time is given by Figure 5.11

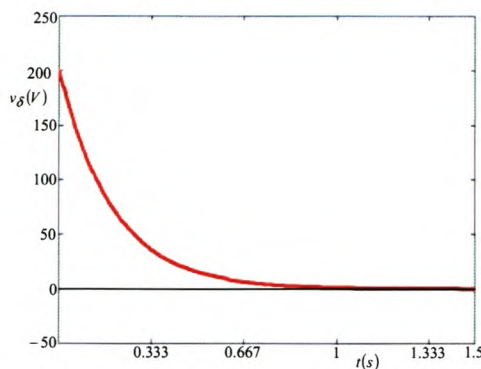


Figure 5.11: Natural balancing of v_δ using theory

Figure 5.11 shows that v_δ exponentially decays to zero, further proving the validity of natural balancing under APOD/POD PWM modulation.

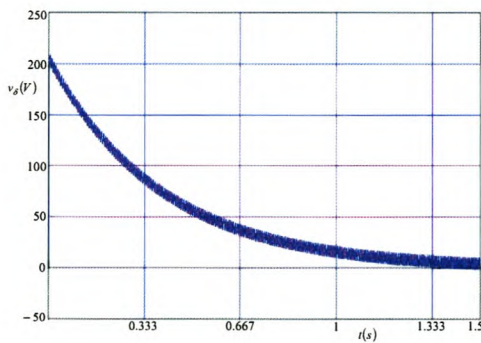


Figure 5.12: Natural balancing of capacitor voltage difference v_δ using simulation of practical converter

Figure 5.12 shows natural balancing using a simulation of a practical converter. Figures 5.11 and 5.12 are approximately the same. Thus we conclude that the capacitor voltage difference v_δ balance under APOD/POD modulation. From Figure 4.9 in section 4.1 of Chapter 4 the largest component of $|F_2|$ occurs at twice the switching frequency; hence the balancing mechanism of the NPC inverter can be enhanced by decreasing the load impedance at 12 kHz. From section 3.8 a simple filter, referred to as a balancing circuit, can be used to enhance the natural balancing. For the parameters of this balancing circuit we assume that its capacitance is $5\mu F$ and its resistance is 0.05Ω . We now calculate the inductance, bandwidth and quality factor. We represent balancing circuit capacitance by C_b , inductance by L_b and resistance by R_b .

$$\omega_0 = \frac{1}{\sqrt{L_b C_b}}$$

$$4 \times \pi \times 6000 = \frac{1}{\sqrt{L_b C_b}}$$

Hence the balancing circuit inductance is given by

$$\begin{aligned} L_b &= \left(\frac{1}{4 \times \pi \times 6000} \right)^2 \times \frac{1}{5\mu F} \\ &= 35.18\mu H \end{aligned}$$

the bandwidth is given by

$$\begin{aligned} \beta &= \frac{R_b}{L_b} \\ &= 1422 \end{aligned}$$

and the quality factor is given by

$$\begin{aligned} Q &= \sqrt{\frac{L_b}{R_b^2 C_b}} \\ &= 53 \end{aligned}$$

Table 5.4 shows the parameters used to design the balancing circuit.

Table 5.4: Balancing circuit parameters under APOD/POD

Balancing circuit inductance	L_b	$35.18 \mu H$
Balancing circuit capacitance	C_b	$5 \mu F$
Balancing circuit resistance	R_b	0.05Ω

Figure 5.13 shows the faster exponential decay of v_δ to zero when a balancing booster is connected parallel to the filter.

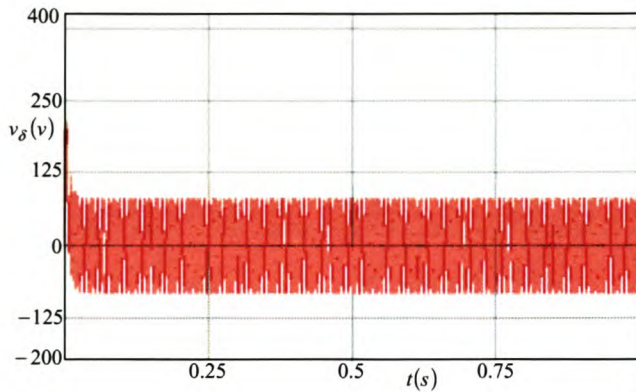


Figure 5.13: Natural balancing v_δ using simulation of practical converter with a balancing booster

5.3 Natural balancing under PD modulation

In this section we give simulation results derived from both the theoretical results and from the practical converter, which proves the theoretical results obtained in Chapter 4 under PD modulation. Table 5.5 shows the parameters used to obtain the figures in this section. Appendix D.2 shows the Simplorer simulation setup used and Appendix D.1 shows the FFT program used.

Table 5.5: Simulation parameters without using balancing circuit under PD

<i>DC – bus voltage</i>	V_t	800 V
<i>DC – bus capacitance</i>	C_d	2 500 μF
<i>Switching frequency</i>	f_s	6 kHz
<i>Modulation index</i>	m_a	0.8
<i>Filter inductance</i>	L	10 mH
<i>Filter capacitance</i>	C	7.036 μF
<i>Load resistance</i>	R	10 Ω

Figures 5.14 and 5.15 show the simulated and theoretical values of the harmonics of S_α and S_β , while Figures 5.16 and 5.17 show the simulated and theoretical values of the harmonics of S'_α and S'_β . Close investigation of these figures shows that magnitudes of the harmonics of S_α and S_β ; and S'_α and S'_β are the same. The spectra shown in Figures 5.14 and 5.16(or 5.15 and 5.17) do not overlap. This ensures balancing in the steady state.

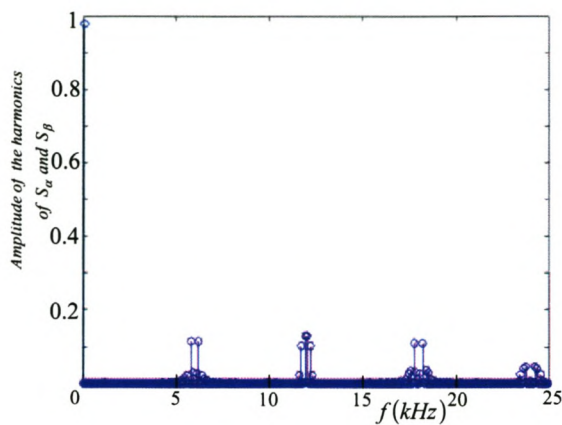


Figure 5.14: Harmonics for S_α and S_β derived from simulation of practical converter

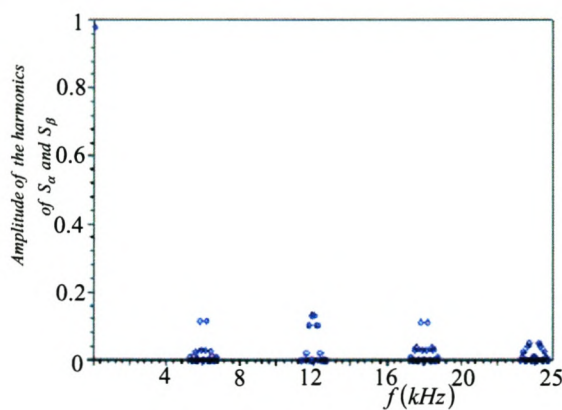


Figure 5.15: Harmonics of S_α and S_β derived from theory

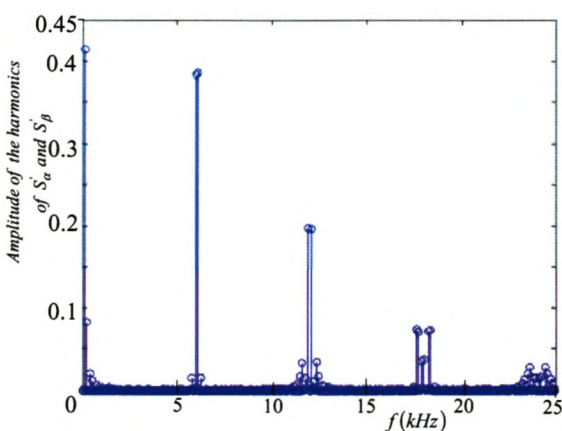


Figure 5.16: Harmonics for S'_α and S'_β derived from simulation of practical converter

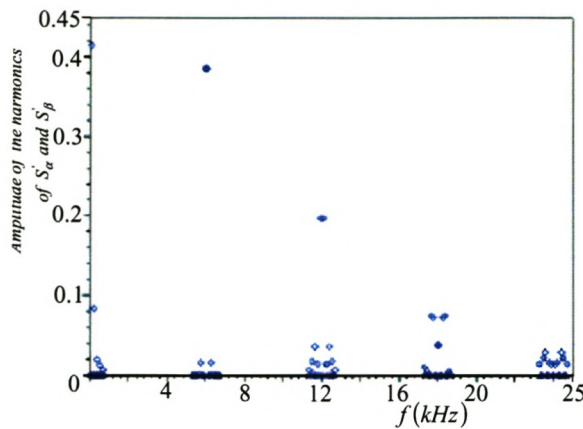


Figure 5.17: Harmonics of S'_α and S'_β derived from theory

Using equation 5.2 and the program in Appendix C.2, the plot of v_δ versus time is given by Figure 5.18.

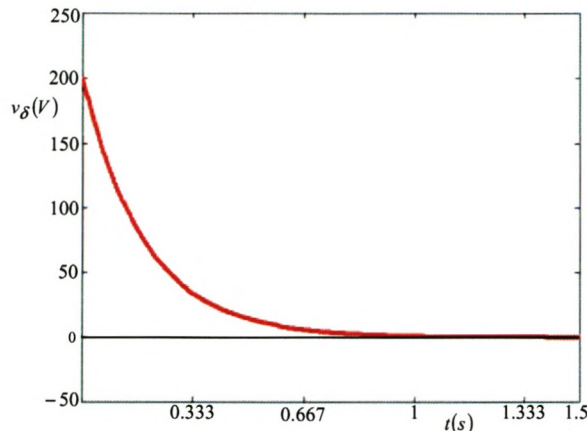


Figure 5.18: Natural balancing of v_δ using theory

Figure 5.18 shows that v_δ exponentially decays to zero, further proving the validity of natural balancing under PD PWM modulation.

Figure 5.19 shows natural balancing using simulation of practical converter.

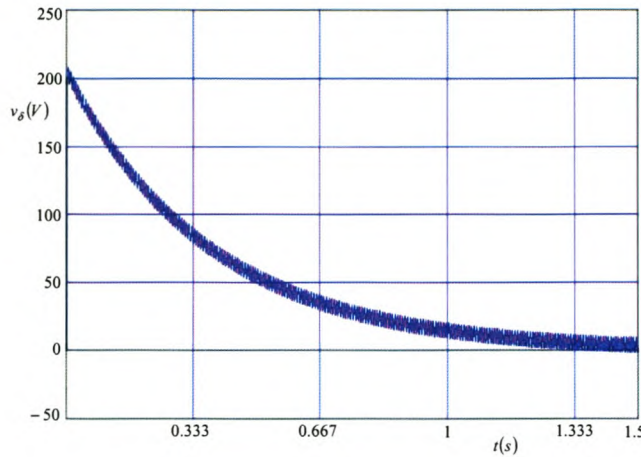


Figure 5.19: Natural balancing v_δ using simulation of practical converter with a balancing booster

From Figure 4.17 in section 4.2 of Chapter 4 the largest component of $|F_2|$ occurs at the switching frequency; hence the balancing mechanism of the NPC inverter can be enhanced by decreasing the load impedance at 6 kHz. Figure 5.20 shows the faster exponential decay of v_δ to zero when a balancing booster is connected parallel to the filter. Using the theory developed in section 3.8 of Chapter 3 we obtain the balancing circuit parameters shown in Table 5.6 for Figure 5.20.

Table 5.6: Balancing circuit parameters under PD

Balancing circuit inductance	L_b	140.7 mH
Balancing circuit capacitance	C_b	5 μF
Balancing circuit resistance	R_b	0.1 Ω

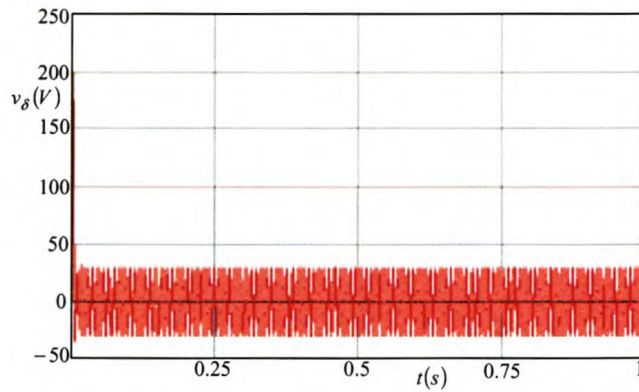


Figure 5.20: Natural balancing using simulation of practical converter with a balancing booster

5.4 Conclusion

In this chapter we compared simulation results from theory using Maple/Matlab packages with simulation results of the practical converter using Simplorer package. Simulation results for switching functions from both theory using Maple/Matlab packages and practical converters using Simplorer were found to be the same. These results are shown in Figures 5.7 and 5.8 (5.9 and 5.10) for APOD/POD PWM modulation and Figures 5.14 and 5.15 (5.16 and 5.17) for PD PWM modulation. We further showed that the exponential decay of the DC-bus capacitor voltage difference (v_δ) from theory and simulation of the practical converter are approximately the same. These results are shown in Figures 5.11 and 5.12 for APOD/POD PWM modulation and in Figures 5.18 and 5.19 for PD PWM modulation. The balancing circuit was used to enhance natural balancing. The results are shown in Figures 5.13 and 5.20 for APOD/POD PWM and PD PWM modulation respectively. We observed that v_δ balances slightly faster under PD PWM modulation as compared to APOD/POD modulation. Hence PD PWM modulation is the better choice for natural balancing of DC-bus capacitor voltages.

Chapter 6

Simulations of NPC Inverter under Vector Control

In section 2.2 of Chapter 2 we discussed vector control of the two-level converter. In this chapter we discuss simulations for natural balancing of the three-level NPC PWM inverter under vector control. Vector control is an alternative method to APOD, POD and PD PWM modulation methods for the study of natural balancing of the three-level NPC PWM inverter discussed in Chapters 3 and 4. We give an insight into the formulas used in the simulations done for natural balancing of NPC inverter under vector control studied in [3]. We first give the switching state vectors for the three phases A, B and C then transform these switching state vectors to α - β parameters using Clarke's transformation method. We also calculate the duty cycles for each region in the first sector and indicate the boundaries for each region. Finally we give some of the simulation results arrived at. The paper [3] and sections 3.1 to 3.4 of Chapter 3 are essential for comprehensive understanding of this chapter.

6.1 Switching Vectors

In this section we give the switching vectors of the three-level voltage source inverter. There are 27 different switching states for the three-level voltage source inverters. These switching states are then arranged into 19 different switching vectors as shown in Figure 6.1 due to similarities of coordinates in the α - β parameter. X_0 is the zero vector, ($X_1 - X_6$) are small vectors, ($X_7 - X_{12}$) are medium vectors and ($X_{13} - X_{18}$) are large vectors.

These vectors in Figure 6.1 represent inverter output line voltages in two-dimensional (V_{ab} , V_{bc} and V_{ca}) plane and are produced by switching different states of the inverter as shown in Tables 6.1, 6.2, 6.3 and 6.4. Tables 6.1, 6.2, 6.3 and 6.4 represent the 19 switching vectors grouped into zero vectors, small vectors, medium vectors and large vectors respectively. These groups are composed of switching vectors for $s_a s_b s_c$ where s_a ,

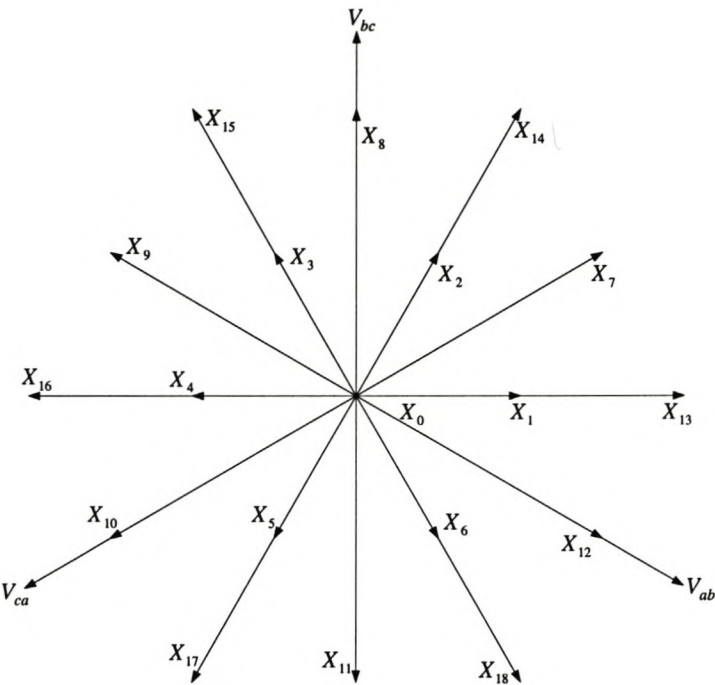


Figure 6.1: Switching vectors of a three-level NPC inverter

s_b and s_c represent switching states of phases A, B and C as shown in equations 3.1, 3.2 and 3.3.

Equations 3.1, 3.2 and 3.3 imply that each phase A, B or C can be connected to either the positive(1), negative(-1) or the neutral(0) point of the dc link. For example switching vector X_9 represented by switching state -110 shows that phase C output is connected to the neutral point, which results in the current i_c disturbing the neutral point voltage balance.

Switching vectors for s_α and s_β are given by

$$\begin{bmatrix} s_\alpha \\ s_\beta \end{bmatrix} = A \begin{bmatrix} s_a \\ s_b \\ s_c \end{bmatrix} \quad (6.1)$$

Switching vectors for s'_α and s'_β are given by

$$\begin{bmatrix} s'_\alpha \\ s'_\beta \end{bmatrix} = A \begin{bmatrix} |s_a| \\ |s_b| \\ |s_c| \end{bmatrix} \quad (6.2)$$

Table 6.1: Zero switching vectors

<i>Vectors</i>	$s_a s_b s_c$	s_α	s_β	s'_α	s'_β
X_0	111	0	0	0	0
	000	0	0	0	0
	-1-1-1	0	0	0	0

Table 6.2: Small switching vectors

<i>Vectors</i>	$s_a s_b s_c$	s_α	s_β	s'_α	s'_β
X_1	100	$\sqrt{\frac{2}{3}}$	0	$\sqrt{\frac{2}{3}}$	0
	0-1-1	$-\sqrt{\frac{2}{3}}$	0	$-\sqrt{\frac{2}{3}}$	0
X_2	110	$\frac{1}{\sqrt{6}}$	$\frac{1}{\sqrt{2}}$	$\frac{1}{\sqrt{6}}$	$\frac{1}{\sqrt{2}}$
	00-1	$-\frac{1}{\sqrt{6}}$	$\frac{1}{\sqrt{2}}$	$-\frac{1}{\sqrt{6}}$	$-\frac{1}{\sqrt{2}}$
X_3	010	$-\frac{1}{\sqrt{6}}$	$\frac{1}{\sqrt{2}}$	$-\frac{1}{\sqrt{6}}$	$\frac{1}{\sqrt{2}}$
	-10-1	$-\frac{1}{\sqrt{6}}$	$\frac{1}{\sqrt{2}}$	$\frac{1}{\sqrt{6}}$	$-\frac{1}{\sqrt{2}}$
X_4	011	$-\sqrt{\frac{2}{3}}$	0	$-\sqrt{\frac{2}{3}}$	0
	-100	$-\sqrt{\frac{2}{3}}$	0	$\sqrt{\frac{2}{3}}$	0
X_5	001	$-\frac{1}{\sqrt{6}}$	$-\frac{1}{\sqrt{2}}$	$-\frac{1}{\sqrt{6}}$	$-\frac{1}{\sqrt{2}}$
	-1-10	$-\frac{1}{\sqrt{6}}$	$-\frac{1}{\sqrt{2}}$	$\frac{1}{\sqrt{6}}$	$\frac{1}{\sqrt{2}}$
X_6	101	$\frac{1}{\sqrt{6}}$	$-\frac{1}{\sqrt{2}}$	$\frac{1}{\sqrt{6}}$	$-\frac{1}{\sqrt{2}}$
	0-10	$\frac{1}{\sqrt{6}}$	$-\frac{1}{\sqrt{2}}$	$-\frac{1}{\sqrt{6}}$	$\frac{1}{\sqrt{2}}$

Table 6.3: Medium switching vectors

<i>Vectors</i>	$s_a s_b s_c$	s_α	s_β	s'_α	s'_β
X_7	10-1	$\sqrt{\frac{3}{2}}$	$\frac{1}{\sqrt{2}}$	$\frac{1}{\sqrt{6}}$	$-\frac{1}{\sqrt{2}}$
X_8	01-1	0	$\sqrt{2}$	$-\sqrt{\frac{2}{3}}$	0
X_9	-110	$-\sqrt{\frac{3}{2}}$	$\frac{1}{\sqrt{2}}$	$\frac{1}{\sqrt{6}}$	$\frac{1}{\sqrt{2}}$
X_{10}	-101	$-\sqrt{\frac{3}{2}}$	$-\frac{1}{\sqrt{2}}$	$\frac{1}{\sqrt{6}}$	$-\frac{1}{\sqrt{2}}$
X_{11}	0-11	0	$-\sqrt{2}$	$-\sqrt{\frac{2}{3}}$	0
X_{12}	1-10	$\sqrt{\frac{3}{2}}$	$-\frac{1}{\sqrt{2}}$	$\frac{1}{\sqrt{6}}$	$\frac{1}{\sqrt{2}}$

Table 6.4: Large switching vectors

Vectors	$s_a s_b s_c$	s_α	s_β	s'_α	s'_β
X_{13}	1-1-1	$2\sqrt{\frac{2}{3}}$	0	0	0
X_{14}	11-1	$\sqrt{\frac{2}{3}}$	$\sqrt{2}$	0	0
X_{15}	-11-1	$-\sqrt{\frac{2}{3}}$	$\sqrt{2}$	0	0
X_{16}	-111	$-2\sqrt{\frac{2}{3}}$	0	0	0
X_{17}	-1-11	$-\sqrt{\frac{2}{3}}$	$-\sqrt{2}$	0	0
X_{18}	1-11	$\sqrt{\frac{2}{3}}$	$-\sqrt{2}$	0	0

6.2 Duty Cycles

In this section we discuss the duty cycles for the first sector which consists of four regions. These duty cycles are obtained by synthesising the reference vector using the space vector modulation of the three switching state vectors nearest to the reference vector at every sampling instant. The duty cycles of other sectors have the same magnitude but are shifted in phase.

Duty cycle(D_T) is the ratio of the duration(time) that a signal is on to the total period of the signal and is given by

$$D_T = \frac{\Delta t}{T_s}$$

where T_s is the switching period and Δt is the on time.

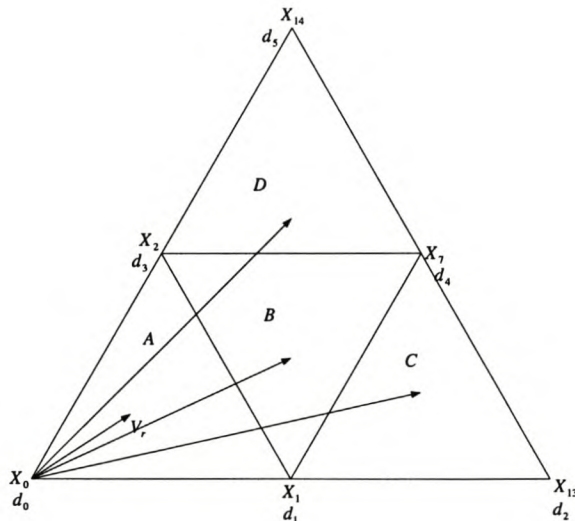
**Figure 6.2:** Regions of vector modulation of the NPC inverter in the first sector.

Figure 6.2 shows the first sector of the switching state vectors of three-level NPC inverter and the four regions within this sector. The reference vector V_r is synthesised using the space vector modulation of the three switching state vectors nearest to the reference vector at every sampling instant. The nearest three switching state vectors are selected by locating the reference vector in one of the four regions as shown in Figure 6.2. The reference vector is given by the general formula

$$V_r = d_p X_e + d_q X_f + d_r X_g$$

where d_p , d_q and d_r are the duty cycles/durations for the switching vectors X_e , X_f and X_g respectively.

Below we calculate duty cycles for each of the regions A, B, C and D in sector I.

Region A:

$$V_r = d_0 X_0 + d_1 X_1 + d_3 X_2$$

$$(m_a \cos \omega t, m_a \sin \omega t) = d_0(0, 0) + d_1\left(\sqrt{\frac{2}{3}}, 0\right) + d_3\left(\frac{1}{\sqrt{6}}, \frac{1}{\sqrt{2}}\right)$$

where m_a is modulation index.

$$m_a \cos \omega t = \sqrt{\frac{2}{3}}d_1 + \frac{1}{\sqrt{6}}d_3$$

$$m_a \sin \omega t = \frac{1}{\sqrt{2}}d_3$$

$$d_3 = \sqrt{2}m_a \sin \omega t$$

$$m_a \cos \omega t = \sqrt{\frac{2}{3}}d_1 + \frac{1}{\sqrt{3}}m_a \sin \omega t$$

$$d_1 = \sqrt{\frac{3}{2}}m_a \cos \omega t - \frac{1}{\sqrt{2}}m_a \sin \omega t$$

$$\begin{aligned} d_0 &= 1 - \sqrt{2}m_a \sin \omega t - \sqrt{\frac{3}{2}}m_a \cos \omega t + \frac{1}{\sqrt{2}}m_a \sin \omega t \\ &= 1 - \frac{1}{\sqrt{2}}m_a \sin \omega t - \sqrt{\frac{3}{2}}m_a \cos \omega t \end{aligned}$$

Region B:

$$V_r = d_1 X_0 + d_3 X_1 + d_4 X_2$$

$$(m_a \cos \omega t, m_a \sin \omega t) = d_1\left(\sqrt{\frac{2}{3}}, 0\right) + d_4\left(\sqrt{\frac{3}{2}}, \frac{1}{\sqrt{2}}\right) + d_3\left(\frac{1}{\sqrt{6}}, \frac{1}{\sqrt{2}}\right)$$

$$m_a \cos \omega t = \sqrt{\frac{2}{3}}d_1 + \sqrt{\frac{3}{2}}d_4 + \frac{1}{\sqrt{6}}d_3$$

$$m_a \sin \omega t = \frac{1}{\sqrt{2}}d_4 + \frac{1}{\sqrt{2}}d_3$$

$$d_3 = \sqrt{2}m_a \sin \omega t - d_4$$

$$\begin{aligned} m_a \cos \omega t &= \sqrt{\frac{2}{3}}d_1 + \sqrt{\frac{3}{2}}d_4 + \frac{1}{\sqrt{6}}\sqrt{2}m_a \sin \omega t - \frac{1}{\sqrt{6}}d_4 \\ &= \sqrt{\frac{2}{3}}d_1 + \sqrt{\frac{2}{3}}d_4 + \frac{1}{\sqrt{3}}m_a \sin \omega t \end{aligned}$$

$$d_1 + d_4 + d_3 = 1$$

$$\begin{aligned} d_1 &= 1 - \sqrt{2}m_a \sin \omega t + d_4 - d_3 \\ &= 1 - \sqrt{2}m_a \sin \omega t \end{aligned}$$

$$m_a \cos \omega t = \sqrt{\frac{2}{3}} - \frac{2}{\sqrt{3}}m_a \sin \omega t + \sqrt{\frac{2}{3}}d_4 + \frac{1}{\sqrt{3}}m_a \sin \omega t$$

$$d_4 = \sqrt{\frac{3}{2}}m_a \cos \omega t - 1 + \frac{1}{\sqrt{2}}m_a \sin \omega t$$

$$\begin{aligned} d_3 &= \sqrt{2}m_a \sin \omega t + 1 - \sqrt{\frac{3}{2}}m_a \cos \omega t - \frac{1}{\sqrt{2}}m_a \sin \omega t \\ &= 1 + \frac{1}{\sqrt{2}}m_a \sin \omega t - \sqrt{\frac{3}{2}}m_a \cos \omega t \end{aligned}$$

Region C:

$$V_r = d_1X_1 + d_2X_{13} + d_4X_7$$

$$(m_a \cos \omega t, m_a \sin \omega t) = d_1(\sqrt{\frac{2}{3}}, 0) + d_2(2\sqrt{\frac{2}{3}}, 0) + d_4(\sqrt{\frac{3}{2}}, \frac{1}{\sqrt{2}})$$

$$m_a \cos \omega t = \sqrt{\frac{2}{3}}d_1 + 2\sqrt{\frac{2}{3}}d_2 + \sqrt{\frac{3}{2}}d_4$$

$$m_a \sin \omega t = \frac{1}{\sqrt{2}}d_4$$

$$d_4 = \sqrt{2}m_a \sin \omega t$$

$$m_a \cos \omega t = \sqrt{\frac{2}{3}}d_1 + 2\sqrt{\frac{2}{3}}d_2 + \sqrt{\frac{3}{2}}\sqrt{2}m_a \sin \omega t$$

$$d_1 + d_2 + d_4 = 1$$

$$d_1 = 1 - d_2 - \sqrt{2}m_a \sin \omega t$$

$$m_a \cos \omega t = \sqrt{\frac{2}{3}} - \sqrt{\frac{2}{3}}d_2 - \sqrt{2}\sqrt{\frac{2}{3}}m_a \sin \omega t + 2\sqrt{\frac{2}{3}}d_2 + \sqrt{3}m_a \sin \omega t$$

$$\sqrt{\frac{2}{3}}d_2 = m_a \cos \omega t - \frac{1}{\sqrt{3}}m_a \sin \omega t - \sqrt{\frac{2}{3}}$$

$$d_2 = \sqrt{\frac{3}{2}}m_a \cos \omega t - \frac{1}{\sqrt{2}}m_a \sin \omega t - 1$$

$$\begin{aligned} d_1 &= 1 - \sqrt{\frac{3}{2}}m_a \cos \omega t + \frac{1}{\sqrt{2}}m_a \sin \omega t + 1 - \sqrt{2}m_a \sin \omega t \\ &= 2 - \sqrt{\frac{3}{2}}m_a \cos \omega t - \frac{1}{\sqrt{2}}m_a \sin \omega t \end{aligned}$$

Region D:

$$V_r = d_3X_2 + d_4X_7 + d_5X_{14}$$

$$(m_a \cos \omega t, m_a \sin \omega t) = d_3(\frac{1}{\sqrt{6}}, \frac{1}{\sqrt{2}}) + d_4(\sqrt{\frac{2}{3}}, \frac{1}{\sqrt{2}}) + d_5(\sqrt{\frac{2}{3}}, \sqrt{2})$$

$$m_a \cos \omega t = \frac{1}{\sqrt{6}}d_3 + \sqrt{\frac{3}{2}}d_4 + \sqrt{\frac{2}{3}}d_5$$

$$m_a \sin \omega t = \frac{1}{\sqrt{2}}d_3 + \frac{1}{\sqrt{2}}d_4 + \sqrt{2}d_5$$

$$d_3 = \sqrt{2}m_a \sin \omega t - d_4 - 2d_5$$

$$\begin{aligned} m_a \cos \omega t &= \frac{1}{\sqrt{6}}\sqrt{2}m_a \sin \omega t - \frac{1}{\sqrt{6}}d_4 - \frac{1}{\sqrt{6}}2d_5 + \sqrt{\frac{3}{2}}d_4 + \frac{2}{3}d_5 \\ &= \frac{1}{\sqrt{3}}m_a \sin \omega t - \frac{1}{\sqrt{6}}d_4 - \sqrt{\frac{2}{3}}d_5 + \sqrt{\frac{3}{2}}d_4 + \sqrt{\frac{2}{3}}d_5 \\ &= \frac{1}{\sqrt{3}}m_a \sin \omega t + \sqrt{\frac{2}{3}}d_4 \end{aligned}$$

$$d_4 = \sqrt{\frac{3}{2}}m_a \cos \omega t - \frac{1}{\sqrt{2}}m_a \sin \omega t$$

$$\begin{aligned}d_3 &= \sqrt{2}m_a \sin \omega t - \sqrt{\frac{3}{2}}m_a \cos \omega t + \frac{1}{\sqrt{2}}m_a \sin \omega t - 2d_5 \\&= \frac{3}{\sqrt{2}}m_a \sin \omega t - \sqrt{\frac{3}{2}}m_a \cos \omega t - 2d_5\end{aligned}$$

$$\begin{aligned}d_5 &= 1 - d_4 - d_3 \\&= 1 - \sqrt{\frac{3}{2}}m_a \cos \omega t + \frac{1}{\sqrt{2}}m_a \sin \omega t - \frac{3}{\sqrt{2}}m_a \sin \omega t + \sqrt{\frac{3}{2}}m_a \cos \omega t + 2d_5 \\&= 1 - \sqrt{2}m_a \sin \omega t + 2d_5 \\d_5 &= \sqrt{2}m_a \sin \omega t - 1\end{aligned}$$

$$\begin{aligned}d_3 &= \frac{3}{2}m_a \sin \omega t - \sqrt{\frac{3}{2}}m_a \cos \omega t - 2\sqrt{2}m_a \sin \omega t + 2 \\&= -\frac{1}{\sqrt{2}}m_a \sin \omega t - \sqrt{\frac{3}{2}}m_a \cos \omega t + 2\end{aligned}$$

Boundary for Regions A, B, C and D:

Below we show boundary equations for Regions A, B, C and D. It is important to be able to determine the boundaries in order to decide in which sector we are.

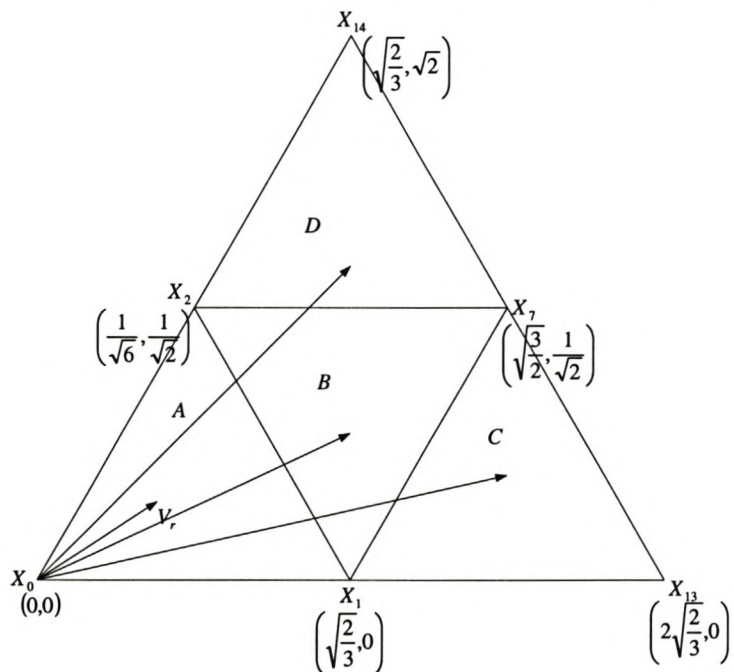


Figure 6.3: Sector I with coordinates for each region

Equations for the line and gradient are given by

$$y - y_1 = m(x - x_1)$$

and

$$m = \frac{y_2 - y_1}{x_2 - x_1}$$

Region A:

$$m = \frac{\frac{1}{\sqrt{2}} - 0}{\frac{1}{\sqrt{6}} - \sqrt{\frac{2}{3}}} = -\sqrt{3}$$

$$\begin{aligned} y - 0 &\leq -\sqrt{3} \left(x - \sqrt{\frac{2}{3}} \right) \\ &\leq -\sqrt{3}x + \sqrt{2} \end{aligned}$$

$$y + \sqrt{3}x \leq \sqrt{2}$$

Region B:

$$\begin{aligned} y - 0 &\geq \sqrt{3} \left(x - \sqrt{\frac{2}{3}} \right) \\ &\geq \sqrt{3}x - \sqrt{2} \end{aligned}$$

$$\sqrt{3}x - y \leq \sqrt{2}$$

$$y \leq \frac{1}{\sqrt{2}}$$

$$y + \sqrt{3}x \geq \sqrt{2}$$

Region C:

$$\sqrt{3}x - y \leq \sqrt{2}$$

Region D:

$$y \geq \frac{1}{\sqrt{2}}$$

Since both the s'_α and s'_β are zero for the large vectors, it follows from equation 3.15 that the zero and large vectors do not influence the neutral point voltage. Each small vector is associated with two different switching states. A small vector that connects a phase current to the neutral point without changing the sign of the current is referred to as a positive small vector. A small vector that connects the phase current to the

negative sign is referred to as a negative small vector [16]. The values of s'_α and s'_β are of opposite signs for the two different switching states associated with a particular small vector. This observation is important in the natural balancing of three-level NPC inverter. Each medium vector is associated with one switching state and medium vectors are the major source of capacitor voltage ripple. The alternative small vector selection technique is used to select small vectors. This implies that in regions A and B switching pairs 100 and 110 are selected for the one sampling period, while 0-1-1 and 00-1 are selected for the next sampling instant. Similarly in region C switching pairs 100 and 0-1-1 are selected alternatively, and in region D switching pairs 110 and 00-1 are selected alternatively. The main advantage of this technique is that the waveforms of switching functions s_α and s_β repeat at the sampling frequency, while those of s'_α and s'_β repeat at half the sampling frequency. This results in orthogonality for the switching functions in the frequency domain, which is a requirement for natural balancing [3].

6.3 Simulation results

In this section we give simulation results of natural balancing of three-level NPC inverter under space vector modulation. The simulation parameters are as shown in Table 6.5 and the simulation setup is shown in Appendix D.3 with NPC inverter not shown. NPC inverter setup is the same as in Appendix D.2.

Table 6.5: *Simulation parameters*

<i>DC – bus voltage</i>	V_t	800 V
<i>DC – bus capacitance</i>	C_d	2 500 μF
<i>Switching frequency</i>	f_s	6 kHz
<i>Modulation index</i>	m_a	0.8
<i>Filter inductance</i>	L	469 μH
<i>Filter capacitance</i>	C	150 μF
<i>Load resistance</i>	R	10 Ω
<i>Balancing circuit inductance</i>	L_b	187.6 μH
<i>Balancing circuit capacitance</i>	C_b	15 μF
<i>Balancing circuit resistance</i>	R_b	0.1 Ω

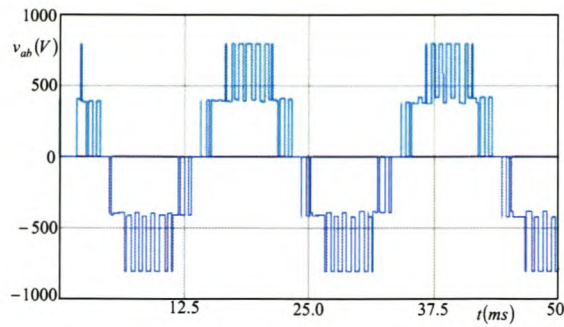


Figure 6.4: Unfiltered line-to-line output voltage waveform

Figure 6.4 shows the unfiltered line-to-line output voltage waveform of the NPC inverter under vector control modulation with switching frequency set at 1.2kHz.

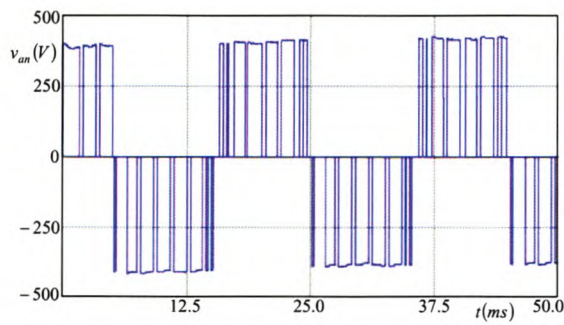


Figure 6.5: Unfiltered phase voltage waveform

Figure 6.5 shows the unfiltered phase voltage waveform of the NPC inverter under vector control modulation with switching frequency set at 1.2kHz.

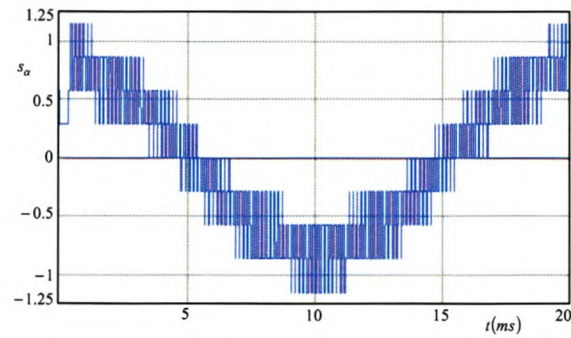


Figure 6.6: Switching function of s_α in time domain

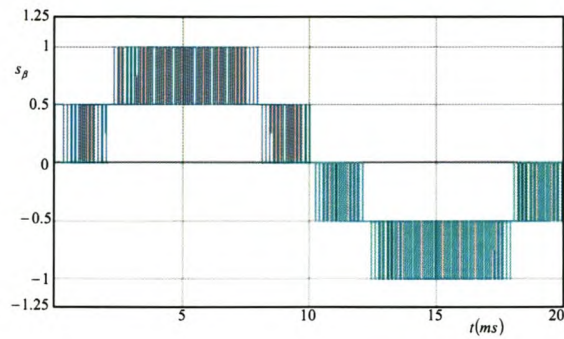


Figure 6.7: Switching function of s_β in time domain

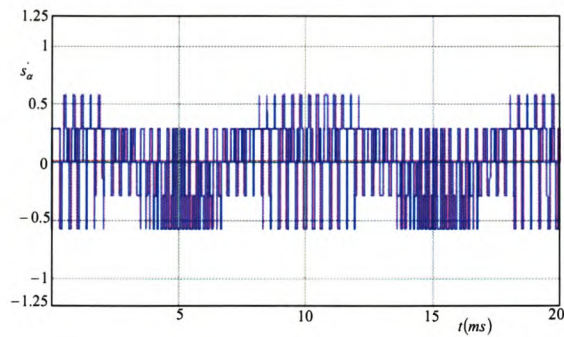


Figure 6.8: Switching function of s'_α in time domain

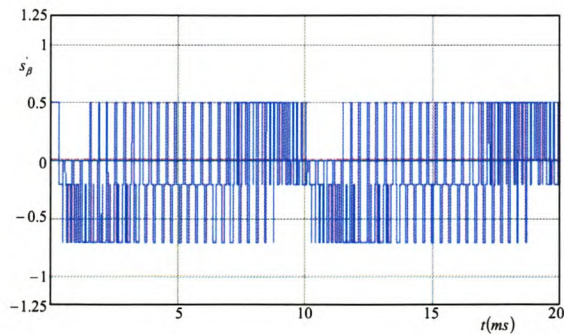


Figure 6.9: Switching function of s'_β in time domain

Figures 6.6, 6.7, 6.8 and 6.9 show the switching functions of s_α , s_β , s'_α and s'_β in the time domain over one fundamental cycle respectively.

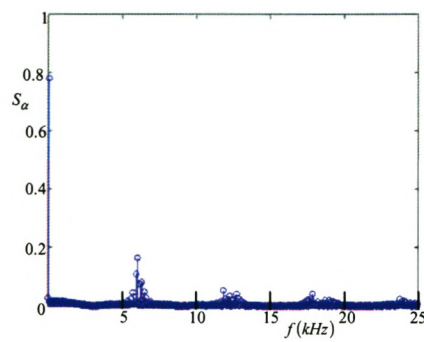


Figure 6.10: Switching function of s_α in frequency domain

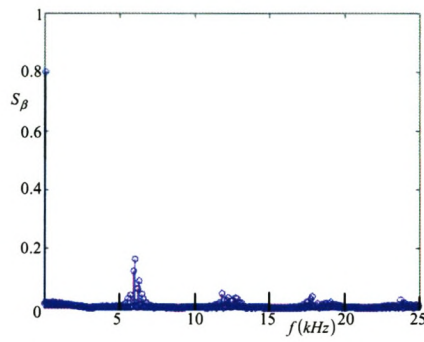


Figure 6.11: Switching function of s_β in frequency domain

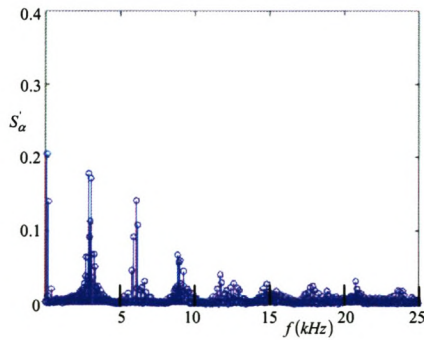


Figure 6.12: Switching function of s'_α in frequency domain

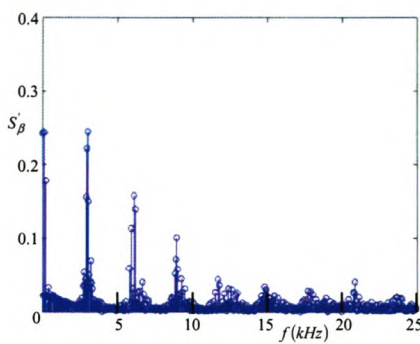


Figure 6.13: Switching function of s'_β in frequency domain

Figures 6.10, 6.11, 6.12 and 6.13 show the switching functions of s_α , s_β , s'_α and s'_β in the frequency domain over one fundamental cycle respectively.

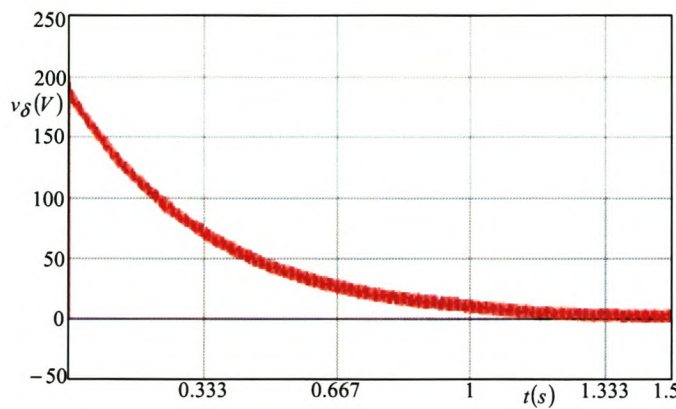


Figure 6.14: Natural balancing of capacitor voltages of NPC inverter

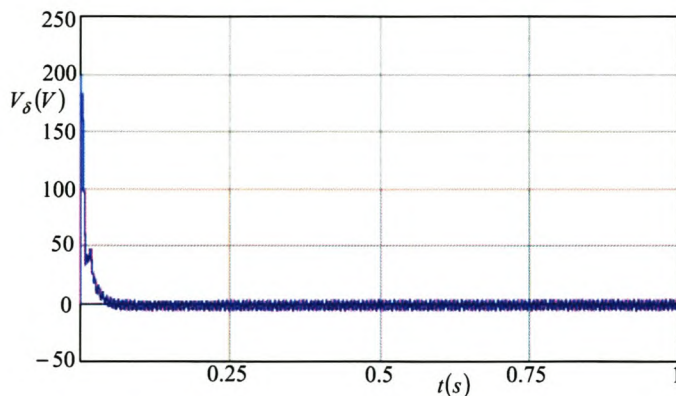


Figure 6.15: Natural balancing with balancing booster

Figure 6.14 shows the natural balancing of capacitor voltages of the NPC inverter without a balancing circuit, whilst Figure 6.15 shows the natural balancing with a balancing circuit. From these figures we notice that the balancing circuit enhances the balancing mechanism.

From equation 3.15 in Chapter 3, one of the factors affecting balancing of the capacitor voltages of the three-level NPC inverter is the impedance of the output filter and load. To illustrate this fact, we replace the load impedance of the NPC inverter by three sinusoidal current sources that are phase shifted by 120° . For this simulation we use the parameters given in Table 6.6.

Table 6.6: *Simulation parameters*

<i>Current source frequency</i>	f_c	50 Hz
<i>Current source amplitude</i>	A_c	40

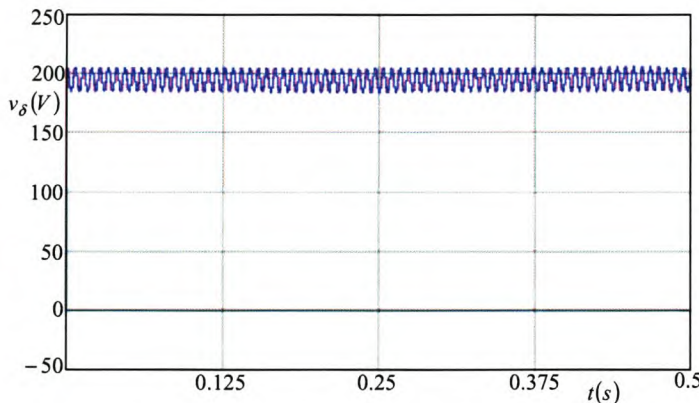


Figure 6.16: *Load replaced by sinusoidal current source*

Figure 6.16 shows that the capacitor voltages do not rebalance and v_δ oscillates at 200 V indefinitely. This is due to the fact that the current source load presents an infinite impedance at odd multiples of the sampling frequency.

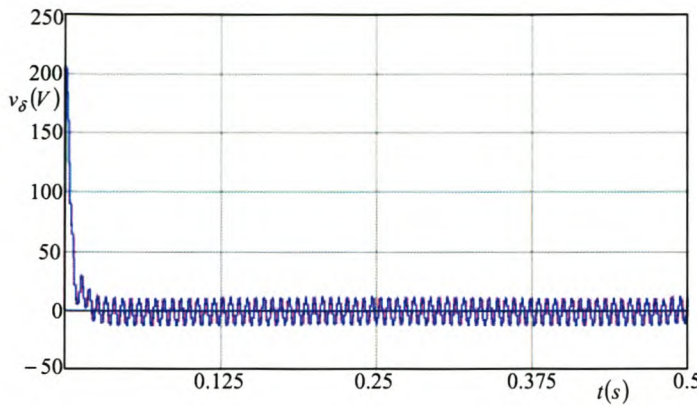


Figure 6.17: Load replaced by sinusoidal current source with balancing circuit connected

Figure 6.17 shows that v_δ exponentially decays to 0 V when the balancing circuit is connected parallel to each sinusoidal current source. The initial stored energy associated with the unbalance of v_1 and v_2 is dissipated in the resistor R_b of the balancing circuit.

6.4 Conclusion

In this chapter we gave an insight into formulas used in the simulations of three-level three-phase NPC inverter under vector control. We then gave some of the simulation results obtained in [3] for natural balancing of three-level NPC PWM inverters under vector control. These simulation results show that the steady-state balancing of the DC-bus voltages depends on the overlap of the spectra of the switching functions as well as the load impedance. These results further show that vector control satisfies the requirements for natural balancing. Further discussions of the theory used in [3] were shown in sections 3.1 to 3.4 of Chapter 3.

Chapter 7

Conclusion

This chapter summarises the previous chapters of this thesis. It then presents the thesis's contribution, followed by suggestions for future work.

7.1 Summary

This thesis studied the neutral-point voltage balancing problem of the three-level NPC inverter with the focus on the steady-state imbalance. The background on multilevel inverters and the research objective were given in the introduction. Chapter 2 gave an overview on sampling methods, switching schemes and strategies used by other authors in the study of the balancing problem of the neutral point of the NPC inverter.

The theory in the paper by [3] was elaborated and the key equation 3.15, which is used in the analysis of capacitor voltage balancing, was presented in Chapter 3. We further derived the equation for the time constant used to plot the exponential decay of capacitor voltage difference. Equations used to determine the parameters of the output filter and the balancing circuit were also derived. Chapter 4 presented the spectra of the switching functions. We used Carrara's PWM technique, Bennet's geometric technique and Bowes's double Fourier series method to calculate the coefficients of the switching functions. Using these coefficients and the theory developed in Chapter 3 we plotted the harmonics of the switching functions in the $\alpha\beta$ plane. Through calculations and plotting of harmonics using equation 3.15, we learned that the DC-bus capacitor voltage difference v_δ decays to zero in the steady state for APOD/POD and PD modulation.

Chapter 5 provided the verification of the theory developed in Chapters 3 and 4. We compared the harmonics of the switching functions in the $\alpha\beta$ plane obtained using the theory and FFT analysis of the simulated inverter and observed that they are the same. The exponential decay of the DC-bus capacitor voltage difference v_δ from the theory and simulated inverter was found to be approximately the same. The addition of the balancing circuit parallel to the output filter and load enhanced the natural balancing for both

APOD/POD and PD modulation. We observed that there is not much difference in the natural balancing when we compare APOD/POD and PD modulation. PD modulation was found to be slightly better than APOD/POD modulation.

Chapter 6 presented natural balancing under vector control. We gave an insight into duty cycles and equations for the boundaries of the regions in the first sector that are used in the simulations. We also observed that the DC-bus capacitor voltage difference v_δ exponentially decays to zero at approximately the same point as in APOD/POD and PD modulation. Similarly the connection of the balancing circuit enhanced the natural balancing.

7.2 Thesis Contribution

The following are the main contribution of this thesis:

- This thesis studied the natural balancing of DC-bus capacitor voltages of the three-level NPC inverter under APOD/POD and PD PWM modulation technique;
- The techniques were the use of a geometric mathematical model and double Fourier series to calculate the magnitude of the harmonics of the switched waveforms;
- It was shown that the steady-state balancing of the DC-bus voltages depends on the overlap of the spectra of the switching functions as well as the load impedance;
- An equation for the balancing time constant is derived and it is shown how a balancing booster can be used to enhance the balancing mechanisms;
- It is proven formally that APOD/POD and PD PWM satisfies the requirements for natural balancing;
- The simulations results provided prove the validity of the theory.

7.3 Future Work

The focus of future work that can follow from this thesis are as follows:

- Experimental verification of the natural balancing of DC-bus capacitor voltages of the three-level NPC converter under APOD/POD and PD PWM modulation techniques;
- Mathematical verification of the spectra of the switching functions and the exponential decay of DC-bus capacitor voltage difference v_δ under vector modulation;

- Study of natural balancing using other switching schemes and topologies;
- An investigation of the natural balancing of the NPC converter under transients and non-linear load conditions.

Bibliography

- [1] A. Nabae, I. Takahashi, and H. Akagi, "A new neutral-point-clamped PWM inverter," IEEE Trans. Ind. App., vol. IA-17, no. 5, pp. 518-523, Sept./Oct. 1981.
- [2] J. S Lai and F. Z Peng, "Multilevel converters - A new breed of power converters," IEEE Trans. Ind. App., vol. 32, no. 3, pp. 509-517, May/June 1996.
- [3] H. du T. Mouton, "Natural balancing of three-level neutral-point-clamped PWM inverters," IEEE Trans. Ind. Electron., vol. 49, no. 5, pp. 1017-1025, Oct. 2002.
- [4] N. Mohan, T. M. Undeland and W. P. Robbins, "Power Electronics," John Wiley and sons, Inc., Second Edition, pp. 200-245, 1995.
- [5] T. A. Meynard, and H. Foch, "Multi-level conversion: high voltage choppers and voltage-source inverters," IEEE PESC'92 Conf. Proc., Toledo, Spain, pp. 397-403, June 1992.
- [6] J. Rodriguez, J-S. Lai and F. Z Peng, "Multilevel inverters: A survey of topologies, controls, and applications," IEEE Trans. Ind. Applications, vol. 49, no. 4, pp. 724-738, August 2002.
- [7] R. Rojas, T. Ohnishi, and T. Suzuki, "An improved voltage vector control method for neutral-point-clamped inverters," IEEE Trans. Power Electron., vol. 10, no. 6, pp. 666-672, Nov. 1995.
- [8] R. Rojas, T. Ohnishi, and T. Suzuki, "Neutral-point-clamped inverter with improved voltage waveform and control range," IEEE Trans. Power Electron., vol. 42, no. 6, pp. 587-594, Dec. 1995.
- [9] H. L. Liu and G. H. Cho, "Three-level space vector PWM in low index modulation region avoiding narrow pulse problem," IEEE Trans. Power Electron., vol. 9, no. 5, pp. 481-487, Sept. 1994.
- [10] Y. H. Lee, B. S. Suh and D. S. Hyun, "A novel PWM scheme for a three-level voltage source inverter with GTO thyristors," IEEE Trans. Ind. App., vol. 32, no. 2, pp. 260-268, March/April 1996.

- [11] G. C. Cho, G. H. Jung, N. S. Choi, and G. H. Cho, "Analysis and controller design of static var compensator using three-level GTO inverter," *IEEE Trans. Power Electron.*, vol. 11, no. 1, pp. 57-65, Jan.1996.
- [12] J. Steinke, "Switching frequency optimal PWM control of a three-level inverter," *IEEE Trans. Power Electron.*, vol. 7, no. 3, pp. 487-496, July 1992.
- [13] C. Hochgraf,R. Lasseter,D. Divan, and T. A. Lipo, "Comparison of multilevel inverters for static var compensation," in Conf. Rec. IEEE-IAS Annu. Meeting, pp. 921-928, Oct. 1994.
- [14] L. M. Tolbert, F. Z. Peng, T. Cunningham and J. N. Chiasson, "Charge balance control schemes for cascade multilevel converter in hybrid electric vehicles," *IEEE Trans. Ind. Electron.*, vol. 49, no. 5, pp. 1058-1064, Oct. 2002.
- [15] C. Hochgraf and R. H. Lasseter, "A transformer-less static synchronous compensator employing a multi-level inverter," *IEEE PES Meeting*, pp. 1-7, July28-Aug.1 1996.
- [16] N. Celanovic and D. Boroyevich, "A comprehensive study of neutral-point voltage balancing problem in three-level neutral-point-clamped voltage source PWM inverters," *IEEE Trans. Power Electron.*, vol. 15, no. 2, pp. 242-249, March 2000.
- [17] H. S. Black, " Modulation theory," New York: Van Nostrand, pp. 263-281, 1953.
- [18] S. R. Bowes, and B. M. Bird "Novel approach to the analysis and synthesis of modulation processes in power converters," *Proc. IEE*, vol. 122, no. 5, pp. 507-513, May 1975.
- [19] G. Carrara,S. Gardella,M. Marchesoni,R. Salutari and G. Sciutto, "A New Multilevel PWM Method: A Theoretical Analysis," *IEEE Trans. Power Electron.*, vol. 7, no. 3, pp. 497-505, July 1992.
- [20] B. P. McGrath and D. G. Holmes "A Comparison of Multicarrier PWM Strategies for Cascaded and Neutral Point Clamped Multilevel Inverters," *IEEE PESC'2000 Conf. Proc.*, pp. 674-679, 2000.
- [21] S. R. Bowes "New sinusoidal pulsewidth-modulated invertor," *Proc. IEE*, vol. 122, no. 11, pp. 1279-1285, Nov. 1975.
- [22] J. Hamman and F. S. Van der Merwe "Voltage Harmonics Generated by Voltage-Fed Inverters Using PWM Natural Sampling," *IEEE Trans. Power Electron.*, vol. 3, no. 3, pp. 297-302 July 1988.

- [23] D. G. Holmes "A General Analytical Method for Determining the Theoretical Harmonic Components of Carrier Based PWM Strategies," in Conf. Rec. IEEE-IAS Annu. Meeting, pp. 1207-1214, 1998.
- [24] J. F. Moynihan, M. G. Egan and J. M. D. Murphy "Theoretical spectra of space-vector-modulated waveforms," IEE Proc.-Electr. Power Appl., vol. 145, no. 1, pp. 17-24, Jan. 1998.
- [25] J. T. Boys and P. G. Handley "Harmonic analysis of space vector modulated PWM waveform," IEE Proc., vol. 137, no. 4, pp. 197-204, July 1990.
- [26] H. W. Van der Broeck, H. C. Skudelny and G. V. Stanke "Analysis and Realization of a Pulsewidth Modulator Based on Voltage Space Vectors", IEEE Trans. on Industrial Applications, vol. 24, no. 1, pp. 142-150, Jan./Feb. 1988.
- [27] W. R. Bennett "New results in the calculation of modulation products," Bell syst. Tech.J., vol. 12, pp. 228-243, 1933.
- [28] A. von Jouanne, S. Dai and H. Zhang "A simple method for balancing the DC-link voltage of three-level inverters," IEEE PESC'2001 Conf. Proc., pp. 1341-1345, June 2001.
- [29] D. Zhou "A self-balancing space vector switching modulator for three-level motor drives," IEEE Trans. Power Electron., vol. 17, no. 6, pp. 1024-1031, Nov. 2002.
- [30] S. Fukuda "Optimal-regulator-based control of NPC boost rectifiers for unity power factor and reduced neutral-point-potential variations," IEEE Trans. Ind. Electron., vol. 46, no. 3, pp. 527-534, June 1999.
- [31] K. Zhou and D. Wang "Relationship between space-vector modulation and three-phase carrier-based PWM: A comprehensive analysis," IEEE Trans. Ind. Electron., vol. 49, no. 1, pp. 186-196, Feb. 2002.
- [32] J. W. Nilsson and S. A. Riedel "Electric Circuits," Prentice Hall, Sixth Edition, pp. 719-722, 2000.
- [33] J. W. Nilsson and S. A. Riedel "Electric Circuits," Prentice Hall, Sixth Edition, pp. 433-437, pp. 541-572, 2000.
- [34] H. Akagi, Y. Kanazawa and A. Nabae "Generalized theory of the instantaneous reactive power in three-phase circuits," IPEC'83-Int. Power Electronics Conf., Tokyo, Japan, pp. 1375-1386, 1983.

- [35] H. Akagi, Y. Kanazawa and A. Nabae “Instantaneous reactive power compensators comprising switching devices without energy storage components,” IEEE Trans. Ind. App., vol. 20, no. 3, pp. 625-630, May/June 1984.
- [36] I. S. Gradshteyn and I. M. Ryzhik “Tables of Integrals, Series, and Products,” Fifth Edition, pp. 942-1003, 1994.
- [37] F. Oberhettinger “Tables of Bessel Transforms,” pp. 279-281, 1972.

Appendix A

Harmonics using APOD/POD PWM technique

A.1 Coefficients of $(s_\alpha \times \frac{V_t}{2})$ and $(s_\beta \times \frac{V_t}{2})$ under APOD/POD PWM.

In this section we calculate the coefficients of equation 4.2 in section 4.1 using Figure 4.3. We thereafter use the calculated results in the first part of subsection 4.1.1.

For $m = 0$

$$\begin{aligned}
A_{0n} + jB_{0n} &= \frac{1}{2\pi^2} \int_0^{2\pi} \int_0^{2\pi} F(x, y) e^{j(ny)} dx dy \\
&= \frac{1}{2\pi^2} \left\{ \int_0^\pi \int_0^{2\pi} F(x, y) e^{j(ny)} dx dy + \int_\pi^{2\pi} \int_0^{2\pi} F(x, y) e^{j(ny)} dx dy \right\} \\
&= \frac{1}{2\pi^2} \left[\int_0^\pi \left\{ \int_0^{m_a \pi \sin y} \frac{V_t}{2} e^{j(ny)} dx + \int_{2\pi - m_a \pi \sin y}^{2\pi} \frac{V_t}{2} e^{j(ny)} dx \right\} dy \right. \\
&\quad \left. + \int_\pi^{2\pi} \left\{ \int_0^{-m_a \pi \sin y} \frac{-V_t}{2} e^{j(ny)} dx + \int_{2\pi + m_a \pi \sin y}^{2\pi} \frac{-V_t}{2} e^{j(ny)} dx \right\} dy \right] \\
&= \frac{1}{2\pi^2} \frac{V_t}{2} \left[\int_0^\pi e^{j(ny)} \{m_a \pi \sin y + 2\pi - (2\pi - m_a \pi \sin y)\} dy + \right. \\
&\quad \left. \int_\pi^{2\pi} e^{j(ny)} \{ -(-m_a \pi \sin y + 2\pi - (2\pi + m_a \pi \sin y)) \} dy \right] \\
&= \frac{V_t}{4\pi^2} \left[\int_0^\pi e^{j(ny)} (2m_a \pi \sin y) dy + \int_\pi^{2\pi} e^{j(ny)} (2m_a \pi \sin y) dy \right] \\
&= \frac{V_t}{4\pi^2} \int_0^{2\pi} e^{j(ny)} (2m_a \pi \sin y) dy \\
&= \frac{V_t m_a (e^{2j\pi n} - 1)}{2\pi (n^2 - 1)}
\end{aligned} \tag{A.1}$$

For $m = 0$ and $n = 1$

$$\begin{aligned}
A_{01} + jB_{01} &= \frac{1}{2\pi^2} \int_0^{2\pi} \int_0^{2\pi} F(x, y) e^{j(y)} dx dy \\
&= \frac{1}{2\pi^2} \left\{ \int_0^\pi \int_0^{2\pi} F(x, y) e^{j(y)} dx dy + \int_\pi^{2\pi} \int_0^{2\pi} F(x, y) e^{j(y)} dx dy \right\}
\end{aligned}$$

$$\begin{aligned}
&= \frac{1}{2\pi^2} \left[\int_0^\pi \left\{ \int_0^{m_a \pi \sin y} \frac{V_t}{2} e^{j(y)} dx + \int_{2\pi - m_a \pi \sin y}^{2\pi} \frac{V_t}{2} e^{j(y)} dx \right\} dy \right. \\
&\quad \left. + \int_\pi^{2\pi} \left\{ \int_0^{-m_a \pi \sin y} \frac{-V_t}{2} e^{j(y)} dx + \int_{2\pi + m_a \pi \sin y}^{2\pi} \frac{-V_t}{2} e^{j(y)} dx \right\} dy \right] \\
&= \frac{1}{2\pi^2} \frac{V_t}{2} \left[\int_0^\pi e^{j(y)} \{m_a \pi \sin y + 2\pi - (2\pi - m_a \pi \sin y)\} dy + \right. \\
&\quad \left. \int_\pi^{2\pi} e^{j(y)} \{-(-m_a \pi \sin y + 2\pi - (2\pi + m_a \pi \sin y))\} dy \right] \\
&= \frac{V_t}{4\pi^2} \left[\int_0^\pi e^{j(y)} (2m_a \pi \sin y) dy + \int_\pi^{2\pi} e^{j(y)} (2m_a \pi \sin y) dy \right] \\
&= \frac{V_t}{4\pi^2} \int_0^{2\pi} e^{j(y)} (2m_a \pi \sin y) dy \\
&= \frac{jV_t m_a}{2}
\end{aligned} \tag{A.2}$$

For $m \neq 0$

$$\begin{aligned}
A_{mn} + jB_{mn} &= \frac{1}{2\pi^2} \int_0^{2\pi} \int_0^{2\pi} F(x, y) e^{j(mx+ny)} dx dy \\
&= \frac{1}{2\pi^2} \left\{ \int_0^\pi \int_0^{2\pi} F(x, y) e^{j(mx+ny)} dx dy + \int_\pi^{2\pi} \int_0^{2\pi} F(x, y) e^{j(mx+ny)} dx dy \right\} \\
&= \frac{1}{2\pi^2} \left[\int_0^\pi \left\{ \int_0^{m_a \pi \sin(y)} \frac{V_t}{2} e^{j(mx+ny)} dx + \int_{m_a \pi \sin(y)}^{2\pi - m_a \pi \sin(y)} 0 e^{j(mx+ny)} dx \right. \right. \\
&\quad \left. \left. + \int_{2\pi - m_a \pi \sin(y)}^{2\pi} \frac{V_t}{2} e^{j(mx+ny)} dx \right\} dy + \int_\pi^{2\pi} \left\{ \int_0^{-m_a \pi \sin(y)} \left(-\frac{V_t}{2} \right) e^{j(mx+ny)} dx \right. \right. \\
&\quad \left. \left. + \int_{-m_a \pi \sin(y)}^{2\pi + m_a \pi \sin(y)} 0 e^{j(mx+ny)} dx + \int_{2\pi + m_a \pi \sin(y)}^{2\pi} \left(\frac{-V_t}{2} \right) e^{j(mx+ny)} dx \right\} dy \right] \\
&= \frac{1}{2\pi^2} \left[\int_0^\pi \left\{ \int_0^{m_a \pi \sin(y)} \frac{V_t}{2} e^{j(mx+ny)} dx + \int_{2\pi - m_a \pi \sin(y)}^{2\pi} \frac{V_t}{2} e^{j(mx+ny)} dx \right\} dy \right. \\
&\quad \left. + \int_\pi^{2\pi} \left\{ \int_0^{-m_a \pi \sin(y)} \left(-\frac{V_t}{2} \right) e^{j(mx+ny)} dx + \int_{2\pi + m_a \pi \sin(y)}^{2\pi} \left(\frac{-V_t}{2} \right) e^{j(mx+ny)} dx \right\} dy \right] \\
&= \frac{1}{2\pi} \frac{V_t}{2mj} \left[\int_0^\pi \left\{ e^{jny} (e^{jm(m_a \pi \sin(y))} - e^{jn(0)}) \right. \right. \\
&\quad \left. \left. + e^{jny} (e^{jm(2\pi)} - e^{jm(2\pi - m_a \pi \sin(y))}) \right\} dy \right. \\
&\quad \left. - \int_\pi^{2\pi} \left\{ e^{jny} (e^{jm(-m_a \pi \sin(y))} - e^{jm(0)}) \right. \right. \\
&\quad \left. \left. + e^{jny} (e^{jm(2\pi)} - e^{jm(2\pi + m_a \pi \sin(y))}) \right\} dy \right] \\
&= \frac{-jV_t}{4\pi^2 m} \left[\int_0^\pi \left\{ e^{jny} e^{jm \pi m_a \sin(y)} - e^{jny} e^{jm(2\pi - m_a \pi \sin(y))} \right\} dy \right]
\end{aligned}$$

$$\begin{aligned}
& - \int_{\pi}^{2\pi} \left\{ e^{jny} e^{jm\pi(-m_a \sin(y))} - e^{jny} e^{jm(2\pi+m_a \pi \sin(y))} \right\} dy \Big] \\
& = \frac{-jV_t}{4\pi^2 m} \left[\int_0^{\pi} \left\{ e^{jny} (e^{jm\pi m_a \sin(y)} - e^{-jm\pi m_a \sin(y)}) \right\} dy \right. \\
& \quad \left. - \int_{\pi}^{2\pi} \left\{ e^{jny} (e^{-jm\pi m_a \sin(y)} - e^{jm\pi m_a \sin(y)}) \right\} dy \right] \\
& = \frac{-jV_t}{4\pi^2 m} \left\{ \int_0^{\pi} e^{jny} e^{jm\pi m_a \sin(y)} dy + \int_{\pi}^{2\pi} e^{jny} e^{jm\pi m_a \sin(y)} dy \right. \\
& \quad \left. - \int_0^{\pi} e^{jny} e^{-jm\pi m_a \sin(y)} dy - \int_{\pi}^{2\pi} e^{jny} e^{-jm\pi m_a \sin(y)} dy \right\} \\
& = \frac{-jV_t}{4\pi^2 m} \left\{ \int_0^{2\pi} e^{jny} e^{jm\pi m_a \sin(y)} dy - \int_0^{2\pi} e^{jny} e^{-jm\pi m_a \sin(y)} dy \right\}
\end{aligned}$$

Let $\theta = y - \pi$ then $d\theta = dy$ and $\theta = \begin{cases} -\pi & \text{as } y = 0 \\ \pi & \text{as } y = 2\pi \end{cases}$

$$\begin{aligned}
A_{mn} + jB_{mn} &= \frac{-jV_t}{4\pi^2 m} \left\{ \int_{-\pi}^{\pi} e^{jn(\theta+\pi)} e^{-jm\pi m_a \sin(\theta)} d\theta - \int_{-\pi}^{\pi} e^{jn(\theta+\pi)} e^{jm\pi m_a \sin(\theta)} d\theta \right\} \\
&= \frac{-jV_t}{2m\pi} e^{jn\pi} \left\{ \frac{1}{2\pi} \int_{-\pi}^{\pi} e^{jn\theta} e^{-jm\pi m_a \sin \theta} d\theta - \frac{1}{2\pi} \int_{-\pi}^{\pi} e^{jn\theta} e^{jm\pi m_a \sin \theta} d\theta \right\} \\
&= \frac{-jV_t}{2m\pi} e^{jn\pi} \{ J_{-n}(-m\pi m_a) - J_{-n}(m\pi m_a) \} \\
&= \frac{-jV_t}{2m\pi} e^{jn\pi} \{ J_n(m\pi m_a) - (-1)^n J_n(m\pi m_a) \}
\end{aligned} \tag{A.3}$$

where J is a Bessel function given by

$$J_n(m\pi m_a) = \frac{1}{2\pi} \int_{-\pi}^{\pi} e^{-i(m\pi m_a)} e^{in\theta} d\theta$$

A.2 Derivation of s_α under APOD/POD PWM

We now derive the Fourier series equation for s_α which is used in the first part of subsection 4.1.1 and in subsection 4.1.2.

$$\begin{aligned}
s_\alpha &= \sqrt{\frac{2}{3}} (s_a - s_b/2 - s_c/2) \\
&= \sqrt{\frac{2}{3}} \left[\frac{1}{2} A_{00} + \sum_{n=1}^{\infty} (A_{0n} \cos n\omega_1 t + B_{0n} \sin n\omega_1 t) + \sum_{m=1}^{\infty} (A_{m0} \cos m\omega_s t + B_{m0} \sin m\omega_s t) \right. \\
&\quad \left. + \sum_{m=1}^{\infty} \sum_{n=\pm 1}^{\pm\infty} (A_{mn} \cos ((m\omega_s + n\omega_1) t) + B_{mn} \sin ((m\omega_s + n\omega_1) t)) \right. \\
&\quad \left. - \frac{1}{2} \left\{ \frac{1}{2} A_{00} + \sum_{n=1}^{\infty} \left(A_{0n} \cos n\omega_1 \left(t - \frac{2\pi}{3\omega_1} \right) + B_{0n} \sin n\omega_1 \left(t - \frac{2\pi}{3\omega_1} \right) \right) \right\} \right]
\end{aligned}$$

$$\begin{aligned}
& + \sum_{m=1}^{\infty} \left(A_{m0} \cos m\omega_s \left(t - \frac{2\pi}{3\omega_1} \right) + B_{m0} \sin m\omega_s \left(t - \frac{2\pi}{3\omega_1} \right) \right) \\
& + \sum_{m=1}^{\infty} \sum_{n=\pm 1}^{\pm \infty} \left\{ A_{mn} \cos \left((m\omega_s + n\omega_1) \left(t - \frac{2\pi}{3\omega_1} \right) \right) \right. \\
& \quad \left. + B_{mn} \sin \left((m\omega_s + n\omega_1) \left(t - \frac{2\pi}{3\omega_1} \right) \right) \right\} \\
& + \frac{1}{2} \left\{ \frac{1}{2} A_{00} + \sum_{n=1}^{\infty} \left(A_{0n} \cos n\omega_1 \left(t + \frac{2\pi}{3\omega_1} \right) + B_{0n} \sin n\omega_1 \left(t + \frac{2\pi}{3\omega_1} \right) \right) \right. \\
& \quad \left. + \sum_{m=1}^{\infty} \left(A_{m0} \cos m\omega_s \left(t + \frac{2\pi}{3\omega_1} \right) + B_{m0} \sin m\omega_s \left(t + \frac{2\pi}{3\omega_1} \right) \right) \right. \\
& \quad \left. + \sum_{m=1}^{\infty} \sum_{n=\pm 1}^{\pm \infty} \left\{ A_{mn} \cos \left((m\omega_s + n\omega_1) \left(t + \frac{2\pi}{3\omega_1} \right) \right) \right. \right. \\
& \quad \left. \left. + B_{mn} \sin \left((m\omega_s + n\omega_1) \left(t + \frac{2\pi}{3\omega_1} \right) \right) \right\} \right] \\
= & \sqrt{\frac{2}{3}} \left[\sum_{n=1}^{\infty} \left\{ A_{0n} \cos n\omega_1 t + B_{0n} \sin n\omega_1 t - \frac{1}{2} A_{0n} \cos n\omega_1 \left(t - \frac{2\pi}{3\omega_1} \right) \right. \right. \\
& \quad \left. - \frac{1}{2} B_{0n} \sin n\omega_1 \left(t - \frac{2\pi}{3\omega_1} \right) - \frac{1}{2} A_{0n} \cos n\omega_1 \left(t + \frac{2\pi}{3\omega_1} \right) \right. \\
& \quad \left. - \frac{1}{2} B_{0n} \sin n\omega_1 \left(t + \frac{2\pi}{3\omega_1} \right) \right\} \\
& \quad + \sum_{m=1}^{\infty} \left\{ A_{m0} \cos m\omega_s t + B_{m0} \sin m\omega_s t - \frac{1}{2} A_{m0} \cos m\omega_s \left(t - \frac{2\pi}{3\omega_1} \right) \right. \\
& \quad \left. - \frac{1}{2} B_{m0} \sin m\omega_s \left(t - \frac{2\pi}{3\omega_1} \right) - \frac{1}{2} A_{m0} \cos m\omega_s \left(t + \frac{2\pi}{3\omega_1} \right) \right. \\
& \quad \left. - \frac{1}{2} B_{m0} \sin m\omega_s \left(t + \frac{2\pi}{3\omega_1} \right) \right\} \\
& \quad + \sum_{m=1}^{\infty} \sum_{n=\pm 1}^{\pm \infty} \left\{ A_{mn} \cos ((m\omega_s + n\omega_1) t) + B_{mn} \sin ((m\omega_s + n\omega_1) t) \right. \\
& \quad \left. - \frac{1}{2} A_{mn} \cos \left((m\omega_s + n\omega_1) \left(t - \frac{2\pi}{3\omega_1} \right) \right) - \frac{1}{2} B_{mn} \sin \left((m\omega_s + n\omega_1) \left(t - \frac{2\pi}{3\omega_1} \right) \right) \right. \\
& \quad \left. - \frac{1}{2} A_{mn} \cos \left((m\omega_s + n\omega_1) \left(t + \frac{2\pi}{3\omega_1} \right) \right) - \frac{1}{2} B_{mn} \sin \left((m\omega_s + n\omega_1) \left(t + \frac{2\pi}{3\omega_1} \right) \right) \right\} \\
= & \sqrt{\frac{2}{3}} \left[\sum_{n=1}^{\infty} \left\{ A_{0n} \left(\cos n\omega_1 t - \frac{1}{2} \cos n\omega_1 \left(t - \frac{2\pi}{3\omega_1} \right) - \frac{1}{2} \cos n\omega_1 \left(t + \frac{2\pi}{3\omega_1} \right) \right) \right. \right. \\
& \quad \left. + B_{0n} \left(\sin n\omega_1 t - \frac{1}{2} \sin n\omega_1 \left(t - \frac{2\pi}{3\omega_1} \right) - \frac{1}{2} \sin n\omega_1 \left(t + \frac{2\pi}{3\omega_1} \right) \right) \right\} \\
& \quad + \sum_{m=1}^{\infty} \left\{ A_{m0} \left(\cos m\omega_s t - \frac{1}{2} \cos m\omega_s \left(t - \frac{2\pi}{3\omega_1} \right) - \frac{1}{2} \cos m\omega_s \left(t + \frac{2\pi}{3\omega_1} \right) \right) \right. \\
& \quad \left. + B_{m0} \left(\sin m\omega_s t - \frac{1}{2} \sin m\omega_s \left(t - \frac{2\pi}{3\omega_1} \right) - \frac{1}{2} \sin m\omega_s \left(t + \frac{2\pi}{3\omega_1} \right) \right) \right\}
\end{aligned}$$

$$\begin{aligned}
& + \sum_{m=1}^{\infty} \sum_{n=\pm 1}^{\pm \infty} \left\{ A_{mn} \left(\cos((m\omega_s + n\omega_1)t) - \frac{1}{2} \cos \left((m\omega_s + n\omega_1) \left(t - \frac{2\pi}{3\omega_1} \right) \right) \right. \right. \\
& \quad \left. \left. - \frac{1}{2} \cos \left((m\omega_s + n\omega_1) \left(t + \frac{2\pi}{3\omega_1} \right) \right) \right) \right. \\
& \quad \left. + B_{mn} \left(\sin((m\omega_s + n\omega_1)t) - \frac{1}{2} \sin \left((m\omega_s + n\omega_1) \left(t - \frac{2\pi}{3\omega_1} \right) \right) \right. \right. \\
& \quad \left. \left. - \frac{1}{2} \sin \left((m\omega_s + n\omega_1) \left(t + \frac{2\pi}{3\omega_1} \right) \right) \right) \right\}
\end{aligned}$$

That is

$$\begin{aligned}
s_\alpha = & \sqrt{\frac{2}{3}} \left[\sum_{n=1}^{\infty} \left\{ A_{0n} \overbrace{\left(\cos n\omega_1 t - \frac{1}{2} \cos n\omega_1 \left(t - \frac{2\pi}{3\omega_1} \right) - \frac{1}{2} \cos n\omega_1 \left(t + \frac{2\pi}{3\omega_1} \right) \right)}^1 \right. \right. \\
& \quad \left. \left. + B_{0n} \left(\sin n\omega_1 t - \frac{1}{2} \sin n\omega_1 \left(t - \frac{2\pi}{3\omega_1} \right) - \frac{1}{2} \sin n\omega_1 \left(t + \frac{2\pi}{3\omega_1} \right) \right) \right\}^2 \right] \\
& + \sum_{m=1}^{\infty} \left\{ A_{m0} \overbrace{\left(\cos m\omega_s t - \frac{1}{2} \cos m\omega_s \left(t - \frac{2\pi}{3\omega_1} \right) - \frac{1}{2} \cos m\omega_s \left(t + \frac{2\pi}{3\omega_1} \right) \right)}^3 \right. \right. \\
& \quad \left. \left. + B_{m0} \left(\sin m\omega_s t - \frac{1}{2} \sin m\omega_s \left(t - \frac{2\pi}{3\omega_1} \right) - \frac{1}{2} \sin m\omega_s \left(t + \frac{2\pi}{3\omega_1} \right) \right) \right\}^4 \right] \\
& + \sum_{m=1}^{\infty} \sum_{n=\pm 1}^{\pm \infty} \left\{ A_{mn} \overbrace{\left(\cos((m\omega_s + n\omega_1)t) - \frac{1}{2} \cos \left((m\omega_s + n\omega_1) \left(t - \frac{2\pi}{3\omega_1} \right) \right) \right.}^5 \right. \\
& \quad \left. \left. - \frac{1}{2} \cos \left((m\omega_s + n\omega_1) \left(t + \frac{2\pi}{3\omega_1} \right) \right) \right) \right. \\
& \quad \left. + B_{mn} \overbrace{\left(\sin((m\omega_s + n\omega_1)t) - \frac{1}{2} \sin \left((m\omega_s + n\omega_1) \left(t - \frac{2\pi}{3\omega_1} \right) \right) \right.}^6 \right. \\
& \quad \left. \left. - \frac{1}{2} \sin \left((m\omega_s + n\omega_1) \left(t + \frac{2\pi}{3\omega_1} \right) \right) \right) \right\}^6 \right] \quad (A.4)
\end{aligned}$$

We divided equation A.4 into six parts in order to make simplifying easy. Now we simplify equation A.4 by solving each part separately.

For part 1 we have

$$\begin{aligned} \cos n\omega_1 t - \frac{1}{2} \cos n\omega_1 \left(t - \frac{2\pi}{3\omega_1} \right) - \frac{1}{2} \cos n\omega_1 \left(t + \frac{2\pi}{3\omega_1} \right) &= \cos n\omega_1 t \left(1 - \cos \frac{2n\pi}{3} \right) \\ &= \begin{cases} \frac{3}{2} \cos n\omega_1 t & \text{if } n \neq 3k \\ 0 & \text{if } n = 3k \end{cases} \end{aligned}$$

where k is an integer.

For part 2 we have

$$\begin{aligned} \sin n\omega_1 t - \frac{1}{2} \sin n\omega_1 \left(t - \frac{2\pi}{3\omega_1} \right) - \frac{1}{2} \sin n\omega_1 \left(t + \frac{2\pi}{3\omega_1} \right) &= \sin n\omega_1 t \left(1 - \cos \frac{2n\pi}{3} \right) \\ &= \begin{cases} \frac{3}{2} \sin n\omega_1 t & \text{if } n \neq 3k \\ 0 & \text{if } n = 3k \end{cases} \end{aligned}$$

where k is an integer.

For part 3 we have

$$\begin{aligned} \cos m\omega_s t - \frac{1}{2} \cos m\omega_s \left(t - \frac{2\pi}{3\omega_1} \right) - \frac{1}{2} \cos m\omega_s \left(t + \frac{2\pi}{3\omega_1} \right) &= \cos m\omega_s t (1 - \cos 2mk\pi) \\ &= 0 \\ \sin m\omega_s t - \frac{1}{2} \sin m\omega_s \left(t - \frac{2\pi}{3\omega_1} \right) - \frac{1}{2} \sin m\omega_s \left(t + \frac{2\pi}{3\omega_1} \right) &= \sin m\omega_s t (1 - \cos 2mk\pi) \\ &= 0 \end{aligned}$$

For part 4 we have

$$\cos ((m\omega_s + n\omega_1) t) - \frac{1}{2} \cos \left((m\omega_s + n\omega_1) \left(t - \frac{2\pi}{3\omega_1} \right) \right) - \frac{1}{2} \cos \left((m\omega_s + n\omega_1) \left(t + \frac{2\pi}{3\omega_1} \right) \right)$$

For part 5 we have

$$\begin{aligned} &= \cos ((m\omega_s + n\omega_1) t) \left\{ 1 - \cos \left(2mk\pi + \frac{2n\pi}{3} \right) \right\} \\ &= \cos ((m\omega_s + n\omega_1) t) \left(1 - \cos \frac{2n\pi}{3} \right) \\ &= \begin{cases} \frac{3}{2} \cos ((m\omega_s + n\omega_1) t) & \text{if } n \neq 3k \\ 0 & \text{if } n = 3k \end{cases} \end{aligned}$$

where k is an integer.

For part 6 we have

$$\begin{aligned} &\sin ((m\omega_s + n\omega_1) t) - \frac{1}{2} \sin \left((m\omega_s + n\omega_1) \left(t - \frac{2\pi}{3\omega_1} \right) \right) - \frac{1}{2} \sin \left((m\omega_s + n\omega_1) \left(t + \frac{2\pi}{3\omega_1} \right) \right) \\ &= \sin ((m\omega_s + n\omega_1) t) \left(1 - \cos \frac{2n\pi}{3} \right) \\ &= \begin{cases} \frac{3}{2} \sin ((m\omega_s + n\omega_1) t) & \text{if } n \neq 3k \\ 0 & \text{if } n = 3k \end{cases} \end{aligned}$$

where k is an integer.

Now substituting solutions of these parts back into equation A.4 we obtain

$$\begin{aligned} s_\alpha &= \sqrt{\frac{2}{3}} \left[\sum_{n=1}^{\infty} \{A_{0n} \cos n\omega_1 t + B_{0n} \sin n\omega_1 t\} \right. \\ &\quad \left. + \sum_{m=1}^{\infty} \sum_{n=\pm 1}^{\pm \infty} \{A_{mn} \cos ((m\omega_s + n\omega_1) t) + B_{mn} \sin ((m\omega_s + n\omega_1) t)\} \right] \end{aligned} \quad (\text{A.5})$$

for $m_f = \frac{\omega_s}{\omega_1} = 3k$ and $n \neq 3k$

where k is an integer.

That is

$$\begin{aligned} s_\alpha &= \sqrt{\frac{3}{2}} \left[\sum_{\substack{n=1 \\ n \neq 3k}}^{\infty} \{A_{0n} \cos n\omega_1 t + B_{0n} \sin n\omega_1 t\} \right. \\ &\quad \left. + \sum_{m=1}^{\infty} \sum_{\substack{n=\pm 1 \\ n \neq 3k}}^{\pm \infty} \{A_{mn} \cos ((m\omega_s + n\omega_1) t) + B_{mn} \sin ((m\omega_s + n\omega_1) t)\} \right] \end{aligned} \quad (\text{A.6})$$

A.3 Derivation of s_β under APOD/POD PWM.

Now we derive the Fourier series equation for s_β which is used in the first part of subsection 4.1.1 and in subsection 4.1.2.

$$\begin{aligned} s_\beta &= \frac{1}{\sqrt{2}} (s_b - s_c) \\ &= \frac{1}{\sqrt{2}} \left[\left\{ \frac{1}{2} A_{00} + \sum_{n=1}^{\infty} \left(A_{0n} \cos n\omega_1 \left(t - \frac{2\pi}{3\omega_1} \right) + B_{0n} \sin n\omega_1 \left(t - \frac{2\pi}{3\omega_1} \right) \right) \right. \right. \\ &\quad \left. \left. + \sum_{m=1}^{\infty} \left(A_{m0} \cos m\omega_s \left(t - \frac{2\pi}{3\omega_1} \right) + B_{m0} \sin m\omega_s \left(t - \frac{2\pi}{3\omega_1} \right) \right) \right\} \right. \\ &\quad \left. - \left\{ \frac{1}{2} A_{00} + \sum_{n=1}^{\infty} \left(A_{0n} \cos n\omega_1 \left(t + \frac{2\pi}{3\omega_1} \right) + B_{0n} \sin n\omega_1 \left(t + \frac{2\pi}{3\omega_1} \right) \right) \right. \right. \\ &\quad \left. \left. + \sum_{m=1}^{\infty} \left(A_{m0} \cos m\omega_s \left(t + \frac{2\pi}{3\omega_1} \right) + B_{m0} \sin m\omega_s \left(t + \frac{2\pi}{3\omega_1} \right) \right) \right\} \right. \\ &\quad \left. + \sum_{m=1}^{\infty} \sum_{n=\pm 1}^{\pm \infty} \left(A_{mn} \cos ((m\omega_s + n\omega_1) \left(t - \frac{2\pi}{3\omega_1} \right)) \right. \right. \\ &\quad \left. \left. + B_{mn} \sin ((m\omega_s + n\omega_1) \left(t - \frac{2\pi}{3\omega_1} \right)) \right) \right. \\ &\quad \left. - \sum_{m=1}^{\infty} \sum_{n=\pm 1}^{\pm \infty} \left(A_{mn} \cos ((m\omega_s + n\omega_1) \left(t + \frac{2\pi}{3\omega_1} \right)) \right) \right] \end{aligned}$$

$$\begin{aligned}
& + B_{mn} \sin \left((m\omega_s + n\omega_1) \left(t + \frac{2\pi}{3\omega_1} \right) \right) \Big] \\
= & \frac{1}{\sqrt{2}} \left[\sum_{n=1}^{\infty} \left\{ A_{0n} \left(\cos n\omega_1 \left(t - \frac{2\pi}{3\omega_1} \right) - \cos n\omega_1 \left(t + \frac{2\pi}{3\omega_1} \right) \right) \right. \right. \\
& + B_{0n} \left(\sin n\omega_1 \left(t - \frac{2\pi}{3\omega_1} \right) - \sin n\omega_1 \left(t + \frac{2\pi}{3\omega_1} \right) \right) \Big\} \\
& + \sum_{m=1}^{\infty} \left\{ A_{m0} \left(\cos m\omega_s \left(t - \frac{2\pi}{3\omega_1} \right) - \cos m\omega_s \left(t + \frac{2\pi}{3\omega_1} \right) \right) \right. \\
& + B_{m0} \left(\sin m\omega_s \left(t - \frac{2\pi}{3\omega_1} \right) - \sin m\omega_s \left(t + \frac{2\pi}{3\omega_1} \right) \right) \Big\} \\
& + \sum_{m=1}^{\infty} \sum_{n=\pm 1}^{\pm \infty} \left\{ A_{mn} \left(\cos \left((m\omega_s + n\omega_1) \left(t - \frac{2\pi}{3\omega_1} \right) \right) \right. \right. \\
& - \cos \left((m\omega_s + n\omega_1) \left(t + \frac{2\pi}{3\omega_1} \right) \right) \Big) \\
& \left. \left. + B_{mn} \left(\sin \left((m\omega_s + n\omega_1) \left(t - \frac{2\pi}{3\omega_1} \right) \right) - \sin \left((m\omega_s + n\omega_1) \left(t + \frac{2\pi}{3\omega_1} \right) \right) \right) \right\} \Big]
\end{aligned}$$

That is

$$\begin{aligned}
s_{\beta} = & \frac{1}{\sqrt{2}} \left[\sum_{n=1}^{\infty} \left\{ A_{0n} \overbrace{\left(\cos n\omega_1 \left(t - \frac{2\pi}{3\omega_1} \right) - \cos n\omega_1 \left(t + \frac{2\pi}{3\omega_1} \right) \right)}^1 \right. \right. \\
& + B_{0n} \overbrace{\left(\sin n\omega_1 \left(t - \frac{2\pi}{3\omega_1} \right) - \sin n\omega_1 \left(t + \frac{2\pi}{3\omega_1} \right) \right)}^2 \Big\} \\
& + \sum_{m=1}^{\infty} \left\{ A_{m0} \overbrace{\left(\cos m\omega_s \left(t - \frac{2\pi}{3\omega_1} \right) - \cos m\omega_s \left(t + \frac{2\pi}{3\omega_1} \right) \right)}^3 \right. \\
& + B_{m0} \overbrace{\left(\sin m\omega_s \left(t - \frac{2\pi}{3\omega_1} \right) - \sin m\omega_s \left(t + \frac{2\pi}{3\omega_1} \right) \right)}^4 \Big\} \\
& + \sum_{m=1}^{\infty} \sum_{n=\pm 1}^{\pm \infty} \left\{ A_{mn} \overbrace{\left(\cos \left((m\omega_s + n\omega_1) \left(t - \frac{2\pi}{3\omega_1} \right) \right) \right)}^5 \right. \\
& \left. \left. - \cos \left((m\omega_s + n\omega_1) \left(t + \frac{2\pi}{3\omega_1} \right) \right) \right\} \right] \quad (A.7)
\end{aligned}$$

$$+B_{mn} \left[\overbrace{\left(\sin \left((m\omega_s + n\omega_1) \left(t - \frac{2\pi}{3\omega_1} \right) \right) - \sin \left((m\omega_s + n\omega_1) \left(t + \frac{2\pi}{3\omega_1} \right) \right) \right)}^6 \right]$$

We divided equation A.7 into six parts in order to make simplifying easy. Now we simplify equation A.7 by solving each part separately.

For part 1 we have

$$\begin{aligned} \cos \left(n\omega_1 t - \frac{2n\pi}{3} \right) - \cos \left(n\omega_1 t + \frac{2n\pi}{3} \right) &= 2 \sin n\omega_1 t \sin \frac{2n\pi}{3} \\ &= \begin{cases} \sqrt{3} \sin n\omega_1 t & \text{if } n = 3k + 1 \\ -\sqrt{3} \sin n\omega_1 t & \text{if } n = 3k + 2 \\ 0 & \text{if } n = 3k \end{cases} \end{aligned}$$

where k is an integer

For part 2 we have

$$\begin{aligned} \sin \left(n\omega_1 t - \frac{2n\pi}{3} \right) - \sin \left(n\omega_1 t + \frac{2n\pi}{3} \right) &= 2 \cos n\omega_1 t \sin \frac{2n\pi}{3} \\ &= \begin{cases} -\sqrt{3} \cos n\omega_1 t & \text{if } n = 3k + 1 \\ \sqrt{3} \cos n\omega_1 t & \text{if } n = 3k + 2 \\ 0 & \text{if } n = 3k \end{cases} \end{aligned}$$

where k is an integer.

For part 3 we have

$$\begin{aligned} \cos(m\omega_s t - 2mk\pi) - \cos(m\omega_s t + 2mk\pi) &= 2 \sin m\omega_s t \sin 2mk\pi \\ &= 0 \end{aligned}$$

For part 4 we have

$$\begin{aligned} \sin(m\omega_s t - 2mk\pi) - \sin(m\omega_s t + 2mk\pi) &= -2 \cos m\omega_s t \sin 2mk\pi \\ &= 0 \end{aligned}$$

For part 5 we have

$$\cos \left((m\omega_s t + n\omega_1 t) - \left(2mk\pi + \frac{2n\pi}{3} \right) \right) - \cos \left((m\omega_s t + n\omega_1 t) + \left(2mk\pi + \frac{2n\pi}{3} \right) \right)$$

$$\begin{aligned}
&= 2 \sin(m\omega_s t + n\omega_1 t) \sin \frac{2n\pi}{3} \\
&= \begin{cases} \sqrt{3} \sin(m\omega_s t + n\omega_1 t) & \text{if } n = 3k + 1 \\ -\sqrt{3} \sin(m\omega_s t + n\omega_1 t) & \text{if } n = 3k + 2 \\ 0 & \text{if } n = 3k \end{cases}
\end{aligned}$$

where k is an integer.

For part 6 we have

$$\begin{aligned}
&\sin \left((m\omega_s t + n\omega_1 t) - \left(2mk\pi + \frac{2n\pi}{3} \right) \right) - \sin \left((m\omega_s t + n\omega_1 t) + \left(2mk\pi + \frac{2n\pi}{3} \right) \right) \\
&= -2 \cos(m\omega_s t + n\omega_1 t) \sin \left(2mk\pi + \frac{2n\pi}{3} \right) \\
&= \begin{cases} -\sqrt{3} \sin(m\omega_s t + n\omega_1 t) & \text{if } n = 3k + 1 \\ \sqrt{3} \sin(m\omega_s t + n\omega_1 t) & \text{if } n = 3k + 2 \\ 0 & \text{if } n = 3k \end{cases}
\end{aligned}$$

where k is an integer.

Now substituting solutions of these parts back into equation A.7 we obtain

$$\begin{aligned}
s_\beta &= \frac{1}{\sqrt{2}} \sqrt{3} \left[\sum_{n=1}^{\infty} \{A_{0n} \sin n\omega_1 t - B_{0n} \cos n\omega_1 t\} \right. \\
&\quad \left. + \sum_{m=1}^{\infty} \sum_{n=\pm 1}^{\pm \infty} \{A_{mn} \sin(m\omega_s t + n\omega_1 t) - B_{mn} \cos(m\omega_s t + n\omega_1 t)\} \right] \\
&= \frac{1}{\sqrt{2}} \sqrt{3} \left[\sum_{n=1}^{\infty} \left\{ A_{0n} \cos \left(n\omega_1 t - \frac{\pi}{2} \right) + B_{0n} \sin \left(n\omega_1 t - \frac{\pi}{2} \right) \right\} \right. \\
&\quad \left. + \sum_{m=1}^{\infty} \sum_{n=\pm 1}^{\pm \infty} \left\{ A_{mn} \cos \left((m\omega_s t + n\omega_1 t) - \frac{\pi}{2} \right) + B_{mn} \cos \left((m\omega_s t + n\omega_1 t) - \frac{\pi}{2} \right) \right\} \right]
\end{aligned}$$

if $n = 3k + 1$

for $m_f = \frac{\omega_s}{\omega_1} = 3k$ and $n \neq 3k$ where k is an integer

or

$$\begin{aligned}
s_\beta &= -\frac{1}{\sqrt{2}} \sqrt{3} \left[\sum_{n=1}^{\infty} \{A_{0n} \sin n\omega_1 t - B_{0n} \cos n\omega_1 t\} \right. \\
&\quad \left. + \sum_{m=1}^{\infty} \sum_{n=\pm 1}^{\pm \infty} \{A_{mn} \sin(m\omega_s t + n\omega_1 t) - B_{mn} \cos(m\omega_s t + n\omega_1 t)\} \right] \\
&= -\frac{1}{\sqrt{2}} \sqrt{3} \left[\sum_{n=1}^{\infty} \left\{ A_{0n} \cos \left(n\omega_1 t - \frac{\pi}{2} \right) + B_{0n} \sin \left(n\omega_1 t - \frac{\pi}{2} \right) \right\} \right. \\
&\quad \left. + \sum_{m=1}^{\infty} \sum_{n=\pm 1}^{\pm \infty} \left\{ A_{mn} \cos \left((m\omega_s t + n\omega_1 t) - \frac{\pi}{2} \right) + B_{mn} \cos \left((m\omega_s t + n\omega_1 t) - \frac{\pi}{2} \right) \right\} \right]
\end{aligned}$$

if $n = 3k + 2$

for $m_f = \frac{\omega_s}{\omega_1} = 3k$ and $n \neq 3k$ where k is an integer.

That is

$$\begin{aligned}
 s_\beta &= \sqrt{\frac{3}{2}} \left[\sum_{\substack{n=1 \\ n=3k+1}}^{\infty} \left\{ A_{0n} \cos \left(n\omega_1 t - \frac{\pi}{2} \right) + B_{0n} \sin \left(n\omega_1 t - \frac{\pi}{2} \right) \right\} \right. \\
 &\quad - \sum_{\substack{n=1 \\ n=3k+2}}^{\infty} \left\{ A_{0n} \cos \left(n\omega_1 t - \frac{\pi}{2} \right) + B_{0n} \sin \left(n\omega_1 t - \frac{\pi}{2} \right) \right\} \\
 &\quad + \sum_{m=1}^{\infty} \left[\sum_{\substack{n=\pm 1 \\ n=3k+1}}^{\pm \infty} \left\{ A_{mn} \cos \left((m\omega_s t + n\omega_1 t) - \frac{\pi}{2} \right) + B_{mn} \cos \left((m\omega_s t + n\omega_1 t) - \frac{\pi}{2} \right) \right\} \right. \\
 &\quad \left. \left. - \sum_{\substack{n=\pm 1 \\ n=3k+2}}^{\pm \infty} \left\{ A_{mn} \cos \left((m\omega_s t + n\omega_1 t) - \frac{\pi}{2} \right) + B_{mn} \cos \left((m\omega_s t + n\omega_1 t) - \frac{\pi}{2} \right) \right\} \right] \right]
 \end{aligned} \tag{A.8}$$

A.4 Harmonics for S_α and S_β using theory and MATLAB package under APOD/POD

(This program calculates the harmonics for S_α and S_β under APOD/POD modulation. This is done by using the theory developed in the first part of subsection 4.1.1. The resulting harmonics are shown in Figure 4.5.)

clear all

ws=2*pi*6000;

w1=2*pi*50;

A=0.8;

Vhrec(1)=sqrt(3/2)*A;

frec(1)=50*2*pi;

l=2;

for m=1:1:5

for n=0

frec(l)=n*w1;

if mod(n,2)==0

wrec(l)=frec(l)/(2*pi);

$Vhrec(l) = \sqrt{3/2} * (1/2) * (2 * A) * (\exp(2 * j * pi * n) - 1) / (pi * (n^2 - 1));$

l=l+1;

else

wrec(l)=frec(l)/(2*pi);

$Vhrec(l) = \sqrt{3/2} * (1/2) * (2 * A) * (\exp(2 * j * pi * n) - 1) / (pi * (n^2 - 1));$

```

l=l+1;
end;
end;
end;
for m=1:1:5
for n=2:1:15
frec(l)=n*w1;
if mod(n,2)==0
wrec(l)=frec(l)/(2*pi);
 $Vhrec(l) = \sqrt{3/2} * (1/2) * (2 * A) * (\exp(2 * j * pi * n) - 1) / (pi * (n^2 - 1));$ 
l=l+1;
else
wrec(l)=frec(l)/(2*pi);
 $Vhrec(l) = \sqrt{3/2} * (1/2) * (2 * A) * (\exp(2 * j * pi * n) - 1) / (pi * (n^2 - 1));$ 
l=l+1;
end;
end;
end;

for m=1:1:5
for n=-15:1:15
frec(l)=m*ws+n*w1;
if mod(n,3)==0
Vhrec(l)=0;
else
wrec(l)=frec(l)/(2*pi);
 $Vhrec(l) = \sqrt{3/2} * (-j * 2) / (2 * pi * m) * \exp(j * pi * n) * (besselj(n, m * A * pi) - besselj(-n, m * A * pi));$ 
l=l+1;

end;
end;
stem(frec/(2*pi),abs(Vhrec));
axis([0,25000,0,1]);
xlabel('f(Hz)');
ylabel('V');

```

A.5 Coefficients of $(s'_\alpha \times \frac{V_t}{2})$ and $(s'_\beta \times \frac{V_t}{2})$ under APOD/POD PWM.

(In this section we calculate the coefficients of equation 4.2 in section 4.1 using Figure 4.6. We thereafter use the calculated results in the second part of subsection 4.1.1 and in subsection 4.1.2.)

For $m = 0$

$$\begin{aligned}
 A_{0n} + jB_{0n} &= \frac{1}{2\pi^2} \int_0^{2\pi} \int_0^{2\pi} F(x, y) e^{jny} dx dy \\
 &= \frac{1}{2\pi^2} \left[\int_0^\pi \left\{ \int_0^{m_a \pi \sin(y)} \frac{V_t}{2} e^{jny} dx + \int_{m_a \pi \sin(y)}^{2\pi - m_a \pi \sin(y)} 0 e^{jny} dx \right. \right. \\
 &\quad \left. \left. + \int_{2\pi - m_a \pi \sin(y)}^{2\pi} \frac{V_t}{2} e^{jny} dx \right\} dy \right. \\
 &\quad \left. + \int_\pi^{2\pi} \left\{ \int_0^{-m_a \pi \sin(y)} \frac{V_t}{2} e^{jny} dx + \int_{-m_a \pi \sin(y)}^{2\pi + m_a \pi \sin(y)} 0 e^{jny} dx \right. \right. \\
 &\quad \left. \left. + \int_{2\pi + m_a \pi \sin(y)}^{2\pi} \frac{V_t}{2} e^{jny} dx \right\} dy \right] \\
 &= \frac{1}{2\pi^2} \frac{V_t}{2} \left[\int_0^\pi e^{jny} \{ (m_a \pi \sin y) + (2\pi) - (2\pi - m_a \pi \sin y) \} dy \right. \\
 &\quad \left. + \int_\pi^{2\pi} e^{jny} \{ (-m_a \pi \sin y) + (2\pi) - (2\pi + m_a \pi \sin y) \} dy \right] \\
 &= \frac{V_t}{4\pi^2} \left[\int_0^\pi e^{jny} (2m_a \pi \sin y) dy + \int_\pi^{2\pi} e^{jny} (-2m_a \pi \sin y) dy \right] \\
 &= -\frac{1}{2} V_t m_a \left\{ \frac{2e^{jn\pi} + 1 + e^{2jn\pi}}{\pi(n^2 - 1)} \right\} \tag{A.9}
 \end{aligned}$$

For $m = 0$ and $n = 1$

$$\begin{aligned}
 A_{01} + jB_{01} &= \frac{1}{2\pi^2} \int_0^{2\pi} \int_0^{2\pi} F(x, y) e^{jy} dx dy \\
 &= \frac{1}{2\pi^2} \left[\int_0^\pi \left\{ \int_0^{m_a \pi \sin(y)} \frac{V_t}{2} e^{jy} dx + \int_{m_a \pi \sin(y)}^{2\pi - m_a \pi \sin(y)} 0 e^{jy} dx \right. \right. \\
 &\quad \left. \left. + \int_{2\pi - m_a \pi \sin(y)}^{2\pi} \frac{V_t}{2} e^{jy} dx \right\} dy \right. \\
 &\quad \left. + \int_\pi^{2\pi} \left\{ \int_0^{-m_a \pi \sin(y)} \frac{V_t}{2} e^{jy} dx + \int_{-m_a \pi \sin(y)}^{2\pi + m_a \pi \sin(y)} 0 e^{jy} dx \right. \right. \\
 &\quad \left. \left. + \int_{2\pi + m_a \pi \sin(y)}^{2\pi} \frac{V_t}{2} e^{jy} dx \right\} dy \right]
 \end{aligned}$$

$$\begin{aligned}
&= \frac{1}{2\pi^2} \frac{V_t}{2} \left[\int_0^\pi e^{jy} \{(m_a\pi \sin y) + (2\pi) - (2\pi - m_a\pi \sin y)\} dy \right. \\
&\quad \left. + \int_\pi^{2\pi} e^{jy} \{(-m_a\pi \sin y) + (2\pi) - (2\pi + m_a\pi \sin y)\} dy \right] \\
&= \frac{V_t}{4\pi^2} \left[\int_0^\pi e^{jy} (2m_a\pi \sin y) dy + \int_\pi^{2\pi} e^{jy} (-2m_a\pi \sin y) dy \right] \\
&= 0 \tag{A.10}
\end{aligned}$$

For $m \neq 0$

$$\begin{aligned}
A_{mn} + jB_{mn} &= \frac{1}{2\pi^2} \int_0^{2\pi} \int_0^{2\pi} F(x, y) e^{j(mx+ny)} dx dy \\
&= \frac{1}{2\pi^2} \left\{ \int_0^\pi \int_0^{2\pi} F(x, y) e^{j(mx+ny)} dx dy + \int_\pi^{2\pi} \int_0^{2\pi} F(x, y) e^{j(mx+ny)} dx dy \right\} \\
&= \frac{1}{2\pi^2} \int_0^\pi \left\{ \int_0^{m_a\pi \sin(y)} \frac{V_t}{2} e^{j(mx+ny)} dx + \int_{m_a\pi \sin(y)}^{2\pi - m_a\pi \sin(y)} 0 e^{j(mx+ny)} dx \right. \\
&\quad \left. + \int_{2\pi - m_a\pi \sin(y)}^{2\pi} \frac{V_t}{2} e^{j(mx+ny)} dx \right\} dy + \int_\pi^{2\pi} \left\{ \int_0^{-m_a\pi \sin(y)} \left(\frac{V_t}{2}\right) e^{j(mx+ny)} dx \right. \\
&\quad \left. + \int_{-m_a\pi \sin(y)}^{2\pi + m_a\pi \sin(y)} 0 e^{j(mx+ny)} dx + \int_{2\pi + m_a\pi \sin(y)}^{2\pi} \left(\frac{V_t}{2}\right) e^{j(mx+ny)} dx \right\} dy \\
&= \frac{1}{2\pi^2} \int_0^\pi \left\{ \int_0^{m_a\pi \sin(y)} \frac{V_t}{2} e^{j(mx+ny)} dx + \int_{2\pi - m_a\pi \sin(y)}^{2\pi} \frac{V_t}{2} e^{j(mx+ny)} dx \right\} dy \\
&\quad + \int_\pi^{2\pi} \left\{ \int_0^{-m_a\pi \sin(y)} \left(\frac{V_t}{2}\right) e^{j(mx+ny)} dx + \int_{2\pi + m_a\pi \sin(y)}^{2\pi} \left(\frac{V_t}{2}\right) e^{j(mx+ny)} dx \right\} dy \\
&= \frac{1}{2\pi} \frac{V_t}{2mj} \left\{ \int_0^\pi \left\{ e^{jny} (e^{jm(m_a\pi \sin(y))} - e^{jm(0)}) \right. \right. \\
&\quad \left. \left. + e^{jny} (e^{jm(2\pi)} - e^{jm(2\pi - m_a\pi \sin(y))}) \right\} dy \right. \\
&\quad \left. + \int_\pi^{2\pi} \left\{ e^{jny} (e^{jm(-m_a\pi \sin(y))} - e^{jm(0)}) \right. \right. \\
&\quad \left. \left. + e^{jny} (e^{jm(2\pi)} - e^{jm(2\pi + m_a\pi \sin(y))}) \right\} dy \right\} \\
&= \frac{-jV_t}{4\pi^2 m} \left\{ \int_0^\pi \left\{ e^{jny} e^{jm\pi m_a \sin(y)} - e^{jny} e^{-jm\pi m_a \sin(y)} \right\} dy \right. \\
&\quad \left. + \int_\pi^{2\pi} \left\{ e^{jny} e^{-jm\pi m_a \sin(y)} - e^{jny} e^{jm\pi m_a \sin(y)} \right\} dy \right\} \\
&= \frac{-jV_d}{4\pi^2 m} \left\{ \int_0^\pi e^{jny} e^{jm\pi m_a \sin(y)} dy - \int_\pi^{2\pi} e^{jny} e^{jm\pi m_a \sin(y)} dy \right. \\
&\quad \left. - \int_0^\pi e^{jny} e^{-jm\pi m_a \sin(y)} dy + \int_\pi^{2\pi} e^{jny} e^{-jm\pi m_a \sin(y)} dy \right\}
\end{aligned}$$

Changing integral limits to be from 0 to π we have

$$\begin{aligned}
 A_{mn} + jB_{mn} &= \frac{-jV_t}{4m\pi^2} \left\{ \int_0^\pi e^{jny} e^{jm\pi m_a \sin y} dy - (-1)^n \int_0^\pi e^{jny} e^{-jm\pi m_a \sin y} dy \right. \\
 &\quad \left. - \int_0^\pi e^{jny} e^{-jm\pi m_a \sin y} dy + (-1)^n \int_0^\pi e^{jny} e^{jm\pi m_a \sin y} dy \right\} \\
 &= \frac{-jV_t}{4m\pi^2} \left\{ \int_0^\pi e^{jny} e^{jm\pi m_a \sin y} dy - \int_0^\pi e^{jny} e^{-jm\pi m_a \sin y} dy \right\} \{1 + (-1)^n\} \\
 &= \frac{-jV_d}{4m\pi^2} \left[\int_0^\pi \cos(ny + m\pi m_a \sin y) dy + j \int_0^\pi \sin(ny + m\pi m_a \sin y) dy \right. \\
 &\quad \left. - \int_0^\pi \cos(ny - m\pi m_a \sin y) dy - j \int_0^\pi \sin(ny - m\pi m_a \sin y) dy \right] \{1 + (-1)^n\} \\
 &= \frac{-jV_t}{4\pi m} [J_{-n}(m\pi m_a) - jE_{-n}(m\pi m_a) - J_{-n}(-m\pi m_a) \\
 &\quad + jE_{-n}(-m\pi m_a)] \{1 + (-1)^n\} \tag{A.11}
 \end{aligned}$$

where J is an Anger function given by

$$J_n(m\pi m_a) = \frac{1}{\pi} \int_0^\pi \cos((m\pi m_a) \sin \theta - n\theta) d\theta$$

and E is a Weber function given by

$$E_n(m\pi m_a) = -\frac{1}{\pi} \int_0^\pi \sin((m\pi m_a) \sin \theta - n\theta) d\theta$$

A.6 Harmonics for S'_α and S'_β under APOD/POD PWM using theory and MAPLE package

(This program calculates the harmonics for S'_α and S'_β under APOD/POD PWM. This is done by using the theory developed in the second part of subsection 4.1.1. The resulting harmonics are shown in Figure 4.7.)

restart:

```

with(plots);
ws:=2*Pi*6000;
w1:=2*Pi*50;
A:=0.8;
l:=1;
for n from 0 to 0 do
if modp(n,2)=0 then
frec[l]:=n * w1;
wrec[l]:=frec[l]/(2 * Pi);

```

```

Vhrec[l] := 0;
l := l + 1;
else
  freqc[l] := n * w1;
  wrec[l] := freqc[l]/(2 * Pi);
  Vhrec[l] := 0;
  l := l + 1;
fi;
od;

for n from 1 to 1 do
if modp(n, 2) = 0 then
  freqc[l] := n * w1;
  wrec[l] := freqc[l]/(2 * Pi);
  Vhrec[l] := 0;
  l := l + 1;
else
  freqc[l] := n * w1;
  wrec[l] := freqc[l]/(2 * Pi);
  Vhrec[l] := 0;
  l := l + 1;
fi;
od;

for n from 2 to 15 do
if modp(n, 3) = 0 then
  freqc[l] := n * w1;
  wrec[l] := freqc[l]/(2 * Pi);
  Vhrec[l] := 0;
  l := l + 1;
else
  freqc[l] := n * w1;
  wrec[l] := freqc[l]/(2 * Pi);
  Vhrec[l] := -sqrt(3/2) * (1/2) * 2 * A * ((2 * exp(I * n * Pi) * cos(Pi) - 2 * exp(I * n * Pi) * I * n * sin(Pi) - 1 - exp(2 * I * n * Pi) * cos(2 * Pi) + exp(2 * I * n * Pi) * I * n * sin(2 * Pi)) / (Pi * (I^2 * n^2 + 1)));
  l := l + 1;
fi;
od;

```

```

for m from 1 to 5 do
for n from -15 to 15 do
  freq[l] := m * ws + n * w1;
  if modp(n, 3) = 0 then
    Vhrec[l] := 0;
    wrec[l] := freq[l]/(2 * Pi);
  else
    wrec[l] := freq[l]/(2 * Pi);
  Vhrec[l] := sqrt(3/2)*(-I*2)/(4*Pi*m)*(AngerJ(n, -m*A*Pi)+I*WeberE(n, -m*
  A*Pi)-AngerJ(n, m*A*Pi)-I*WeberE(n, m*A*Pi))*(1+(-1)^n);
  l := l + 1;
fi;
od;
od;
l;
Vhrec[l];
plot([[freq[1]/(2 * Pi), abs(Vhrec[1])], [freq[2]/(2 * Pi), abs(Vhrec[2])], [freq[3]/(2 * Pi),
abs(Vhrec[3])], [freq[4]/(2 * Pi), abs(Vhrec[4])], [freq[5]/(2 * Pi), abs(Vhrec[5])],
[freq[6]/(2 * Pi), abs(Vhrec[6])], [freq[7]/(2 * Pi), abs(Vhrec[7])], [freq[8]/(2 * Pi),
abs(Vhrec[8])], [freq[9]/(2 * Pi), abs(Vhrec[9])], [freq[10]/(2 * Pi), abs(Vhrec[10])],
[freq[11]/(2 * Pi), abs(Vhrec[11])], [freq[12]/(2 * Pi), abs(Vhrec[12])], [freq[13]/(2 * Pi),
abs(Vhrec[13])], [freq[14]/(2 * Pi), abs(Vhrec[14])], [freq[15]/(2 * Pi), abs(Vhrec[15])],
[freq[16]/(2 * Pi), abs(Vhrec[16])], [freq[17]/(2 * Pi), abs(Vhrec[17])], [freq[18]/(2 * Pi),
abs(Vhrec[18])], [freq[19]/(2 * Pi), abs(Vhrec[19])], [freq[20]/(2 * Pi), abs(Vhrec[20])],
)[freq[21]/(2 * Pi), abs(Vhrec[21])], [freq[22]/(2 * Pi), abs(Vhrec[22])], [freq[23]/(2 * Pi),
abs(Vhrec[23])], [freq[24]/(2 * Pi), abs(Vhrec[24])], [freq[25]/(2 * Pi), abs(Vhrec[25])],
[freq[26]/(2 * Pi), abs(Vhrec[26])], [freq[27]/(2 * Pi), abs(Vhrec[27])], [freq[28]/(2 * Pi),
abs(Vhrec[28])], [freq[29]/(2 * Pi), abs(Vhrec[29])], [freq[30]/(2 * Pi), abs(Vhrec[30])],
[freq[31]/(2 * Pi), abs(Vhrec[31])], [freq[32]/(2 * Pi), abs(Vhrec[32])], [freq[33]/(2 * Pi),
abs(Vhrec[33])], [freq[34]/(2 * Pi), abs(Vhrec[34])], [freq[35]/(2 * Pi), abs(Vhrec[35])],
[freq[36]/(2 * Pi), abs(Vhrec[36])], [freq[37]/(2 * Pi), abs(Vhrec[37])], [freq[38]/(2 * Pi),
abs(Vhrec[38])], [freq[39]/(2 * Pi), abs(Vhrec[39])], [freq[40]/(2 * Pi), abs(Vhrec[40])],
[freq[41]/(2 * Pi), abs(Vhrec[41])], [freq[42]/(2 * Pi), abs(Vhrec[42])], [freq[43]/(2 * Pi),
abs(Vhrec[43])], [freq[44]/(2 * Pi), abs(Vhrec[44])], [freq[45]/(2 * Pi), abs(Vhrec[45])],
[freq[46]/(2 * Pi), abs(Vhrec[46])], [freq[47]/(2 * Pi), abs(Vhrec[47])], [freq[48]/(2 * Pi),
abs(Vhrec[48])], [freq[49]/(2 * Pi), abs(Vhrec[49])], [freq[50]/(2 * Pi), abs(Vhrec[50])],
[freq[51]/(2 * Pi), abs(Vhrec[51])], [freq[52]/(2 * Pi), abs(Vhrec[52])], [freq[53]/(2 * Pi),
abs(Vhrec[53])], [freq[54]/(2 * Pi), abs(Vhrec[54])], [freq[55]/(2 * Pi), abs(Vhrec[55])],

```

```
[freq[56]/(2 * Pi), abs(Vhrec[56])], [freq[57]/(2 * Pi), abs(Vhrec[57])], [freq[58]/(2 * Pi),
abs(Vhrec[58])], [freq[59]/(2 * Pi), abs(Vhrec[59])], [freq[60]/(2 * Pi), abs(Vhrec[60])],
[freq[61]/(2 * Pi), abs(Vhrec[61])], [freq[62]/(2 * Pi), abs(Vhrec[62])], [freq[63]/(2 * Pi),
abs(Vhrec[63])], [freq[64]/(2 * Pi), abs(Vhrec[64])], [freq[65]/(2 * Pi), abs(Vhrec[65])],
[freq[66]/(2 * Pi), abs(Vhrec[66])], [freq[67]/(2 * Pi), abs(Vhrec[67])], [freq[68]/(2 * Pi),
abs(Vhrec[68])], [freq[69]/(2 * Pi), abs(Vhrec[69])], [freq[70]/(2 * Pi), abs(Vhrec[70])],
[freq[71]/(2 * Pi), abs(Vhrec[71])], [freq[72]/(2 * Pi), abs(Vhrec[72])], [freq[73]/(2 * Pi),
abs(Vhrec[73])], [freq[74]/(2 * Pi), abs(Vhrec[74])], [freq[75]/(2 * Pi), abs(Vhrec[75])],
[freq[76]/(2 * Pi), abs(Vhrec[76])], [freq[77]/(2 * Pi), abs(Vhrec[77])], [freq[78]/(2 * Pi),
abs(Vhrec[78])], [freq[79]/(2 * Pi), abs(Vhrec[79])], [freq[80]/(2 * Pi), abs(Vhrec[80])],
[freq[81]/(2 * Pi), abs(Vhrec[81])], [freq[82]/(2 * Pi), abs(Vhrec[82])], [freq[83]/(2 * Pi),
abs(Vhrec[83])], [freq[84]/(2 * Pi), abs(Vhrec[84])], [freq[85]/(2 * Pi), abs(Vhrec[85])],
[freq[86]/(2 * Pi), abs(Vhrec[86])], [freq[87]/(2 * Pi), abs(Vhrec[87])], [freq[88]/(2 * Pi),
abs(Vhrec[88])], [freq[89]/(2 * Pi), abs(Vhrec[89])], [freq[90]/(2 * Pi), abs(Vhrec[90])],
[freq[91]/(2 * Pi), abs(Vhrec[91])], [freq[92]/(2 * Pi), abs(Vhrec[92])], [freq[93]/(2 * Pi),
abs(Vhrec[93])], [freq[94]/(2 * Pi), abs(Vhrec[94])], [freq[95]/(2 * Pi), abs(Vhrec[95])],
[freq[96]/(2 * Pi), abs(Vhrec[96])], [freq[97]/(2 * Pi), abs(Vhrec[97])], [freq[98]/(2 * Pi),
abs(Vhrec[98])], [freq[99]/(2 * Pi), abs(Vhrec[99])], [freq[100]/(2 * Pi),
abs(Vhrec[100])], [freq[101]/(2 * Pi), abs(Vhrec[101])], [freq[102]/(2 * Pi),
abs(Vhrec[102])], [freq[103]/(2 * Pi), abs(Vhrec[103])], [freq[104]/(2 * Pi),
abs(Vhrec[104])], [freq[105]/(2 * Pi), abs(Vhrec[105])], [freq[106]/(2 * Pi),
abs(Vhrec[106])], [freq[107]/(2 * Pi), abs(Vhrec[107])], [freq[108]/(2 * Pi),
abs(Vhrec[108])], [freq[109]/(2 * Pi), abs(Vhrec[109])], [freq[110]/(2 * Pi),
abs(Vhrec[110])], [freq[111]/(2 * Pi), abs(Vhrec[111])], [freq[112]/(2 * Pi),
abs(Vhrec[112])], [freq[113]/(2 * Pi), abs(Vhrec[113])], [freq[114]/(2 * Pi),
abs(Vhrec[114])], [freq[115]/(2 * Pi), abs(Vhrec[115])], [freq[116]/(2 * Pi),
abs(Vhrec[116])], [freq[117]/(2 * Pi), abs(Vhrec[117])]], 0..25000, 0..0.45, style = point);
```

A.7 Harmonics for $|F_1|$ under APOD/POD PWM

(This program calculates the harmonics for $|F_1|$ under APOD/POD PWM. The resulting harmonics are shown in Figure 4.8.)

restart:

with(plots):

$ws := 2 * Pi * 6000;$

$w1 := 2 * Pi * 50;$

$A := 0.8;$

```

l := 1;
for n from 0 to 0 do
if modp(n, 2) = 0 then
frec[l] := n * w1;
wrec[l] := frec[l]/(2 * Pi);
Vhrec[l] := (conjugate(-sqrt(3/2) * (1/2) * 2 * A * ((2 * exp(I * n * Pi) * cos(Pi)-
2 * exp(I * n * Pi) * I * n * sin(Pi) - 1 - exp(2 * I * n * Pi) * cos(2 * Pi) + exp(2 * I * n * Pi)*
I * n * sin(2 * Pi))/(Pi * (I2 * n2 + 1)))) * sqrt(3/2) * (1/2) * 2 * A *
(exp(2 * I * Pi * n) - 1)/(Pi * (n2 - 1));
l := l + 1;
else
frec[l] := n * w1;
wrec[l] := frec[l]/(2 * Pi);
Vhrec[l] := (conjugate(-sqrt(3/2) * (1/2) * 2 * A * ((2 * exp(I * n * Pi) * cos(Pi)-
2 * exp(I * n * Pi) * I * n * sin(Pi) - 1 - exp(2 * I * n * Pi) * cos(2 * Pi) + exp(2 * I * n * Pi)*
I * n * sin(2 * Pi))/(Pi * (I2 * n2 + 1)))) * sqrt(3/2) * (1/2) * 2 * A *
(exp(2 * I * Pi * n) - 1)/(Pi * (n2 - 1));
l := l + 1;
fi;
od;
for n from 1 to 1 do
if modp(n, 2) = 0 then
frec[l] := n * w1;
wrec[l] := frec[l]/(2 * Pi);
Vhrec[l] := (Conjugate(-sqrt(3/2) * (1/2) * 2 * A * (1 - 3 * cos((Pi)(2)) - 2 * I *
cos(Pi) * sin(Pi) + 2 * cos((Pi)(4)) + 2 * I * cos((Pi)(3)) * sin(Pi))/Pi))*
((1/2) * I * 2 * A);
l := l + 1;
else
frec[l] := n * w1;
wrec[l] := frec[l]/(2 * Pi);
Vhrec[l] := (Conjugate(-sqrt(3/2) * (1/2) * 2 * A * (1 - 3 * cos((Pi)(2)) - 2 * I *
cos(Pi) * sin(Pi) + 2 * cos((Pi)(4)) + 2 * I * cos((Pi)(3)) * sin(Pi))/Pi))*
((1/2) * I * 2 * A);
l := l + 1;
fi;
od;

```

```

for n from 2 to 15 do
if modp(n, 2) = 0 then
  freq[l] := n * w1;
  wrec[l] := freq[l]/(2 * Pi);
  Vhrec[l] := (conjugate(-sqrt(3/2) * (1/2) * 2 * A * ((2 * exp(I * n * Pi) * cos(Pi) -
  2 * exp(I * n * Pi) * I * n * sin(Pi) - 1 - exp(2 * I * n * Pi) * cos(2 * Pi) + exp(2 * I * n * Pi) *
  I * n * sin(2 * Pi))/(Pi * (I2 * n2 + 1)))) * sqrt(3/2) * (1/2) * 2 * A *
  (exp(2 * I * Pi * n) - 1)/(Pi * (n2 - 1));
  l := l + 1;
else
  freq[l] := n * w1;
  wrec[l] := freq[l]/(2 * Pi);
  Vhrec[l] := (conjugate(-sqrt(3/2) * (1/2) * 2 * A * ((2 * exp(I * n * Pi) * cos(Pi) -
  2 * exp(I * n * Pi) * I * n * sin(Pi) - 1 - exp(2 * I * n * Pi) * cos(2 * Pi) + exp(2 * I * n * Pi) *
  I * n * sin(2 * Pi))/(Pi * (I2 * n2 + 1)))) * sqrt(3/2) * (1/2) * 2 * A *
  (exp(2 * I * Pi * n) - 1)/(Pi * (n2 - 1));
  l := l + 1;
fi;
od;

for m from 1 to 5 do
for n from -15 to 15 do
  freq[l] := m * ws + n * w1;
  if modp(n, 3) = 0 then
    Vhrec[l] := 0;
    wrec[l]:=freq[l]/(2*Pi);
  else
    Vhrec[l] := (conjugate(sqrt(3/2) * (-I * 2)/(4 * Pi * m) * (AngerJ(n, -m * A * Pi) +
    I * WeberE(n, -m * A * Pi) - AngerJ(n, m * A * Pi) - I * WeberE(n, m * A * Pi)) *
    (1 + (-1)n)) * sqrt(3/2) * (-I * 2)/(2 * Pi * m) * exp(I * n * Pi) * (BesselJ(-n, -m * A) -
    BesselJ(-n, m * A)));
    l := l + 1;
  fi;
  od;
  od;
l;
Vhrec[l];
plot([[freq[1]/(2 * Pi), abs(Vhrec[1])], [freq[2]/(2 * Pi), abs(Vhrec[2])], [freq[3]/(2 * Pi),

```



```

abs(Vhrec[98])), [freq[99]/(2 * Pi), abs(Vhrec[99])], [freq[100]/(2 * Pi),
abs(Vhrec[100])], [freq[101]/(2 * Pi), abs(Vhrec[101])], [freq[102]/(2 * Pi),
abs(Vhrec[102])], [freq[103]/(2 * Pi), abs(Vhrec[103])], [freq[104]/(2 * Pi),
abs(Vhrec[104])], [freq[105]/(2 * Pi), abs(Vhrec[105])], [freq[106]/(2 * Pi),
abs(Vhrec[106])], [freq[107]/(2 * Pi), abs(Vhrec[107])], [freq[108]/(2 * Pi),
abs(Vhrec[108])], [freq[109]/(2 * Pi), abs(Vhrec[109])], [freq[110]/(2 * Pi),
abs(Vhrec[110])], [freq[111]/(2 * Pi), abs(Vhrec[111])], [freq[112]/(2 * Pi),
abs(Vhrec[112])], [freq[113]/(2 * Pi), abs(Vhrec[113])], [freq[114]/(2 * Pi),
abs(Vhrec[114])], [freq[115]/(2 * Pi), abs(Vhrec[115])], [freq[116]/(2 * Pi),
abs(Vhrec[116])], [freq[117]/(2 * Pi), abs(Vhrec[117])]], 0..25000, 0..0.18, style = point);

```

A.8 Harmonics for $|F_2|$ under APOD/POD

(This program calculates the harmonics for $|F_2|$ under APOD/POD PWM. The resulting harmonics are shown in Figure 4.9.)

restart:

```

with(plots):
ws:=2*Pi*6000;
w1:=2*Pi*50;
A:=0.8;
l:=1;
for n from 0 to 0 do
if modp(n,2)=0 then
freq[l]:=n*w1;
wrec[l]:=freq[l]/(2*Pi);
Vhrec[l] := (conjugate(-sqrt(3/2) * (1/2) * 2 * A * ((2 * exp(I * n * Pi) * cos(Pi)-
2 * exp(I * n * Pi) * I * n * sin(Pi) - 1 - exp(2 * I * n * Pi) * cos(2 * Pi) + exp(2 * I * n * Pi) *
I * n * sin(2 * Pi))/(Pi * (I^2 * n^2 + 1)))) * (-sqrt(3/2) * (1/2) * 2 * A * ((2 *
exp(I * n * Pi) * cos(Pi) - 2 * exp(I * n * Pi) * I * n * sin(Pi) - 1 - exp(2 * I * n * Pi) *
cos(2 * Pi) + exp(2 * I * n * Pi) * I * n * sin(2 * Pi))/(Pi * (I^2 * n^2 + 1))));;
l:=l+1;
else
freq[l]:=n*w1;
wrec[l]:=freq[l]/(2*Pi);
Vhrec[l] := (conjugate(-sqrt(3/2) * (1/2) * 2 * A * ((2 * exp(I * n * Pi) * cos(Pi)-
2 * exp(I * n * Pi) * I * n * sin(Pi) - 1 - exp(2 * I * n * Pi) * cos(2 * Pi) + exp(2 * I * n * Pi) *
I * n * sin(2 * Pi))/(Pi * (I^2 * n^2 + 1)))) * (-sqrt(3/2) * (1/2) * 2 * A * ((2 *

```

```

exp(I * n * Pi) * cos(Pi) - 2 * exp(I * n * Pi) * I * n * sin(Pi) - 1 - exp(2 * I * n * Pi)*
cos(2 * Pi) + exp(2 * I * n * Pi) * I * n * sin(2 * Pi))/(Pi * (I2 * n2 + 1))));

l:=l+1;
fi;
od;
for n from 1 to 1 do
if modp(n,2)=0 then
frec[l]:=n*w1;
wrec[l]:=frec[l]/(2*Pi);
Vhrec[l] := (Conjugate(-sqrt(3/2) * (1/2) * 2 * A * (1 - 3 * cos((Pi)(2)) - 2 * I *
cos(Pi) * sin(Pi) + 2 * cos((Pi)(4)) + 2 * I * cos((Pi)(3)) * sin(Pi))/Pi))*
(-sqrt(3/2) * (1/2) * 2 * A * (1 - 3 * cos((Pi)(2)) - 2 * I * cos(Pi) * sin(Pi) + 2*
cos((Pi)(4)) + 2 * I * cos((Pi)(3)) * sin(Pi))/Pi);

l:=l+1;
else
frec[l]:=n*w1;
wrec[l]:=frec[l]/(2*Pi);
Vhrec[l] := (Conjugate(-sqrt(3/2) * (1/2) * 2 * A * (1 - 3 * cos((Pi)(2)) - 2 * I *
cos(Pi) * sin(Pi) + 2 * cos((Pi)(4)) + 2 * I * cos((Pi)(3)) * sin(Pi))/Pi))*
(-sqrt(3/2) * (1/2) * 2 * A * (1 - 3 * cos((Pi)(2)) - 2 * I * cos(Pi) * sin(Pi) + 2*
cos((Pi)(4)) + 2 * I * cos((Pi)(3)) * sin(Pi))/Pi);

l:=l+1;
fi;
od;
for n from 2 to 15 do
if modp(n,2)=0 then
frec[l]:=n*w1;
wrec[l]:=frec[l]/(2*Pi);
Vhrec[l] := (conjugate(-sqrt(3/2) * (1/2) * 2 * A * ((2 * exp(I * n * Pi) * cos(Pi)-
2 * exp(I * n * Pi) * I * n * sin(Pi) - 1 - exp(2 * I * n * Pi) * cos(2 * Pi) + exp(2 * I * n * Pi)*
I * n * sin(2 * Pi))/(Pi * (I2 * n2 + 1)))) * (-sqrt(3/2) * (1/2) * 2 * A * ((2*
exp(I * n * Pi) * cos(Pi) - 2 * exp(I * n * Pi) * I * n * sin(Pi) - 1 - exp(2 * I * n * Pi)*
cos(2 * Pi) + exp(2 * I * n * Pi) * I * n * sin(2 * Pi))/(Pi * (I2 * n2 + 1))));

l:=l+1;
else
frec[l]:=n*w1;
wrec[l]:=frec[l]/(2*Pi);
Vhrec[l] := (conjugate(-sqrt(3/2) * (1/2) * 2 * A * ((2 * exp(I * n * Pi) * cos(Pi)-

```

```

2 * exp(I * n * Pi) * I * n * sin(Pi) - 1 - exp(2 * I * n * Pi) * cos(2 * Pi) + exp(2 * I * n * Pi) *
I * n * sin(2 * Pi)) / (Pi * (I2 * n2 + 1)))) * (-sqrt(3/2) * (1/2) * 2 * A * ((2 *
exp(I * n * Pi) * cos(Pi) - 2 * exp(I * n * Pi) * I * n * sin(Pi) - 1 - exp(2 * I * n * Pi) *
cos(2 * Pi) + exp(2 * I * n * Pi) * I * n * sin(2 * Pi)) / (Pi * (I2 * n2 + 1))));
```

l:=l+1;
fi;
od;

for m from 1 to 5 do

for n from -15 to 15 do

freq[l]:=m*ws+n*w1;

if modp(n,3)=0 then

Vhrec[l]:=0;

wrec[l]:=freq[l]/(2*Pi);

else

```

Vhrec[l] := (conjugate(sqrt(3/2) * (-I * 2)/(4 * Pi * m) * (AngerJ(n, -m * A * Pi) +
I * WeberE(n, -m * A * Pi) - AngerJ(n, m * A * Pi) - I * WeberE(n, m * A * Pi)) *
(1 + (-1)n))) * sqrt(3/2) * (-I * 2)/(4 * Pi * m) * (AngerJ(n, -m * A * Pi) + I *
WeberE(n, -m * A * Pi) - AngerJ(n, m * A * Pi) - I * WeberE(n, m * A * Pi)) * (1 + (-1)n);
```

l:=l+1;

fi;

od;

od;

l;

Vhrec[l];

```

plot([[freq[1]/(2*Pi), abs(Vhrec[1])], [freq[2]/(2*Pi), abs(Vhrec[2])], [freq[3]/(2*Pi),
abs(Vhrec[3])], [freq[4]/(2 * Pi), abs(Vhrec[4])], [freq[5]/(2 * Pi), abs(Vhrec[5])],
[freq[6]/(2 * Pi), abs(Vhrec[6])], [freq[7]/(2 * Pi), abs(Vhrec[7])], [freq[8]/(2 * Pi),
abs(Vhrec[8])], [freq[9]/(2 * Pi), abs(Vhrec[9])], [freq[10]/(2 * Pi), abs(Vhrec[10])],
[freq[11]/(2 * Pi), abs(Vhrec[11])], [freq[12]/(2 * Pi), abs(Vhrec[12])], [freq[13]/(2 * Pi),
abs(Vhrec[13])], [freq[14]/(2 * Pi), abs(Vhrec[14])], [freq[15]/(2 * Pi), abs(Vhrec[15])],
[freq[16]/(2 * Pi), abs(Vhrec[16])], [freq[17]/(2 * Pi), abs(Vhrec[17])], [freq[18]/(2 * Pi),
abs(Vhrec[18])], [freq[19]/(2 * Pi), abs(Vhrec[19])], [freq[20]/(2 * Pi), abs(Vhrec[20])],
)[freq[21]/(2 * Pi), abs(Vhrec[21])], [freq[22]/(2 * Pi), abs(Vhrec[22])], [freq[23]/(2 * Pi),
abs(Vhrec[23])], [freq[24]/(2 * Pi), abs(Vhrec[24])], [freq[25]/(2 * Pi), abs(Vhrec[25])],
[freq[26]/(2 * Pi), abs(Vhrec[26])], [freq[27]/(2 * Pi), abs(Vhrec[27])], [freq[28]/(2 * Pi),
abs(Vhrec[28])], [freq[29]/(2 * Pi), abs(Vhrec[29])], [freq[30]/(2 * Pi), abs(Vhrec[30])],
```

[freq[31]/(2 * Pi), abs(Vhrec[31])], [freq[32]/(2 * Pi), abs(Vhrec[32])], [freq[33]/(2 * Pi),
 abs(Vhrec[33])], [freq[34]/(2 * Pi), abs(Vhrec[34])], [freq[35]/(2 * Pi), abs(Vhrec[35])],
 [freq[36]/(2 * Pi), abs(Vhrec[36])], [freq[37]/(2 * Pi), abs(Vhrec[37])], [freq[38]/(2 * Pi),
 abs(Vhrec[38])], [freq[39]/(2 * Pi), abs(Vhrec[39])], [freq[40]/(2 * Pi), abs(Vhrec[40])],
 [freq[41]/(2 * Pi), abs(Vhrec[41])], [freq[42]/(2 * Pi), abs(Vhrec[42])], [freq[43]/(2 * Pi),
 abs(Vhrec[43])], [freq[44]/(2 * Pi), abs(Vhrec[44])], [freq[45]/(2 * Pi), abs(Vhrec[45])],
 [freq[46]/(2 * Pi), abs(Vhrec[46])], [freq[47]/(2 * Pi), abs(Vhrec[47])], [freq[48]/(2 * Pi),
 abs(Vhrec[48])], [freq[49]/(2 * Pi), abs(Vhrec[49])], [freq[50]/(2 * Pi), abs(Vhrec[50])],
 [freq[51]/(2 * Pi), abs(Vhrec[51])], [freq[52]/(2 * Pi), abs(Vhrec[52])], [freq[53]/(2 * Pi),
 abs(Vhrec[53])], [freq[54]/(2 * Pi), abs(Vhrec[54])], [freq[55]/(2 * Pi), abs(Vhrec[55])],
 [freq[56]/(2 * Pi), abs(Vhrec[56])], [freq[57]/(2 * Pi), abs(Vhrec[57])], [freq[58]/(2 * Pi),
 abs(Vhrec[58])], [freq[59]/(2 * Pi), abs(Vhrec[59])], [freq[60]/(2 * Pi), abs(Vhrec[60])],
 [freq[61]/(2 * Pi), abs(Vhrec[61])], [freq[62]/(2 * Pi), abs(Vhrec[62])], [freq[63]/(2 * Pi),
 abs(Vhrec[63])], [freq[64]/(2 * Pi), abs(Vhrec[64])], [freq[65]/(2 * Pi), abs(Vhrec[65])],
 [freq[66]/(2 * Pi), abs(Vhrec[66])], [freq[67]/(2 * Pi), abs(Vhrec[67])], [freq[68]/(2 * Pi),
 abs(Vhrec[68])], [freq[69]/(2 * Pi), abs(Vhrec[69])], [freq[70]/(2 * Pi), abs(Vhrec[70])],
 [freq[71]/(2 * Pi), abs(Vhrec[71])], [freq[72]/(2 * Pi), abs(Vhrec[72])], [freq[73]/(2 * Pi),
 abs(Vhrec[73])], [freq[74]/(2 * Pi), abs(Vhrec[74])], [freq[75]/(2 * Pi), abs(Vhrec[75])],
 [freq[76]/(2 * Pi), abs(Vhrec[76])], [freq[77]/(2 * Pi), abs(Vhrec[77])], [freq[78]/(2 * Pi),
 abs(Vhrec[78])], [freq[79]/(2 * Pi), abs(Vhrec[79])], [freq[80]/(2 * Pi), abs(Vhrec[80])],
 [freq[81]/(2 * Pi), abs(Vhrec[81])], [freq[82]/(2 * Pi), abs(Vhrec[82])], [freq[83]/(2 * Pi),
 abs(Vhrec[83])], [freq[84]/(2 * Pi), abs(Vhrec[84])], [freq[85]/(2 * Pi), abs(Vhrec[85])],
 [freq[86]/(2 * Pi), abs(Vhrec[86])], [freq[87]/(2 * Pi), abs(Vhrec[87])], [freq[88]/(2 * Pi),
 abs(Vhrec[88])], [freq[89]/(2 * Pi), abs(Vhrec[89])], [freq[90]/(2 * Pi), abs(Vhrec[90])],
 [freq[91]/(2 * Pi), abs(Vhrec[91])], [freq[92]/(2 * Pi), abs(Vhrec[92])], [freq[93]/(2 * Pi),
 abs(Vhrec[93])], [freq[94]/(2 * Pi), abs(Vhrec[94])], [freq[95]/(2 * Pi), abs(Vhrec[95])],
 [freq[96]/(2 * Pi), abs(Vhrec[96])], [freq[97]/(2 * Pi), abs(Vhrec[97])], [freq[98]/(2 * Pi),
 abs(Vhrec[98])], [freq[99]/(2 * Pi), abs(Vhrec[99])], [freq[100]/(2 * Pi),
 abs(Vhrec[100])], [freq[101]/(2 * Pi), abs(Vhrec[101])], [freq[102]/(2 * Pi),
 abs(Vhrec[102])], [freq[103]/(2 * Pi), abs(Vhrec[103])], [freq[104]/(2 * Pi),
 abs(Vhrec[104])], [freq[105]/(2 * Pi), abs(Vhrec[105])], [freq[106]/(2 * Pi),
 abs(Vhrec[106])], [freq[107]/(2 * Pi), abs(Vhrec[107])], [freq[108]/(2 * Pi),
 abs(Vhrec[108])], [freq[109]/(2 * Pi), abs(Vhrec[109])], [freq[110]/(2 * Pi),
 abs(Vhrec[110])], [freq[111]/(2 * Pi), abs(Vhrec[111])], [freq[112]/(2 * Pi),
 abs(Vhrec[112])], [freq[113]/(2 * Pi), abs(Vhrec[113])], [freq[114]/(2 * Pi),
 abs(Vhrec[114])], [freq[115]/(2 * Pi), abs(Vhrec[115])], [freq[116]/(2 * Pi),
 abs(Vhrec[116])], [freq[117]/(2 * Pi), abs(Vhrec[117])]], 0..25000, 0..0.18, style = point);

Appendix B

Harmonics using PD PWM technique

B.1 Coefficients of $(s_\alpha \times \frac{V_t}{2})$ and $(s_\beta \times \frac{V_t}{2})$ under PD PWM

(In this section we calculate the coefficients of equation 4.2 using figure 4.12. We thereafter use the calculated results in subsection 4.2.)

For $m = 0$

$$\begin{aligned}
 A_{0n} + jB_{0n} &= \frac{1}{2\pi^2} \int_0^{2\pi} \int_0^{2\pi} F(x, y) e^{j(ny)} dx dy \\
 &= \frac{1}{2\pi^2} \left\{ \int_0^\pi \int_0^{2\pi} F(x, y) e^{j(ny)} dx dy + \int_\pi^{2\pi} \int_0^{2\pi} F(x, y) e^{j(ny)} dx dy \right\} \\
 &= \frac{1}{2\pi^2} \left[\int_0^\pi \left\{ \int_{\pi - m_a \pi \sin y}^{\pi + m_a \pi \sin y} \frac{V_t}{2} e^{j(ny)} dx \right\} dy \right. \\
 &\quad \left. + \int_\pi^{2\pi} \left\{ \int_0^{-m_a \pi \sin y} \frac{-V_t}{2} e^{j(ny)} dx + \int_{2\pi + m_a \pi \sin y}^{2\pi} \frac{-V_t}{2} e^{j(ny)} dx \right\} dy \right] \\
 &= \frac{1}{2\pi^2} \frac{V_t}{2} \left[\int_0^\pi e^{j(ny)} \{(\pi + m_a \pi \sin y) - (\pi - m_a \pi \sin y)\} dy + \right. \\
 &\quad \left. \int_\pi^{2\pi} e^{j(ny)} \{-(-m_a \pi \sin y + 2\pi - (2\pi + m_a \pi \sin y))\} dy \right] \\
 &= \frac{V_t}{4\pi^2} \left[\int_0^\pi e^{j(ny)} (2m_a \pi \sin y) dy + \int_\pi^{2\pi} e^{j(ny)} (2m_a \pi \sin y) dy \right] \\
 &= \frac{V_t}{4\pi^2} \int_0^{2\pi} e^{j(ny)} (2m_a \pi \sin y) dy \\
 &= \frac{V_t m_a}{2\pi} \frac{(e^{2j\pi n} - 1)}{(n^2 - 1)}
 \end{aligned} \tag{B.1}$$

For $m = 0$ and $n = 1$

$$\begin{aligned}
 A_{01} + jB_{01} &= \frac{1}{2\pi^2} \int_0^{2\pi} \int_0^{2\pi} F(x, y) e^{j(y)} dx dy \\
 &= \frac{1}{2\pi^2} \left\{ \int_0^\pi \int_0^{2\pi} F(x, y) e^{j(y)} dx dy + \int_\pi^{2\pi} \int_0^{2\pi} F(x, y) e^{j(y)} dx dy \right\}
 \end{aligned}$$

$$\begin{aligned}
&= \frac{1}{2\pi^2} \left[\int_0^\pi \left\{ \int_{\pi-m_a\pi \sin y}^{\pi+m_a\pi \sin y} \frac{V_t}{2} e^{j(y)} dx \right\} dy \right. \\
&\quad \left. + \int_\pi^{2\pi} \left\{ \int_0^{-m_a\pi \sin y} -\frac{V_t}{2} e^{j(y)} dx + \int_{2\pi+m_a\pi \sin y}^{2\pi} -\frac{V_t}{2} e^{j(y)} dx \right\} dy \right] \\
&= \frac{1}{2\pi^2} \frac{V_t}{2} \left[\int_0^\pi e^{j(y)} \{(\pi + m_a\pi \sin y) - (\pi - m_a\pi \sin y)\} dy + \right. \\
&\quad \left. \int_\pi^{2\pi} e^{j(y)} \{-(-m_a\pi \sin y + 2\pi - (2\pi + m_a\pi \sin y))\} dy \right] \\
&= \frac{V_t}{4\pi^2} \left[\int_0^\pi e^{j(y)} (2m_a\pi \sin y) dy + \int_\pi^{2\pi} e^{j(y)} (2m_a\pi \sin y) dy \right] \\
&= \frac{V_t}{4\pi^2} \int_0^{2\pi} e^{j(y)} (2m_a\pi \sin y) dy \\
&= \frac{jV_t m_a}{2}
\end{aligned} \tag{B.2}$$

For $m \neq 0$

$$\begin{aligned}
A_{mn} + jB_{mn} &= \frac{1}{2\pi^2} \int_0^{2\pi} \int_0^{2\pi} F(x, y) e^{j(mx+ny)} dxdy \\
&= \frac{1}{2\pi^2} \left\{ \int_0^\pi \int_0^{2\pi} F(x, y) e^{j(mx+ny)} dxdy + \int_\pi^{2\pi} \int_0^{2\pi} F(x, y) e^{j(mx+ny)} dxdy \right\} \\
&= \frac{1}{2\pi^2} \left[\int_0^\pi \left\{ \int_0^{\pi-m_a\pi \sin(y)} 0e^{j(mx+ny)} dx + \int_{\pi-m_a\pi \sin(y)}^{\pi+m_a\pi \sin(y)} \frac{V_t}{2} e^{j(mx+ny)} dx \right. \right. \\
&\quad \left. \left. + \int_{\pi+m_a\pi \sin(y)}^{2\pi} 0e^{j(mx+ny)} dx \right\} dy + \int_\pi^{2\pi} \left\{ \int_0^{-m_a\pi \sin(y)} \left(-\frac{V_t}{2}\right) e^{j(mx+ny)} dx \right. \right. \\
&\quad \left. \left. + \int_{-m_a\pi \sin(y)}^{2\pi+m_a\pi \sin(y)} 0e^{j(mx+ny)} dx + \int_{2\pi+m_a\pi \sin(y)}^{2\pi} \left(\frac{-V_t}{2}\right) e^{j(mx+ny)} dx \right\} dy \right] \\
&= \frac{1}{2\pi^2} \left[\int_0^\pi \left\{ \int_{\pi-m_a\pi \sin(y)}^{\pi+m_a\pi \sin(y)} \frac{V_t}{2} e^{j(mx+ny)} dx \right\} dy \right. \\
&\quad \left. + \int_\pi^{2\pi} \left\{ \int_0^{-m_a\pi \sin(y)} \left(-\frac{V_t}{2}\right) e^{j(mx+ny)} dx \right. \right. \\
&\quad \left. \left. + \int_{2\pi+m_a\pi \sin(y)}^{2\pi} \left(\frac{-V_t}{2}\right) e^{j(mx+ny)} dx \right\} dy \right] \\
&= \frac{1}{2\pi} \frac{V_t}{2mj} \left[\int_0^\pi \left\{ e^{jny} (e^{jm(\pi+m_a\pi \sin(y))} - e^{jn(\pi-m_a\pi \sin(y))}) \right\} dy \right. \\
&\quad \left. - \int_\pi^{2\pi} \left\{ e^{jny} (e^{jm(-m_a\pi \sin(y))} - e^{jm(0)}) \right. \right. \\
&\quad \left. \left. + e^{jny} (e^{jm(2\pi)} - e^{jm(2\pi+m_a\pi \sin(y))}) \right\} dy \right] \\
&= \frac{-jV_t}{4\pi^2 m} \left[\int_0^\pi \left\{ e^{jny} e^{jm(\pi+\pi m_a \sin(y))} - e^{jny} e^{jm(\pi-m_a\pi \sin(y))} \right\} dy \right. \\
&\quad \left. - \int_\pi^{2\pi} \left\{ e^{jny} e^{jm\pi(-m_a \sin(y))} - e^{jny} e^{jm(2\pi+m_a\pi \sin(y))} \right\} dy \right]
\end{aligned}$$

For m even

$$\begin{aligned}
 A_{mn} + jB_{mn} &= \frac{-jV_t}{4\pi^2 m} \left[\int_0^\pi \left\{ e^{jny} (e^{jm\pi m_a \sin(y)} - e^{-jm\pi m_a \sin(y)}) \right\} dy \right. \\
 &\quad \left. - \int_\pi^{2\pi} \left\{ e^{jny} (e^{-jm\pi m_a \sin(y)} - e^{jm\pi m_a \sin(y)}) \right\} dy \right] \\
 &= \frac{-jV_t}{4\pi^2 m} \left\{ \int_0^\pi e^{jny} e^{jm\pi m_a \sin(y)} dy + \int_\pi^{2\pi} e^{jny} e^{jm\pi m_a \sin(y)} dy \right. \\
 &\quad \left. - \int_0^\pi e^{jny} e^{-jm\pi m_a \sin(y)} dy - \int_\pi^{2\pi} e^{jny} e^{-jm\pi m_a \sin(y)} dy \right\} \\
 &= \frac{-jV_t}{4\pi^2 m} \left\{ \int_0^{2\pi} e^{jny} e^{jm\pi m_a \sin(y)} dy - \int_0^{2\pi} e^{jny} e^{-jm\pi m_a \sin(y)} dy \right\}
 \end{aligned}$$

Let $\theta = y - \pi$ then $d\theta = dy$ and $\theta = \begin{cases} -\pi & \text{as } y = 0 \\ \pi & \text{as } y = 2\pi \end{cases}$

$$\begin{aligned}
 A_{mn} + jB_{mn} &= \frac{-jV_t}{4\pi^2 m} \left\{ \int_{-\pi}^\pi e^{jn(\theta+\pi)} e^{-jm\pi m_a \sin(\theta)} d\theta - \int_{-\pi}^\pi e^{jn(\theta+\pi)} e^{jm\pi m_a \sin(\theta)} d\theta \right\} \\
 &= \frac{-jV_t}{2m\pi} e^{jn\pi} \left\{ \frac{1}{2\pi} \int_{-\pi}^\pi e^{jn\theta} e^{-jm\pi m_a \sin \theta} d\theta - \frac{1}{2\pi} \int_{-\pi}^\pi e^{jn\theta} e^{jm\pi m_a \sin \theta} d\theta \right\} \\
 &= \frac{-jV_t}{2m\pi} e^{jn\pi} \{ J_{-n}(-m\pi m_a) - J_{-n}(m\pi m_a) \} \\
 &= \frac{-jV_t}{2m\pi} e^{jn\pi} \{ J_n(m\pi m_a) - (-1)^n J_n(m\pi m_a) \} \tag{B.3}
 \end{aligned}$$

where J is a Bessel function given by

$$J_n(m\pi m_a) = \frac{1}{2\pi} \int_{-\pi}^\pi e^{-i(m\pi m_a)} e^{in\theta} d\theta$$

For m odd

$$\begin{aligned}
 &= \frac{-jV_t}{4\pi^2 m} \left\{ \int_0^\pi \left\{ e^{jny} e^{-jm\pi m_a \sin(y)} - e^{jny} e^{jm\pi m_a \sin(y)} \right\} dy \right. \\
 &\quad \left. - \int_\pi^{2\pi} \left\{ e^{jny} e^{-jm\pi m_a \sin(y)} - e^{jny} e^{jm\pi m_a \sin(y)} \right\} dy \right\} \\
 &= \frac{-jV_t}{4\pi^2 m} \left\{ \int_0^\pi e^{jny} e^{-jm\pi m_a \sin(y)} dy - \int_\pi^{2\pi} e^{jny} e^{-jm\pi m_a \sin(y)} dy \right. \\
 &\quad \left. - \int_0^\pi e^{jny} e^{jm\pi m_a \sin(y)} dy + \int_\pi^{2\pi} e^{jny} e^{jm\pi m_a \sin(y)} dy \right\}
 \end{aligned}$$

Changing integral limits to be from 0 to π we have

$$\begin{aligned}
 A_{mn} + jB_{mn} &= \frac{-jV_t}{4m\pi^2} \left\{ \int_0^\pi e^{jny} e^{-jm\pi m_a \sin y} dy - (-1)^n \int_0^\pi e^{jny} e^{jm\pi m_a \sin y} dy \right. \\
 &\quad \left. - \int_0^\pi e^{jny} e^{jm\pi m_a \sin y} dy + (-1)^n \int_0^\pi e^{jny} e^{-jm\pi m_a \sin y} dy \right\}
 \end{aligned}$$

$$\begin{aligned}
&= \frac{-jV_t}{4m\pi^2} \left\{ \int_0^\pi e^{jny} e^{-jm\pi m_a \sin y} dy - \int_0^\pi e^{jny} e^{jm\pi m_a \sin y} dy \right\} \{1 + (-1)^n\} \\
&= \frac{-jV_t}{4m\pi^2} \left[\int_0^\pi \cos(ny - m\pi m_a \sin y) dy + j \int_0^\pi \sin(ny - m\pi m_a \sin y) dy \right. \\
&\quad \left. - \int_0^\pi \cos(ny + m\pi m_a \sin y) dy \right. \\
&\quad \left. - j \int_0^\pi \sin(ny + m\pi m_a \sin y) dy \right] \{1 + (-1)^n\} \\
&= \frac{-jV_t}{4\pi m} [J_{-n}(-m\pi m_a) - jE_{-n}(-m\pi m_a) - J_{-n}(m\pi m_a) \\
&\quad + jE_{-n}(m\pi m_a)] \{1 + (-1)^n\} \tag{B.4}
\end{aligned}$$

where J is an Anger function given by

$$J_n(m\pi m_a) = \frac{1}{\pi} \int_0^\pi \cos((m\pi m_a) \sin \theta - n\theta) d\theta$$

and E is a Weber function given by

$$E_n(m\pi m_a) = -\frac{1}{\pi} \int_0^\pi \sin((m\pi m_a) \sin \theta - n\theta) d\theta$$

B.2 Coefficients of $(s_\alpha' \times \frac{V_t}{2})$ and $(s_\beta' \times \frac{V_t}{2})$ under PD PWM

In this section we calculate the coefficients of equation 4.2 using figure 4.14. We thereafter use the calculated results in section 4.2.

For $m = 0$

$$\begin{aligned}
A_{0n} + jB_{0n} &= \frac{1}{2\pi^2} \int_0^{2\pi} \int_0^{2\pi} F(x, y) e^{j(ny)} dx dy \\
&= \frac{1}{2\pi^2} \left\{ \int_0^\pi \int_0^{2\pi} F(x, y) e^{j(ny)} dx dy + \int_\pi^{2\pi} \int_0^{2\pi} F(x, y) e^{j(ny)} dx dy \right\} \\
&= \frac{1}{2\pi^2} \left[\int_0^\pi \left\{ \int_{\pi-m_a\pi \sin y}^{\pi+m_a\pi \sin y} \frac{V_t}{2} e^{j(ny)} dx \right\} dy \right. \\
&\quad \left. + \int_\pi^{2\pi} \left\{ \int_0^{-m_a\pi \sin y} \frac{V_t}{2} e^{j(ny)} dx + \int_{2\pi+m_a\pi \sin y}^{2\pi} \frac{V_t}{2} e^{j(ny)} dx \right\} dy \right] \\
&= \frac{1}{2\pi^2} \frac{V_t}{2} \left[\int_0^\pi e^{j(ny)} \{(\pi + m_a\pi \sin y) - (\pi - m_a\pi \sin y)\} dy + \right. \\
&\quad \left. \int_\pi^{2\pi} e^{j(ny)} \{(-m_a\pi \sin y + 2\pi - (2\pi + m_a\pi \sin y))\} dy \right] \\
&= \frac{V_t}{4\pi^2} \left[\int_0^\pi e^{jny} (2m_a\pi \sin y) dy + \int_\pi^{2\pi} e^{jny} (-2m_a\pi \sin y) dy \right] \\
&= -\frac{1}{2} V_t m_a \left\{ \frac{2e^{jn\pi} + 1 + e^{2jn\pi}}{\pi(n^2 - 1)} \right\} \tag{B.5}
\end{aligned}$$

For $m = 0$ and $n = 1$

$$\begin{aligned}
 A_{01} + jB_{01} &= \frac{1}{2\pi^2} \int_0^{2\pi} \int_0^{2\pi} F(x, y) e^{jy} dx dy \\
 &= \frac{1}{2\pi^2} \left[\int_0^\pi \left\{ \int_{\pi-m_a\pi \sin y}^{\pi+m_a\pi \sin y} \frac{V_t}{2} e^{j(y)} dx \right\} dy \right. \\
 &\quad \left. + \int_\pi^{2\pi} \left\{ \int_0^{-m_a\pi \sin y} \frac{V_t}{2} e^{j(y)} dx + \int_{2\pi+m_a\pi \sin y}^{2\pi} \frac{V_t}{2} e^{j(y)} dx \right\} dy \right] \\
 &= \frac{1}{2\pi^2} \frac{V_t}{2} \left[\int_0^\pi e^{j(y)} \{(\pi + m_a\pi \sin y) - (\pi - m_a\pi \sin y)\} dy + \right. \\
 &\quad \left. \int_\pi^{2\pi} e^{j(y)} \{(-m_a\pi \sin y + 2\pi - (2\pi + m_a\pi \sin y))\} dy \right] \\
 &= \frac{V_t}{4\pi^2} \left[\int_0^\pi e^{jy} (2m_a\pi \sin y) dy + \int_\pi^{2\pi} e^{jy} (-2m_a\pi \sin y) dy \right] \\
 &= 0
 \end{aligned} \tag{B.6}$$

For $m \neq 0$

$$\begin{aligned}
 A_{mn} + jB_{mn} &= \frac{1}{2\pi^2} \int_0^{2\pi} \int_0^{2\pi} F(x, y) e^{j(mx+ny)} dx dy \\
 &= \frac{1}{2\pi^2} \left\{ \int_0^\pi \int_0^{2\pi} F(x, y) e^{j(mx+ny)} dx dy + \int_\pi^{2\pi} \int_0^{2\pi} F(x, y) e^{j(mx+ny)} dx dy \right\} \\
 &= \frac{1}{2\pi^2} \left[\int_0^\pi \left\{ \int_0^{\pi-m_a\pi \sin(y)} 0e^{j(mx+ny)} dx + \int_{\pi-m_a\pi \sin(y)}^{\pi+m_a\pi \sin(y)} \frac{V_t}{2} e^{j(mx+ny)} dx \right. \right. \\
 &\quad \left. \left. + \int_{\pi+m_a\pi \sin(y)}^{2\pi} 0e^{j(mx+ny)} dx \right\} dy + \int_\pi^{2\pi} \left\{ \int_0^{-m_a\pi \sin(y)} \left(\frac{V_t}{2} \right) e^{j(mx+ny)} dx \right. \right. \\
 &\quad \left. \left. + \int_{-m_a\pi \sin(y)}^{2\pi+m_a\pi \sin(y)} 0e^{j(mx+ny)} dx + \int_{2\pi+m_a\pi \sin(y)}^{2\pi} \left(\frac{V_t}{2} \right) e^{j(mx+ny)} dx \right\} dy \right] \\
 &= \frac{1}{2\pi^2} \left[\int_0^\pi \left\{ \int_{\pi-m_a\pi \sin(y)}^{\pi+m_a\pi \sin(y)} \frac{V_t}{2} e^{j(mx+ny)} dx \right\} dy \right. \\
 &\quad \left. + \int_\pi^{2\pi} \left\{ \int_0^{-m_a\pi \sin(y)} \left(\frac{V_t}{2} \right) e^{j(mx+ny)} dx \right. \right. \\
 &\quad \left. \left. + \int_{2\pi+m_a\pi \sin(y)}^{2\pi} \left(\frac{V_t}{2} \right) e^{j(mx+ny)} dx \right\} dy \right] \\
 &= \frac{1}{2\pi} \frac{V_t}{2m_j} \left\{ \int_0^\pi \left\{ e^{jny} \left(e^{jm(\pi+m_a\pi \sin(y))} - e^{jm(\pi+m_a\pi \sin(y))} \right) \right\} dy \right. \\
 &\quad \left. + \int_\pi^{2\pi} \left\{ e^{jny} \left(e^{jm(-m_a\pi \sin(y))} - e^{jm(0)} \right) \right. \right. \\
 &\quad \left. \left. + e^{jny} \left(e^{jm(2\pi)} - e^{jm(2\pi+m_a\pi \sin(y))} \right) \right\} dy \right\}
 \end{aligned}$$

For m even

$$\begin{aligned} A_{mn} + jB_{mn} &= \frac{-jV_t}{4\pi^2 m} \left\{ \int_0^\pi \left\{ e^{jny} e^{jm\pi m_a \sin(y)} - e^{jny} e^{-jm\pi m_a \sin(y)} \right\} dy \right. \\ &\quad \left. + \int_\pi^{2\pi} \left\{ e^{jny} e^{-jm\pi m_a \sin(y)} - e^{jny} e^{jm\pi m_a \sin(y)} \right\} dy \right\} \\ &= \frac{-jV_t}{4\pi^2 m} \left\{ \int_0^\pi e^{jny} e^{jm\pi m_a \sin(y)} dy - \int_\pi^{2\pi} e^{jny} e^{jm\pi m_a \sin(y)} dy \right. \\ &\quad \left. - \int_0^\pi e^{jny} e^{-jm\pi m_a \sin(y)} dy + \int_\pi^{2\pi} e^{jny} e^{-jm\pi m_a \sin(y)} dy \right\} \end{aligned}$$

Changing integral limits to be from 0 to π we have

$$\begin{aligned} A_{mn} + jB_{mn} &= \frac{-jV_t}{4m\pi^2} \left\{ \int_0^\pi e^{jny} e^{jm\pi m_a \sin y} dy - (-1)^n \int_0^\pi e^{jny} e^{-jm\pi m_a \sin y} dy \right. \\ &\quad \left. - \int_0^\pi e^{jny} e^{-jm\pi m_a \sin y} dy + (-1)^n \int_0^\pi e^{jny} e^{jm\pi m_a \sin y} dy \right\} \\ &= \frac{-jV_t}{4m\pi^2} \left\{ \int_0^\pi e^{jny} e^{jm\pi m_a \sin y} dy - \int_0^\pi e^{jny} e^{-jm\pi m_a \sin y} dy \right\} \{1 + (-1)^n\} \\ &= \frac{-jV_t}{4m\pi^2} \left[\int_0^\pi \cos(ny + m\pi m_a \sin y) dy + j \int_0^\pi \sin(ny + m\pi m_a \sin y) dy \right. \\ &\quad \left. - \int_0^\pi \cos(ny - m\pi m_a \sin y) dy - j \int_0^\pi \sin(ny - m\pi m_a \sin y) dy \right] \{1 + (-1)^n\} \\ &= \frac{-jV_t}{4\pi m} [J_{-n}(m\pi m_a) - jE_{-n}(m\pi m_a) - J_{-n}(-m\pi m_a) \\ &\quad + jE_{-n}(-m\pi m_a)] \{1 + (-1)^n\} \end{aligned} \tag{B.7}$$

where J is an Anger function given by

$$J_n(m\pi m_a) = \frac{1}{\pi} \int_0^\pi \cos((m\pi m_a) \sin \theta - n\theta) d\theta$$

and E is a Weber function given by

$$E_n(m\pi m_a) = -\frac{1}{\pi} \int_0^\pi \sin((m\pi m_a) \sin \theta - n\theta) d\theta$$

For m odd

$$\begin{aligned} A_{mn} + jB_{mn} &= \frac{-jV_t}{4\pi^2 m} \left[\int_0^\pi \left\{ e^{jny} \left(e^{-jm\pi m_a \sin(y)} - e^{jm\pi m_a \sin(y)} \right) \right\} dy \right. \\ &\quad \left. + \int_\pi^{2\pi} \left\{ e^{jny} \left(e^{-jm\pi m_a \sin(y)} - e^{jm\pi m_a \sin(y)} \right) \right\} dy \right] \\ &= \frac{-jV_t}{4\pi^2 m} \left\{ \int_0^{2\pi} e^{jny} e^{-jm\pi m_a \sin(y)} dy - \int_0^{2\pi} e^{jny} e^{jm\pi m_a \sin(y)} dy \right\} \end{aligned}$$

Let $\theta = y - \pi$ then $d\theta = dy$ and $\theta = \begin{cases} -\pi & \text{as } y = 0 \\ \pi & \text{as } y = 2\pi \end{cases}$

$$\begin{aligned}
A_{mn} + jB_{mn} &= \frac{-jV_t}{4\pi^2 m} \left\{ \int_{-\pi}^{\pi} e^{jn(\theta+\pi)} e^{jm\pi m_a \sin(\theta)} d\theta - \int_{-\pi}^{\pi} e^{jn(\theta+\pi)} e^{-jm\pi m_a \sin(\theta)} d\theta \right\} \\
&= \frac{-jV_t}{2m\pi} e^{jn\pi} \left\{ \frac{1}{2\pi} \int_{-\pi}^{\pi} e^{jn\theta} e^{jm\pi m_a \sin \theta} d\theta - \frac{1}{2\pi} \int_{-\pi}^{\pi} e^{jn\theta} e^{-jm\pi m_a \sin \theta} d\theta \right\} \\
&= \frac{-jV_t}{2m\pi} e^{jn\pi} \{ J_{-n}(m\pi m_a) - J_{-n}(-m\pi m_a) \} \\
&= \frac{-jV_t}{2m\pi} e^{jn\pi} \{ (-1)^n J_n(m\pi m_a) - J_n(m\pi m_a) \}
\end{aligned} \tag{B.8}$$

where J is a Bessel function given by

$$J_n(m\pi m_a) = \frac{1}{2\pi} \int_{-\pi}^{\pi} e^{-i(m\pi m_a)} e^{in\theta} d\theta$$

B.3 Maple program for S_α and S_β under PD PWM

(This program calculates the harmonics for S_α and S_β under PD PWM. This is done by using the theory developed in subsection 4.2.1. The resulting harmonics are shown in Figure 4.13.)

restart:

with(plots):

ws:=2*Pi*6000;

w1:=2*Pi*50;

A:=0.8;

Vhrec[1] := sqrt(3/2) * A;

frec[1]:=2*Pi*50;

l:=2;

for m from 2 to 2 do

for n from -15 to 15 do

frec[l]:=m*ws+n*w1;

if modp(n,3)=0 then

Vhrec[l]:=0;

wrec[l]:=frec[l]/(2*Pi);

elif modp(n,3)=1 then

Vhrec[l] := sqrt(3/2) * (-I * 2)/(2 * Pi * m) * exp(I * n * Pi) * (BesselJ(-n, -m * A * Pi) - BesselJ(-n, m * A * Pi));

l:=l+1;

else

Vhrec[l] := -sqrt(3/2) * (-I * 2)/(2 * Pi * m) * exp(I * n * Pi) * (BesselJ(-n, -m * A *

```

 $Pi) - BesselJ(-n, m * A * Pi));$ 
l:=l+1;
fi;
od;
od;
for m from 4 to 4 do
for n from -15 to 15 do
frec[l]:=m*ws+n*w1;
if modp(n,3)=0 then
Vhrec[l]:=0;
wrec[l]:=frec[l]/(2*Pi);
elif modp(n,3)=1 then
Vhrec[l] := sqrt(3/2) * (-I * 2)/(2 * Pi * m) * exp(I * n * Pi) * (BesselJ(-n, -m * A *
Pi) - BesselJ(-n, m * A * Pi));
l:=l+1;
else
Vhrec[l] := -sqrt(3/2) * (-I * 2)/(2 * Pi * m) * exp(I * n * Pi) * (BesselJ(-n, -m * A *
Pi) - BesselJ(-n, m * A * Pi));
l:=l+1;
fi;
od;
od;
for m from 1 to 1 do
for n from -15 to 15 do
frec[l]:=m*ws+n*w1;
if modp(n,3)=0 then
Vhrec[l]:=0;
wrec[l]:=frec[l]/(2*Pi);
else
wrec[l]:=frec[l]/(2*Pi);
Vhrec[l] := sqrt(3/2) * (-I * 2)/(4 * Pi * m) * (AngerJ(-n, -m * A * Pi)-
I * WeberE(-n, -m * A * Pi) - AngerJ(-n, m * A * Pi) +
I * WeberE(-n, m * A * Pi)) * (1 + (-1)n);
l:=l+1;
fi;
od;
od;

```



```

abs(Vhrec[106]]], [freq[107]/(2 * Pi), abs(Vhrec[107])], [freq[108]/(2 * Pi),
abs(Vhrec[108])], [freq[109]/(2 * Pi), abs(Vhrec[109])], [freq[110]/(2 * Pi),
abs(Vhrec[110])], [freq[111]/(2 * Pi), abs(Vhrec[111])], [freq[112]/(2 * Pi),
abs(Vhrec[112])], [freq[113]/(2 * Pi), abs(Vhrec[113])], [freq[114]/(2 * Pi),
abs(Vhrec[114])], [freq[115]/(2 * Pi), abs(Vhrec[115])], [freq[116]/(2 * Pi),
abs(Vhrec[116])], [freq[117]/(2 * Pi), abs(Vhrec[117])]], 0..25000, 0..0.18, style = point);

```

B.4 Maple program for S'_α and S'_β under PD PWM

(This program calculates the harmonics for S'_α and S'_β under PD PWM. This is done by using the theory developed in section 4.2.1. The resulting harmonics are shown in Figure 4.15.)

restart:

with(plots):

ws:=2*Pi*6000;

w1:=2*Pi*50;

A:=0.8;

l:=1;

for n from 0 to 0 do

if modp(n,2)=0 then

freq[l]:=n*w1;

wrec[l]:=freq[l]/(2*Pi);

Vhrec[l]:=0;

l:=l+1;

else

freq[l]:=n*w1;

wrec[l]:=freq[l]/(2*Pi);

Vhrec[l]:=0;

l:=l+1;

fi;

od;

for n from 1 to 1 do

if modp(n,2)=0 then

freq[l]:=n*w1;

wrec[l]:=freq[l]/(2*Pi);

Vhrec[l]:=0;

```

l:=l+1;
else
frec[l]:=n*w1;
wrec[l]:=frec[l]/(2*Pi);
Vhrec[l]:=0;
l:=l+1;
fi;
od;

for n from 2 to 15 do
if modp(n,3)=0 then
frec[l]:=n*w1;
wrec[l]:=frec[l]/(2*Pi);
Vhrec[l]:=0;
l:=l+1;
else
frec[l]:=n*w1;
wrec[l]:=frec[l]/(2*Pi);
Vhrec[l] := -sqrt(3/2) * (1/2) * 2 * A * ((2 * exp(I * n * Pi) * cos(Pi)-
2 * exp(I * n * Pi) * I * n * sin(Pi) - 1 - exp(2 * I * n * Pi) * cos(2 * Pi) +
exp(2 * I * n * Pi) * I * n * sin(2 * Pi))/(Pi * (I^2 * n^2 + 1)));
l:=l+1;
fi;
od;

for m from 1 to 1 do
for n from -15 to 15 do
frec[l]:=m*ws+n*w1;
if modp(n,3)=0 then
Vhrec[l]:=0;
wrec[l]:=frec[l]/(2*Pi);
elif modp(n,3)=1 then
Vhrec[l] := sqrt(3/2) * (-I * 2)/(2 * Pi * m) * exp(I * n * Pi) * (BesselJ(-n, m * A *
Pi) - BesselJ(-n, -m * A * Pi));
l:=l+1;
else
Vhrec[l] := -sqrt(3/2) * (-I * 2)/(2 * Pi * m) * exp(I * n * Pi) * (BesselJ(-n, m * A *
Pi) - BesselJ(-n, -m * A * Pi));
l:=l+1;

```

fi;

od;

od;

for m from 3 to 3 do

for n from -15 to 15 do

frec[l]:=m*ws+n*w1;

if modp(n,3)=0 then

Vhrec[l]:=0;

wrec[l]:=frec[l]/(2*Pi);

elif modp(n,3)=1 then

$Vhrec[l] := \sqrt{3/2} * (-I * 2) / (2 * Pi * m) * \exp(I * n * Pi) * (BesselJ(-n, m * A * Pi) - BesselJ(-n, -m * A * Pi));$

l:=l+1;

else

$Vhrec[l] := \sqrt{3/2} * (-I * 2) / (2 * Pi * m) * \exp(I * n * Pi) * (BesselJ(-n, m * A * Pi) - BesselJ(-n, -m * A * Pi));$

l:=l+1;

fi;

od;

od;

for m from 5 to 5 do

for n from -15 to 15 do

frec[l]:=m*ws+n*w1;

if modp(n,3)=0 then

Vhrec[l]:=0;

wrec[l]:=frec[l]/(2*Pi);

elif modp(n, 3) = 1 then

$Vhrec[l] := \sqrt{3/2} * (-I * 2) / (2 * Pi * m) * \exp(I * n * Pi) * (BesselJ(-n, m * A * Pi) - BesselJ(-n, -m * A * Pi));$

l:=l+1;

else

$Vhrec[l] := \sqrt{3/2} * (-I * 2) / (2 * Pi * m) * \exp(I * n * Pi) * (BesselJ(-n, m * A * Pi) - BesselJ(-n, -m * A * Pi));$

l:=l+1;

fi;

od;

od;

for m from 2 to 2 do

for n from -15 to 15 do

frec[l]:=m*ws+n*w1;

if modp(n,3)=0 then

Vhrec[l]:=0;

wrec[l]:=frec[l]/(2*Pi);

else

wrec[l]:=frec[l]/(2*Pi);

$Vhrec[l] := \sqrt{3/2} * (-I * 2) / (4 * Pi * m) * (AngerJ(-n, m * A * Pi) -$

$I * WeberE(-n, m * A * Pi) - AngerJ(-n, -m * A * Pi) +$

$I * WeberE(-n, -m * A * Pi)) * (1 + (-1)^n);$

l:=l+1;

fi;

od;

od;

for m from 4 to 4 do

for n from -15 to 15 do

frec[l]:=m*ws+n*w1;

if modp(n,3)=0 then

Vhrec[l]:=0;

wrec[l]:=frec[l]/(2*Pi);

else

wrec[l]:=frec[l]/(2*Pi);

$Vhrec[l] := \sqrt{3/2} * (-I * 2) / (4 * Pi * m) * (AngerJ(-n, m * A * Pi) -$

$I * WeberE(-n, m * A * Pi) - AngerJ(-n, -m * A * Pi) +$

$I * WeberE(-n, -m * A * Pi)) * (1 + (-1)^n);$

l:=l+1;

fi;

od;

od;

for m from 3 to 3 do

for n from -15 to 15 do

frec[l]:=m*ws+n*w1;

if modp(n,3)=0 then

```

Vhrec[l]:=0;
wrec[l]:=freq[l]/(2*Pi);
else
wrec[l]:=freq[l]/(2*Pi);
Vhrec[l] := sqrt(3/2) * (-I * 2)/(4 * Pi * m) * (AngerJ(-n, -m * A * Pi)-
I * WeberE(-n, -m * A * Pi) - AngerJ(-n, m * A * Pi) +
I * WeberE(-n, m * A * Pi)) * (1 + (-1)^n);
l:=l+1;
fi;
od;
od;

for m from 5 to 5 do
for n from -15 to 15 do
freq[l]:=m*ws+n*w1;
if modp(n,3)=0 then
Vhrec[l]:=0;
wrec[l]:=freq[l]/(2*Pi);
else
wrec[l] := freq[l]/(2 * Pi);
Vhrec[l] := sqrt(3/2) * (-I * 2)/(4 * Pi * m) * (AngerJ(-n, -m * A * Pi)-
I * WeberE(-n, -m * A * Pi) - AngerJ(-n, m * A * Pi) +
I * WeberE(-n, m * A * Pi)) * (1 + (-1)^n);
l:=l+1;
fi;
od;
od;
l;
Vhrec[l];
plot([[freq[1]/(2 * Pi), abs(Vhrec[1])], [freq[2]/(2 * Pi), abs(Vhrec[2])], [freq[3]/(2 * Pi),
abs(Vhrec[3])], [freq[4]/(2 * Pi), abs(Vhrec[4])], [freq[5]/(2 * Pi), abs(Vhrec[5])],
[freq[6]/(2 * Pi), abs(Vhrec[6])], [freq[7]/(2 * Pi), abs(Vhrec[7])], [freq[8]/(2 * Pi),
abs(Vhrec[8])], [freq[9]/(2 * Pi), abs(Vhrec[9])], [freq[10]/(2 * Pi), abs(Vhrec[10])],
[freq[11]/(2 * Pi), abs(Vhrec[11])], [freq[12]/(2 * Pi), abs(Vhrec[12])], [freq[13]/(2 * Pi),
abs(Vhrec[13])], [freq[14]/(2 * Pi), abs(Vhrec[14])], [freq[15]/(2 * Pi), abs(Vhrec[15])],
[freq[16]/(2 * Pi), abs(Vhrec[16])], [freq[17]/(2 * Pi), abs(Vhrec[17])], [freq[18]/(2 * Pi),
abs(Vhrec[18])], [freq[19]/(2 * Pi), abs(Vhrec[19])], [freq[20]/(2 * Pi), abs(Vhrec[20])],
)[freq[21]/(2 * Pi), abs(Vhrec[21])], [freq[22]/(2 * Pi), abs(Vhrec[22])], [freq[23]/(2 * Pi),

```



```
abs(Vhrec[114])], [freq[115]/(2 * Pi), abs(Vhrec[115])], [freq[116]/(2 * Pi),
abs(Vhrec[116])], [freq[117]/(2 * Pi), abs(Vhrec[117])]], 0..25000, 0..0.18, style = point);
```

B.5 Maple program for $|F_1|$ under PD PWM

(This program calculates the harmonics for $|F_1|$ under PD PWM. The resulting harmonics are shown in Figure 4.16.)

restart:

with(plots):

ws:=2*Pi*6000;

w1:=2*Pi*50;

A:=0.8;

l:=1;

for n from 0 to 0 do

if modp(n,2)=0 then

freq[l]:=n*w1;

wrec[l]:=freq[l]/(2*Pi);

$Vhrec[l] := (\text{conjugate}(-\sqrt{3}/2) * (1/2) * 2 * A * ((2 * \exp(I * n * \text{Pi}) * \cos(\text{Pi}) - 2 * \exp(I * n * \text{Pi}) * I * n * \sin(\text{Pi}) - 1 - \exp(2 * I * n * \text{Pi}) * \cos(2 * \text{Pi}) + \exp(2 * I * n * \text{Pi}) * I * n * \sin(2 * \text{Pi})) / (\text{Pi} * (I^2 * n^2 + 1)))) * \sqrt{3}/2 * (1/2) * 2 * A * (\exp(2 * I * \text{Pi} * n) - 1) / (\text{Pi} * (n^2 - 1));$

l:=l+1;

else

freq[l]:=n*w1;

wrec[l]:=freq[l]/(2*Pi);

$Vhrec[l] := (\text{conjugate}(-\sqrt{3}/2) * (1/2) * 2 * A * ((2 * \exp(I * n * \text{Pi}) * \cos(\text{Pi}) - 2 * \exp(I * n * \text{Pi}) * I * n * \sin(\text{Pi}) - 1 - \exp(2 * I * n * \text{Pi}) * \cos(2 * \text{Pi}) + \exp(2 * I * n * \text{Pi}) * I * n * \sin(2 * \text{Pi})) / (\text{Pi} * (I^2 * n^2 + 1)))) * \sqrt{3}/2 * (1/2) * 2 * A * (\exp(2 * I * \text{Pi} * n) - 1) / (\text{Pi} * (n^2 - 1));$

l:=l+1;

fi;

od;

for n from 1 to 1 do

if modp(n,2)=0 then

freq[l]:=n*w1;

wrec[l]:=freq[l]/(2*Pi);

$Vhrec[l] := (\text{conjugate}(-\sqrt{3}/2) * (1/2) * 2 * A * (1 - 3 * \cos((\text{Pi})^{(2)}) - 2 * I * \cos(\text{Pi}) * \sin(\text{Pi}) + 2 * \cos((\text{Pi})^{(4)}) + 2 * I * \cos((\text{Pi})^{(3)}) * \sin(\text{Pi})) / \text{Pi}) * ((1/2) * I * 2 * A);$

l:=l+1;

```

else
frec[l]:=n*w1;
wrec[l]:=frec[l]/(2*Pi);
Vhrec[l] := (conjugate(-sqrt(3/2) * (1/2) * 2 * A * (1 - 3 * cos((Pi)^2)) - 2 * I * cos(Pi) *
sin(Pi) + 2 * cos((Pi)^4)) + 2 * I * cos((Pi)^3) * sin(Pi))/Pi) * ((1/2) * I * 2 * A);
l:=l+1;
fi;
od;
for n from 2 to 15 do
if modp(n,2)=0 then
frec[l]:=n*w1;
wrec[l]:=frec[l]/(2*Pi);
Vhrec[l] := (conjugate(-sqrt(3/2) * (1/2) * 2 * A * ((2 * exp(I * n * Pi) * cos(Pi) - 2 *
exp(I*n*Pi)*I*n*sin(Pi)-1-exp(2*I*n*Pi)*cos(2*Pi)+exp(2*I*n*Pi)*I*n*sin(2*
Pi))/(Pi*(I^2*n^2+1)))) * sqrt(3/2) * (1/2) * 2 * A * (exp(2 * I * Pi * n) - 1)/(Pi * (n^2 - 1));
l:=l+1;
else
frec[l]:=n*w1;
wrec[l]:=frec[l]/(2*Pi);
Vhrec[l] := (conjugate(-sqrt(3/2) * (1/2) * 2 * A * ((2 * exp(I * n * Pi) * cos(Pi) - 2 *
exp(I*n*Pi)*I*n*sin(Pi)-1-exp(2*I*n*Pi)*cos(2*Pi)+exp(2*I*n*Pi)*I*n*sin(2*
Pi))/(Pi*(I^2*n^2+1)))) * sqrt(3/2) * (1/2) * 2 * A * (exp(2 * I * Pi * n) - 1)/(Pi * (n^2 - 1));
l:=l+1;
fi;
od;
for m from 1 to 1 do
for n from -15 to 15 do
frec[l]:=m*ws+n*w1;
if modp(n,3)=0 then
Vhrec[l]:=0;
wrec[l]:=frec[l]/(2*Pi);
l:=l+1;
elif modp(n,3)=1 then
Vhrec[l] := (conjugate(sqrt(3/2) * (-I * 2)/(4 * Pi * m) * (AngerJ(-n, -m * A * Pi) -
I * WeberE(-n, -m * A * Pi) - AngerJ(-n, m * A * Pi) + I * WeberE(-n, m * A * Pi)) *
(1 + (-1)^n)) * (sqrt(3/2) * (-I * 2)/(2 * Pi * m) * exp(I * n * Pi) * (BesselJ(-n, m * A *
Pi) - BesselJ(-n, -m * A * Pi))));
```

l:=l+1;

else

$Vhrec[l] := (\text{conjugate}(\sqrt{3/2}) * (-I * 2) / (4 * Pi * m) * (\text{AngerJ}(-n, -m * A * Pi) - I * \text{WeberE}(-n, -m * A * Pi) - \text{AngerJ}(-n, m * A * Pi) + I * \text{WeberE}(-n, m * A * Pi)) * (1 + (-1)^n)) * (\sqrt{3/2} * (-I * 2) / (2 * Pi * m) * \exp(I * n * Pi) * (\text{BesselJ}(-n, m * A * Pi) - \text{BesselJ}(-n, -m * A * Pi))));$

l:=l+1;

fi;

od;

od;

for m from 3 to 3 do

for n from -15 to 15 do

frec[l]:=m*ws+n*w1;

if modp(n,3)=0 then

$Vhrec[l]:=0;$

wrec[l]:=frec[l]/(2*Pi);

l:=l+1;

elif modp(n,3)=1 then

$Vhrec[l] := (\text{conjugate}(\sqrt{3/2}) * (-I * 2) / (4 * Pi * m) * (\text{AngerJ}(-n, -m * A * Pi) - I * \text{WeberE}(-n, -m * A * Pi) - \text{AngerJ}(-n, m * A * Pi) + I * \text{WeberE}(-n, m * A * Pi)) * (1 + (-1)^n)) * (\sqrt{3/2} * (-I * 2) / (2 * Pi * m) * \exp(I * n * Pi) * (\text{BesselJ}(-n, m * A * Pi) - \text{BesselJ}(-n, -m * A * Pi))));$

l:=l+1;

else

$Vhrec[l] := (\text{conjugate}(\sqrt{3/2}) * (-I * 2) / (4 * Pi * m) * (\text{AngerJ}(-n, -m * A * Pi) - I * \text{WeberE}(-n, -m * A * Pi) - \text{AngerJ}(-n, m * A * Pi) + I * \text{WeberE}(-n, m * A * Pi)) * (1 + (-1)^n)) * (\sqrt{3/2} * (-I * 2) / (2 * Pi * m) * \exp(I * n * Pi) * (\text{BesselJ}(-n, m * A * Pi) - \text{BesselJ}(-n, -m * A * Pi))));$

l:=l+1;

fi;

od;

od;

for m from 5 to 5 do

for n from -15 to 15 do

frec[l]:=m*ws+n*w1;

if modp(n,3)=0 then

$Vhrec[l]:=0;$

```
wrec[l]:=freq[l]/(2*Pi);
l:=l+1;
elif modp(n,3)=1 then
  Vhrec[l] := (conjugate(sqrt(3/2) * (-I * 2)/(4 * Pi * m) * (AngerJ(-n, -m * A * Pi) -
  I * WeberE(-n, -m * A * Pi) - AngerJ(-n, m * A * Pi) + I * WeberE(-n, m * A * Pi)) *
  (1 + (-1)^n)) * (sqrt(3/2) * (-I * 2)/(2 * Pi * m) * exp(I * n * Pi) * (BesselJ(-n, m * A *
  Pi) - BesselJ(-n, -m * A * Pi)))); 
l:=l+1;
else
  Vhrec[l] := (conjugate(sqrt(3/2) * (-I * 2)/(4 * Pi * m) * (AngerJ(-n, -m * A * Pi) -
  I * WeberE(-n, -m * A * Pi) - AngerJ(-n, m * A * Pi) + I * WeberE(-n, m * A * Pi)) *
  (1 + (-1)^n)) * (sqrt(3/2) * (-I * 2)/(2 * Pi * m) * exp(I * n * Pi) * (BesselJ(-n, m * A *
  Pi) - BesselJ(-n, -m * A * Pi)))); 
l:=l+1;
fi;
od;
od;

for m from 2 to 2 do
for n from -15 to 15 do
  freq[l]:=m*ws+n*w1;
  if modp(n,3)=0 then
    Vhrec[l]:=0;
    wrec[l]:=freq[l]/(2*Pi);
    l:=l+1;
  elif modp(n,3)=1 then
    Vhrec[l] := (conjugate(sqrt(3/2) * (-I * 2)/(2 * Pi * m) * exp(I * n * Pi) * (BesselJ(-n,
    -m * A * Pi) - BesselJ(-n, m * A * Pi)) * (sqrt(3/2) * (-I * 2)/(4 * Pi * m) * (AngerJ(-n,
    m * A * Pi) - I * WeberE(-n, m * A * Pi) - AngerJ(-n, -m * A * Pi) + I * WeberE
    (-n, -m * A * Pi)) * (1 + (-1)^n)));
    l:=l+1;
  else
    wrec[l]:=freq[l]/(2*Pi);
    Vhrec[l] := (conjugate(-sqrt(3/2) * (-I * 2)/(2 * Pi * m) * exp(I * n * Pi) * (BesselJ(-n,
    -m * A * Pi) - BesselJ(-n, m * A * Pi)) * (sqrt(3/2) * (-I * 2)/(4 * Pi * m) * (AngerJ
    (-n, m * A * Pi) - I * WeberE(-n, m * A * Pi) - AngerJ(-n, -m * A * Pi) + I *
    WeberE(-n, -m *
    A * Pi)) * (1 + (-1)^n)));
  end if;
end if;
end if;
end if;
```

```

l:=l+1;
fi;
od;
od;

for m from 4 to 4 do
for n from -15 to 15 do
frec[l]:=m*ws+n*w1;
if modp(n,3)=0 then
Vhrec[l]:=0;
wrec[l]:=frec[l]/(2*Pi);
l:=l+1;
elif modp(n,3)=1 then
Vhrec[l] := (conjugate(sqrt(3/2)*(-I*2)/(2*Pi*m)*exp(I*n*Pi)*(BesselJ(-n,
-m*A*Pi)-BesselJ(-n,m*A*Pi)))*(sqrt(3/2)*(-I*2)/(4*Pi*m)*(AngerJ(-n,
m*A*Pi)-I*WeberE(-n,m*A*Pi)-AngerJ(-n,-m*A*Pi)+I*WeberE
(-n,-m*A*Pi))*(1+(-1)^n)));
l:=l+1;
else
wrec[l]:=frec[l]/(2*Pi);
Vhrec[l] := (conjugate(-sqrt(3/2)*(-I*2)/(2*Pi*m)*exp(I*n*Pi)*(BesselJ(-n,
-m*A*Pi)-BesselJ(-n,m*A*Pi)))*(sqrt(3/2)*(-I*2)/(4*Pi*m)*(AngerJ
(-n,m*A*Pi)-I*WeberE(-n,m*A*Pi)-AngerJ(-n,-m*A*Pi)+I*WeberE
(-n,-m*A*Pi))*(1+(-1)^n)));
l:=l+1;
fi;
od;
od;
l;
Vhrec[l];
plot([[frec[1]/(2*Pi),abs(Vhrec[1])],[frec[2]/(2*Pi),abs(Vhrec[2])],[frec[3]/(2*Pi),
abs(Vhrec[3])],[frec[4]/(2*Pi),abs(Vhrec[4])],[frec[5]/(2*Pi),abs(Vhrec[5])],
[frec[6]/(2*Pi),abs(Vhrec[6])],[frec[7]/(2*Pi),abs(Vhrec[7])],[frec[8]/(2*Pi),
abs(Vhrec[8])],[frec[9]/(2*Pi),abs(Vhrec[9])],[frec[10]/(2*Pi),abs(Vhrec[10])],
[frec[11]/(2*Pi),abs(Vhrec[11])],[frec[12]/(2*Pi),abs(Vhrec[12])],[frec[13]/(2*Pi),
abs(Vhrec[13])],[frec[14]/(2*Pi),abs(Vhrec[14])],[frec[15]/(2*Pi),abs(Vhrec[15])],
[frec[16]/(2*Pi),abs(Vhrec[16])],[frec[17]/(2*Pi),abs(Vhrec[17])],[frec[18]/(2*Pi),
abs(Vhrec[18])],[frec[19]/(2*Pi),abs(Vhrec[19])],[frec[20]/(2*Pi),abs(Vhrec[20])]],

```

)[freq[21]/(2 * Pi), abs(Vhrec[21])], [freq[22]/(2 * Pi), abs(Vhrec[22])], [freq[23]/(2 * Pi),
abs(Vhrec[23])], [freq[24]/(2 * Pi), abs(Vhrec[24])], [freq[25]/(2 * Pi), abs(Vhrec[25])],
[freq[26]/(2 * Pi), abs(Vhrec[26])], [freq[27]/(2 * Pi), abs(Vhrec[27])], [freq[28]/(2 * Pi),
abs(Vhrec[28])], [freq[29]/(2 * Pi), abs(Vhrec[29])], [freq[30]/(2 * Pi), abs(Vhrec[30])],
[freq[31]/(2 * Pi), abs(Vhrec[31])], [freq[32]/(2 * Pi), abs(Vhrec[32])], [freq[33]/(2 * Pi),
abs(Vhrec[33])], [freq[34]/(2 * Pi), abs(Vhrec[34])], [freq[35]/(2 * Pi), abs(Vhrec[35])],
[freq[36]/(2 * Pi), abs(Vhrec[36])], [freq[37]/(2 * Pi), abs(Vhrec[37])], [freq[38]/(2 * Pi),
abs(Vhrec[38])], [freq[39]/(2 * Pi), abs(Vhrec[39])], [freq[40]/(2 * Pi), abs(Vhrec[40])],
[freq[41]/(2 * Pi), abs(Vhrec[41])], [freq[42]/(2 * Pi), abs(Vhrec[42])], [freq[43]/(2 * Pi),
abs(Vhrec[43])], [freq[44]/(2 * Pi), abs(Vhrec[44])], [freq[45]/(2 * Pi), abs(Vhrec[45])],
[freq[46]/(2 * Pi), abs(Vhrec[46])], [freq[47]/(2 * Pi), abs(Vhrec[47])], [freq[48]/(2 * Pi),
abs(Vhrec[48])], [freq[49]/(2 * Pi), abs(Vhrec[49])], [freq[50]/(2 * Pi), abs(Vhrec[50])],
[freq[51]/(2 * Pi), abs(Vhrec[51])], [freq[52]/(2 * Pi), abs(Vhrec[52])], [freq[53]/(2 * Pi),
abs(Vhrec[53])], [freq[54]/(2 * Pi), abs(Vhrec[54])], [freq[55]/(2 * Pi), abs(Vhrec[55])],
[freq[56]/(2 * Pi), abs(Vhrec[56])], [freq[57]/(2 * Pi), abs(Vhrec[57])], [freq[58]/(2 * Pi),
abs(Vhrec[58])], [freq[59]/(2 * Pi), abs(Vhrec[59])], [freq[60]/(2 * Pi), abs(Vhrec[60])],
[freq[61]/(2 * Pi), abs(Vhrec[61])], [freq[62]/(2 * Pi), abs(Vhrec[62])], [freq[63]/(2 * Pi),
abs(Vhrec[63])], [freq[64]/(2 * Pi), abs(Vhrec[64])], [freq[65]/(2 * Pi), abs(Vhrec[65])],
[freq[66]/(2 * Pi), abs(Vhrec[66])], [freq[67]/(2 * Pi), abs(Vhrec[67])], [freq[68]/(2 * Pi),
abs(Vhrec[68])], [freq[69]/(2 * Pi), abs(Vhrec[69])], [freq[70]/(2 * Pi), abs(Vhrec[70])],
[freq[71]/(2 * Pi), abs(Vhrec[71])], [freq[72]/(2 * Pi), abs(Vhrec[72])], [freq[73]/(2 * Pi),
abs(Vhrec[73])], [freq[74]/(2 * Pi), abs(Vhrec[74])], [freq[75]/(2 * Pi), abs(Vhrec[75])],
[freq[76]/(2 * Pi), abs(Vhrec[76])], [freq[77]/(2 * Pi), abs(Vhrec[77])], [freq[78]/(2 * Pi),
abs(Vhrec[78])], [freq[79]/(2 * Pi), abs(Vhrec[79])], [freq[80]/(2 * Pi), abs(Vhrec[80])],
[freq[81]/(2 * Pi), abs(Vhrec[81])], [freq[82]/(2 * Pi), abs(Vhrec[82])], [freq[83]/(2 * Pi),
abs(Vhrec[83])], [freq[84]/(2 * Pi), abs(Vhrec[84])], [freq[85]/(2 * Pi), abs(Vhrec[85])],
[freq[86]/(2 * Pi), abs(Vhrec[86])], [freq[87]/(2 * Pi), abs(Vhrec[87])], [freq[88]/(2 * Pi),
abs(Vhrec[88])], [freq[89]/(2 * Pi), abs(Vhrec[89])], [freq[90]/(2 * Pi), abs(Vhrec[90])],
[freq[91]/(2 * Pi), abs(Vhrec[91])], [freq[92]/(2 * Pi), abs(Vhrec[92])], [freq[93]/(2 * Pi),
abs(Vhrec[93])], [freq[94]/(2 * Pi), abs(Vhrec[94])], [freq[95]/(2 * Pi), abs(Vhrec[95])],
[freq[96]/(2 * Pi), abs(Vhrec[96])], [freq[97]/(2 * Pi), abs(Vhrec[97])], [freq[98]/(2 * Pi),
abs(Vhrec[98])], [freq[99]/(2 * Pi), abs(Vhrec[99])], [freq[100]/(2 * Pi),
abs(Vhrec[100])], [freq[101]/(2 * Pi), abs(Vhrec[101])], [freq[102]/(2 * Pi),
abs(Vhrec[102])], [freq[103]/(2 * Pi), abs(Vhrec[103])], [freq[104]/(2 * Pi),
abs(Vhrec[104])], [freq[105]/(2 * Pi), abs(Vhrec[105])], [freq[106]/(2 * Pi),
abs(Vhrec[106])], [freq[107]/(2 * Pi), abs(Vhrec[107])], [freq[108]/(2 * Pi),
abs(Vhrec[108])], [freq[109]/(2 * Pi), abs(Vhrec[109])], [freq[110]/(2 * Pi),
abs(Vhrec[110])], [freq[111]/(2 * Pi), abs(Vhrec[111])], [freq[112]/(2 * Pi),

```

abs(Vhrec[112])), [freq[113]/(2 * Pi), abs(Vhrec[113])], [freq[114]/(2 * Pi),
abs(Vhrec[114])], [freq[115]/(2 * Pi), abs(Vhrec[115])], [freq[116]/(2 * Pi),
abs(Vhrec[116])], [freq[117]/(2 * Pi), abs(Vhrec[117])], [freq[118]/(2 * Pi),
abs(Vhrec[118])], [freq[119]/(2 * Pi), abs(Vhrec[119])], [freq[120]/(2 * Pi),
abs(Vhrec[120])], [freq[121]/(2 * Pi), abs(Vhrec[121])], [freq[122]/(2 * Pi),
abs(Vhrec[122])], [freq[123]/(2 * Pi), abs(Vhrec[123])], [freq[124]/(2 * Pi),
abs(Vhrec[124])], [freq[125]/(2 * Pi), abs(Vhrec[125])], [freq[126]/(2 * Pi),
abs(Vhrec[126])], [freq[127]/(2 * Pi), abs(Vhrec[127])], [freq[128]/(2 * Pi),
abs(Vhrec[128])], [freq[129]/(2 * Pi), abs(Vhrec[129])], [freq[130]/(2 * Pi),
abs(Vhrec[130])], [freq[131]/(2 * Pi), abs(Vhrec[131])], [freq[132]/(2 * Pi),
abs(Vhrec[132])], [freq[133]/(2 * Pi), abs(Vhrec[133])], [freq[134]/(2 * Pi),
abs(Vhrec[134])], [freq[135]/(2 * Pi), abs(Vhrec[135])], [freq[136]/(2 * Pi),
abs(Vhrec[136])], [freq[137]/(2 * Pi), abs(Vhrec[137])], [freq[138]/(2 * Pi),
abs(Vhrec[138])], [freq[139]/(2 * Pi), abs(Vhrec[139])], [freq[140]/(2 * Pi),
abs(Vhrec[140])], [freq[141]/(2 * Pi), abs(Vhrec[141])], [freq[142]/(2 * Pi),
abs(Vhrec[142])], [freq[143]/(2 * Pi), abs(Vhrec[143])], [freq[144]/(2 * Pi),
abs(Vhrec[144])], [freq[145]/(2 * Pi), abs(Vhrec[145])], [freq[146]/(2 * Pi),
abs(Vhrec[146])], [freq[147]/(2 * Pi), abs(Vhrec[147])], [freq[148]/(2 * Pi),
abs(Vhrec[148])], [freq[149]/(2 * Pi), abs(Vhrec[149])], [freq[150]/(2 * Pi),
abs(Vhrec[150])], [freq[151]/(2 * Pi), abs(Vhrec[151])], [freq[152]/(2 * Pi),
abs(Vhrec[152])], [freq[153]/(2 * Pi), abs(Vhrec[153])], [freq[154]/(2 * Pi),
abs(Vhrec[154])], [freq[155]/(2 * Pi), abs(Vhrec[155])], [freq[156]/(2 * Pi),
abs(Vhrec[156])], [freq[157]/(2 * Pi), abs(Vhrec[157])], [freq[158]/(2 * Pi),
abs(Vhrec[158])], [freq[159]/(2 * Pi), abs(Vhrec[159])], [freq[160]/(2 * Pi),
abs(Vhrec[160])], [freq[161]/(2 * Pi), abs(Vhrec[161])], [freq[162]/(2 * Pi),
abs(Vhrec[162])], [freq[163]/(2 * Pi), abs(Vhrec[163])], [freq[164]/(2 * Pi),
abs(Vhrec[164])], [freq[165]/(2 * Pi), abs(Vhrec[165])], [freq[166]/(2 * Pi),
abs(Vhrec[166])], [freq[167]/(2 * Pi), abs(Vhrec[167])], [freq[168]/(2 * Pi),
abs(Vhrec[168])], [freq[169]/(2 * Pi), abs(Vhrec[169])], [freq[170]/(2 * Pi),
abs(Vhrec[170])], [freq[171]/(2 * Pi), abs(Vhrec[171])], [freq[172]/(2 * Pi),
abs(Vhrec[172])]], 0..25000, 0..0.18, style = point);

```

B.6 Maple program for $|F_2|$ under PD PWM

(This program calculates the harmonics for $|F_2|$ under PD PWM. The resulting harmonics are shown in Figure 4.17.)

restart:

```
with(plots);
ws:=2*Pi*6000;
w1:=2*Pi*50;
A:=0.8;
l:=1;
for n from 0 to 0 do
if modp(n,2)=0 then
frec[l]:=n*w1;
wrec[l]:=frec[l]/(2*Pi);
Vhrec[l]:=0;
l:=l+1;
else
frec[l]:=n*w1;
wrec[l]:=frec[l]/(2*Pi);
Vhrec[l]:=0;
l:=l+1;
fi;
od;
for n from 1 to 1 do
if modp(n,2)=0 then
frec[l]:=n*w1;
wrec[l]:=frec[l]/(2*Pi);
Vhrec[l]:=0;
l:=l+1;
else
frec[l]:=n*w1;
wrec[l]:=frec[l]/(2*Pi);
Vhrec[l]:=0;
l:=l+1;
fi;
od;

for n from 2 to 15 do
if modp(n,3)=0 then
frec[l]:=n*w1;
wrec[l]:=frec[l]/(2*Pi);
Vhrec[l]:=0;
l:=l+1;
```

```

else
freq[l]:=n*w1;
wrec[l]:=freq[l]/(2*Pi);
Vhrec[l] := (conjugate(-sqrt(3/2) * (1/2) * 2 * A * ((2 * exp(I * n * Pi) * cos(Pi) - 2 *
exp(I * n * Pi) * I * n * sin(Pi) - 1 - exp(2 * I * n * Pi) * cos(2 * Pi) + exp(2 * I * n * Pi)*
I * n * sin(2 * Pi))/(Pi * (I^2 * n^2 + 1)))) * (-sqrt(3/2) * (1/2) * 2 * A * ((2 * exp(I * n*
Pi) * cos(Pi) - 2 * exp(I * n * Pi) * I * n * sin(Pi) - 1 - exp(2 * I * n * Pi) * cos(2 * Pi)+
exp(2 * I * n * Pi) * I * n * sin(2 * Pi))/(Pi * (I^2 * n^2 + 1))));;
l:=l+1;
fi;
od;

for m from 1 to 1 do
for n from -15 to 15 do
freq[l]:=m*ws+n*w1;
if modp(n,3)=0 then
Vhrec[l]:=0;
wrec[l]:=freq[l]/(2*Pi);
elif modp(n,3)=1 then
Vhrec[l] := (conjugate(sqrt(3/2)*(-I*2)/(2*Pi*m)*exp(I*n*Pi)*(BesselJ(-n,m*
A*Pi) - BesselJ(-n,-m*A*Pi))) * (sqrt(3/2)*(-I*2)/(2*Pi*m)*exp(I*n*
Pi)*(BesselJ(-n,m*A*Pi) - BesselJ(-n,-m*A*Pi)));
l:=l+1;
else
Vhrec[l] := (conjugate(-sqrt(3/2)*(-I*2)/(2*Pi*m)*exp(I*n*Pi)*(BesselJ(-n,
m*A*Pi) - BesselJ(-n,-m*A*Pi))) * (-sqrt(3/2)*(-I*2)/(2*Pi*m)*exp(
I*n*Pi)*(BesselJ(-n,m*A*Pi) - BesselJ(-n,-m*A*Pi)));
l:=l+1;
fi;
od;
od;

for m from 3 to 3 do
for n from -15 to 15 do
freq[l]:=m*ws+n*w1;
if modp(n,3)=0 then
Vhrec[l]:=0;
wrec[l]:=freq[l]/(2*Pi);

```

```

elseif modp(n,3)=1 then
Vhrec[l] := (conjugate(sqrt(3/2)*(-I*2)/(2*Pi*m)*exp(I*n*Pi)*(BesselJ(-n,m*
A*Pi) - BesselJ(-n,-m*A*Pi))) * (sqrt(3/2)*(-I*2)/(2*Pi*m)*exp(I*n*Pi) *
(BesselJ(-n,m*A*Pi) - BesselJ(-n,-m*A*Pi)));
l:=l+1;
else
Vhrec[l] := (conjugate(sqrt(3/2)*(-I*2)/(2*Pi*m)*exp(I*n*Pi)*(BesselJ(-n,m*
A*Pi) - BesselJ(-n,-m*A*Pi))) * (sqrt(3/2)*(-I*2)/(2*Pi*m)*exp(I*n*Pi) *
(BesselJ(-n,m*A*Pi) - BesselJ(-n,-m*A*Pi)));
l:=l+1;
fi;
od;
od;

for m from 5 to 5 do
for n from -15 to 15 do
frec[l]:=m*ws+n*w1;
if modp(n,3)=0 then
Vhrec[l]:=0;
wrec[l]:=frec[l]/(2*Pi);
elseif modp(n,3)=1 then
Vhrec[l] := (conjugate(sqrt(3/2)*(-I*2)/(2*Pi*m)*exp(I*n*Pi)*(BesselJ(-n,m*
A*Pi) - BesselJ(-n,-m*A*Pi))) * (sqrt(3/2)*(-I*2)/(2*Pi*m)*exp(I*n*Pi) *
(BesselJ(-n,m*A*Pi) - BesselJ(-n,-m*A*Pi)));
l:=l+1;
else
Vhrec[l] := (conjugate(sqrt(3/2)*(-I*2)/(2*Pi*m)*exp(I*n*Pi)*(BesselJ(-n,m*
A*Pi) - BesselJ(-n,-m*A*Pi))) * (sqrt(3/2)*(-I*2)/(2*Pi*m)*exp(I*n*Pi) *
(BesselJ(-n,m*A*Pi) - BesselJ(-n,-m*A*Pi)));
l:=l+1;
fi;
od;
od;

for m from 2 to 2 do
for n from -15 to 15 do
frec[l]:=m*ws+n*w1;
if modp(n,3)=0 then

```

```

Vhrec[l]:=0;
wrec[l]:=freq[l]/(2*Pi);
else
wrec[l]:=freq[l]/(2*Pi);
Vhrec[l] := (conjugate(sqrt(3/2) * (-I * 2)/(4 * Pi * m) * (AngerJ(-n, m * A * Pi) - I *
WeberE(-n, m * A * Pi) - AngerJ(-n, -m * A * Pi) + I * WeberE(-n, -m * A * Pi)) * (1 +
(-1)^n)) * (sqrt(3/2) * (-I * 2)/(4 * Pi * m) * (AngerJ(-n, m * A * Pi) - I * WeberE(-n, m *
A * Pi) - AngerJ(-n, -m * A * Pi) + I * WeberE(-n, -m * A * Pi)) * (1 + (-1)^n));
l:=l+1;
fi;
od;
od;

for m from 4 to 4 do
for n from -15 to 15 do
freq[l]:=m*ws+n*w1;
if modp(n,3)=0 then
Vhrec[l]:=0;
wrec[l]:=freq[l]/(2*Pi);
else
wrec[l]:=freq[l]/(2*Pi);
Vhrec[l] := (conjugate(sqrt(3/2) * (-I * 2)/(4 * Pi * m) * (AngerJ(-n, m * A * Pi) - I *
WeberE(-n, m * A * Pi) - AngerJ(-n, -m * A * Pi) + I * WeberE(-n, -m * A * Pi)) * (1 +
(-1)^n)) * (sqrt(3/2) * (-I * 2)/(4 * Pi * m) * (AngerJ(-n, m * A * Pi) - I * WeberE(-n, m *
A * Pi) - AngerJ(-n, -m * A * Pi) + I * WeberE(-n, -m * A * Pi)) * (1 + (-1)^n));
l:=l+1;
fi;
od;
od;

for m from 3 to 3 do
for n from -15 to 15 do
freq[l]:=m*ws+n*w1;
if modp(n,3)=0 then
Vhrec[l]:=0;
wrec[l]:=freq[l]/(2*Pi);
else
wrec[l]:=freq[l]/(2*Pi);

```

```

Vhrec[l] := (conjugate(sqrt(3/2) * (-I * 2)/(4 * Pi * m) * (AngerJ(-n, -m * A * Pi)-
I * WeberE(-n, -m * A * Pi) - AngerJ(-n, m * A * Pi) + I * WeberE(-n, m * A * Pi)))*
(1 + (-1)^n)) * (sqrt(3/2) * (-I * 2)/(4 * Pi * m) * (AngerJ(-n, -m * A * Pi) - I *
WeberE(-n, -m * A * Pi) - AngerJ(-n, m * A * Pi) + I * WeberE(-n, m * A * Pi)))*
(1 + (-1)^n));
l:=l+1;
fi;
od;
od;

for m from 5 to 5 do
for n from -15 to 15 do
freq[l]:=m*ws+n*w1;
if modp(n,3)=0 then
Vhrec[l]:=0;
wrec[l]:=freq[l]/(2*Pi);
else
wrec[l]:=freq[l]/(2*Pi);
Vhrec[l] := (conjugate(sqrt(3/2) * (-I * 2)/(4 * Pi * m) * (AngerJ(-n, -m * A * Pi)-
I * WeberE(-n, -m * A * Pi) - AngerJ(-n, m * A * Pi) + I * WeberE(-n, m * A * Pi)))*
(1 + (-1)^n)) * (sqrt(3/2) * (-I * 2)/(4 * Pi * m) * (AngerJ(-n, -m * A * Pi) - I *
WeberE(-n, -m * A * Pi) - AngerJ(-n, m * A * Pi) + I * WeberE(-n, m * A * Pi)))*
(1 + (-1)^n));
l:=l+1;
fi;
od;
od;
l;
Vhrec[l];
plot([[freq[1]/(2 * Pi), abs(Vhrec[1])], [freq[2]/(2 * Pi), abs(Vhrec[2])], [freq[3]/(2 * Pi),
abs(Vhrec[3])], [freq[4]/(2 * Pi), abs(Vhrec[4])], [freq[5]/(2 * Pi), abs(Vhrec[5])],
[freq[6]/(2 * Pi), abs(Vhrec[6])], [freq[7]/(2 * Pi), abs(Vhrec[7])], [freq[8]/(2 * Pi),
abs(Vhrec[8])], [freq[9]/(2 * Pi), abs(Vhrec[9])], [freq[10]/(2 * Pi), abs(Vhrec[10])],
[freq[11]/(2 * Pi), abs(Vhrec[11])], [freq[12]/(2 * Pi), abs(Vhrec[12])], [freq[13]/(2 * Pi),
abs(Vhrec[13])], [freq[14]/(2 * Pi), abs(Vhrec[14])], [freq[15]/(2 * Pi), abs(Vhrec[15])],
[freq[16]/(2 * Pi), abs(Vhrec[16])], [freq[17]/(2 * Pi), abs(Vhrec[17])], [freq[18]/(2 * Pi),
abs(Vhrec[18])], [freq[19]/(2 * Pi), abs(Vhrec[19])], [freq[20]/(2 * Pi), abs(Vhrec[20])],
)[freq[21]/(2 * Pi), abs(Vhrec[21])], [freq[22]/(2 * Pi), abs(Vhrec[22])], [freq[23]/(2 * Pi),

```



```
abs(Vhrec[114])), [freq[115]/(2 * Pi), abs(Vhrec[115])], [freq[116]/(2 * Pi),
abs(Vhrec[116])), [freq[117]/(2 * Pi), abs(Vhrec[117])], [freq[118]/(2 * Pi),
abs(Vhrec[118])], [freq[119]/(2 * Pi), abs(Vhrec[119])], [freq[120]/(2 * Pi),
abs(Vhrec[120])], [freq[121]/(2 * Pi), abs(Vhrec[121])], [freq[122]/(2 * Pi),
abs(Vhrec[122])], [freq[123]/(2 * Pi), abs(Vhrec[123])], [freq[124]/(2 * Pi),
abs(Vhrec[124])], [freq[125]/(2 * Pi), abs(Vhrec[125])], [freq[126]/(2 * Pi),
abs(Vhrec[126])], [freq[127]/(2 * Pi), abs(Vhrec[127])], [freq[128]/(2 * Pi),
abs(Vhrec[128])], [freq[129]/(2 * Pi), abs(Vhrec[129])], [freq[130]/(2 * Pi),
abs(Vhrec[130])], [freq[131]/(2 * Pi), abs(Vhrec[131])], [freq[132]/(2 * Pi),
abs(Vhrec[132])], [freq[133]/(2 * Pi), abs(Vhrec[133])], [freq[134]/(2 * Pi),
abs(Vhrec[134])], [freq[135]/(2 * Pi), abs(Vhrec[135])], [freq[136]/(2 * Pi),
abs(Vhrec[136])], [freq[137]/(2 * Pi), abs(Vhrec[137])], [freq[138]/(2 * Pi),
abs(Vhrec[138])], [freq[139]/(2 * Pi), abs(Vhrec[139])], [freq[140]/(2 * Pi),
abs(Vhrec[140])], [freq[141]/(2 * Pi), abs(Vhrec[141])], [freq[142]/(2 * Pi),
abs(Vhrec[142])], [freq[143]/(2 * Pi), abs(Vhrec[143])], [freq[144]/(2 * Pi),
abs(Vhrec[144])], [freq[145]/(2 * Pi), abs(Vhrec[145])], [freq[146]/(2 * Pi),
abs(Vhrec[146])], [freq[147]/(2 * Pi), abs(Vhrec[147])], [freq[148]/(2 * Pi),
abs(Vhrec[148])], [freq[149]/(2 * Pi), abs(Vhrec[149])], [freq[150]/(2 * Pi),
abs(Vhrec[150])], [freq[151]/(2 * Pi), abs(Vhrec[151])], [freq[152]/(2 * Pi),
abs(Vhrec[152])], [freq[153]/(2 * Pi), abs(Vhrec[153])], [freq[154]/(2 * Pi),
abs(Vhrec[154])], [freq[155]/(2 * Pi), abs(Vhrec[155])], [freq[156]/(2 * Pi),
abs(Vhrec[156])], [freq[157]/(2 * Pi), abs(Vhrec[157])]],
0..25000, 0..0.18, style = point);
```

Appendix C

Exponential decay

C.1 Exponential decay of v_δ under APOD/POD PWM

(This program calculates the exponential decay curve under APOD/POD PWM. The resulting curve is shown in Figure 5.11.)

restart:

with(plots):

$ws := 2 * Pi * 6000;$

$w1 := 2 * Pi * 50;$

$C := 1.759 * 10^{(-6)}$;

$R := 10;$

$L := 10 * 10^{(-3)}$;

$A := 0.8;$

$Cd := 2500 * 10^{(-6)}$;

$wrec := n * w1;$

$Vhrec2 := \text{sum}'((\text{conjugate}(-\sqrt{3/2} * (1/2) * 2 * A * (2 * \exp(I * \text{Pi} * (3 * k + 2))) + 1 + \exp(2 * I * \text{Pi} * (3 * k + 2))) / (\text{Pi} * ((3 * k + 2)^2 - 1))) * (-\sqrt{3/2} * (1/2) * 2 * A * (2 * \exp(I * \text{Pi} * (3 * k + 2))) + 1 + \exp(2 * I * \text{Pi} * (3 * k + 2))) / (\text{Pi} * ((3 * k + 2)^2 - 1))) / (((-(3 * k + 2) * w1)^2 + (1 / (R * C)) * I * (3 * k + 2) * w1 + (1 / (L * C))) / ((1 / L) * I * (3 * k + 2) * w1 + (1 / (L * R * C))))', k' = 0..4);$

$Vhrec1 := \text{sum}'((\text{conjugate}(-\sqrt{3/2} * (1/2) * 2 * A * (2 * \exp(I * \text{Pi} * (3 * k + 1))) + 1 + \exp(2 * I * \text{Pi} * (3 * k + 1))) / (\text{Pi} * ((3 * k + 1)^2 - 1))) * (-\sqrt{3/2} * (1/2) * 2 * A * (2 * \exp(I * \text{Pi} * (3 * k + 1))) + 1 + \exp(2 * I * \text{Pi} * (3 * k + 1))) / (\text{Pi} * ((3 * k + 1)^2 - 1))) / (((-(3 * k + 1) * w1)^2 + (1 / (R * C)) * I * (3 * k + 1) * w1 + (1 / (L * C))) / ((1 / L) * I * (3 * k + 1) * w1 + (1 / (L * R * C))))', k' = 1..4);$

$Vh0 := \text{simplify}((Vhrec1 + Vhrec2));$

$Vhrec3 := \text{sum}'((\text{conjugate}(\sqrt{3/2} * (-I * 2) / (4 * \text{Pi} * m)) * (\text{AngerJ}(-(3 * k + 1), m *$

```


$$A * Pi) - I * WeberE(-(3 * k + 1), m * A * Pi) - AngerJ(-(3 * k + 1), -m * A * Pi) + I * WeberE(-(3 * k + 1), -m * A * Pi)) * (1 + (-1)^(3 * k + 1))) * (sqrt(3/2) * (-I * 2) / (4 * Pi * m) * (AngerJ(-(3 * k + 1), m * A * Pi) - I * WeberE(-(3 * k + 1), m * A * Pi) - AngerJ(-(3 * k + 1), -m * A * Pi) + I * WeberE(-(3 * k + 1), -m * A * Pi)) * (1 + (-1)^(3 * k + 1))) / (((((3 * k + 1) * w1 + m * ws)^2) + (1 / (R * C)) * I * ((3 * k + 1) * w1 + m * ws) + (1 / (L * C)))) / ((1 / L) * I * ((3 * k + 1) * w1 + m * ws) + (1 / (L * R * C))))))' , k' = -5..4) + sum('((conjugate(sqrt(3/2) * (-I * 2) / (4 * Pi * m) * (AngerJ(-(3 * k + 2), m * A * Pi) - I * WeberE(-(3 * k + 2), m * A * Pi) - AngerJ(-(3 * k + 2), -m * A * Pi) + I * WeberE(-(3 * k + 2), -m * A * Pi)) * (1 + (-1)^(3 * k + 2))) * (sqrt(3/2) * (-I * 2) / (4 * Pi * m) * (AngerJ(-(3 * k + 2), m * A * Pi) - I * WeberE(-(3 * k + 2), m * A * Pi) - AngerJ(-(3 * k + 2), -m * A * Pi) + I * WeberE(-(3 * k + 2), -m * A * Pi)) * (1 + (-1)^(3 * k + 2))) / (((((3 * k + 2) * w1 + m * ws)^2) + (1 / (R * C)) * I * ((3 * k + 2) * w1 + m * ws) + (1 / (L * C)))) / ((1 / L) * I * ((3 * k + 2) * w1 + m * ws) + (1 / (L * R * C))))))' , k' = -5..4); Vh1 := sum('Vhrec3' , m' = 1..20);$$


```

```
V1 := Cd / (Re(Vh1 + Vh0));
```

```
Vf := (V1);
plot([200 * exp(-t/Vf)], t = 0..1.5);
```

C.2 Exponential decay of v_δ under PD PWM

(This program calculates the exponential decay curve under PD PWM. The resulting curve is shown in Figure 5.18.)

restart:

```
with(plots):
```

```
ws := 2 * Pi * 6000;
```

```
w1 := 2 * Pi * 50;
```

```
C := 7.036 * 10^(-6);
```

```
R:=10;
```

```
L := 10 * 10^(-3);
```

```
A:=0.8;
```

```
Cd := 2500 * 10^(-6);
```

```
wrec := n * w1;
```

```
Vhrec2 := sum('((conjugate(-sqrt(3/2) * (1/2) * 2 * A * (2 * exp(I * Pi * (3 * k + 2))) + 1 + exp(2 * I * Pi * (3 * k + 2))) / (Pi * ((3 * k + 2)^2 - 1))) * (-sqrt(3/2) * (1/2) * 2 * A * (2 * exp(I * Pi * (3 * k + 2))) + 1 + exp(2 * I * Pi * (3 * k + 2))) / (Pi * ((3 * k + 2)^2 - 1))) / (((((3 * k + 2) * w1)^2) + (1 / (R * C)) * I * ((3 * k + 2) * w1 + (1 / (L * C)))) / ((1 / L) * I * ((3 * k + 2) * w1 + (1 / (L * R * C))))))' , k' = 0..4);
```

```
Vhrec1 := sum('((conjugate(-sqrt(3/2) * (1/2) * 2 * A * (2 * exp(I * Pi * (3 * k + 1))) + 1 + exp(2 * I * Pi * (3 * k + 1))) / (Pi * ((3 * k + 1)^2 - 1))) * (-sqrt(3/2) * (1/2) * 2 * A * (2 * exp(I * Pi * (3 * k + 1))) + 1 + exp(2 * I * Pi * (3 * k + 1))) / (Pi * ((3 * k + 1)^2 - 1))) / (((((3 * k + 1) * w1)^2) + (1 / (R * C)) * I * ((3 * k + 1) * w1 + (1 / (L * C)))) / ((1 / L) * I * ((3 * k + 1) * w1 + (1 / (L * R * C))))))' , k' = 0..4);
```

$$I*Pi*(3*k+1)))/(Pi*((3*k+1)^2-1))))*(-sqrt(3/2)*(1/2)*2*A*(2*exp(I*Pi*(3*k+1))+1+exp(2*I*Pi*(3*k+1)))/(Pi*((3*k+1)^2-1)))/((-(((3*k+1)*w1)^2)+(1/(R*C))*I*(3*k+1)*w1+(1/(L*C)))/((1/L)*I*(3*k+1)*w1+(1/(L*R*C)))))', k' = 1..4);$$

$Vh0 := \text{simplify}((Vhrec1 + Vhrec2));$

$$Vhrec3 := \text{sum}'((\text{conjugate}(sqrt(3/2)*(-I*2)/(4*Pi*m)*(AngerJ(-(3*k+1), m*A*Pi) - I*WeberE(-(3*k+1), m*A*Pi) - AngerJ(-(3*k+1), -m*A*Pi) + I*WeberE(-(3*k+1), -m*A*Pi))*(1+(-1)^(3*k+1)))*(sqrt(3/2)*(-I*2)/(4*Pi*m)*(AngerJ(-(3*k+1), m*A*Pi) - I*WeberE(-(3*k+1), m*A*Pi) - AngerJ(-(3*k+1), -m*A*Pi) + I*WeberE(-(3*k+1), -m*A*Pi))*(1+(-1)^(3*k+1)))/((-(((3*k+1)*w1+m*ws)^2)+(1/(R*C))*I*((3*k+1)*w1+m*ws)+(1/(L*C)))))', k' = -5..4) + \text{sum}'((\text{conjugate}(sqrt(3/2)*(-I*2)/(4*Pi*m)*(AngerJ(-(3*k+2), m*A*Pi) - I*WeberE(-(3*k+2), m*A*Pi) - AngerJ(-(3*k+2), -m*A*Pi) + I*WeberE(-(3*k+2), -m*A*Pi))*(1+(-1)^(3*k+2)))*(sqrt(3/2)*(-I*2)/(4*Pi*m)*(AngerJ(-(3*k+2), m*A*Pi) - I*WeberE(-(3*k+2), m*A*Pi) - AngerJ(-(3*k+2), -m*A*Pi) + I*WeberE(-(3*k+2), -m*A*Pi))*(1+(-1)^(3*k+2)))/((-(((3*k+2)*w1+m*ws)^2)+(1/(R*C))*I*((3*k+2)*w1+m*ws)+(1/(L*C)))))/((1/L)*I*((3*k+2)*w1+m*ws)+(1/(L*R*C)))))', k' = -5..4);$$

$Vh1 := \text{sum}'(Vhrec3', m' = 1..20);$

$V1 := Cd/(Re(Vh1 + Vh0));$

$Vf := (V1);$

$\text{plot}([200 * \text{exp}(-t/Vf)], t = 0..1.5);$

Appendix D

FFT analysis and simulation setup

D.1 FFT for switching functions

(This program is used for plotting harmonics of s_α , s'_α , s_β , s'_β using simulated results of NPC inverter.)

```
x=SALPHA/SBETA/SALPHAP/SBETAP;
y=fft(x);
N=length(x);
y=y/(N/2);
mag=abs(y);
phase=angle(y);
T=20e-3;
f=0:1/T:(N-1)/T;
f1=f(1:500);
mag1=mag(1:500);
stem(f1,mag1);
```

D.2 Simulation setup using APOD/POD and PD.

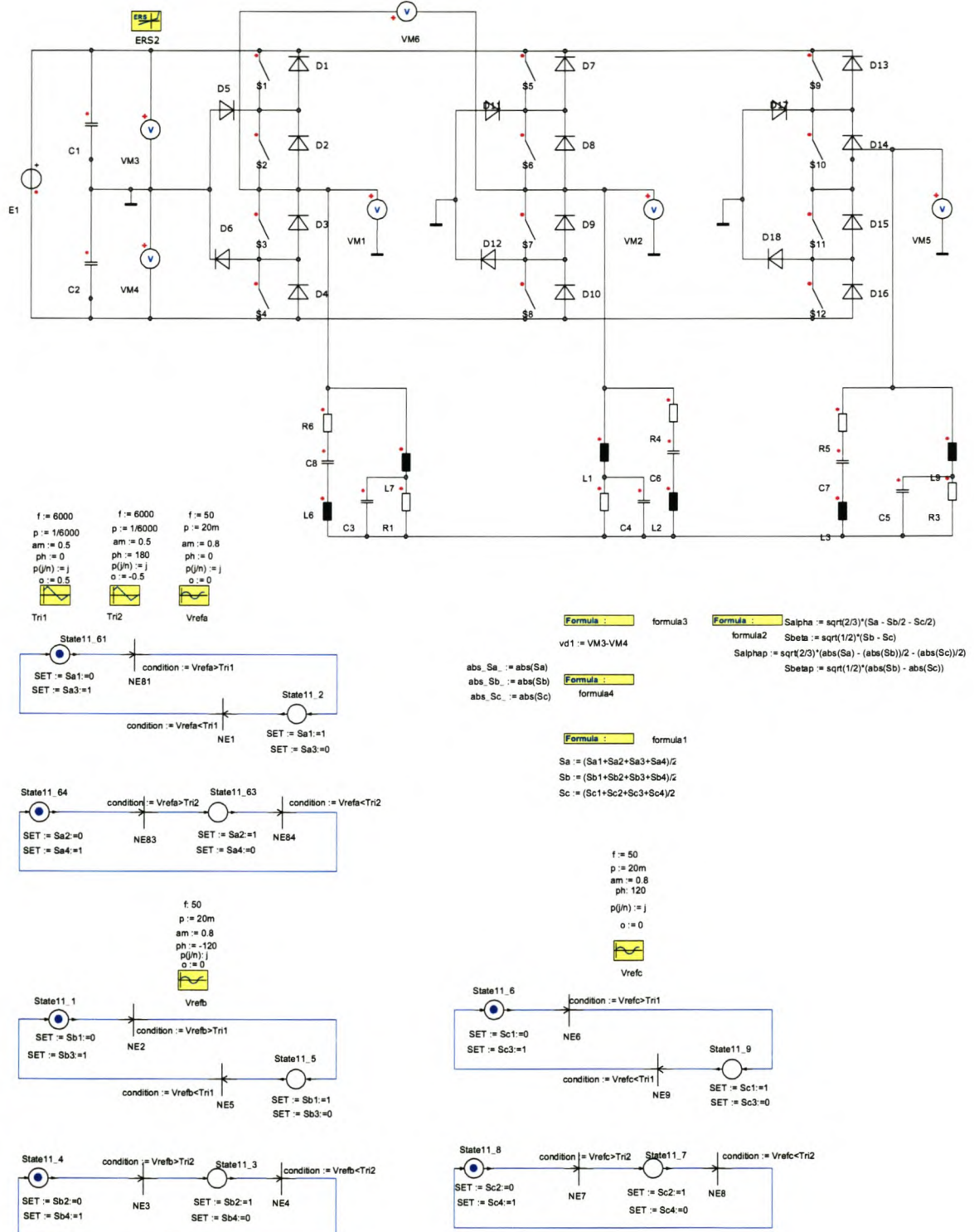


Figure D.1: Simulation setup for NPC inverter using APOD/POD and PD PWM.

D.3 Simulation setup using vector control

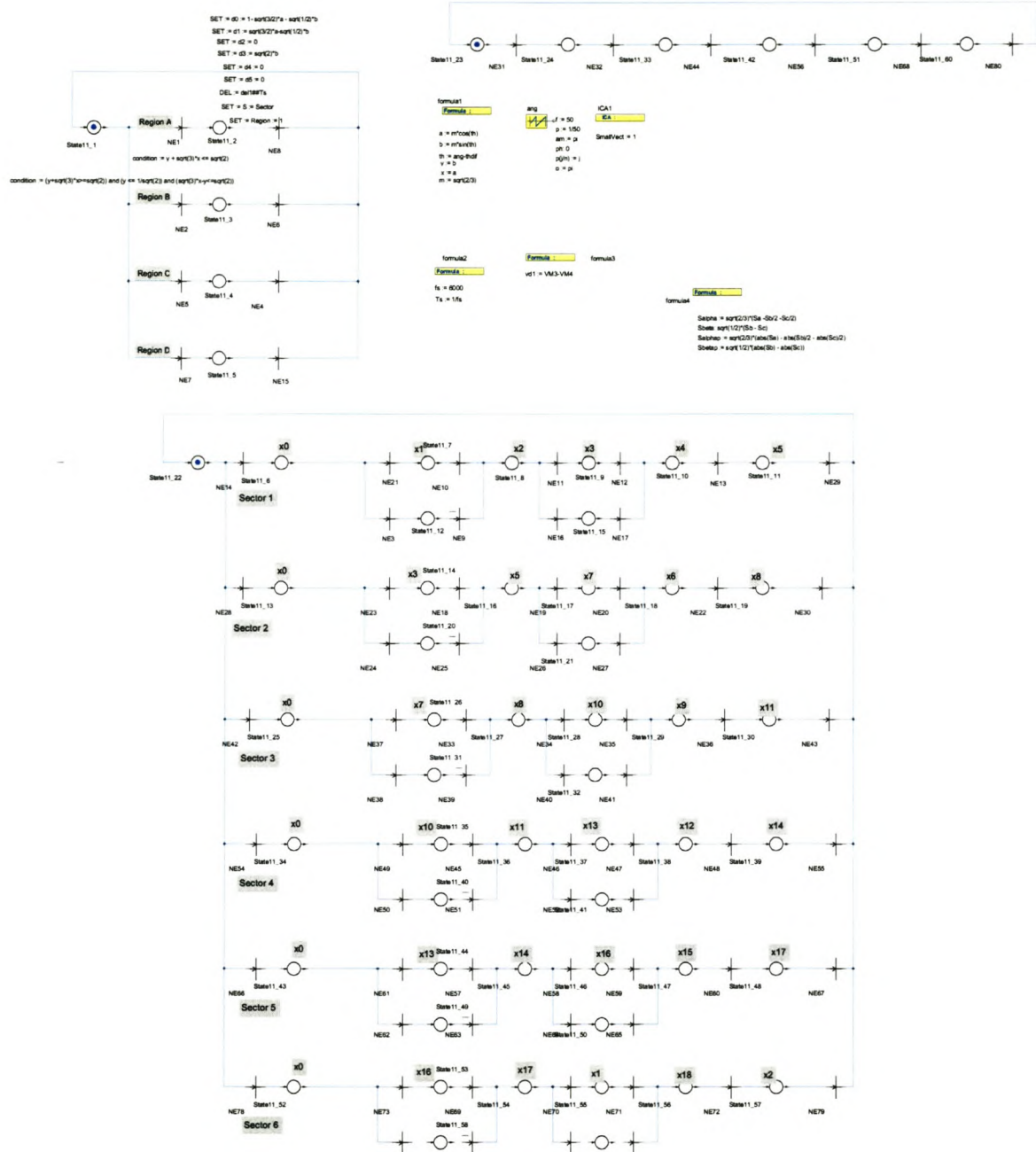


Figure D.2: Simulation setup for NPC inverter using vector control.